Khfagi, Amir Mohamed Ibrahim (2023) *Investigation of entropy generation and thermohydraulics of forced and mixed convection of Al₂O₃-Cu/water in a parabolic trough receiver tube.* PhD thesis.

https://theses.gla.ac.uk/83735/

Investigation of entropy generation and thermohydraulics of forced and mixed convection of Al_2O_3-Cu/water in a parabolic trough receiver tube

Amir Mohamed Ibrahim Khfagi

Submitted in fulfilment of the requirements for the Degree of Doctor of Philosophy in Mechanical Engineering at the University of Glasgow

James Watt School of Engineering

College of Science and Engineering

University of Glasgow

March 2023

Declaration

I declare that this thesis is my own work, and it has not been submitted for any other degree at the University of Glasgow or any other institution. It was carried out in the James Watt School of Engineering at the Glasgow University during the period from June 2019 to March 2023. The author conducted all the work in this thesis, except where explicitly stated otherwise in the text.

………………………

Amir Khfagi

March 2023

Abstract

Heat transfer has long been a vital part of human life. Many sources have focused on increased heat transfer. Various industries, such as solar water heating systems, solar chemistry, solar desalination plants, and concentrating solar power plants, food processing plants, petrochemical plants, refrigeration systems and air conditioning equipment, and condensing central heating exchangers, etc., face the challenges of effective utilisation, conservation, and recovery of heat. In modern times, increasing the rate of heat transfer in concentrating solar collectors such as parabolic troughs by using various passive approaches have proven to be very effective. When passive approaches are used, more pumping power is needed to move the fluid through the receiver. Manufacturing of parabolic trough receiver tubes requires a significant financial commitment due to the high expenses of both capital and operation. Therefore, it is essential to develop parabolic trough receivers that are efficient. Several methods, such as heat transfer enhancement and minimisation of entropy generation, are used to do this. The current investigation makes use of tube insert technology and nanoparticle flow to achieve optimal thermohydraulic and thermodynamic designs.

Previous research on fluid flow and heat transfer in a regular pipe (PT) and a pipe equipped with an elliptical-cut twisted tape insert (TECT) and a traditional twisted tape insert (TPT) has not been conducted, particularly emphasizing the utilization of hybrid nanofluid as the working medium. However, previous works on water and nanofluid do exist. In addition, the Bejan number and the generation of total entropy are not examined on tubes supplied with an elliptical-cut and classical twisted tape insert for different fluids. Hence, in this study, heat transfer and entropy generation in a turbulent flow of an Al_2O_3-Cu/water hybrid nanofluid in a plain tube with classical and elliptical-cut twisted tape inserts are investigated numerically.

The current study focuses on the heat transmission augmentation and thermodynamic irreversibility of steady and unsteady turbulent flows through pipes with elliptical-cut and classical twisted tape introduced under uniform or non-uniform well heat flux for water, hybrid-nanofluids (Al_2O_3-Cu/water), and nanofluids (CuO/water). This work uses Star-CCM+ for numerical simulations. The realizable k-ε model is employed to simulate the turbulent flow computationally. The findings are utilised to determine which type of tube and fluid provides the highest performance by quantifying gains in steady state (friction factor, heat transfer, and thermal performance factor) and unsteady state (transient heat transfer). The total entropy

generation has been examined in this PhD study to determine the type of tube and fluid that reduces entropy generation.

The results indicate that the heat transfer augmentation and thermal performance factor provided by the tube fitted with elliptical-cut twisted tape are greater than those provided by the tube supplied with classical twisted tape and the ordinary tube. This is because the pipe supplied with elliptical-cut twisted tape mixes the fluids better than the tube supplied with traditional twisted tape and the ordinary tube. Also, when the number of nanoparticles increases, heat transmission and thermal performance factors increase. Furthermore, TECT, hybrid nanofluids, and mass concentrations of nanoparticles affect the rate of total entropy production.

The mixed convection of Al_2O_3-Cu/water hybrid nanofluid is also investigated in a vertical pipe supplied with elliptical-cut twisted tape inserts. Further, the local and total entropy production as well as Bejan number of the system are calculated. The results clearly demonstrate the effect of mixed convection on heat transfer, thermal performance factor, and entropy production. Where the factor of thermal performance and the rate of heat transfer increase of pipe systems under mixed convection exceed those under forced convection. Moreover, mixed convection has a significant impact on the minimisation of the total entropy production.

Acknowledgements

In the Name of Allah, the Most Beneficent, the Most Compassionate. All praise and thanks to Allah, who gave me strength, health, and patience to reach this stage.

Dr Nader Karimi, my director of studies before he moved to Queen Mary University of London and became a second supervisor, deserves my gratitude for his assistance during my research. Your continuous encouragement, constructive criticism, and wonderful comments will be remembered forever. Thank you for making time for this research despite your busy schedules and new responsibilities at Queen Mary University of London. I owe you a huge debt of gratitude for your continuous cooperation and support during your time in Glasgow and after you moved.

I would also like to thank my supervisors at the University of Glasgow, Prof Manosh Paul, and Dr Graeme Hunt for all their guidance, excellent leadership, and unwavering support throughout the research and PhD process. I appreciate their support, advice, and constructive feedbacks in order to enhance my work. All your interest for this research has been a continuous source of motivation.

Thanks to the Libyan government and Ministry of Higher Education for funding my doctoral studies at University of Glasgow.

School of Engineering of the University of Glasgow for this study is gratefully appreciated. Grateful thanks are due to the members of IT Support Team of School of Engineering.

I would like to thank my local and international friends and colleagues for their time spent with me during the previous several years of my research. I am incredibly grateful to everyone who helped make my research a success in whatever way.

Finally, and most importantly, I am thankful for my wonderful family. I would like to thank my mom and dad for the love and support I have received since the day I was born, as well as my sisters and brothers. Their faith and prayers have inspired and encouraged me to keep going with this research. I would also like to express my gratitude to my family for their support, sympathy, and patience throughout this study journey. I would like to express my gratitude to my wife and our gorgeous children. Your happiness and affection have always lifted my spirits during the ups and downs of the last four years.

Table of Contents

List of Figures

List of Tables

List of Symbols

Roman Symbols

a	Short diameter ratio (m)
b	Long diameter ratio (m)
Be	Bejan number.
$C_1, C_2, C_3, C_{1\varepsilon}, C_{3\varepsilon}, C_\mu$	Model constant
C_p	Specific heat of fluids (J Kg^{-1} K^{-1})
D	Diameter of tube (m)
f	Friction Factor
g	Gravitational acceleration (m s^{-2})
g_i	Gravitational vector component in the ith direction (m s^{-2})
G_k	Kinetic energy produced by turbulent flow (J Kg^{-1})
G_b	Turbulence kinetic energy generation caused by buoyancy
G_r	Grashof number
h	Thermal transfer coefficient (W m^{-2} K^{-1})
I	Turbulence intensity
k_c	Thermal conductivity of fluids (Wm^{-1}K^{-1})
k_{c_t}	Fluid thermal conductivity during turbulent flow (Wm^{-1}K^{-1})
k	Kinetic energy of turbulent fluids (JKg^{-1})
L	Length of tube (m)
$\dot{m}$	Mass flow rate (Kg. s^{-1})
Nu	Nusselt number
p	Pressure (Pa)
Pr_t	Turbulent Prandtl number
q	Heat flux (W m^{-2})
Re	Reynolds number
Ri	Richardson number
S	Modulus of the average rate-of-strain tensor
S_ε, S_k	Terms of source
S_{ij}	Fluid element's linear deformation rate
$S_{F,F}$	Friction-induced entropy generation (W m^{-3} K^{-1})
$S_{H,T}$	Thermal-induced entropy generation (W m^{-3} K^{-1})

List of Symbols

$S_{g,t}$	Total entropy generation (W m^{-3} K^{-1})
t	Time (s)
T	Temperature (K)
T_0	Reference Fluid temperature (K)
u	Velocity of fluid (m s^{-1})
u_i, u_j, u, v, w	Component of velocity in Cartesian coordinates (m s^{-1})
u'	Turbulent behavior of the velocity component
w	Twisted tape width (m)
y	Twisted tape pitch (m)
Y_M	Dissipation rate due to fluctuating dilatation in compressible flow

Greek symbols

β	Thermal expansion coefficient
ρ	Fluid density (Kg m^{-3})
ρ_0	Flow density reference (Kg m^{-3})
μ	Viscosity of fluid dynamics (Pa-S)
μ_t	Flow dynamics turbulent viscosity (Pa-S)
$\emptyset$	Amount of solid volume
η	Factor of thermal efficiency
Δp	Pressure drops (Pa)
σ_ε	Prandtl Turbulent Numbers for ε
σ_k	Prandtl Turbulent Numbers for k
δ	Thickness (m)
δ_{ij}	Kronecker-Delta
τ_{ij}	Stress tensor
ε	Dissipation rate of Turbulent kinetic energy (m^2 s^{-3})
ω_k	Specific dissipation rate (s^{-1})

Subscripts

b	Bulk
eff	Effective
bf	Basic fluid
nf	Nanofluid
hnf	Hybrid-nanofluid
i	Inlet
o	Reference
p	Simple pipe

List of Acronyms

PT	Ordinary Tube
TATCT	Tube containing twisted tape with alternate-axis triangular cuts
TECT	Tube containing elliptical cut twisted tape
TPT	Tube containing solid twisted tape

Chapter 1 Introduction

1.1 Background

Many countries possess abundant natural resources such as sun, wind, and natural gas, yet a significant portion of their energy production still relies on fossil fuels. In recent years, there has been a growing global interest in harnessing renewable energy sources as a means to diversify energy portfolios and decrease reliance on fossil fuels. Solar energy, in particular, holds great potential in regions with high solar irradiation, such as desert areas (Figure 1-1). Alongside solar power, wind energy systems have emerged as promising renewable alternatives [1].

Governments worldwide have acknowledged this potential and set ambitious targets to increase the share of renewable energy in their respective energy mixes. For instance, there are national goals to generate a certain percentage of electricity from renewable sources by specific years [1, 2]. Both solar and wind energy play critical roles in achieving these objectives. It has been noted that many regions receive an annual solar radiation level of approximately 7.5 kWh/m2/day, coupled with an average of 3000 to 3500 sunshine hours per year. Furthermore, the average wind speed ranges between 6 to 7.5 meters per second (m/s) at a height of 40 meters [1].These favourable conditions enable the potential to meet future electricity needs [1].

Despite the ambitious targets and potential benefits, the implementation of renewable energy projects has encountered challenges globally, including inadequate regulations, limited funding, and political instability in some countries. However, several initiatives and projects have emerged in recent years, such as the establishment of solar power plants, deployment of solar-powered water pumps, and the development of small-scale wind energy projects [3, 4]. Overall, the renewable energy sector is still in its nascent stages across many regions. However, with the implementation of appropriate policies and investments, it holds significant promise in meeting energy needs and contributing to sustainable development. Consequently, governments aim to fully exploit renewable energy sources by 2050, ensuring the satisfaction of all energy requirements and potentially enabling energy exports. This transformation would mark a reversal from the current situation, with renewable energy surpassing fossil energy consumption (Figure 1-2).

One specific type of renewable energy that has gained attention in recent years is solar thermal energy. According to the MED-CSP vision (Trans Mediterranean interconnection for

concentrated solar power), solar thermal energy is expected to hold the highest proportion of renewable energy sources until 2050 [5].

1.2 Solar thermal energy

Solar thermal energy is a technology that harnesses the heat from the sun to generate electricity. Thermal energy can be obtained from solar radiation by using Concentrated Solar Power (CSP) or Photovoltaic (PV) systems. The electricity generated through PV plants can be stored in batteries, but CSP technologies use Thermal Energy Storage (TES) systems to do so. One of the system's main features (Figure 1-3) is that it includes the thermal energy storage system (two-tank system) which can store the thermal energy and enable continuous operation of the power block during cloud cover conditions or in the absence of sunlight. A parabolic trough receiver is a component of a concentrated solar power (CSP) system that is designed to collect and focus the sun's energy onto a fluid-filled pipe, called a heat transfer fluid (HTF), located at the focal point of the trough. It uses mirrors or lenses to concentrate the sun's energy onto receiver tubes that heat up the Heat Transfer Fluid (HTF) contained within the tubes (Figure 1-4). The HTF is then circulated to a heat exchanger, where the thermal energy is transferred to a working fluid, which is used to generate electricity.

The performance of concentrated solar power plants can be enhanced or optimized by improving thermal energy storage, heat transfer fluids, and, even more importantly, the methods by which solar radiation is concentrated. The main challenges in the parabolic trough receiver are poor fluid quality causing corrosion and clogging, high fluid temperature leading to thermal degradation and reduced heat transfer efficiency, and poor fluid circulation leading to uneven temperature distribution and reduced heat transfer efficiency. Such issues can result in decreased performance and reduced efficiency of the solar thermal power plant. This is in addition to the durability and longevity of the receiver in the harsh operating environment [6]. Researchers are actively working to improve these aspects through material and design advancements to make solar thermal power a more viable form of renewable energy.
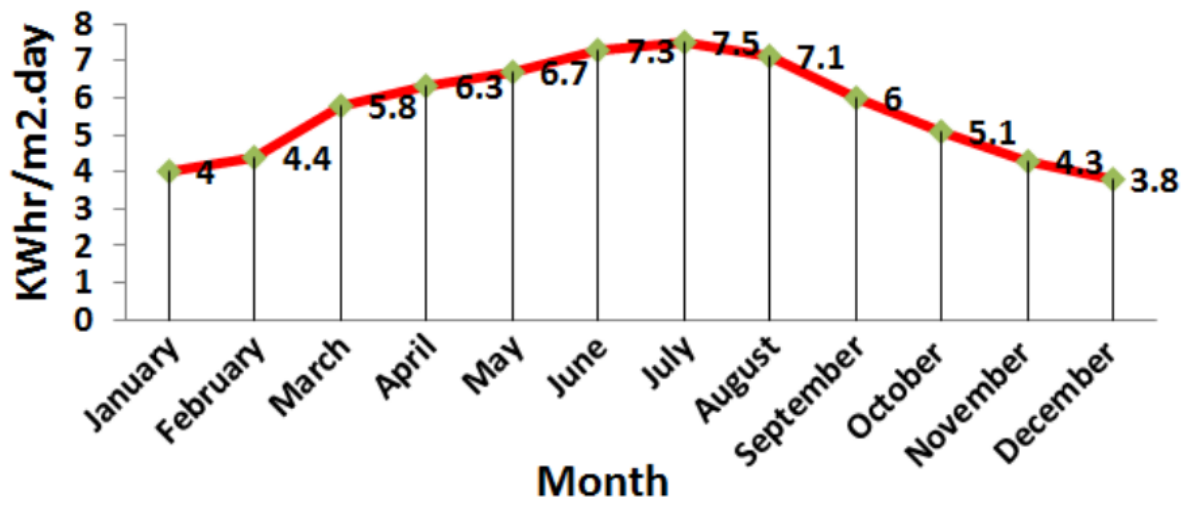
Figure 1-1 Monthly solar radiation average [2].
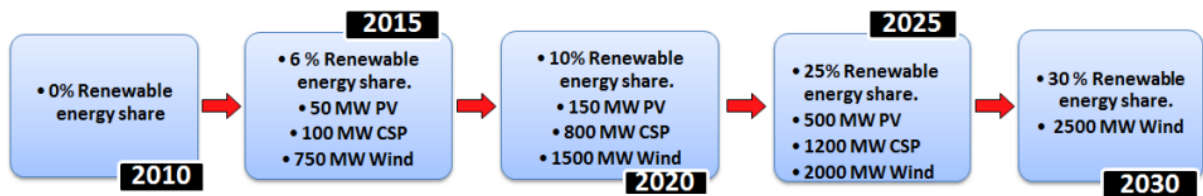
Figure 1-2 Action plans of renewable energy authority [2].
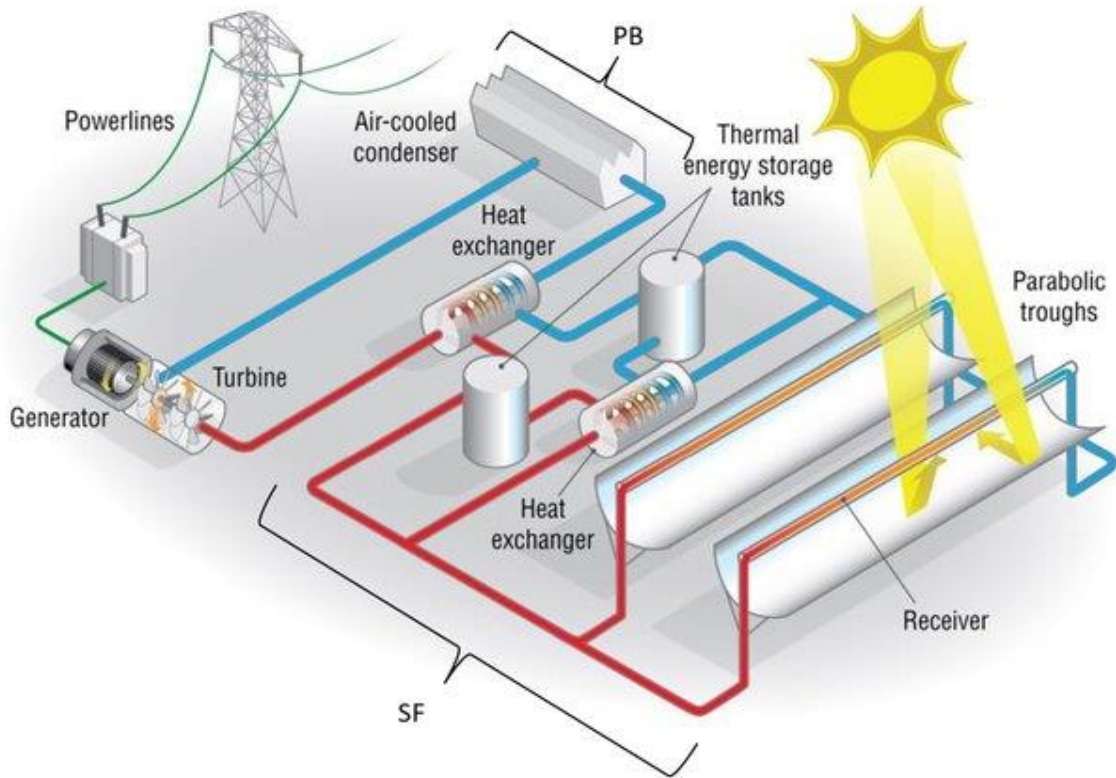
Figure 1-3 Scheme for a solar thermal power plant with a parabolic trough [7].

Figure 1-4 Parabolic trough collectors [8].

1.3 Heat Transfer

Heat is a form of energy that is transferred when the temperature of a system and its surroundings are different. Numerous studies have been conducted in this subject throughout the years, the majority of which have aimed to improve and accelerate heat transfer. As a result, this science remains one of the most vital areas of inquiry and study for academics and scientists. The optimization of heat transfer and thermohydraulic performance remains an important issue due to its importance in a wide range of engineering and power-associated uses, including solar thermal energy, heat exchangers, refrigeration of electronic devices, and manufacturing systems [9]. Convective heat transfer is the most often employed method of heat transfer [10].

In general, there are three types of convection: free, forced, and mixed. The motion of fluids in free convection is caused by changes in gravity as a result of changes in fluid density. In the process of forced convection, a driving force is provided to the fluid to get it moving. "Mixed convection" refers to both free and forced convections in the heat transfer process [10, 11].

Solar receiver tubes are an important part of the system of parabolic trough solar thermal production that converts solar radiation to thermal energy, accounting for about 30% of the material costs associated with the building of a solar field [12]. With energy costs continuing to rise, significant savings in total costs can be made by using increasingly more efficient receiver tubes. Because of this, a lot of effort has been put into finding ways to improve the efficiency of heat transfer in solar receiver tubes. Research is also being done to learn more about the basic mechanisms of heat transmission. This study aims to continue in the same direction, with a focus on solar receiver tubes. According to a study by Wang and Sunden [13], a heat transfer improvement technique leads to lower capital costs.

In general, an augmentation in heat transmission rate is accompanied by a rise in pressure drop, which requires a high pumping power demand. Researchers have been attempting to develop techniques that improve heat transfer at the lowest feasible pressure drop. These methods include the forced flow of fluids, including oil, water, ethylene glycol, air, and other nanofluids, across a heated surface.

Heat transfer enhancement, augmentation, or intensification refers to methods employed to increase heat transmission efficiency [14]. These methods can be used effectively in a variety of solar thermal energy applications, such as solar water heating systems, solar chemistry [15],

solar desalination plants, and concentrating solar power plants [16]. In addition, air-cooled heat pipe heat exchangers are employed in industrial operations for inner heat exchangers and radiators, and also in household uses like heat dissipation cycles, condensing central heating exchangers, refrigeration systems, and radiators in rooms [13, 17-19].

Heat transfer enhancement strategies are classed as passive methods, active methods, and compound methods [20, 21]. Passive techniques for improving heat transmission require no external power. As part of these approaches, the flow channel is modified geometrically or surface-wise, for instance surfaces treated, extended surfaces, rough surfaces, as well as enhanced surfaces, or integrate extra devices, such as swirl flow devices (twisted tape inserts), surface tension devices, spiral pipes, gases additives, liquid additives, etc. The active approaches of improving heat transmission need direct use of external power. Surface vibration, fluid vibration, mechanical assistance, electric and/ or magnetic fields, etc., fall under this category. Due to their complexity and reliance on external power, these technologies have not demonstrated significant promise, and have therefore found limited uses. Compound heat transfer augmentation refers to the use of several methods working together to improve heat transfer (a combined approach of passive and active techniques). Tubes fitted with a twisted tape insert and spirally corrugated pipes are two examples of this technique.

As an enhancement strategy, passive methods are by far the most frequent. Liquid additives and twisted tape designed to fit inside of tubes are two obvious examples. An increase in heat transfer may be achieved by creating a flow disturbance that causes the velocity and thermal boundary layers to separate. It is essential to overcome the predominant barrier to heat transmission over a primary surface in order to increase heat transmission through a receiver tube. For these situations, the coefficient of heat transmission and the exposed surface area are the only two determinants of heat transfer. The two are connected in the sense that any rise in one lead in a commensurate drop in the other. By increasing the flow velocity parallel to the pipe or the pipe axis the heat transfer coefficient is increased as reported by Lane and Heggs [17] and Manglik and Bergles [22]. In addition, researchers anticipate that fluids containing solid metallic particles will have much higher thermal conductivities than traditional heat transfer fluids [23-25]. Furthermore, hybrid nanofluids containing these nanoparticles have been demonstrated to improve the conductivity of thermal and heat transfer performance of base fluids [26-28]. Twisted tape insertion techniques and hybrid-nanofluid are used in this work to enhance heat transfer.

Advantages of tube insert technology have made it a dependable method of improving heat transmission. The tape, for instance, may be placed into and removed from the tube without any special training or equipment, which simplifies the installation process. Additionally, twisted tape has a low manufacturing cost when compared to other heat transport augmentation methods such as, springs, heatex wire matrix, fins, etc. Due to its simplicity, it makes an appealing choice for moulding jobs [14, 29-31], as opposed to heatex wire matrix, springs, fins, etc. On the other hand, by combining two or more nanoparticles in a base fluid, a hybrid nanofluid is created. A hybrid material is a substance that gives the combined physical and chemical properties of many distinct materials in a single, unified form. The amazing physicochemical features shown in synthetic hybrid nanomaterials are not seen in the individual components [32, 33].

Typically constructed from a thin metallic strip, twisted tape falls under the umbrella term "swirl flow device" [34]. Some factors are responsible for the improved heat transport in pipes with twisted tape inserts. This can include reducing hydraulic diameter (that improves the rate of heat transmission), swirl mixing and secondary motion caused by the twisted tape (that also enhances the convective ratio), the cross-sections of the pipe fluid are divided and blocked by the tape (that causes a heightened flow velocity), and spiral flow (that produces eddies in the fluid) [35]. In addition, the conductivity of thermal is a crucial metric for enhancing heat transfer in hybrid nanofluids. The heat transmission and thermal conductivity parameters for nanofluid depend on a variety of factors, including nanoparticle type, nanoparticle size, stability, base fluid type, fluid temperature, etc [36-38].

Most of the research on the performance analysis of tubes with or without twisted tape are based primarily on the first law of thermodynamics, which does not provide a conception of the energy quality produced by parabolic trough systems. The use of the second law is often advised when determining the quality of energy from a system and optimising the thermal system and its components [39, 40].

The majority of previous studies on the improvement of heat transmission have been conducted on ordinary pipes, pipes supplied with twisted tape, and cut twisted tape for water and nanofluid flows. Despite this, hybrid nanofluid flow in ordinary tubes and tubes with twisted tape have received very little attention. Not only that, but there is also a severe lack of study on tubes fitted with twisted tape and using hybrid nanofluid as working flow according to the second law of thermodynamics. Moreover, the analysis of entropy generation and transient heat

transmission augmentation employing hybrid nanofluids in tubes with twisted tape have largely been neglected. Additionally, no research has been reported on the improvement of transient heat transmission in pipe equipped with twisted tape inserts and non-uniform heat flux. Also, despite their importance in engineering, mixed convection heat transmission and entropy production for mixed convection of turbulent flows in pipes supplied with twisted tape using hybrid nanofluid have been largely ignored. Therefore, the main focuses of interest in this thesis for the parabolic trough receiver tube are heat transmission rates and the analysis of entropy creation. The use of heat transfer rates in order to achieve high thermal efficiency levels and to analyse entropy generation for the purpose of reducing total entropy generation. Analyses were carried out on ordinary pipes (PT) and pipes fitted with elliptical cut (TECT) and classical (TPT) twisted tape inserts, under hybrid nanofluid turbulent flow conditions.

1.4 Publications

Khfagi, A.M., Hunt, G., Paul, M.C. and Karimi, N., 2022. Computational analysis of heat transfer augmentation and thermodynamic irreversibility of hybrid nanofluids in a tube fitted with classical and elliptical-cut twisted tape inserts. *Journal of Thermal Analysis and Calorimetry*, *147*(21), pp.12093-12110.

Khfagi, A.M., Hunt, G., Paul, M.C. and Karimi, N., 2023. Entropy generation and thermohydraulics of mixed convection of hybrid-nanofluid in a vertical tube fitted with elliptical-cut twisted tape inserts-a computational study. *Energy Sources, Part A: Recovery, Utilization, and Environmental Effects*, *45*(2), pp.3369-3391.

1.5 Articles under Review or Preparation

Time-dependent analysis of heat transmission enhancement and entropy generation in a pipe with a solid and elliptical-cut twisted tape insert with non-uniform heat flux for hybrid nanofluids, to be submitted to Energy Sources, Part A: Recovery, Utilization, and Environmental Effects. Accepted with minor corrections.

Chapter 2 Literature review

2.1 Introduction

Scientists estimate that the world's energy consumption will increase by 50% by 2030 and by 70% to 100% by 2050 as a result of rising populations and growing economies [41]. Fossil fuels, for example, are fast dwindling and experiencing price volatility. More importantly, they are destroying the environment irreversibly. The high carbon emission rate from fossil fuels leads to environmental concerns such as global warming, so it is urgent to reduce fossil fuel dependency for commercial power generation. According to the UN Climate Change Conference (COP26) in Glasgow in November 2021, countries need to come up with net zero emissions targets by 2030. Solar and wind energy are excellent sources of renewable energy, which can be used to generate electricity in place of conventional methods. In addition, it addresses the challenges associated with the growing energy needs, particularly in Libya, where ample sunlight is available.

Despite these challenges, there are opportunities for the development of solar thermal energy in Libya. However, as mentioned in Chapter 1, there are several issues faced with heat transfer fluids. Such issues can result in decreased performance and reduced efficiency of the solar thermal power plant. To mitigate these problems, it is imperative to improve the HTF system.

Therefore, the focus will be on parabolic trough technology with the objective of achieving a high level of thermal efficiency. This allows for the efficient conversion of solar energy into electricity. Additionally, parabolic troughs are relatively simple and robust, making them a reliable and cost-effective option for large-scale solar power generation. So, the literature review in this chapter is based on a general overview of parabolic trough receiver tubes. Many of the studies cited are not recent. Also, it is not a comprehensive review of all the studies that have been conducted in this field. In this chapter, the thermal properties of parabolic trough receivers will be outlined. Now, industrial technology relating to heat transfer is heavily focused on developing new tools and researching the application of twisted tape inserts, wavy pipes, as well as expanded surfaces. In addition, nanoparticles are being researched as a way to speed up heat transfer rates [42-44]. This chapter summarises and discusses many numerical and experimental studies on the turbulent steady and unsteady flow of tubes fitted with twisted tape inserts as well as the flow of nanofluids inside tubes. This chapter also includes examples of research on entropy generation analysis. Finally, the thesis's objective is presented.

2.2 Parabolic trough solar collectors

The parabolic trough solar collectors are exceptional technologies since they capture solar thermal energy at a low operating cost. A number of applications of parabolic trough solar collector have been explored [45], such as water heating in the home, industrial operations [46, 47] , solar steam production [48], desalination [49], dehydration process [50], solar cooling [51], power generation [52], and absorption heat pumps [53]. As such, their use could be extended to other areas in order to reduce fossil fuel consumption and reduce greenhouse gas emissions.

A number of earlier studies have described the development of a system to collect solar energy from parabolic troughs and the analysis of its performance. Parabolic trough collectors and their thermohydraulic behaviour were studied by Eck et. al. [54]. Kalogirou [55] developed the parabolic trough collector in order to calculate collector time constants, acceptance angles, and thermal efficiency, as well as incident angle modifiers. A study by Klychev et. al. [56] examined how geometric parameters can be optimized for the parabolic-cylinder-receiver system used in thermal power plants, and they concluded that the optimal opening angles for the parabolic-cylindrical concentrator can enhance solar concentration within the system. A study conducted by Szargut and Stanek [57] addressed the issue of determining the optimal collector area per unit of heat demand. Additionally, the diameter of the collector tubes and the distance between the tube centres in the collector plate were discussed for optimizing the solar collector's performance. According to Bakos [58], two axis parabolic trough collectors can be used for normal weather conditions and have an increase in efficiency of 46% over fixed surfaces. Fisher [59] assessed the efficiency of a parabolic trough collector using European standard EN 12975, which takes into account a diffuse irradiation angle modifier and the effective thermal capacity of the collector in addition to the steady state parameters. Using synthetic oil as working fluid, Liu et. al. [60] studied solar parabolic trough collectors' thermal performance.

To improve the receiver's performance, the receiver surface temperature can be reduced, and heat losses can be reduced from the receiver. It is possible to accomplish this by increasing the rate at which heat is transferred from the receiver's inner surface to the heat transfer fluid [61]. The rate of heat transfer inside the receiver can be enhanced by enhancing surface contact and creating turbulence between the receiver and working fluid. By inserting twisted tape inserts onto the internal surface of the receiver, it is possible to achieve this. Though twisted tape

inserts enhance the rate of heat transmission, the pressure drop in receivers will increase. An analysis of the receiver of the solar parabolic trough is carried out in the following sections using twisted tape.

2.3 Experimental and numerical studies of turbulent steady flow in tubes with twisted tape inserts under forced convection

Experiments and numerical approaches have made invaluable contributions to the study of heat transfer and fluid flow. The next sections discuss some of the experimental and computational studies that were carried out to investigate the flow properties and heat transmission of pipes equipped with different types of twist-tape inserts.

2.3.1 Experimental Studies

Some studies have been performed to enhance heat transmission in pipes by utilising twisted-tape inserts (Figure 2-1) Evans and Sarjant [62], Kreith and Margolis [63], Ibragimov et. al. [64], Brevi et. al. [65], Abu-Khader [66], Manglik and Bergles [67], and Eiamsa et. al. [68]. Compared to standard tubes, the friction factor and Nusselt number have been enhanced.

Figure 2-1 Solid twisted tape [69].

Migay and Golubev [70], Burfoot and Rice [71], and Eiamsa et. al. [72], found that pressure drops in twisted tapes placed intermittently were fewer than those on the tapes of full-length when they conducted experiments on the matter. Swirl reduction in full-length twisted tapes was also cited as a factor in the reduced pressure drop. Heat transfer improvement is sacrificed in order to reduce drop of pressure.

Liao and Xin [73] investigated how three-dimensional interior expanded surfaces and twisted tape inserts could improve convective heat transport in pipes. Heat transmission and friction in tubes were studied using integrated 3D fins and twisted tape inserts. Turbine oil, ethylene glycol, and water were all used in the tests. Compared to a smooth pipe, the finned pipe with twisted tape of continuous had a Stanton number that was up to 5.8 times higher, whereas the

friction factor was nearly 6.5 times higher. Segmented tape inserts decreased the friction factor and Stanton number when compared with continuous tape inserts. According to Ayub and Fahed [74], nine twisted tapes were applied with three various twist ratios and three different tape widths in order to investigate the drop of pressure in turbulent water flow. The results showed that the bigger the distance between the horizontal pipe and the twisted tape, the greater the drop of pressure. When the tape width rises, the pressure drops first increases and then decreases. A similar pattern of findings was observed when the twist ratio was raised. The authors believed that the heat transfer findings would exhibit a similar abnormal pattern.

Kumar and Prasad [75] demonstrated that twisted tape on a solar water heater can improve heat transfer by 18 to 70% compared to a solar water heaters that do not use tape. The investigation also found that compared to a basic solar water heater working in the same conditions, the drop of pressure may be increased by up to 132%. Thermal performance also improved by about 30%. According to the authors, the twisted tape intensifies turbulence. The thermal performance of solar collector increases monotonically over Reynolds number 12000. The system worked better at Re = 12000. Murugesan et. al. [76] analysed the heat transport properties and pressure drop in a pipe supplied with twisted tape inserts with trapezoidal cuts (Figure 2-2). Tape of trapezoidal cut was twisted with a twist ratio of 6.4 and 4.4. On the tape, the trapezoidal cut was performed simultaneously on the upper and bottom, alternating between the two cuts. The correlation between the experimental data from the ordinary pipe and the standard correlation was used to guarantee uniformity of the experiment's findings. The trapezoidal-cut twisted tape had a much greater heat transmission coefficient and friction factor than the ordinary pipe, according to the findings of the experiment. That is, trapezoidal-cut twisted tape had a Nusselt number 1.72 times more than that of ordinary pipe for twist ratios of 4.44 and 6.06. In comparison to the ordinary pipe, the trapezoidal-cut twisted tape with twist ratios of 4.4 and 6.0 had a friction factor of 2.85 and 1.97, respectively. Based on experimental data, friction factor and Nusselt number were found to be within 6% and 5% of these values, respectively.
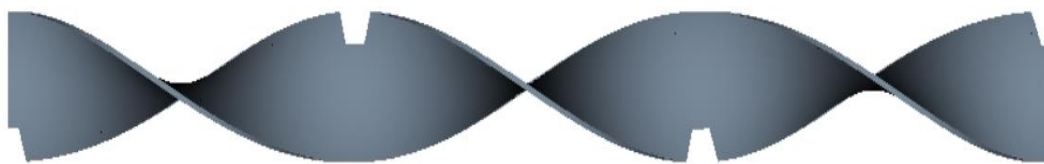
Figure 2-2 Cutting trapezoidal on the tape of twisted [76].

Jaisankar et. al. [77] examined friction factor, heat transfer, as well as thermal performance characteristics for twisted tapes with ratios of twist between 3 and 6 at Reynolds numbers between 3000 and 22000 in a solar water heater. In comparison to plain tubes, their findings demonstrated a rise in heat transport and friction factor upon insertion of twisted tapes of all twist ratios evaluated for their research into plain tubes. The greatest augmentation in convective heat transmission and friction factor occurred with a ratio of twist 3. In addition, they determined that when the twist ratio rises, heat transmission and friction factors decrease owing to a reduction in swirl production.

More recent work by Murusegan et. al. [78] looked at experiments on the heat transmission characteristics of water in a twin tube heat exchanger equipped with plain twisted tubes and square-cut tape twisted twists for twist ratios of 2, 4, and 6 at Reynolds numbers ranging from 2000 to 12000. The square incisions were made alternately on the tape's top and bottom. Square cut twisted tape with twist ratios of 2, 4.4, and 6 showed Nusselt numbers of respectively 1.08, 1.67, and 1.055 times greater than solid twisted tape in the flow system examined. The frictional factors of tubes with simple twisted-tape inserts were 1.09, 1.12, and 1.15 times greater than those with square-cut twisted tape twist ratios of 2, 4.4, and 6, respectively. The Nusselt number and the friction factor were anticipated to be within 6% and 8% of the actual values, respectively.

Eiamsa-ard and colleagues [69] used individual twisted tape (Figure 2-1), twin tapes twisted (Figure 2-3), as well as tape twisted to create flow of individual eddy, flow of reverse eddy, and flow of co-swirl, all at the micron scale. The tapes with reverse eddy had a greater rate of heat transport than the ones with flow of individual eddy or flow of co-swirl, as a result of their experiments. Additionally, the counter twisted tape transmits 12.5% to 44.5% more heat than the individual-twist tape and co-twist tape, respectively, in comparison. The thermal performance factor of tapes with counter swirl is greater than that of tapes with flow of single swirl and flow of co-swirl at constant pumping power. The outcomes of the experiments match well with the established empirical relationships.
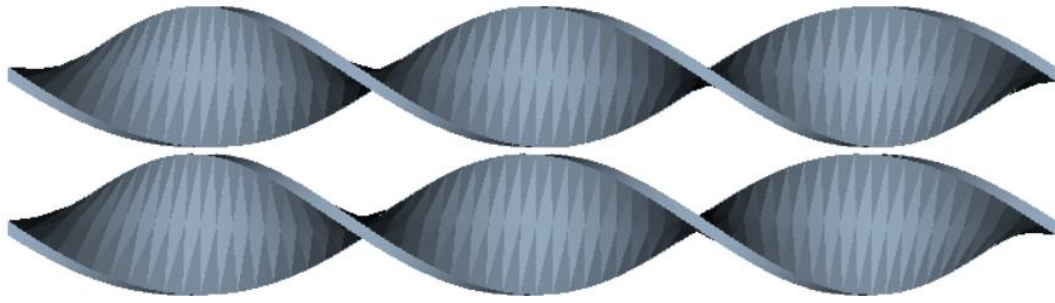
Figure 2-3 Twin counter twisted tape [69].

In square and rectangular pipes with corrugated interior surfaces and inserting twisted-tape with and without teeth oblique Saha's findings [79], discovered turbulent heat transport and pressure drop (Figure 2-4). Because both axial corrugation and twisted tapes have similar pumping power, the combination resulted in improved total heat transfer increase. Compared to tape with oblique teeth, tape without oblique teeth has a lower thermal performance factor.
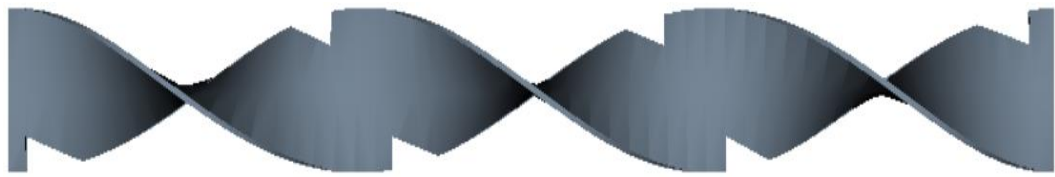
Figure 2-4 Twisted tape for cutting oblique-tooth [79].

Nanan et al [80] measured the friction factor and heat transmission inside pipes with varying perforation diameter ratios (d/w = 0.2, 0.4, and 0.6) along with the ratios of perforation pitch (s/w = 1.5, 2.0), using perforated helical twisted-tapes P-HTTs (Figure 2-5). The thermal enhancement features of the ratios of perforation pitch and diameter were studied. As the diameter pitch ratio increased and the perforation pitch ratio decreased, they found that the heat transmission rate, thermal performance, and pressure loss all decreased. As a result of the ratios of perforation pitch and diameter being 2 and 0.2, respectively, the greatest thermal performance factor was obtained, which was 1.28. The heat transmission and flow resistance of tubes with staggered-winglet perforated tape inserts were examined by Skullong et al [81], who varied the winglet pitch ratios and winglet blockage ratios. Thermal and pressure losses rose as the winglet pitch ratio decreased with increasing winglet blockage ratios. Staggered-

winglet perforated tape, on the other hand, was claimed to have a 20% greater thermal performance than standard winglet tape.
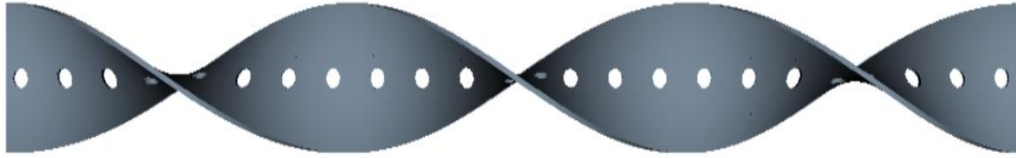
Figure 2-5 Modified twisted tape for perforated heli-cal [80].

Converging-divergent tubes with uniformly spaced twist tapes at varied twist ratios and rotation angles were tested for heat transmission and friction loss in a Reynolds number range of 3400 to 20,000 by Hong et. al. [82]. Twisted-tape with a twist ratio of 4.72 (the lowest twist ratio) and an angle of $\theta=180^o$ degrees was found to have the greatest thermal performance factor, according to their study findings. The thermal performance of the pipe inserts with the ratio of space 48.6 was found to be between 0.85 and 1.21 times greater than that of the ordinary pipe and individual diverging converging pipes. Jaisankar et. al. [83] compared the friction factor as well as heat transfer of thermosyphon solar water heaters using twisted tape and rod in conjunction with spacers. Compared with full length twist tape, twisted tapes equipped with spacers and rods exhibited decreased in the rates of heat transmission of approximately 11% and 19%, respectively, while friction factors were reduced by approximately 18% and 29%. Bhuiya et. al. [84] performed experiments on a tube provided with punctured twisted tape varying between 1.6%, 4.5%, 8.9%, and 14.7% in porosity (Figure 2-6). A uniform wall heat flux boundary condition and air were used as the working fluids for the experiments. The findings revealed that the thermal performance factor, friction factor, and Nusselt number of the pipe supplied with punctured twisted tape were 28–59%, 110–360, and 110–340 more than those of the conventional pipe, respectively.
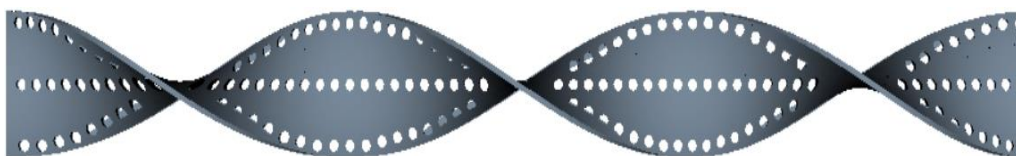
Figure 2-6 Twisted tape for perforated [84].

Ponnada et. al. [85] explored the impact of punctured twisted tape in various axes as well as ordinary twisted tape with the percentages of varied twisted of 3, 4, and 5 on a circular tube. From 3000 to 16,000, the Reynolds number was available. The modified circular tube outperformed the regular circular tube regarding heat performance and friction coefficient. The highest thermal performance factors for twisted tapes of conventional, punctured, and punctured alternative, respectively, were about 1.24, 1.369, and 1.433 for constant pumping power.

2.3.2 Numerical Studies

In 1974, Date [86] performed one of the first numerical studies on the rise in heat transport between pipes having twisted tape inserts in turbulent flows. Many researchers have sought to do more numerical analyses since then to investigate flow friction and heat transmission in pipes with twisted tapes of various geometries [44, 87-90]. The friction factor and Nusselt number are enhanced over the ordinary pipes, resulting in better performance. Wang et. al. [91] conducted a computational fluid dynamics (CFD) analysis to optimise the short-length, regularly spaced twisted tape in a plain pipe (Figure 2-7). It was clear that flow resistance and heat transfer improve as the twisted angle (θ) improves.

Figure 2-7 Twisted tape for regularly spaced short length [91].

Yadav and Padalkar [92] conducted a numerical analysis to examine the heat transport properties of air flow in a circular pipe. This analysis was conducted with partially decaying and partially swirling flow. There was greater heat transport inside the tubes supplied with twisted tape than there was in the ordinary tubes. Chiu and Jang [93] examined the thermal properties for the flow of air inside a pipe containing long tape inserts (including apertures) as well as twisted tape inserts with various turns ($15.3°, 24.4°$ and $34.3°$) (Figure 2-8). To solve the governing equations, numerical simulations have been performed employing the approach of finite volume. The numerical calculations and the experimental outcomes were in excellent agreement. The drop of pressure and the rate of heat transmission in the pipe with long tape

inserts (without perforations) were 100-170% and 7-16% greater than in ordinary pipes, respectively. The drop of pressure and rate of heat transmission were 140-220% and 13-28% greater, respectively, than in ordinary pipes. The pressure drops and heat transmission rate of pipes with twisted-tape inserts were 150-370% and 13-61% greater than those of ordinary pipes, respectively.
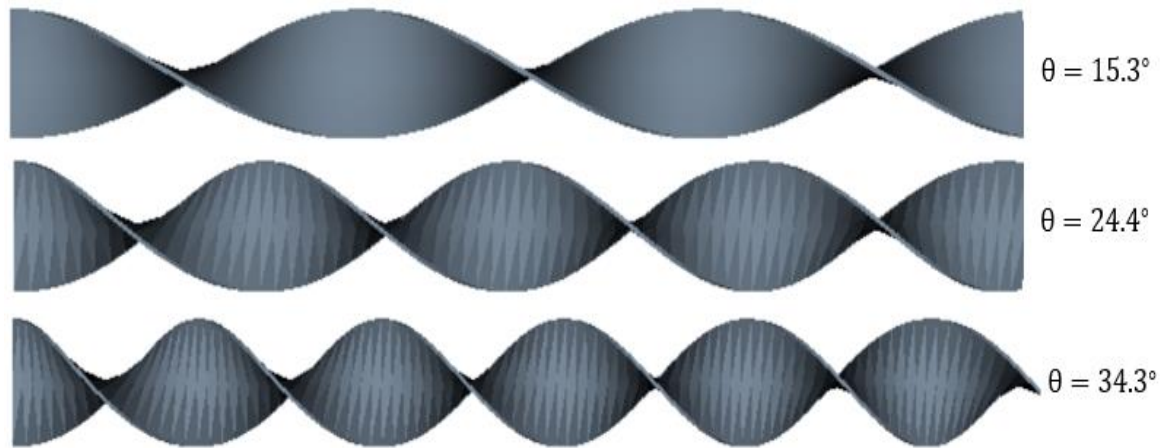
Figure 2-8 Different angles of twisted tape [93].

Eiamsa-ard et. al. [94] studied the physical behaviour of thermal and fluid flow in a pipe supplied by loose-fit twisted tape. Different turbulent models (the Renormalized Group (RNG) $k - \varepsilon$ turbulence model, Shear Stress Transport (SST) $k - \omega$ turbulence model, the standard $k - \omega$ turbulence model, and the standard $k - \varepsilon$ turbulence model) have been used to quantitatively explore the influence of the clearance between the wall and the tape's edge of the hose on the factor of thermal performance, friction factor, as well as the Nusselt number for twisted tape with twist ratios of (2.5 and 5). The simulation findings suggest that the twisted tape has the smallest ratio of clearance (c / D) exhibited the greatest heat transfer augmentation and was the most reliable thermal performance indicator. Cui and Tian [95] studied numerically and experimentally heat transport and drop of pressure in circular ducts equipped with edge-folded and solid twisted tape inserts. Investigations were conducted using RNG turbulence models. Nusselt number and friction factor were found to be greater in tubes generated with edgefold twisted tape inserts compared to plain twisted tape inserts. It was found that numerical findings were in excellent agreement with experimental data, with a variance of 1.6% to 3.6% in the Nusselt number and 8.2% to 13.66% in the friction factor.

Saysroy and Eiamsa- ard [96] investigated the improvement for heat transfer in a pipe equipped with square-cut twisted-tapes at various punctured length proportions and punctured width proportions (Figure 2-9). According to their findings, heat transfer as well as pressure loss rose as the ratio of punctured width to punctured length decreased. Using constant pumping power as a criterion, the highest thermal augmentation factor was 1.32 times superior to that of conventional twisted tape.
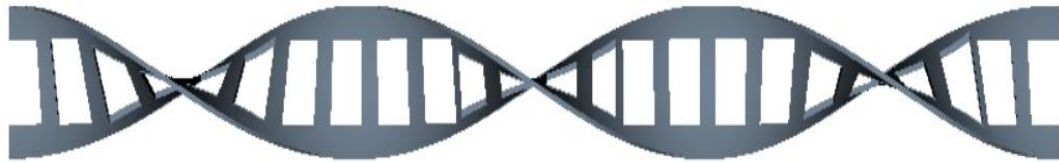
Figure 2-9 Twisted tape for square cut [96].

Oni and Paul [88] investigated numerically the heat transport and flow properties of water in a pipe containing several modified twisted tapes (Figure 2-1 and Figure 2-10). The objective is to determine which tube design provides superior performance relative to a plain tube. According to the concept of turbulent flow, a uniform divider flux is applied to the mass of the pipes. The RNG k-ε model was employed for simulations, and Reynold's number ranged from 5,000 to 20,000. The pipe supplied by alternate-axis triangular cut twisted tape features the best performance, as its friction's factor and Nusselt number are 2.60 to 3.15 and 1.63 to 2.18 times that of the pipe supplied with solid twisted tape, respectively, and its thermal performance factor varies between 1.35 and 1.43 times that of the pipe supplied with solid twisted tape.
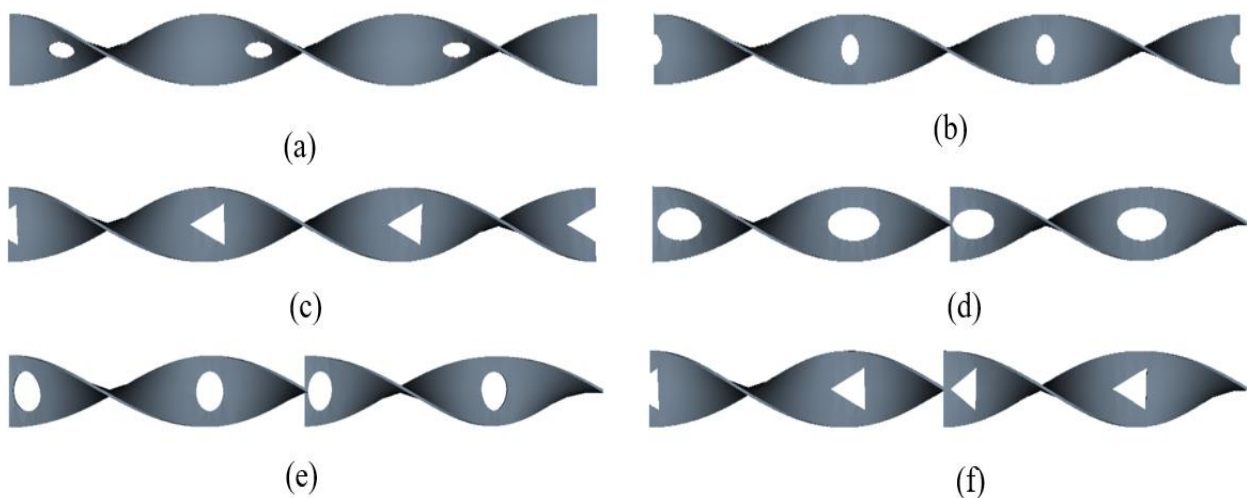
Figure 2-10 Different twisted tapes (a) TECT, (b) TCCT, (c) TTCT, (d) TAECT, (e) TACCT, and (f) TATCT [88].

Nakhchi and Esfahai [97] explored the single-sided and double-sided configurations of rectangular-cut TT (Figure 2-11). The Reynolds number ranged from 5000 to 16,000, and the flow was simulated with a renormalized group (RNG) $k - \epsilon$ model. The findings shown that rectangular-cut enables superior fluid mixing and generates significant centrifugal force near the wall. Both contribute significantly to the enhancement of the local heat transfer. The maximum thermal performance value for the rectangular cut TT may occur at depth and width ratios of 0.75 and 0.5, respectively. Also, they offered a tube with a double V-cut TT (Figure 2-12) [98].
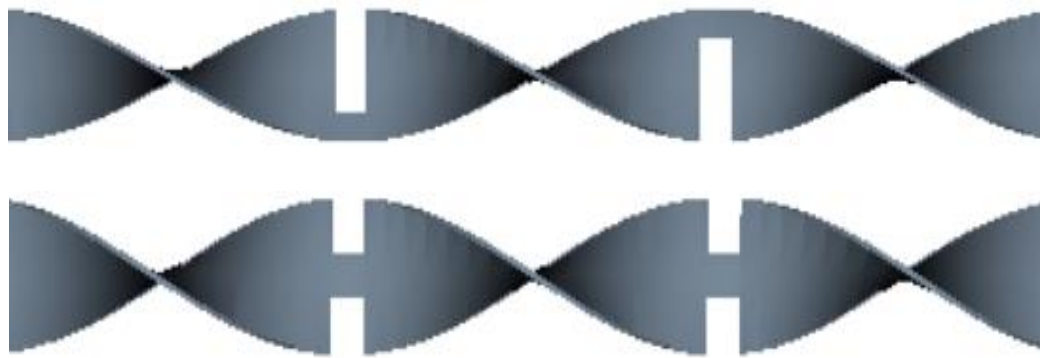
Figure 2-11 Twisted tape for rectangular-cut TT [97].
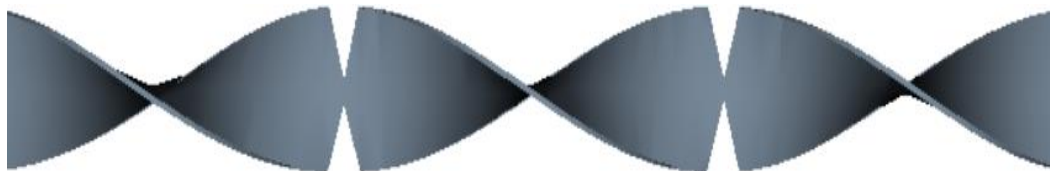
Figure 2-12 Twisted tape for a double V-cut [98].

In computational fluid dynamics (CFD), the resolution of the mesh near the wall is crucial for determining the appropriate turbulence modelling strategies [99]. Typically, there are two approaches to model the near-wall region: the near-wall model and the enhanced-wall function.

The near-wall model utilizes high-order derivative terms to accurately represent turbulent production. On the other hand, the enhanced-wall functions are semi-empirical expressions that serve as a link between the viscosity-affected region near the wall and the log-law area. These functions help characterize the turbulent behaviour in this intermediate region. For further information on the numerical simulation of turbulent pipe flow using the wall y+ approach, you can refer to the research published by [100]. Their work delves into the details of this approach and provides valuable insights into the subject.

In summary, the choice between the near-wall model and the enhanced-wall function depends on how accurately we need to capture turbulent production and bridge the gap between the wall and the log-law area in our simulation.

2.3.3 Studies on Nanofluid Flows

Recently, several experimental [101-103] and numerical [44, 104-106] studies have used various nanofluids in conjunction with twisted tape inserts in a variety of receiver tubes to improve desired characteristics like the rate of heat transport and the efficiency of thermal performance. Flowing nanofluids in a pipe with a variety of turbulence promoters may increase heat transmission. For the first time, Sundar and Sharma [107] examined experimentally the heat transport and friction properties of alumina/water nanofluid. Alumina/water nanofluids with volume concentrations of 0.02 %, 0.1%, and 0.5% were employed as test fluids with 10,000 to 22,000 Reynolds numbers for the experimental investigation. Comparing water with a twist ratio of 5, the greatest rise in convective heat transfer coefficient was 42.17 percent at the Reynolds number of 22,000. They also found that using nanofluids at the same twist ratio values had no appreciable impact on pressure decrease compared to water.

Using longitudinal strip inserts in a pipe, Sundar and Sharma [108] also noticed an increase in friction factor and heat transfer using nanofluid (Al_2O_3) in a pipe with longitudinal strip inserts. Sundar et. al. [109] employed nanofluid (Fe_3O_4) with twisted tape inserts in their experiment. Wongcharee and Eiamsa-ard [110] applied nanofluid of CuO/ water with different twisted tape inserts. Suresh et. al. [111] used nanofluids of CuO/ water and Al_2O_3/ water for helical screw

tape inserts. Nail and Sundar [112] used water/propylene glycol-based CuO nanofluids with twisted tape inserts. Qi et. al. [113] completed an experimental analysis of the flow characteristics and heat transmission in a hose provided by static and rotary twisted tape and a TiO_2 nanofluid. They discovered that a Reynolds number of 4,500 was crucial for the heat transfer ratio improvement. In addition, efficiency of the energy for the pipe supplied with twisted tape was greater than that of the ordinary pipe.

Sharma et. al. [114] attempted to alter flow dynamics by inserting twisted tape into a pipe of the flow for nanofluids in the transition region of Reynolds number. Even at modest flow rates, the tape causes turbulence and interrupts the development of the boundary layer, which is an effective approach for achieving high heat transfer rates. The coefficient of heat transfer of 0.1% Al_2O_3 in a pipe with a twist ratio of 5 was found to be 11.84% higher at Reynolds number of 3000 and 15.80 percent higher at (Re = 9000) compared to flow in the pipe without inserts. Nanofluid friction increased by 3.32% and 16.65% in comparison to flow in a tube at the same concentration, twist ratio, and Reynolds numbers of 3000 and 9000. Most of the experimental work is devoted to determining the heat transport coefficient of Al_2O_3 and Cu nanofluids in an ordinary pipe, while some academics have focused on determining the heat transmission coefficient of nanofluid (Al_2O_3) in a plain pipe with twisted. By using nanofluids (Cu-water) in a pipe with twist tapes, Aliabadi and Eskandari [115] achieved an integration of convective heat transfer and enhanced conductive. Utilizing non-uniform twist tapes with varying twist lengths (low–high, high–low, low–high–low, and high–low–high), they conducted their tests. The joint use of nanofluids and twisted tapes resulted in improved heat transfer, as compared to the use of either approach alone. The examined tapes with the lowest to highest twist lengths had the highest coefficient of heat transfer.

Chougule and Sahu [116] examined the coefficient of heat transfer of nanofluids (CNT/water and Al_2O_3/water) at varying particle volume percentages in a pipe supplied by a helical twisted tape. By combining helical tape with nanofluids, more heat is transmitted than either tape or nanofluids alone. Twisted tape was modified by Maddah et. al. [117] to increase the double tube's heat transfer. Twisted tapes were both shortened and extended as a result of the adjustments. (Figure 2-13) shows the twisted tape alterations conducted by Maddah et. al. [117]. There are three different ways to change the length of a twisted tape: (a), (b), and (c). According to Maddah et. al. [117], compared to a duct with solid twisted tape coupled to nanofluid, using a shorted twisted tape coupled with nanofluid results in the greatest increase

in friction factor and heat transfer of around 28 and 52%. By utilising a longer twisted tape instead of a normal twisted one, the pipe's efficiency decreases.
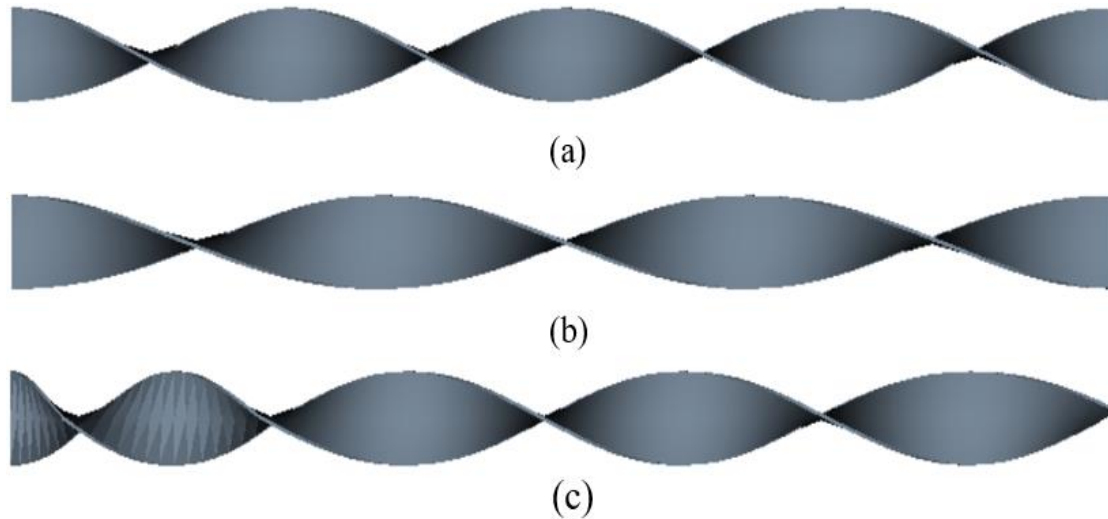
Figure 2-13 Geometries (a) typical twisted tape (b) IGPR twisted tapes (c) RGPR twisted tapes [117].

In all of the previous studies, various nanofluids and turbulent flow were used, as well as twisted tape inserts, in experimentation. Some numerical investigations are detailed in the following section:

Sun et. al. [118] employed CuO nanoparticles with mass fractions ranging from 0.01 to 0.05 in a twisted tape tube to enhance heat transfer. They determined that when CuO/water nanofluids are used, the heat transfer coefficient will be about two times more than the heat transfer coefficient in the horizontal tube. Nakhchi and Esfahani [119] conducted a numerical examination of the flow of nanofluids (Cu–water) within a pipe supplied by twisted pipes of alternate axis (Figure 2-14). Nanoparticle concentrations between 0 and 1.5% were simulated for length ratios between 2 and 2.5, and width ratios between 0.7 and 0.9. Their research indicated that twisted tapes with crosscuts directed the flow of swirls toward walls, resulting in a greater the rate of heat transport and friction coefficient increase of up to 23.20% as the nanoparticle volume fraction increased.
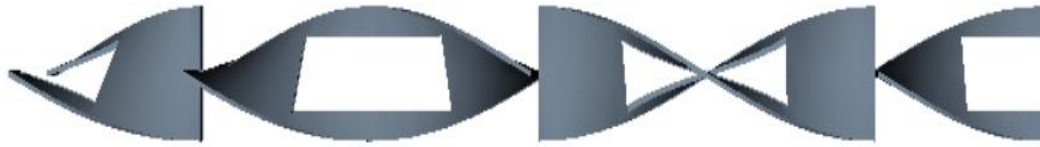
Figure 2-14 Twisted tape for alternate axis crosscut [119].

A numerical study conducted by Jafaryar et. al. [120] examined the heat transmission properties of nanofluid (water-CuO) in a pipe supplied by a twisted-tape turbulator. They evaluated the effects of the height ratio, pitch ratio, and Reynolds number. Based on their findings, the rate of heat transfer improves as the height ratio and Reynolds number improve, whereas it decreases as the pitch ratio increases. Farshad and Sheikhoeslami [121] have also performed simulations of energy loss and heat transfer of a mixture of aluminium oxide and water through a solar collector using twisted tape. They discovered that the rate of heat exchange for Al_2O_3/water improved as the number of rotations increased.

Ahmadi et. al. [44] presented a numerical study in order to determine the impact of utilising elliptical cut twisted tapes with nanofluid (CuO/ water) (volume fraction 1-4 %) as the working fluid on the flow and heat performance inside a tube. For nanofluids alone, the maximum Nusselt number and performance factor will be attained at a 4% volume concentration, however for nanofluids combined with elliptical cut tapes, these values will be 21 times higher. Hosseinnezhad et. al. [122] examined the impact of using double twisted tapes (Figure 2.3) with different twist ratios (2.5-4) in both co-swirl and counter-swirl positions inside a tubular heat exchanger in the turbulent flow regime (Re=10,000-30,000) with aluminium oxide/water as working fluid (1-4% volume fraction) and discovered a rise in average Nusselt number with rise in volume fraction and reduction in twist proportion for the counter swirl. The research also discovered that an improvement in performance assessment for both configurations with counter-swirl resulted in a greater increment.

Mustafa et. al. [123] numerically carried out analyses to study performance evaluation criteria (PEC) of the absorber tube of some parabolic solar collectors that were fitted with three-and four-channel twisted tape and water-copper oxide (CuO) nanofluid. The study was done for Re = 20000 – 80000. By means of the finite volume approach, the governing equations were numerically solved. Moreover, the impacts of the nanofluid on the heat transfer performance are studied using fluids augmented with Cupric Oxide nanoparticles whose nanoparticle concentrations range from 1 to 4%. It was found that nanofluids with a Reynolds number of

80,000 and ($\emptyset$ = 4 %) had the greatest Nusselt number, which was 54.7. As a result, three-channel twisted tape's thermal performance is at its maximum point when the volume percentage is only 4%. Furthermore, the highest efficiency of parabolic solar collectors is linked to nanofluid flow with Re = 80,000 and ($\emptyset$ = 4 %), which is equivalent to 26%. At ($\emptyset$ = 4 %), the nanofluid has the best exergy efficiency. He et. al. [124] numerically examined the performance of CuO nanofluid with different sold concentrations (1 to 4%) in a tube with single (Figure 2.1) and double (Figure 2.3) twisted tapes, the turbulent flow simulation was conducted using Reynolds numbers ranging from 3000 to 36000. They found that a pipe with one twisted tape has a higher performance evaluation criteria (PEC) value than a pipe with two twisted tape inserts. Accordingly, it is fine to use a pipe with one twisted tape from a fluid-thermal perspective.

Bellos et. al. [125] investigated how nanofluids and turbulators increased the performance of parabolic collectors. Different fluid temperatures were analysed using a suitable computational fluid dynamics model using SolidWorks software. The use of nanofluids, internal fins, and their combination increased the thermal efficiency by 0.76 %, 1.10 %, and 1.54 %, respectively, according to the data. Flow and heat transport properties of nanofluids have been computationally examined in various configurations, such as porous twisted tape tubes. Wang et. al. [126] employed porous twisted tapes to enhance the heat transport of silica-water (SiO_2–H_2O) nanofluids in circular and triangular tubes. The findings suggested that the triangular tube had a lower current resistance and a greater heat transfer capacity than the circular tube. The use of nanofluids with triangle tubing may dramatically enhance heat transfer.

2.3.4 Flow Hybrid Nanofluid Studies

A hybrid nanofluid is a type of engineered fluid that is composed of a mixture of two or more types of nanoparticles suspended in a base fluid. These nanoparticles can be made of a wide variety of materials, including metals, ceramics, and polymers. The unique properties of hybrid nanofluids, such as enhanced thermal conductivity and improved mechanical properties, make them useful in a wide range of applications, including heat transfer, lubrication, and energy storage. Hybrid nanofluids are created by combining two or more types of nanoparticles to create a new material with unique properties [33]. Nanofluids have been extensively researched as the working flow in solar systems, as discussed in section 2.2.3. However, the introduction of hybrid nanofluids, which are fluid flow mixtures of at least two nanofluid types, has improved the efficiency of thermal systems [33, 127, 128]. There are limited studies focusing

on using the twisted tape with different hybrid nanofluids simultaneously as an effective heat transfer enhancement method.

Sundar et. al. [129] examined the thermo-hydraulic characteristics of $CNT_{-5e}Fe_4/H_2O$ hybrid nanofluid ($\phi = 0.1\%$ and 0.3%) with twisted tape insert (y=5,10, and 15) under continuous heat flux and turbulent flow regime ($3000 < R_e < 22,000$). Experiments using hybrid nanofluid ($\phi = 0.3\%$) in a plain tube demonstrated a maximum increase of 31.1% in Nusselt number and a corresponding 1.18-fold increase in friction factor compared to base fluid under ideal flow conditions. In addition, utilising twisted tape with the appropriate twist ratio resulted in a maximum rise of 42.51% in Nusselt number, but the friction factor increased by only 1.23 times compared to water in a plain tube. On the basis of experimental data, correlations have been built for Nusselt number and friction factor as a function of twist ratio and volume concentration.

Dalklc et. al. [130] in (2019) examined a horizontal pipe with quad-duct twisted tape and empirical research to investigate the turbulent heat transfer parameters for SiO_2- Graphite/H_2O hybrid nanofluid flow. For the preparation of the hybrid nanofluid, they used two distinct nanoparticles: Graphite (40%) and Siliciumdioxid (60%) dispersed in clean water as the base fluid. With increasing volume concentration, a rise in the Nusselt number was found for the hybrid nanofluid instance. Moreover, increasing the length of the twisted tape insert led to a rise in the Nusselt number. In addition, raising Reynolds number led to pressure drop rises. It is usually larger with longer tape inserts and higher concentrations. As the mass fraction and mass flow rate rose, so did the resistance. Within the deviation region of 10% for friction factor and 5% for Nusselt number, it was determined that the regression equations correlated well with the experiments.

In 2021, Fattahi [131] investigated numerically the heat transfer capacity and the drop of pressure in a solar collector with a hybrid nanofluid of Al_2O_3-CuO/water and a twisted taper. The nanofluid volume fraction (0.02 and 0.04), Reynolds number (10,000 and 20,000), and wall roughness (0.00025m and 0.000050m) of the collector were all altered independently. When nanoparticles were added to the base flow, the pressure drop and Nusselt number increased by 25 - 35% and 60 - 90% correspondingly. The Nusselt number increased by more than 100% because of the increase in the Reynolds numbers. For smaller and larger volume fractions, the pressure decrease was 170 and 200%, respectively. In the same year, Alnaqi et. al. [132] assessed the influence of two twisted tapes positioned within the receiver tube of a

PTC (Parabolic trough collector) while using a hybrid nanofluid as the working medium. The primary objective of this specific research was to examine a variety of tape sizes and permutations of twist direction within each tape. It was discovered that the PEC number (Performance Evaluation Criterion) has its highest values in the majority of instances when the two tapes have counter-swirl flow such that they direct the working medium to the upper portion of the flow tube from the inner side relative to the position between them. Regarding hybrid nanofluid, it was shown that PEC rises with increasing concentration, as predicted.

2.4 Experimental and numerical studies of turbulent transient thermal analysis

The transient heat transport in pipes with twisted tape inserts has not been addressed, despite several analytical solutions and experiments have been documented for the steady state heat transfer. Therefore, transient thermal analysis for parabolic trough solar collector tubes is crucial for using solar thermal energy with varying solar radiation. However, most researchers have only examined this heat transfer improvement utilising twisted tape under steady-state conditions: uniform wall temperature or uniform heat flow. Transients in heat transfer and diffuse solar irradiation have been identified and explained by the authors [133, 134].

The performance of parabolic trough collectors in transient operations was investigated by Xu et. al. [135]. A 3D thermal-hydraulic simulation for a high-temperature engineering test reactor was calculated by Nakagawa and Tochio [136]. They computed steady-state and unsteady-state values. Therefore, when unsteady states occur, the estimated reactor pressure vessel and lower permanent reflector block temperatures are significantly different from the ones that were found. Tandiroglu and Ayhan [137] performed an experimental examination of transient heat transmission of turbulent flow within ordinary tubes using various combinations of baffle inserts and constant surface heat flux. They discovered that the Nusselt's average number was much greater for tubes with baffle inserts than for tubes without baffles for Reynolds numbers between 3000 and 20,000 and in the case of constant heat flux.

Recently, there have been experimental reports on transient heat transmission processes of helium gas using a heater with twisted tape inserts. Zhao et. al. [138] experimentally performed analyses to investigate the impacts of forced convection on helium gas's transient heat transfer at different time periods of exponential growth in heat input to a short, thin, and twisted plate with varying helix angles. A forced convection heat transfer experimental apparatus was used to measure the experimental data. Heat transfer coefficients have been shown to approach quasi-steady-state values for periods longer than one second (s), while they rise for periods less

than one second (s). According to the findings of their experiments, when using twisted plates with broad widths, the heat transfer coefficient is lower than when using narrow widths. At the quasi-steady state, local heat transfer coefficients for twisted plates drop as the x position increases. Local heat transfer coefficients decrease as axial velocity increases. Inlet and outlet positions have more transient heat transfer than the centre position. Liu et. al. [139] conducted experiments to examine forced convection transient heat transfer for helium gas at different times of exponentially increasing heat input to a twisted plate (heater) with various pitches. It was found that the small-pitch heaters have a greater heat transfer rate than big pitch heaters, and the Nusselt values are more than 50% higher than the flat plate heat transfer rate.

2.5 Experimental and computational investigations of mixed convection

As an engineering phenomenon, mixed convection heat transfer is used to address a wide variety of issues. In order to enhance and optimise the performance of diverse industrial applications, a greater knowledge of the processes involved is necessary [140, 141]. Numerous studies and investigations have been conducted on mixed convection under a variety of boundary and operational circumstances due to its importance in the literature.

It is possible to determine the influence of buoyancy forces on a vertical pipe's constant laminar flow. Heat transfer is promoted when flow is upwards past a hot surface (or downwards past a cooled surface) and is impeded when the flow is in the other direction. Thermal diffusivity has nothing to do with these effects. Instead, they are caused by changes in the fluid's velocity field and convection patterns.

Double tube heat exchangers were used in the early stages of research into mixed convection in vertical tubes. In 1939, Watzinger and Johnson [142] described experiments in which external flow cooled water moving downhill in a tube. In this arrangement, free convection assisted forced convection. Shortly afterwards, Martinelli et. al. [143] published studies involving the upward flow of water and oil in tubes with uniform, steam-heated wall temperatures. So far, there are very few investigations of turbulent mixed convection in tubes.

Kurganov and Kaptilnyi [144] reported experimental information on the flow structure, heat transfer, and hydraulic drag of SCP CO_2 heated in a vertical tube moving upward and downward at very high Reynolds numbers between (10^5) and (10^6). The diameter of the tube was $D = 22.7$ mm and the CO_2 pressure was 9.0MPa. With a small Pitot tube and micro-thermocouples, velocity and temperature measurements were performed within the range of

$0 \leqslant r/R \leqslant 0.995$, as well as static pressure measurements throughout the tube length. Through a comparison of test data for upward and downward flows, they concluded that a relative worsening of heat transmission when the flow is upward, as evidenced by the development of a wall temperature peak, is due to the rearrangements of velocity fields and shear stress distributions, which result in the appearance of a fluid layer with reduced turbulence generation. In addition, they discovered that the development of an M-shaped velocity profile in upward flows facilitates the improvement of heat transfer.

Some researchers used experimental studies to investigate laminar and transition mixed convection inside tubes. Piva et. al. [145] studied both computational and experimental laminar water flow convection in a horizontal pipe under a homogenous wall heat flow. Due to the buoyancy influence, pressure drops, and heat transfer increased by 22% and 150%, respectively. In coupled convection of air via a disposed rectangular channel, Lin and Lin [146] investigated the flow, transition, and associated heat transfer processes. These processes are influenced by air's buoyancy. Based on the findings, it was determined that buoyancy improved heat transfer. Thermal instability was accelerated by large negative inclined angles (opposing convection) and/or the increased numbers of Grashof, while it was delayed by large positive inclined angles (assisting convection) and/or very substantial Reynolds numbers. The shift from laminar to turbulent flow was also seen when the Grashof number was raised, or the Reynolds number was lowered.

By using a square channel with a constant wall temperature, Patil and Babu [147] studied the laminar flow of ethylene glycol and water mixed convection. They examined the significance of nondimensional parameters such as the Prandt number. It was determined that as the Reynolds number increased, free convection became weaker, and the Richardson number became smaller. In addition, mixed convection had a superior average Nusselt number relative to forced convection. An increase in the fluids' Richardson and Prandtl values results in a larger average Nusselt number. The heat transfer parameters of mixed convection for air (laminar and transition) with inclined rectangular pipes were investigated by Chong et. al. [148] at seven different inclination angles $(-90° \leq \theta \leq 90°)$. The findings revealed that heat transfer was highest at a $45°$ angle of inclination and subsequently reduced with further inclination. Nusselt number became independent of inclination angles as Reynolds number increased. Increasing Reynolds number led to a decrease in friction factor as inclination angle increased, up to a point. After that point, the coefficient of friction no longer cared about the directional changes.

In terms of numerical work, there are few computational studies of turbulent mixed convection. Using the two-equation model, Abdelmeguid and Spalding [149] conducted numerical predictions of heat transport and turbulent flow in horizontal, vertical, and inclined pipes with buoyancy and uniform heat flow. It is important to note that buoyancy has only a small impact on turbulence when Grashof numbers are below a critical Grashof number, however buoyancy influences both the averaged flow as well as the heat transfer in large Grashof numbers. Farouk and Ball [150] performed both computational and experimental research on the mixed convection transfer of heat from a horizontally rotating cylinder in air across broad ranges of the Grashof number (Gr) and Richardson number (Ri). In the two-dimensional system, they ran numerical simulations. Over the range $1.39 \times 10^3 \leqslant Gr \leqslant 1.39 \times 10^6$ and Pr=0.7, it was seen that the Nusselt number remained almost constant in the range $0 \leqslant Ri \leqslant 1$, which was consistent with their experimental findings. Experimentally, when the rotating speed of the cylinder is progressively raised, a three-dimensional secondary flow and a significant rise in the rate of heat transport are seen.

Oni and Paul [151] performed a numerical analysis for mixed convection to study the heat transport as well as fluid flow properties associated with laminar, transition, and turbulent flows inside a pipe provided with twisted tape triangular-cut at an alternate axis. To simulate turbulent flow, Fluent software and RNG k - ε were used, while transition flow was simulated using SST k - ω. The tube wall was exposed to uniform heat flux at $(15° \leq \theta \leq 90°)$ flow orientation. According to the findings, friction factors and Nusselt numbers obtained in pipes with mixed convection are significantly increased than those obtained in pipes with forced convection in all three flow regimes (laminar, transition, and turbulent). In addition, the friction factor and Nusselt number for mixed convection rose when the flow direction changed from horizontal to vertical 15° to 90°. In terms of the friction coefficient and Nusselt number, the highest values were seen at a flow orientation of 90°, while the least coefficient of friction and Nusselt number were observed at a flow orientation of 15°.

2.6 Entropy Generation

Entropy Generation Minimization, as presented by Bejan [152], is a standard method for determining the quality of energy from a system and optimising the thermal system and its components. The Bejan number was first suggested by Paoletti and co-workers [153]. The underlying concept of lowest entropy production is minimizing the amount of labour necessary for increased convective heat transfer. In each convective heat transfer issue, there is a trade-

off between irreversibility of fluid friction and irreversibility of heat transmission [152, 154]. The entropy production minimization has been applied to forced and free convection situations with various geometries [155-159].

Researchers have used the concepts of entropy production minimisation to define the amount of entropy generated. In one such instance, Ko and Wu [160] studied the entropy production in a curving rectangular pipe under thermal treatment using numerical methods. Similarly, You et. al. [161] assessed the heat transport efficiency of horizontal tubes with conical tape inserts in terms of reducing entropy formation. Mwesigye et. al. [162] used twisted tapes to promote heat transport in parabolic trough receivers while simultaneously generating entropy. Based on their findings, twisted tape inserts substantially reduce the rates of entropy production at low Reynolds numbers. The thermal analysis of a pipe equipped with a twisted tape turbulator was examined by Suri et. al. [163]. According to their findings, the thermal efficiency of numerous perforated twist tapes was much higher.

Kock and Herwing [164] expanded their previous work on the local entropy production in shear turbulent single-phase flows with a numerical model. The model was applied to a turbulent single-phase flow within a heated pipe with a constant heat flow. To create shear flow, they placed a twisted tape inside the pipe. Despite the positive impact on the rate of heat transport, the findings showed that a significant negative pressure drop is generated when the twisted tape is applied. In addition, they found that the entropy production is even 8% less for tubes with a twisted tape slope of $\frac{D}{L_T} = 0.18$ (D is the hose diameter and L_T is the pitch during a 360-degree turn).

Recently, Liu et. al. [165] examined numerically conical strip inserts in the parabolic trough collector system, taking into account the influence of the geometrical factors including a central angle, pitch ratio, and hollow diameter of inserts in addition to various flow circumstances. Using this type of inserts increased the Nusselt number by 45% to 203%, while reducing entropy production and heat losses by 74.2% and 82.1%, respectively, as shown by the results. In addition, the total improvement in thermal and exergetic efficiency improved by 0.02% to 5.04 % and 5.7%, respectively. Moreover, Kumar et. al. [166] explored the generation of entropy in a pipe fitted with punctured twisted tape with numerous V cuts, varying the twist ratio between (2 and 6) and the Reynolds number from 2000 to 25,000. The minimum value of entropy creation was achieved in this research using twisted punctured tape with a ratio of 3.

Recently, scientists and engineers have evaluated the augmentation of heat transmission procedures through the thermodynamics second law via using nanoparticles. A study by Sheikholeslami et. al. [105] investigated the production of entropy in flow of nanofluid through a pipe containing twisted-tape swirlers Pitch ratios and values of Reynolds number were examined, and the findings indicated that increasing the pitch ratio enhanced Bejan number, whereas raising Reynolds number reduced Bejan number. Based on the numerical study conducted by Shamsabadi et. al. [167] entropy generation for flows of nanofluid within a pipe with porous barriers is reduced by 14% and 32%, respectively, by increasing the number of barriers. Farshad and Sheikholeslami [168] investigated entropy production to improve the performance of solar collectors. In their research, five distinct forms of nanoparticle-containing nanofluids were explored. They found that the thermal irreversibility improves as the number of channels reduces. Due to more nanofluid gliding close to the surface, frictional irreversibility increases as pumping power rises. Bahiraei et. al. [169] examined the production of entropy for a hybrid-nanofluid comprising graphene-platinum in a pipe supplied with double twisted tapes that produce a variety of swirling flows. According to the results, employing double counter twisted tapes is recommended based on the second law.

For the entropy generation study on non-uniform heat flux, a recent study by Mwesigye [170] investigated the minimum entropy production under non-uniform heat flow for the receiver of parabolic trough at varying ratios and rim angles of concentration owing to heat transfer and fluid friction. The outcomes reveal that for each given combination of fluid temperature, concentration ratio, and rim angle, the overall entropy production is minimised. Total entropy generation increased with decreasing rim angle, concentration ratio, and fluid temperature. This is owing to high peak temperatures in the absorber tube at these low rim angles.

2.7 Objective of the Thesis

It is clear from the literature study presented above that some researchers have carried out studies in an effort to increase the efficiency of heat transfer and fluid flow. Not only that, but a little research has also been carried out to utilise the entropy generation. Most studies were done on plain tubes and tubes supplied with twisted tape for laminar and turbulent flows of water and nanofluid. However, there is no study on heat transfer and the flow of fluid for ordinary tubes induced by elliptical-cut and classical twisted tape inserts with a focus on hybrid-nanofluid. In addition, there was no study on transient heat transfer and non-uniform heat flux for plain tubes and tubes supplied with elliptical-cut and solid twisted tape inserts. Moreover, the entropy production analysis of tubes fitted with twisted tape receives less attention. Despite its relevance, mixed convection on tubes fitted with twisted tape has been largely ignored, as well as entropy generation for mixed convection.

Consequently, this study aims to achieve the following objectives:

- To investigate the thermo-hydraulic performance of Al_2O_3-Cu/water hybrid nanofluid in a plain pipe (PT), and pipe supplied with elliptical-cut twisted tape (TECT) and solid twisted tape (TPT) in steady flow and unsteady flow, as well as uniform heat flux and non-uniform heat flux.
- To analyse the spatio-temporal evolution trends in temperature, and fluid friction to evaluate the parameters that dominate the heat transfer behaviour under different fluid conditions.
- To assess thermodynamic irreversibility for hybrid-nanofluids in PT, TECT, and TPT.
- To examine the turbulent performance of thermohydraulic for Al_2O_3-Cu/water hybrid nanofluids under mixed convection through a hollow pipe supplied with elliptical-cut tape inserts.
- To compare the thermodynamic irreversibility between mixed and forced convection for a pipe supplied with elliptical-cut twisted tape inserts using Al_2O_3-cu/water hybrid-nanofluid.

2.8 Thesis structure

The structure of this thesis is as follows.

Chapter 1 provides an overview of the various forms of heat transfer and thermodynamics' second law. It describes the methods for increasing heat transfer and their applications. Also, the objectives of the thesis are presented. Additionally, a list of publications is provided.

In Chapter 2, a literature review of prior research reviewing heat transfer and transient heat transfer using tube insert technology is presented. It investigates experimental and computational investigations of heat transfer and transient heat transfer increases in tubes using simple twisted tape as well as modified twisted tape for different fluids. Moreover, experimental, and computational studies of the enhancement of mixed convection heat transfer in pipes are described. Moreover, entropy generation. In addition, the objectives of the present study are outlined.

Chapter 3 contains the mathematical formulae utilised in the numerical research. Explanation of the governing equations for incompressible flow of fluid in steady as well as unstable states for heat transfer using a realizable k-ε turbulence model. Furthermore, numerical methods and boundary conditions are discussed.

Chapter 4 computational analysis of augmentation of heat transport and entropy production analysis for Al_2O_3-Cu/water inside a pipe supplied with elliptical-cut and solid twisted tape inserts is investigated. friction factor, Nusselt number, and thermal preformance factor correlations are also proposed using a non-linear regression analysis.

Chapter 5 computational analysis of transient heat transfer enhancement and entropy production for Al_2O_3-Cu/water inside a pipe supplied by elliptical-cut and solid twisted tape inserts with non-uniform heat flux is expounded.

Chapter 6 computational study of entropy production and thermohydraulics of mixed convection for Al_2O_3-Cu/water in a vertical hose supplied by elliptical-cut twisted tape inserts is presented. The study describes the flow system's response to changes in buoyancy force.

Chapter 7 summarises this study's results and provides recommendations for further research.

Chapter 3 Methodology

3.1 Introduction

Computational fluid dynamics (CFD) simulation processes are an essential tool for any application that involves dealing with fluid flow or heat transfer. The current study employs numerical approaches to explore the thermohydraulic behaviour of water, nanofluids, and hybrid-nanofluids in an ordinary pipe and a pipe supplied by elliptical-cut and classical twisted tape inserts. This study assumes incompressible, Newtonian, turbulent, and stable fluid flow (or unsteady). The governing equations and modelling equations, also an analysis of entropy generation and an explanation of the numerical techniques, are presented in this chapter.

3.2 Governing Equations

To describe the motion of fluid in the system, the Navier-Stokes equations are used, as it is assumed that the fluid is Newtonian. The Navier-Stokes equations are made up of Partial Differential Equations (PDEs) that describe the conservation laws for [171]:

- Mass (continuity equation).
- Momentum (Newton's 2nd Law).
- Energy (1st Law of Thermodynamics).

3.2.1 Under steady flow and with fully developed flow.

Basically, mass conservation is required by the continuity equation. It is expressed as in Cartesian coordinates (x_i):

$$\frac{\partial}{\partial x_i}(\rho u_i) = 0 \tag{3.1}$$

Here u_i is the velocity vector, and ρ is the density of flow.

Momentum must be conserved, as stated by the second conservation principle. All of this is expressed using Cartesian coordinates:

$$\frac{\partial}{\partial x_j}(\rho u_i u_j) = -\frac{\partial p}{\partial x_i} + \frac{\partial}{\partial x_j}\left[\mu_{eff}\left(\frac{\partial u_i}{\partial x_j} + \frac{\partial u_j}{\partial x_i}\right) - \frac{2}{3}\mu_{eff}\frac{\partial u_i}{\partial x_i}\delta_{ij} - \overline{\rho u_i' u_j'}\right] \tag{3.2}$$

Energy equation using Cartesian coordinates as

$$\frac{\partial}{\partial x_j}(\rho u_j C_p T) = \frac{\partial}{\partial x_j}\left(k_{eff}\frac{\partial T}{\partial x_j} + \frac{\mu_t}{\sigma_{h.t}}\frac{\partial(C_p T)}{\partial x_j}\right) + u_j\frac{\partial p}{\partial x_i}$$

$$+ \left[\mu_{eff}\left(\frac{\partial u_i}{\partial x_j} + \frac{\partial u_j}{\partial x_i}\right) - \frac{2}{3}\mu_{eff}\frac{\partial u_i}{\partial x_i}\delta_{ij} - \overline{\rho u_i' u_j'}\right]\frac{\partial u_i}{\partial x_j}$$

$$(3.3)$$

The above conservation equations (3.2) and (3.3) are solved directly for turbulent flow μ_{eff} and k_{eff}. Here k_{eff}, μ_{eff}, and T indicate the thermal conductivity of fluid, dynamic viscosity, and time-averaged temperature, respectively.

Following is a formula for determining the effective viscosity:

$\mu_{eff} = \mu + \mu_t$. And the thermal conductivity $k_{eff} = k_c + k_t$

$$k_t = C_p\frac{\mu_t}{Pr_t} \tag{3.4}$$

where Pr_t, k_t, and μ_t are the Prandtl number of turbulent, thermal conductivity of turbulent, and dynamic viscosity of turbulent, respectively.

The term $(-\overline{\rho u_i' u_j'})$ represents the turbulence effects and Reynolds stresses. The most used method for representing Reynolds stresses is the Boussinesq method, in which Reynolds stresses are connected to mean velocity gradients by [171-173].

$$-\rho\overline{u_i' u_j'} = 2\mu_t S_{ij} - \frac{2}{3}\left(\rho k + \mu_t\frac{\partial u_k}{\partial x_k}\right)\delta_{ij} \tag{3.5}$$

In this equation, S_{ij} is the rate of linear deformation tensor and can be calculated by

$$S_{ij} = \frac{1}{2}\left(\frac{\partial u_i}{\partial x_j} + \frac{\partial u_j}{\partial x_i}\right) \tag{3.6}$$

Such that

$$-\rho\overline{u_i' u_j'} = \mu_t\left(\frac{\partial u_i}{\partial x_j} + \frac{\partial u_j}{\partial x_i}\right) - \frac{2}{3}\left(\rho k + \mu_t\frac{\partial u_k}{\partial x_k}\right)\delta_{ij} \tag{3.7}$$

Here k represents the turbulent kinetic energy.

3.2.2 Under unsteady state

The continuity equation essentially states that mass must be conserved. This is expressed in Cartesian coordinates as (x_i):

$$\frac{\partial}{\partial t}(\rho) + \frac{\partial}{\partial x_i}(\rho u_i) = 0 \tag{3.8}$$

The second principle of conservation is that momentum must be conserved. It is represented as in Cartesian coordinates:

$$\frac{\partial}{\partial t}(\rho u_i) + \frac{\partial}{\partial x_j}(\rho u_i u_j) = -\frac{\partial p}{\partial x_i} + \frac{\partial \tau_{ij}}{\partial x_j} \tag{3.9}$$

In this equation, p denotes the static pressure and τ_{ij} denotes the stress tensor. The stress tensor τ_{ij} for a Newtonian fluid is defined by

$$\tau_{ij} = \left[\mu_{eff} \left(\frac{\partial u_i}{\partial x_j} + \frac{\partial u_j}{\partial x_i} \right) \right] - \frac{2}{3} \mu_{eff} \frac{\partial u_l}{\partial x_l} \delta_{ij} \tag{3.10}$$

On the right-hand side of the equation, the second term represents the impact of volume expansion.

Thus, the equation of momentum can be written as follows:

$$\frac{\partial}{\partial t}(\rho u_i) + \frac{\partial}{\partial x_j}(\rho u_i u_j) = -\frac{\partial p}{\partial x_i} + \frac{\partial}{\partial x_j} \left\{ \mu_{eff} \left(\frac{\partial u_i}{\partial x_j} + \frac{\partial u_j}{\partial x_i} \right) - \frac{2}{3} \mu_{eff} \frac{\partial u_l}{\partial x_l} \delta_{ij} \right\} \tag{3.11}$$

The conservation of energy balance is expressed as [171]:

$$\begin{aligned}
\frac{\partial}{\partial t}(\rho u_i) + \frac{\partial}{\partial x_j}(\rho u_j C_p T) &= \frac{\partial}{\partial x_j}\left(k_{eff} \frac{\partial T}{\partial x_j} + \frac{\mu_t}{\sigma_{h.t}} \frac{\partial (C_p T)}{\partial x_j} \right) + u_j \frac{\partial p}{\partial x_i} \\
&+ \left[\mu_{eff} \left(\frac{\partial u_i}{\partial x_j} + \frac{\partial u_j}{\partial x_i} \right) - \frac{2}{3} \mu_{eff} \frac{\partial u_i}{\partial x_i} \delta_{ij} \right] \frac{\partial u_i}{\partial x_j}
\end{aligned} \tag{3.12}$$

3.2.3 Buoyancy flow

In order to execute the forced convection computations, temperature-dependent fluid characteristics are used. There is a constant formulation for fluid characteristics in buoyancy-influenced convective heat transfer (mixed convection); density, however, density is treated as a function of variance between local and reference temperatures, and is therefore estimated [174] as

$$(\rho)_{hnf} = \rho_0 \left[1 - \beta_{hnf}(T - T_0) \right] \tag{3.13}$$

The mixed convection employs the Boussinesq approximation, and its momentum equations are written as follows [141]:

$$\rho \frac{\partial(u)}{\partial t} + \frac{\partial(\rho uu)}{\partial x} + \frac{\partial(\rho uv)}{\partial y} + \frac{\partial(\rho uw)}{\partial z} =$$
$$-\frac{\partial p}{\partial x} + \mu_{eff} \left(\frac{\partial^2 u}{\partial x^2} + \frac{\partial^2 u}{\partial y^2} + \frac{\partial^2 u}{\partial z^2} \right) + g\cos \theta (\rho - \rho_0) \tag{3.14}$$

$$\rho \frac{\partial(v)}{\partial t} + \frac{\partial(\rho vu)}{\partial x} + \frac{\partial(\rho vv)}{\partial y} + \frac{\partial(\rho vw)}{\partial z} =$$
$$-\frac{\partial p}{\partial y} + \mu_{eff} \left(\frac{\partial^2 v}{\partial x^2} + \frac{\partial^2 v}{\partial y^2} + \frac{\partial^2 v}{\partial z^2} \right) + g\sin \theta (\rho - \rho_0) \tag{3.15}$$

$$\rho \frac{\partial(w)}{\partial t} + \frac{\partial(\rho wu)}{\partial x} + \frac{\partial(\rho wv)}{\partial y} + \frac{\partial(\rho ww)}{\partial z} =$$
$$-\frac{\partial p}{\partial z} + \mu_{eff} \left(\frac{\partial^2 w}{\partial x^2} + \frac{\partial^2 w}{\partial y^2} + \frac{\partial^2 w}{\partial z^2} \right) \tag{3.16}$$

Here u, v and w are the components of velocity.

In the momentum equations (3.12) and (3.13), Boussinesq's model approximates the buoyancy term [175]:

$$(\rho - \rho_0)g \approx -\rho_0 \beta (T - T_0)g$$

where ρ is the density (kg/m^3), ρ_0 is referencing density (kg/m^3), determined from the temperature of reference $T_0(K)$, T is the fluid temperature of fluid (K), μ is the dynamic viscosity (Ns/m^2), p is the pressure (Pa), θ is the angle of inclination, g is the gravitational acceleration, and β is the fluid's thermal expansion coefficient (K^{-1}).

3.2.4 Turbulence model

This study applies the realizable k-ε model to turbulence. It is proposed by Shih et. al. [176] and is a model based on the transport equations for the turbulence kinetic energy (k) and its dissipation rate (ε). The model transport equation for (k) is derived from the exact equation, however the model transport equation for (ε) was derived using physical reasoning and bears little relation to its mathematically precise counterpart. The model transport equations for (k) and (ε) are given by Lam-Bremhorst [177]and shown below.

3.2.4.1 Transport equations for the realizable k-ε model in forced convection

Turbulence kinetic energy (k) equation:

$$\frac{\partial}{\partial t}(\rho k) + \frac{\partial}{\partial x_i}(\rho k u_i) = \frac{\partial}{\partial x_j}\left[\left(\mu + \frac{\mu_t}{\sigma_k}\right)\frac{\partial k}{\partial x_j}\right] + G_k - \rho\varepsilon \tag{3.17}$$

Equation of turbulence dissipation rate (ε)

$$\frac{\partial}{\partial t}(\rho\varepsilon) + \frac{\partial}{\partial x_i}(\rho\varepsilon u_i) = \frac{\partial}{\partial x_j}\left[\left(\mu + \frac{\mu_t}{\sigma_\varepsilon}\right)\frac{\partial\varepsilon}{\partial x_j}\right] + \rho C_1 S_\varepsilon - \rho C_2 \frac{\varepsilon^2}{k + \sqrt{(\mu/\rho)\varepsilon}} \tag{3.18}$$

3.2.4.2 Transport equations for the realizable k-ε model in mixed convection

Turbulence kinetic energy (k) equation:

$$\frac{\partial}{\partial t}(\rho_{hnf}k) + \frac{\partial}{\partial x_i}(\rho_{hnf}k u_i) =$$

$$\frac{\partial}{\partial x_j}\left[\left(\mu + \frac{\mu_t}{\sigma_k}\right)\frac{\partial k}{\partial x_j}\right] + G_b + G_k - \rho\varepsilon - Y_M + S_k \tag{3.19}$$

Equation of turbulence dissipation rate (ε)

$$\frac{\partial}{\partial t}(\rho_{hnf}\varepsilon) + \frac{\partial}{\partial x_i}(\rho_{hnf}\varepsilon u_i) =$$

$$\frac{\partial}{\partial x_j}\left[\left(\mu + \frac{\mu_t}{\sigma_\varepsilon}\right)\frac{\partial \varepsilon}{\partial x_j}\right] + \rho_{hnf}C_1 S_\varepsilon - \rho C_2 \frac{\varepsilon^2}{k + \sqrt{(\mu/\rho)\varepsilon}} + C_{1\varepsilon}\frac{\varepsilon}{k}C_{3\varepsilon}G_b + S_\varepsilon \qquad (3.20)$$

where σ_k and σ_ε denote the turbulent Prandtl numbers for k and ε respectively, G_b is the generation of turbulence kinetic energy due to buoyancy, G_k is the amount of turbulent kinetic energy generated as a result of gradients of mean velocity, Y_M is the dissipation rate due to fluctuating dilatation in compressible flow. $C_{1\varepsilon}, C_{2\varepsilon}$ and $C_{3\varepsilon}$ are model constants. The default values for the constants are given by Lam-Bremhorst [177].

3.2.4.3 Turbulent Viscosity

The turbulent viscosity, μ_t, is determined by turbulent kinetic energy, k, and dissipation rate, ε. As in other k-ε models, the eddy viscosity is computed from.

$$\mu_t = \rho C_\mu \frac{k^2}{\varepsilon} \qquad (3.21)$$

Here, the coefficient C_μ is not a constant. It is computed from [171]:

$$C_\mu = \frac{1}{A_0 + A_s \frac{kU^*}{\epsilon}} \qquad (3.22)$$

where,

$$U^* \equiv \sqrt{S_{ij}S_{ij} + \tilde{\Omega}_{ij}\tilde{\Omega}_{ij}} \qquad (3.23)$$

and

$$\tilde{\Omega}_{ij} = \Omega_{ij} - 2\epsilon_{ijk}\omega_k$$
$$\Omega_{ij} = \overline{\Omega_{ij}} - \epsilon_{ijk}\omega_k$$

where $\overline{\Omega_{ij}}$ is the mean rate-of-rotation tensor viewed in a rotating reference frame with the angular velocity ω_k. The model constants A_0 and A_s are given by

$$A_0 = 4.04, \ A_s = \sqrt{6}\cos \phi$$

where,

$$\phi = \frac{1}{3}\cos^{-1}(\sqrt{6}W), \quad W = \frac{S_{ij}S_{jk}S_{ki}}{\tilde{S}^3}, \quad \tilde{S} = \sqrt{S_{ij}S_{ij}},$$

S_{ij} from Equation (3.6)

3.2.4.4 Modelling turbulent production in the realizable k-ε model

The term G_k, representing the production of turbulence kinetic energy, is modeled identically for the realizable k-ε models. From the exact equation for the transport of k, this term may be defined as

$$G_k = -\rho \overline{u_i' u_j'} \frac{\partial u_j}{\partial x_i} \tag{3.24}$$

To evaluate G_k in a manner consistent with the Boussinesq hypothesis,

$$G_k = \mu_{eff} S^2 \tag{3.25}$$

where S is the modulus of the mean rate-of-strain tensor, defined as

$$S \equiv \sqrt{2S_{ij}S_{ij}} \tag{3.26}$$

3.2.4.5 Model constants

For a realizable k-ε model, the model coefficients C_μ and C_1 are computed, C_μ from equation (3.22) and C_1 using the following equations [171]:

$$C_1 = max\left[0.43, \frac{\eta}{\eta+5}\right] \tag{3.27}$$

Where $\eta = S\frac{k}{\varepsilon}$,

Table 3.1 shows the model constant.

σ_k	σ_ε	C_1	C_2	$C_{1\varepsilon}$	$C_{3\varepsilon}$	C_μ	A_0
1.0	1.2	Equation (3.27)	1.9	1.44	1	Equation (3.22)	4.04

Table 3.1 Model coefficients

3.2.5 Buoyancy Effects on Turbulence in k-ε Models

When a non-zero gravity field and temperature gradient are present simultaneously, the k-ε models in Lam-Bremhorst account for the generation of k due to buoyancy (G_b in Equation (3.19)) and the corresponding contribution to the production of ε in Equation (3.20)

The generation of turbulence due to buoyancy is given by

$$G_b = \beta g_i \frac{\mu_t}{Pr_t} \frac{\partial T}{\partial x_i} \tag{3.28}$$

where Pr_t is the turbulent Prandtl number for energy and g_i is the component of the gravitational vector in the ith direction.

The coefficient of thermal expansion, β, is defined in Equation (3.13).

3.3 Boundary conditions

The present work's numerical simulations are performed on the assumption that the flow is incompressible in both steady and unstable states. The model has three types of geometry: ordinary pipes (PT), and ordinary pipes supplied with elliptical-cut (TECT) or solid (TPT) twisted tape inserts. Pipe walls and elliptical and solid twisted tape surfaces under non-slip conditions, i.e $u_i = 0$. At an entrance temperature of 300K, the thermal properties of water, nanofluid (CuO/water), and hybrid-nanofluid (Al$_2$O$_3$–Cu/water) are calculated. The conditions of pressure outlet are used at the outlet, and the pressure of gauge is set to zero.

In order to achieve the requested Reynolds number at the pipe's inlet, the following velocity is specified:

$$Re = \frac{\rho\, u\, D}{\mu} \tag{3.29}$$

In this equation, Re represents the Reynolds number and μ and ρ represent fluid dynamic viscosity and density of the fluid, respectively.

For turbulent flow, the intensity of turbulence flow (I) can be expressed as follows [178]

$$I = 0.16 Re^{-0.125} \tag{3.30}$$

Grashof number (Gr) is defined for mixed convection [179, 180]

$$Gr = \frac{g\beta(T_o - T_i)^3}{v^2} \qquad (3.31)$$

Here v is fluid kinematic viscosity (m^2/s).

The Richardson number (Ri) was computed as [147]

$$Ri = \frac{Gr}{Re^2} \qquad (3.32)$$

3.4 Confirmatory tests

Three parameters of interest for the present work are: (1) Nusselt number, (2) friction factor, and (3) thermal performance factor, which are respectively used for characterization of friction loss, heat transfer rate, and effectiveness of heat transfer augmentation in the pipe with classical and elliptical-cut twisted tape insert based on a given geometry and flow conditions.

3.4.1 Nusselt number

The Nusselt number (Nu) provides the ratio of the convective to conductive heat transmission taking place across the interface between the walls and the fluid phase, as shown in the equations below [181]:

$$Nu = \frac{1}{L}\int_0^L Nu(x)dx \qquad (3.33)$$

$$Nu = \frac{h\,D}{k_c} \qquad (3.34)$$

Where L is the length of pipe, D is pipe diameter (m), and k_c is the thermal conductivity.

The formula for the coefficient of heat transport, h, can be written in the following way:

$$h = \frac{q}{(T_{ri} - T_{bulk})} \qquad (3.35)$$

3.4.2 Friction factor

In the fully developed flow, the friction factor (f) is determined from measured shear stresses (τ) [182] in the plain pipe (3.36), and the pressure drop (Δp) [88] in tube supplied with twisted tape inserts (3.37), as follows:

$$f = \frac{8 * \tau_w}{\rho \, u^2} \tag{3.36}$$

$$f = \frac{2 \, \Delta p \, D}{\rho \, L u^2} \tag{3.37}$$

3.4.3 Thermal performance factor

This work calculates the thermal performance factor on the basis of ratios of heat transmission to friction factor. For TPT and TECT, and is defined by:

$$\eta = \frac{\left(Nu/Nu_p\right)}{\left(f/f_p\right)^{1/3}} \tag{3.38}$$

where Nu_p, Nu, f_p and f are the Nusselt numbers and friction factors for the plain pipe and the pipe supplied with twisted tape, respectively.

3.5 Second law analysis (Entropy Generation)

There are three main focuses for considering the entropy generation analysis presented here. First, there is the generation rate of volumetric entropy, which displays how much entropy is created within each system component. In this way, it is possible to compare the entropy of each component of the investigated system. Secondly, there is the system's total entropy production. This is the amount of entropy produced by the entire system, as its name suggests. Third, there is the Bejan number, which shows how much entropy is generated by each irreversibility [105].

3.5.1 Local entropy generation

Based on frictional and thermal influences as the only contributors, local volumetric entropy formation was calculated separately for each condition:

$$S_{g,t} = S_{HT} + S_{FF} \tag{3.39}$$

where the first term in the equation on the right-hand (3.39) is the thermal entropy production in addition to the second term is the frictional entropy production. These two terms are defined, respectively. In general, the generation of volumetric entropy can be expressed as follows [183]:

$$S_{H,T} = \frac{k_c}{T^2} \left(\frac{\partial T}{\partial x_i}\right)^2 \tag{3.40}$$

$$S_{F,F} = \frac{\mu}{T} \left\{ 2\left[\left(\frac{\partial u_i}{\partial x_i}\right)^2\right] + \left(\frac{\partial u_i}{\partial x_j} + \frac{\partial u_j}{\partial x_i}\right)^2 \right\} \tag{3.41}$$

3.5.2 Total Entropy generation

In order to calculate the total entropy creation $(S_{g,t})$, the volumetric entropy production components must be integrated across the tube's volume.

$$S_{g,t} = \left\{ \int S_{H,T} + \int S_{F,F} \right\} \partial V \tag{3.42}$$

3.5.3 Bejan number

A Bejan number represents the percentage contribution of every irreversibility to the total production of entropy. It is possible to define the Bejan number as follows [105]:

$$Be = \frac{(S_{gen})_{Heat\ transfer}}{S_{gen,total}} \tag{3.43}$$

3.6 Numerical techniques

To discover solutions to the motion equations, their discrete equivalents must be generated. In this work, finite volume methods (FVM) are employed to discretize the governing partial differential equations. When using the finite volume approach, the domain of computation is divided to group of control volumes, inside which the computing nodes are located. Both momentum and mass are preserved locally inside the control region and across the calculation domain when the governing equations of motion are incorporated into this volume. This study uses a pressure-based finite volume technique to perform numerical computations. The momentum, turbulent kinetic energy, turbulent dissipation rate, and energy equations were discretized using the second order upwind approach. Warming and Beam [184] introduced it. In the case of the coupling of pressure and velocity, the SIMPLE (Semi-Implicit Pressure Linked Equations) approach is employed, which suggested by Patankar and Spalding [185]. Indirectly, the continuity equation was used for this purpose. A control volume can be integrated using this equation, as can the momentum equations. For the SIMPLE computation to begin, a pressure field P^* is estimated. Then, using the estimated pressure, the discretized momentum equations are solved to get the velocity components u^*, v^*. Corrected pressure P', defined as defined as the spread between the assumed and actual pressures, is then used to approximate the pressure field more accurately through the relation $P = P' + P^*$. Next, the corrected findings of *u, v, P* [171] are used to solve the scalar quantity's discretized equation, which includes the corrected velocity))components. This equation is solved using Star-CCM+ iteratively. The numerical solutions are done until the residual of the continuity equation, momentum equations, energy equation, and turbulent kinetic energy rate are less than 10^{-5}. Furthermore, MATLAB was used for solving equations from (3.39) to (3.42).

3.7 Conclusions

The methods used in this work explore the numerical investigation of the thermohydraulic behaviour of hybrid-nanofluids in PT, TPT, and TECT. The tube model has been numerically analysed using FVM. Two Al_2O_3-Cu/water cases have been studied (forced and mixed convection). Both cases studied thermal and hydraulic flows through tubes. Additionally, entropy generation was also analysed using MATLAB codes. According to the numerical results, Al_2O_3-Cu/water is an appropriate fluid to solve fluid flow and heat transfer problems in parabolic receiver tubes.

Chapter 4 Computational analysis of entropy generation and heat transfer augmentation

4.1 Introduction

Heat transfer, an analysis of entropy production, and Bejan number for a hybrid nanofluid (Al_2O_3-Cu/water) turbulent flow in ordinary pipe (PT) as well as pipe supplied with elliptical-cut (TECT) and classical twisted tape (TPT) inserts have been numerically investigated. The research results will have wide-ranging implications for many different systems, including those used in energy-related applications and many engineering such as heat exchangers, solar water heating systems, solar chemistry, solar desalination plants, concentrating solar power plants, solar thermal power, cooling towers, etc. Using twisted tapes to enhance heat transfer has been the topic of a wide-ranging study. According to the literature, twisted tapes are used to maximize fluid mixing between the wall and the centre of the tube. For the purpose of improving the thermal performance of these systems, Oni and Paul [88] have demonstrated that twisted tape with various shapes of cuts can enhance thermal efficiency in a distinctive manner. A further benefit of the use of nano-fluid techniques is the improved heat transmission compared to water [42-44]. Thermal processes can be optimized using entropy production analysis [186]. However, despite the fact that these works have received considerable attention, no numerical or experimental analysis has been provided regarding heat transmission and production of entropy in tubes fitted with elliptical-cut and solid twisted tape in which a hybrid nanofluid is used as the working fluid.

Considering the above, this chapter's objective is to evaluate the rate of heat transmission, the factor of thermal performance, and the production analysis of entropy in PT, TPT, and TECT with a hybrid- nanofluid (Al_2O_3-Cu/water) compared with a nanofluid (Cu/water) under turbulent flow conditions. The objective is achieved through numerical simulations with a variety of Reynolds numbers: 7000, 9000, 11000, 13000, and 15000. Furthermore, an investigation was conducted to ascertain which of the tubes and fluid flows gave the best performance and caused the least entropy generation.

4.2 Model Geometry and physical model

Model geometries consist of ordinary pipe (PT), and ordinary pipe supplied with elliptical cut (TECT) and classical twisted tape (TPT) inserts. Figure 4-1 (a), illustrates a pipe with a length (*L*) of 1m and an inner diameter (*D*) of 0.0195m. The twisted tape inserts have 0.057m pitch (*y*), a 0.019m width (*W*), and 0.0008m thickness (*t*), as demonstrated in Figure 4-1 (b). In the TECT, the twisted tape has elliptical-cut with a long diameter to short ratio of *b/a* = 2 and a ratio of width tape of *a/w* = 0.7, as depicted in Figure 4-1 (c). Figure 4-1 (d) illustrates the configuration of the plain twisted tape and of the elliptical-cut twisted tape. These dimensions were chosen in accordance with the experimental and numerical works in [96] and [44], which are the sources employed to verify the numerical findings of this chapter.

The physical model is simplified by using the following assumptions:
(1) The gravity force is neglected. (2) The numerical study of turbulent flows is performed by means of the realizable *k-ε* model. (3) All the simulations are performed at Reynolds numbers 7000, 9000, 11000, 13000, and 15000. (4) Incompressible and steady flow is assumed. (5) Tube walls receive 600 Wm^{-2} and 4000 Wm^{-2} constant heat fluxes, while the twisted tape is under adiabatic conditions; furthermore, tube walls and elliptical and solid tapes under non-slip conditions.
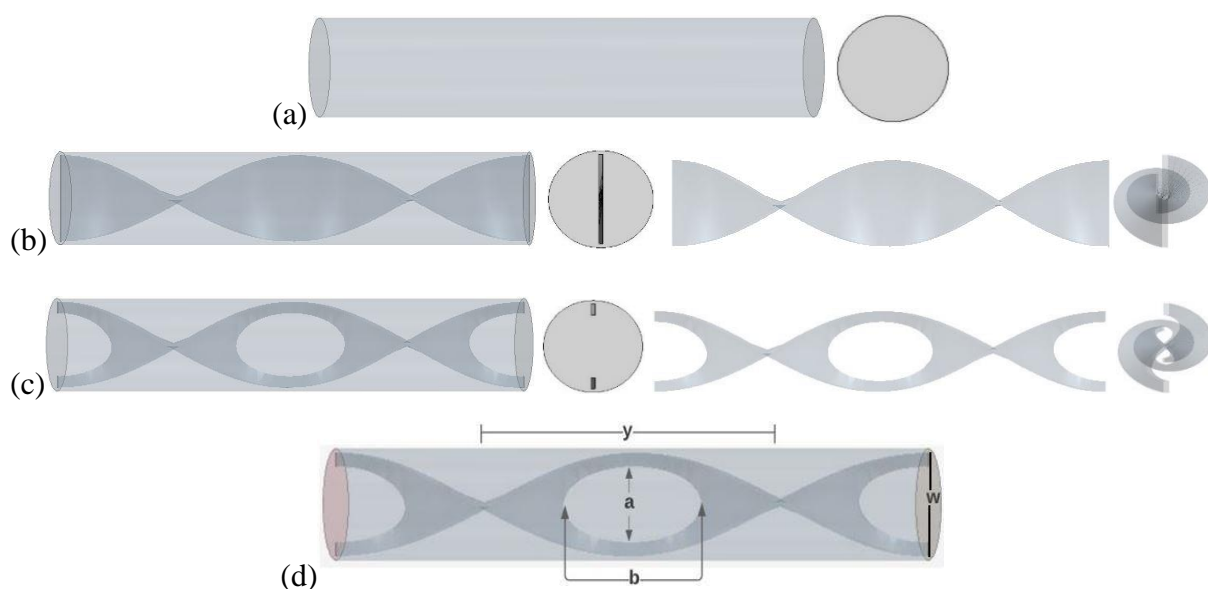
Figure 4-1 Physical models for (a) PT, (b) TPT, (c) TECT, and (d) important dimensions.

4.3 Hybrid-nanofluid properties

Many studies have been conducted to address the problem of low thermal conductivity of the receiver pipe's most common medium. It has been demonstrated in a number of studies that the incorporation of nanoparticles into the water enhances thermal conductivity [187-189]. An Al_2O_3–Cu/water hybrid nanofluid was calculated for different mass concentrations in this study. Moreover, for comparison, a nanofluid (CuO/water) was selected [44]. Table 4.1 summarises the properties of thermophysical for water and Al_2O_3, Cu, CuO nanoparticles, [190]. The following are the properties of the fluid:

Substances	ρ/Kg m^{-3}	C_p/J Kg^{-1} K^{-1}	k_c /Wm^{-1} K^{-1}
Water	997.1	4179	0.613
Al_2O_3	3970	765	40
CuO	6500	535.6	20
Cu	8933	385	401

Table 4.1 Flow properties at T=300K.

A hybrid nanofluid's thermophysical properties are based on the water properties, solid nanoparticle volume friction in the water, and Cu, Al_2O_3, nanoparticles [26]. The volume fractions of the Al_2O_3 and Cu nanoparticles are denoted by $\emptyset_1$ and $\emptyset_2$, respectively. The determining equations for the thermo-physical properties of the hybrid nanofluid of Al_2O_3-Cu/water are depicted in equations (4.1- 4.4). Owing to the precision of its thermo-physical correlations [26], this type of hybrid nanofluid was chosen in this study. Equations for thermo-physical properties of the hybrid nanofluid are represented by [26-28]:

Density:

$$\rho_{hnf} = (1 - \emptyset_2)[(1 - \emptyset_1)\rho_f + \emptyset_1\rho_{n1}] + \emptyset_2\rho_{n2} \qquad (4.1)$$

Specific heat:

$$(\rho C_p)_{hnf} = (1 - \emptyset_2)[(1 - \emptyset_1)(\rho C_p)_f + \emptyset_1(\rho C_p)_{n1}] + \emptyset_2(\rho C_p)_{n2} \quad (4.2)$$

Dynamic viscosity:

$$\mu_{hnf} = \frac{\mu_f}{(1-\emptyset_1)^{2.5}(1-\emptyset_2)^{2.5}} \tag{4.3}$$

Thermal Conductivity:

$$\frac{k_{hnf}}{k_{nf}} = \frac{k_{n2}+2k_{nf}-2\emptyset_2(k_{nf}-k_{n2})}{k_{n2}+2k_{nf}+\emptyset_2(k_{nf}-k_{n2})} \tag{4.4}$$

Where $k_{nf} = \dfrac{k_p+2k_{bf}-2\emptyset(k_{bf}-k_p)}{k_p+2k_{bf}+\emptyset(k_{bf}-k_p)} k_{bf}$

Here, $\emptyset_1$ and $\emptyset_2$ denote the volume fraction of nanoparticles, where $\emptyset_1 + \emptyset_2 = \emptyset$, where $\emptyset$ is the overall volume concentration of two different types of nanoparticles dispersed in a basic fluid in the hybrid nanofluid. Further, the indices n_1 and n_2 refer to the Al₂O₃ and CuO nanoparticles, and *bf, hnf*, and *nf* are acronyms for base fluid, hybrid-nanofluid, and nanofluid, respectively.

Table 4.2 summarizes the thermophysical characteristics of the hybrid nanofluid used in this study.

Al₂O₃-cu/Water Hybrid-nanofluid	ρ/Kg m⁻³	k_c /Wm⁻¹ K⁻¹	$\mu/Pa-s$	C_p/J Kg⁻¹ K⁻¹
1%	1052.24	0.639	0.00114	3955
2%	1106.8	0.658	0.00133	3752.052
3%	1161.314	0.677	0.00155	3568
4%	1215.9	0.697	0.00183	3400

Table 4.2 The characteristics of hybrid nanofluids (Al₂O₃-Cu/water) at different concentrations.

4.4 Grid independency test

A grid-independent study was performed to determine an acceptable grid with high accuracy for the temperature for a variety of mesh sizes. At Re = 11000, the findings are obtained for water flow within an ordinary pipe as well as a pipe supplied by solid and elliptical-cut twisted tape. To apply enhanced wall function technique, the wall y+ is strictly controlled between 35 and 100. According to Figure 4-2, in each pipe, the total number of cells was changed as part of testing grid independence. To demonstrate which number of cells is appropriate for each shape, five grids were used, each with a different number of cells. It depends upon the number of cells divided for the computational outcomes to be convergent with the precise answers. It is shown that in Figure 4-2 (frame (a)), the measured temperatures from grids of 520000, 592000, 624000, and 64000 cells differ by 0.24%, 0.33%, 1.2%, and 1.2% from those obtained from a grid consisting of 496000 cells. In the case of the TPT shown in Figure 4-2 (frame (b)), the temperatures in the grids 1179769, 1234240, 1526023, and 1611011 differ by 0.15%, 0.35%, 0.53%, and 0.53% from those in the grid with cell counts 1008117. Likewise, in TECT, temperature readings in grids with 2892319, 2990608, 3359202, and 3413798 cells vary by 0.17%, 0.49%, 0.73%, and 0.73% compared to grids with 2615663 cells. A grid of 624000 or 640000 cells can be used in the PT, while a grid with cells ranging from 1526023 to 1611011 can be utilized in the TPT. Moreover, any grid with cells from 2990608 to 3413798 would be suitable for TECT, due to the negligible variance in results obtained using these grids. For the fields of PT, TECT, and TECT, the grid with cell counts of 640000, 3413798. and 1611011 are used.

(a)

(b)

(c)
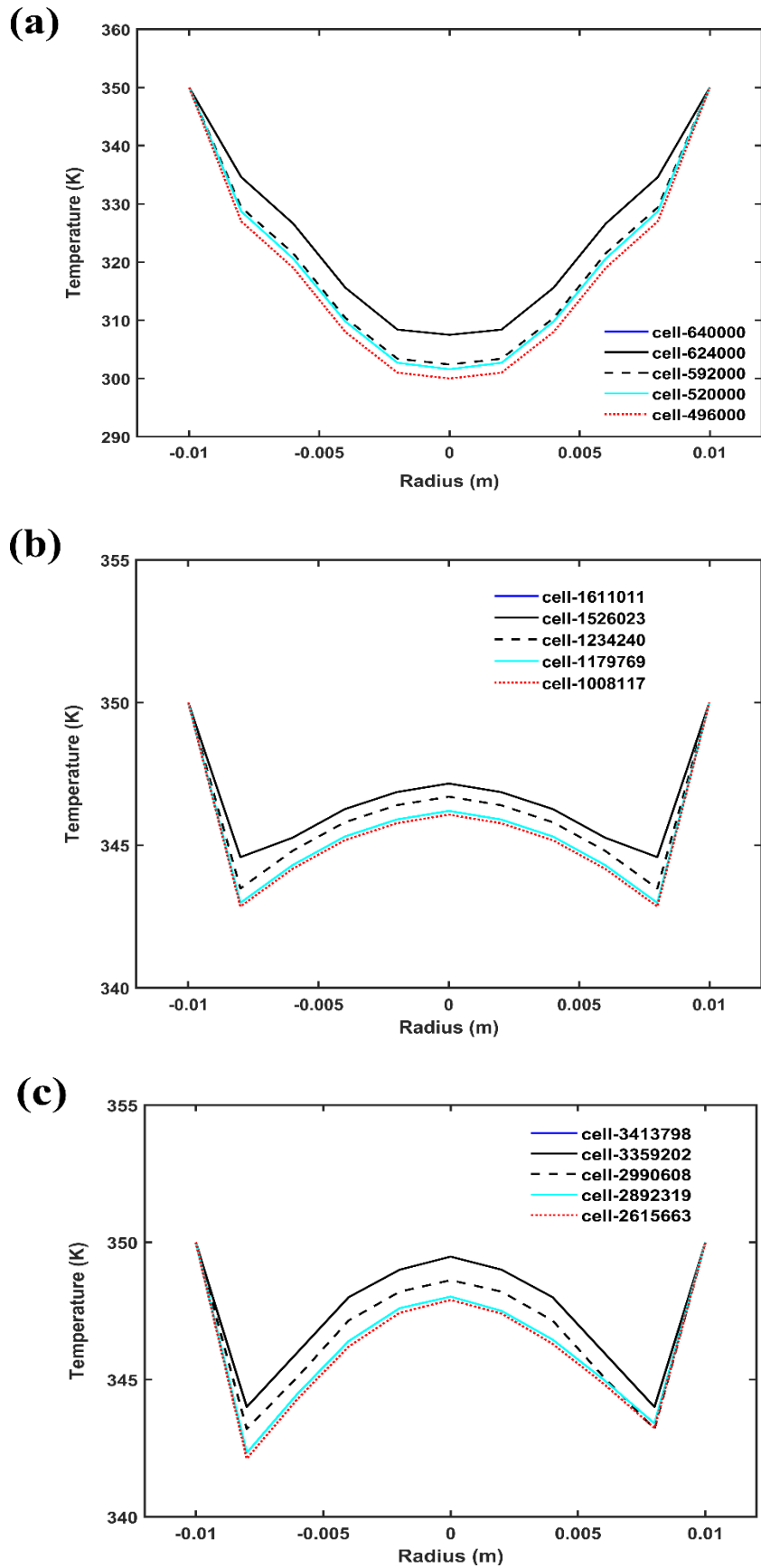
Figure 4-2 Temperature distribution for various grids over the cross-sections in (a) PT, (b) TPT, and (c) TECT at Re = 11000.

4.5 Validation

Various concentrations of nanoparticles were compared with Ahmadi's work [44] at a Reynolds number of 7000 in TECT using the realizable k-ε model model to determine the Nusselt number, friction factor, and the factor of thermal efficiency. For the parameters (Nusselt number, friction factor, and the factor of thermal efficiency), the results under turbulent flow conditions are generally in agreement as shown in Figure 4-3 (a-c). For the aforementioned parameters, the nanoparticle concentrations of 4% caused the highest error percentages, with values of 5.1, 3.5, and 5.5%, respectively.
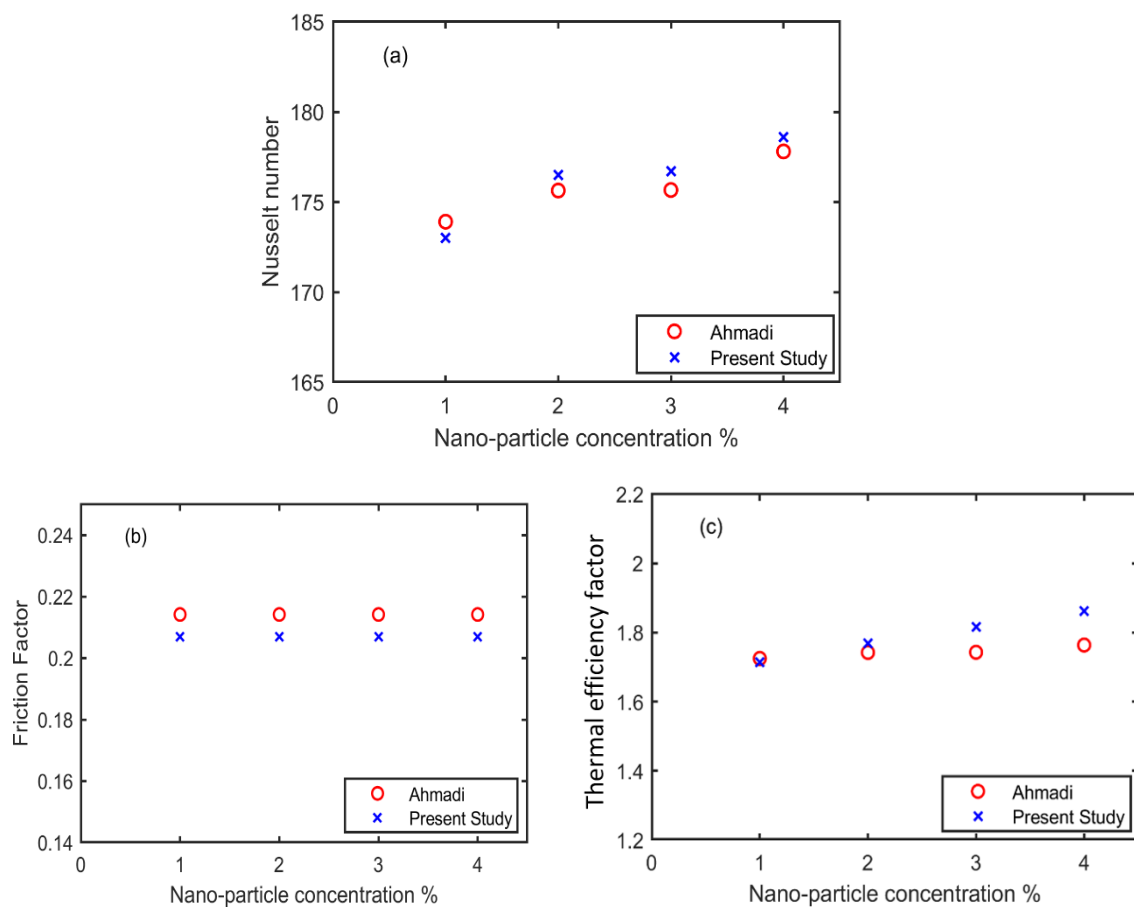
Figure 4-3 The change of (a) Nusselt number, (b) friction factor, and (c) thermal efficiency factor vs Nano-particle concentrations of Ahmadi [44].

4.6 Computational Results and Discussions

The plots of contours, thermal performance factor, Nusselt number, friction factor, and the analysis of entropy production are discussed in this section for the turbulent flow of an Al_2O_3-Cu/water hybrid nanofluid in an ordinary tube and in a tube supplied by solid and elliptical twisted tape inserts. A Reynolds number of Re = 7000 is selected to give an overview of the temperature contour, velocity contour, and the distribution of turbulent kinetic energy. In addition, the spatial distribution of thermal and frictional entropy production is displayed.

4.6.1 Temperature contours

In Figure 4-4, the plot of the temperature at X= 0.57m of three configurations for PT, TPT, and TECT are shown for a turbulent flow of hybrid nanofluid (Al_2O_3-Cu/water) with concentration variations. The wall heat flow is 4000 Wm^{-2}. The contours of temperature in PT are similar as shown in Figure 4-4 (a). The development of the flow at this point may be responsible for this phenomenon. There is an increase in the distribution of temperature in the TPT and TECT tubes in Figure 4-4 (b and c), because of the use of elliptical-cut and solid twisted tape inserts in these tubes. Oni and Pual [88] agree with this. In particular, TECT has a higher temperature gradient than PT and TPT.
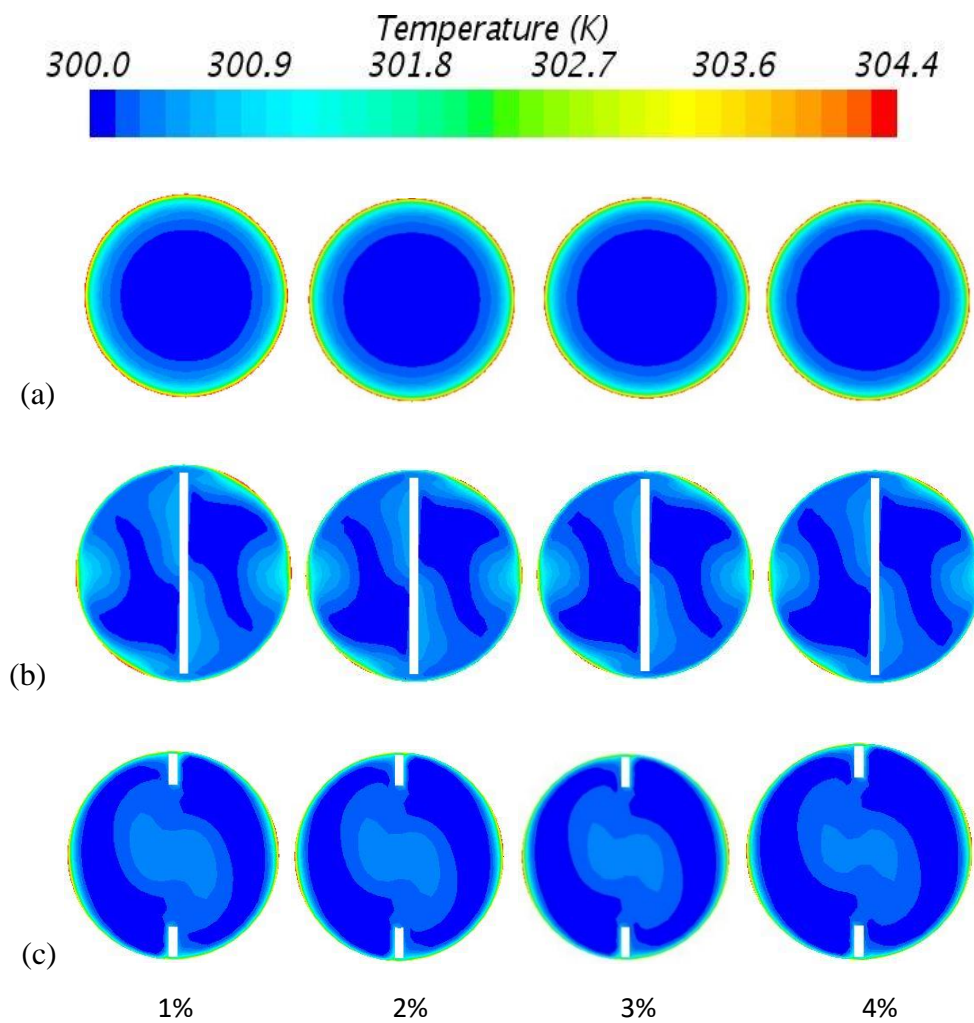
Figure 4-4 Temperature contour for hybrid nanofluid (Al_2O_3-Cu/water) in different concentrations located at $X = 0.57$m and Re = 7000 of (a) PT, (b) TPT, and (c) TECT.

4.6.2 Flow velocity contour

In Figure 4-5 the contours of velocity flow are depicted for the hybrid nanofluid (Al_2O_3-Cu/water) with various nanoparticle concentrations and a Reynolds number of 7000 for PT, TECT, and TPT. The location of $X = 0.57$m was chosen to illustrate the flow within the tube once it has reached a developed state. It can be seen from Figure 4-5, that the concentration of nanoparticles doesn't change the velocity contour, as stated by Ahmedi et. al. [44]. According to Figure 4-5 (a), the velocity at this location appears to be similar, with the maximum velocity occurring at the pipe centre. This suggests that the flow is fully developed at this point. In contrast, in TPT Figure 4-5 (b), there's a prominent eddy about the twisted tapes. An imperative function of longitudinal swirling is to disrupt the boundary layer as well as create a uniform velocity throughout the flow. This is achieved by reducing the spacing between the tape wall and pipe wall. It is observed that the results of the present study and those of [96] are generally in agreement. Similarly, in Figure 4-5 (c), TECT produces swirl flows in the core zone and on the tube walls. Thus, it makes a contribution to more fluid mixing between the near-wall areas and the middle. For TECT and TPT, the cut on the twisted tape and the gap are responsible for uniform velocity; the swirling flow in this region is to blame for this phenomenon. When the gap reduces in TPT, distortion decreases in that zone, also when twisted tape is cut in TECT. As a result, the velocity gradient increases, allowing heat to be more effectively transferred.
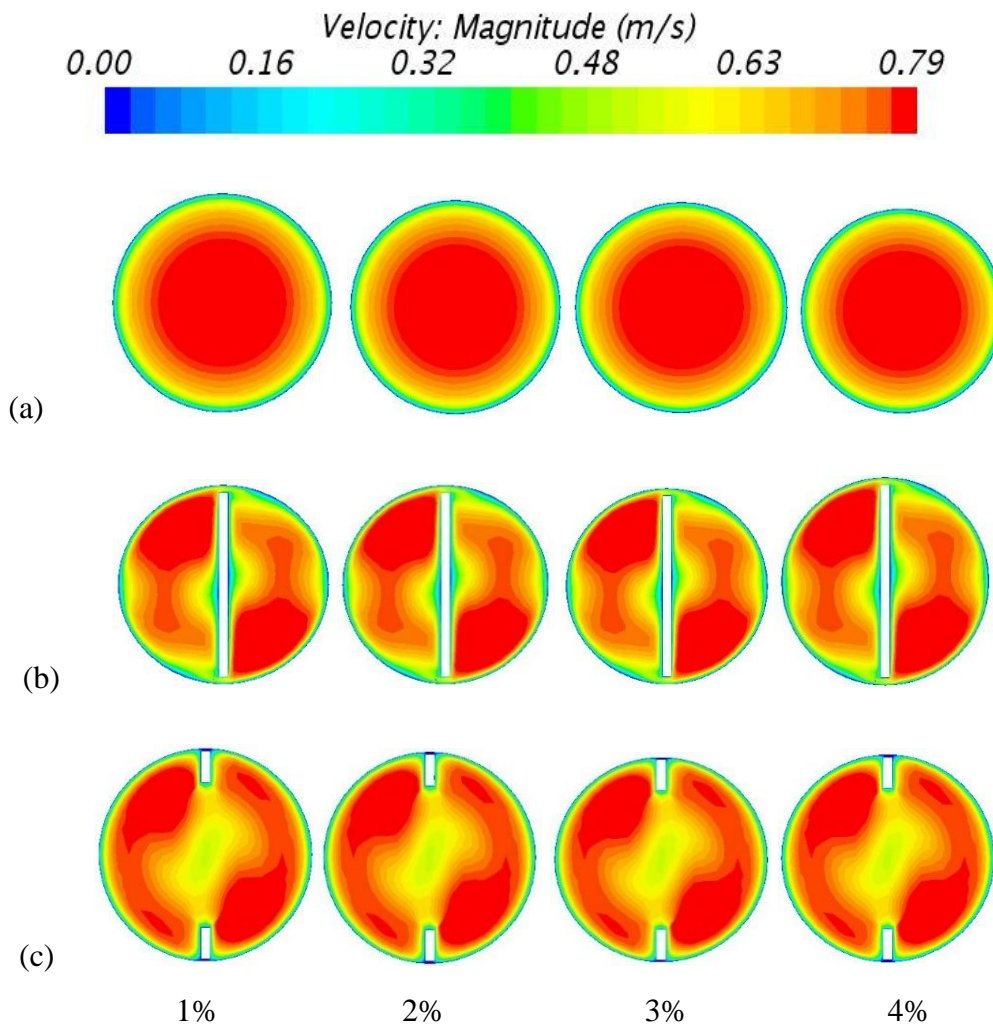
Figure 4-5 Velocity contour for hybrid nanofluid (Al$_2$O$_3$-Cu/water) in different concentrations located at X = 0.57m and Re = 7000 of (a) PT, (b) TPT, and (c) TECT.

4.6.3 Turbulent kinetic energy

In Figure 4-6, different concentrations of hybrid-nanofluid (Al_2O_3-Cu/water) at X= 0.57m are depicted at various locations on the turbulent kinetic energy at Re = 7000. The kinetic energy of turbulent flow is greatest closer to the wall, as is depicted in PT Figure 4-6 (a). Because of the low flow velocity caused by the no-slip situation on the pipe wall [88]. The kinetic energy of turbulent flow is peaked near the tape surface when twisted tape is inserted inside an ordinary pipe as seen in TPT Figure 4-6 (b). This is caused by the existence of the tape, which creates turbulent boundary layers [88]. Due to the elliptical cuts on the twisted tape, the boundary layer disruption in the domains rises compared to TPT. There is agreement between this result and that of Ahmadi et. al. [44].
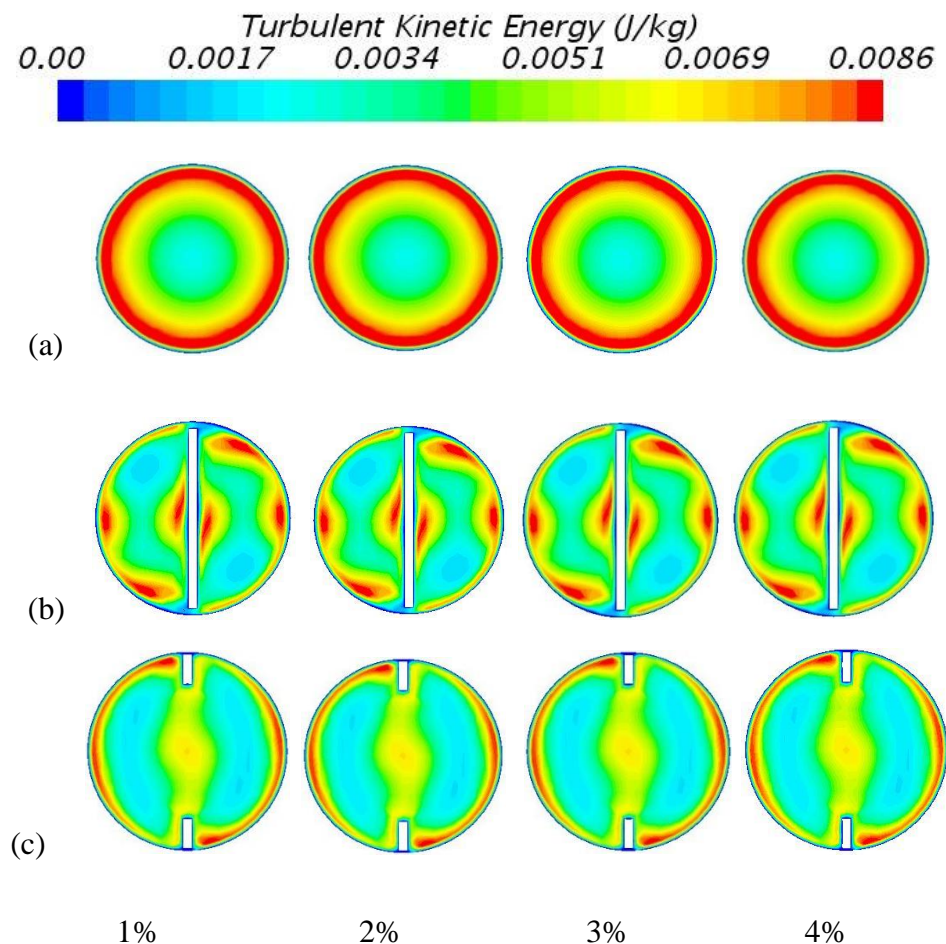
Figure 4-6 Contours of turbulent kinetic energy for hybrid nanofluid (Al_2O_3-Cu/water) in different concentrations located at X = 0.57m and Re = 7000 of (a) PT, (b) TPT, and (c) TECT.

4.6.4 Heat transfer

Heat transmission was assessed using the Nusselt number in this section. Figure 4-7 illustrates the impact of different nanoparticle concentrations on the Nusselt number at a Reynolds number of 7000 for TECT. Furthermore, as displayed in Figure 4-7, the Nusselt number enhanced as nanoparticle concentration was increased. Moreover, when hybrid nanofluid (Al_2O_3-Cu/water) is applied, heat transmission is enhanced in comparison with CuO/water nanofluid [44]. In the figure below $\emptyset$ = 4%, the hybrid-nanofluid (Al_2O_3-Cu/water) has a Nusselt number of 195, which is approximately 3.9% superior to the nanofluid (CuO/water) [44]. In accordance with [191], this is due to an excess of intensity, dynamic viscosity, as well as thermal conductivity.

At various Reynolds numbers, Figure 4-8 (a-d) illustrates the impact of the concentration of nanoparticles on heat transmission in a hybrid Al_2O_3-Cu/water nanofluid flow. In addition, the impact of inserting elliptical-cut and classical twisted tape against plain pipe. Also, higher Reynolds numbers and concentrations of nanoparticles enhance heat transfer. Additionally, PT has a lower Nusselt number than TECT and TPT. Based on [192], this occurs because the Reynolds number causes the turbulence intensity to improve, resulting in the destruction of the boundary layer. Furthermore, as mentioned earlier, a higher concentration of nanoparticles enhances the thermal conductivity for the flow of Al_2O_3-Cu/water, therefore enhancing the rate of heat transmission [191]. Based on the previous numerical investigation [44, 88], the twisted tape accelerates fluid swirling inside pipes, disintegrating thermal boundary layers and improving flow mixing among fluids at both the surface of the wall and the centre. The results in Figure 4-8 (d) demonstrate that at $\emptyset$ = 4% and a Reynolds number of 15000, the rate of heat transmission in TECT and TPT is 1.70 and 1. 57 times greater than that in PT, respectively. Furthermore, TECT is the only system with the highest Nusselt number, 222.
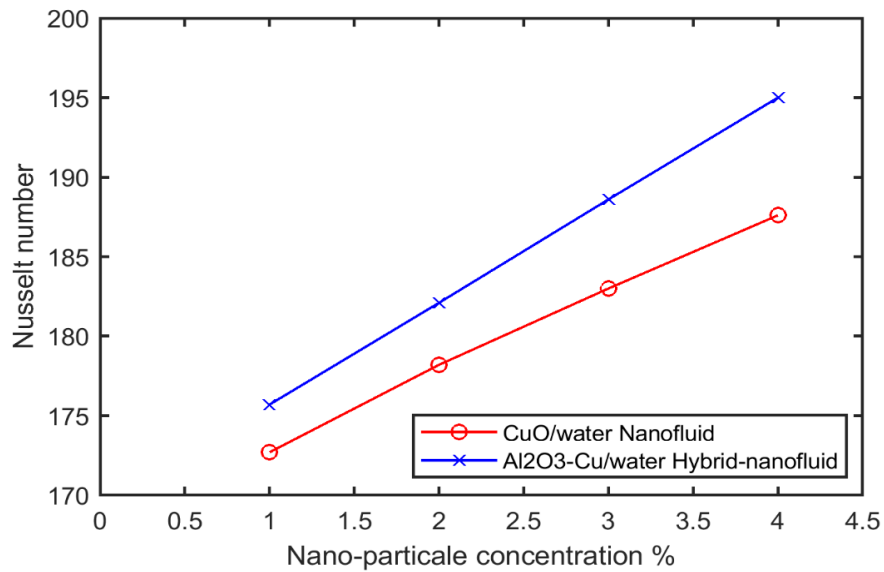
Figure 4-7 The variation of the Nusselt number with the concentration of nanoparticles between Cu/water and Al$_2$O$_3$-Cu/water at Re = 7000.

(a)

(b)

(c)

(d)
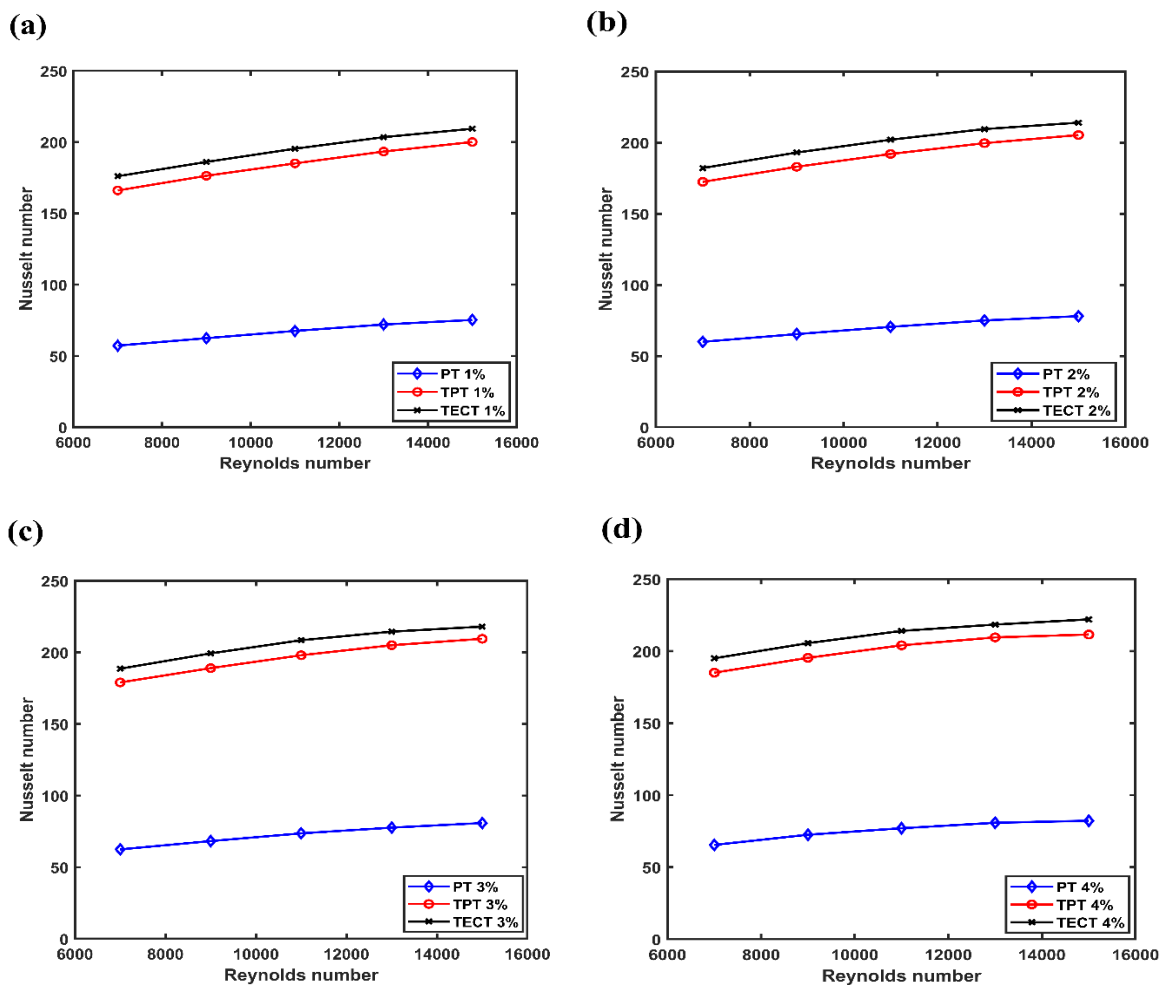
Figure 4-8 Effects of twisted tapes on Nusselt number and Reynolds number with varying concentrations of Al$_2$O$_3$-Cu hybrid nanofluid (a) 1%, (b) 2%, (c) 3%, and (d) 4%.

4.6.5 Friction factor

Figure 4-9 provides a comparison of the friction factor at Re = 11000 with various nanoparticle concentrations for PT, TPT, and TECT. Based on the results of the tests, the friction factor remains constant at all concentrations of nanoparticles. According to[44], friction factors are primarily influenced by Reynolds numbers along with roughness. The friction factor against the Reynolds number for a hybrid nanofluid of Al_2O_3-Cu/water is demonstrated in Figure 4-10 in pipes with elliptical-cut solid twisted tape inserts. Increasing the Reynolds number consistently results in decreasing friction factor. In this scenario, the fluid's viscosity exceeds the Reynolds number, resulting in a reduction in the shear rate between the wall of pipe and the fluid [88]. In pipes with twisted tapes, flow obstruction and swirl flow cause a greater friction factor than in ordinary pipe [192]. In the illustration, there is an unanticipated case at a Reynolds number of 7000, in TECT which has the same friction factor as TPT, at approximately 0.208. It is possible that the low vortex flow intensity at Re =7000 in the TECT might be responsible for this phenomenon.
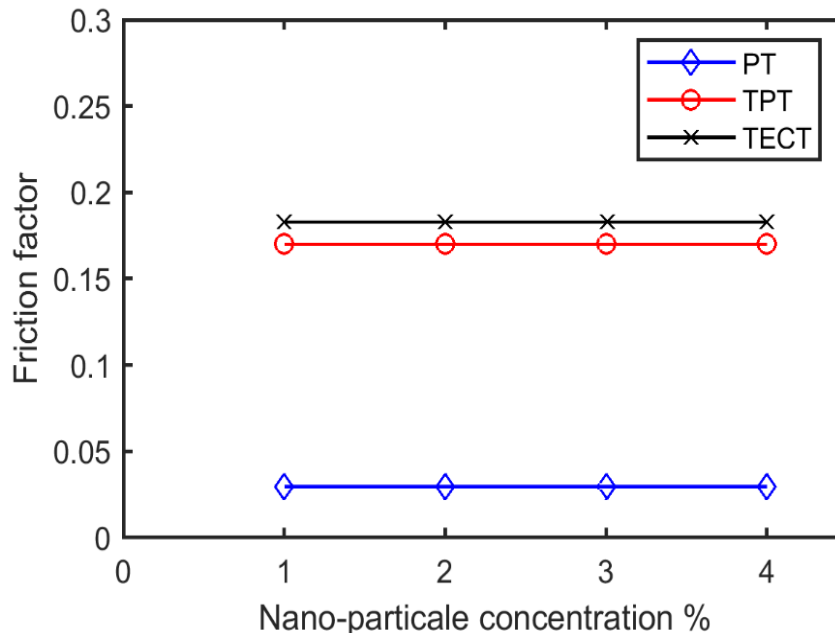
Figure 4-9 Friction factor variation at various nanoparticle concentrations at Re = 11000 for PT, TPT and TECT.
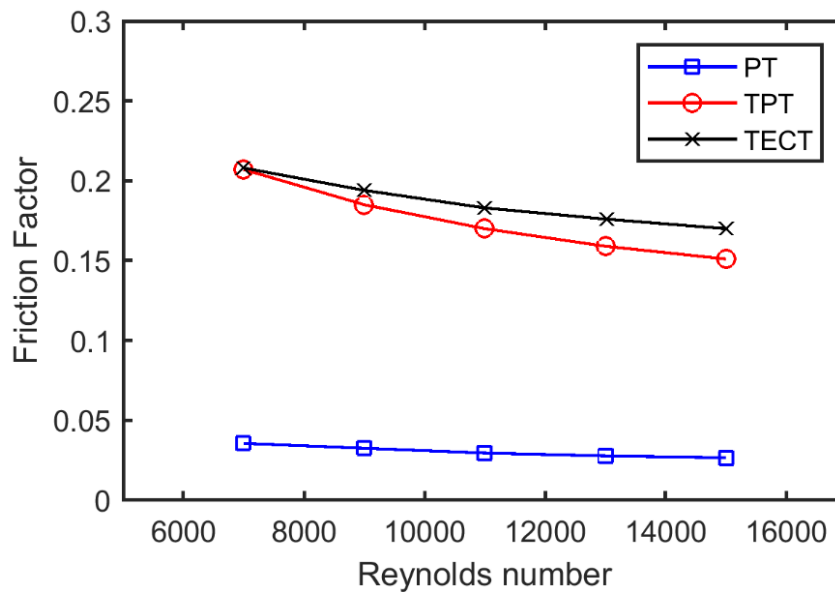
Figure 4-10 Friction factor vs Reynolds number of different tubes.

4.6.6 Thermal performance factor

A comparison of the thermal performance factor between hybrid nanofluids (Al_2O_3-Cu/water) at different mass concentrations is displayed in Figure 4-11, which shows that the factor of thermal performance enhances as the nanoparticle concentration rises. Hybrid nanofluids often exhibit greater thermal conductivity with increasing nanoparticle concentrations, which is accompanied by an increase in viscosity [25]. For the different tube designs and nanoparticle concentrations, Figure 4-12 (a-d) provides a comparison between thermal efficiency fluctuations and Reynolds numbers. It is depicted in the results that there is an increase in the pressure drop performance and the heat transport rate of the twisted tape when the working fluid is a hybrid nanofluid (Al_2O_3-Cu/water). It is also worth noting that the thermal performance factor of TECT is higher than that of TPT. There is no doubt that the performance factor decreases proportionately with increasing Reynolds number. Due to a decrease in pressure when the Reynolds number increases [88]. As demonstrated in Figure 4-12 (d), the maximum factor of thermal efficiency for TECT is about 1.9 at Re =7000 and $\emptyset$ = 4%, which is 7.73% higher than nanofluid for the same geometry.
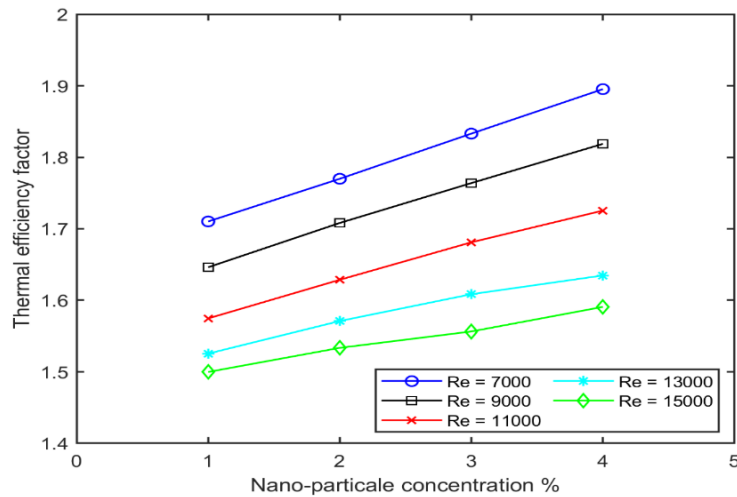
Figure 4-11 Thermal efficiency factor variation of Al$_2$O$_3$-Cu hybrid nanofluid against nano-particle concentration at various Reynolds number for TECT.
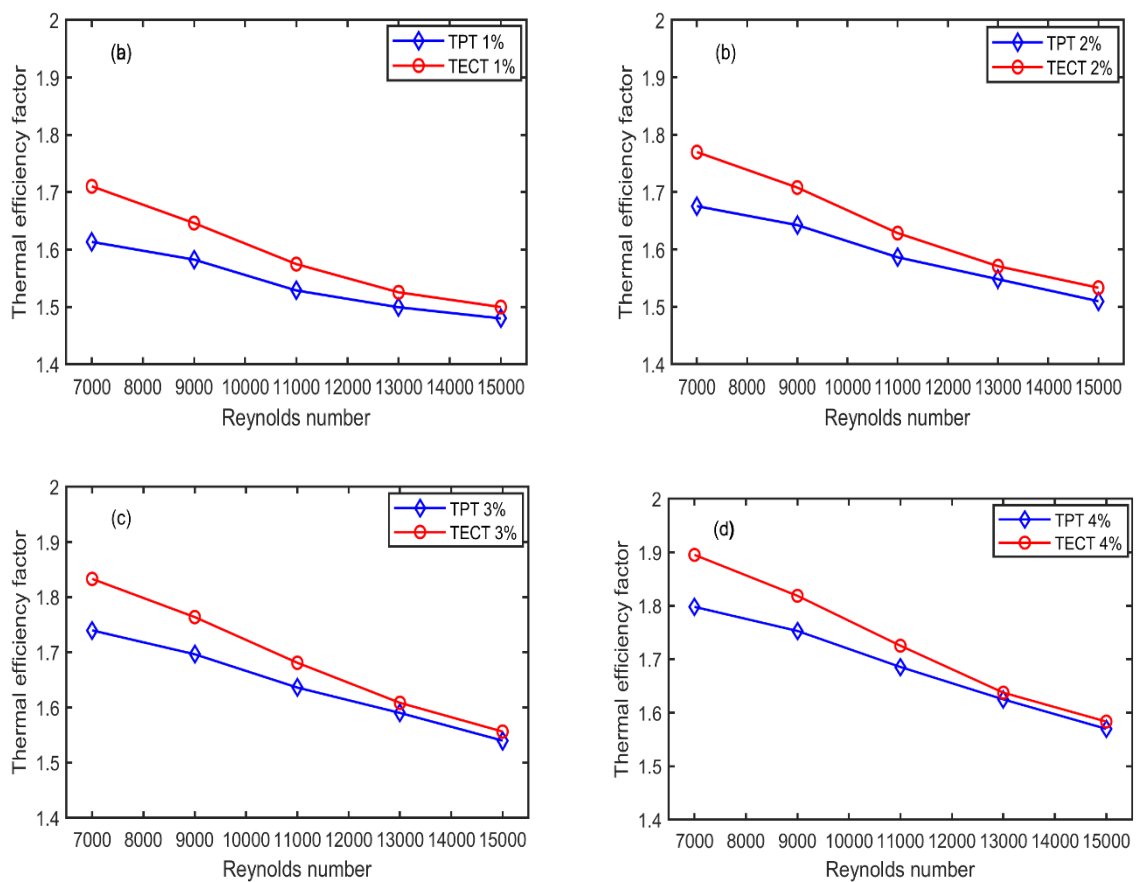
Figure 4-12 The impact of various tube designs with the concentrations of nanoparticles on thermal efficiency factor against Reynolds number (a) 1%, (b) 2%, (c) 3%, and (d) 4%.

63

4.6.7 Entropy generation

The entropy production distribution and Bejan number within an ordinary pipe and a pipe supplied with elliptical-cut and solid twisted tape inserts have been numerically studied for water, hybrid-nanofluid (Al$_2$O$_3$-Cu/water), and nanofluid (CuO/water) at $\emptyset = 4\%$. For different configurations at Re = 7000, entropy production impacts are also presented (Figure 4-13 - Figure 4-16). The production of entropy in thermal systems occurs as a result of heat transmission caused by a temperature difference. Furthermore, it is also caused by irreversible kinetic energy dissipation as a result of fluid friction [183]. This study aims to examine the influence of fluid friction and heat transmission effects on the production of entropy, in an ordinary pipe and pipe supplied with elliptical-cut and solid twisted tape inserts.

4.6.7.1 The local entropy production

A diagram showing the local entropy production grew is displayed in Figure 4-13 and Figure 4-14. The thermodynamic irreversibility of the process due to heat transfer and fluid friction were analysed individually in equations 3.40 and 3.41 by using the MATLAB code. The local thermal entropy production distribution is depicted in Figure 4-13. Figure 4-13 displays the spatial distributions of entropy production for different tube configurations, namely plain tube (PT), twisted classical tape (TPT), and twisted elliptical-cut tape (TECT). The entropy production is assessed for water, CuO/water, and Al$_2$O$_3$-Cu/water hybrid nanofluids. Based on our results, it appears that ordinary pipes create the greatest amount of thermal entropy in close proximity to the wall, where gradients of temperature are more pronounced. Nevertheless, incorporating elliptical-cut and solid twisted tape into the pipes has a significant influence on the production of entropy, as shown for TECT and TPT, where the twisted tape produces a powerful swirling motion between the twisted tape surface and the tube wall, resulting in an increase in thermal entropy. When nanoparticles are added to water, there is a decrease in thermal entropy production. This is to be anticipated due to the improved viscous effects in the vicinity of the near wall, as well as the greater fluid velocity because of the twisted tape. This is consistent with those found in Ref [193]. This is evident in Figures (4-13 - 4-16) (a) is that the production of thermal entropy in TECT and TPT is lower than that in the PT. The reason for this is that TECT and TPT perform better than PT in terms of heat transmission [194]. It is apparent that, the production of thermal entropy reduces with an increase in swirl flow. In the TECT, for example, intensifying swirling flow leads to a decline of the rate of entropy

production of approximately 14.8% and 80% in comparison to the models of TPT and PT, respectively.

Figure 4-14 shows the localised production of the frictional entropy. This figure shows the spatial distributions of entropy production by water, CuO/water, and AL2O3-Cu/water for various tubes PT, TPT, and TECT. As can be seen in Figure 4-14, the PT exhibits high entropy adjacent to the wall as a result of a strong velocity gradient orthogonal to the wall. Furthermore, in TECT and TPT, frictional entropy production displays substantial growth in the vicinity of the rotational axis of the elliptical-cut and classical twisted tape. A major contributing factor to this increase is the development of large gradients in flow velocity by using twisted tape in this area. These gradients are generated by sudden changes in vortex flow direction and tend to reach very high values. As dynamic viscosity increases, frictional entropy is observed to increase as well (see Eq. 3.40 in section 3.5.1). Moreover, frictional entropy is predominant at the pipe inlet, where velocity gradients are high [183].

Figure 4-15 (b) and Figure 4-16 (b) illustrate an important characteristic of TECT geometry that results in enhanced heat transmission, while reducing viscous entropy generation. By adding nanoparticles to the mixture, the velocity gradient increases and disturbances are caused, thus increasing frictional entropy generation [195]. However, twisted tapes minimize thermal entropy [196].
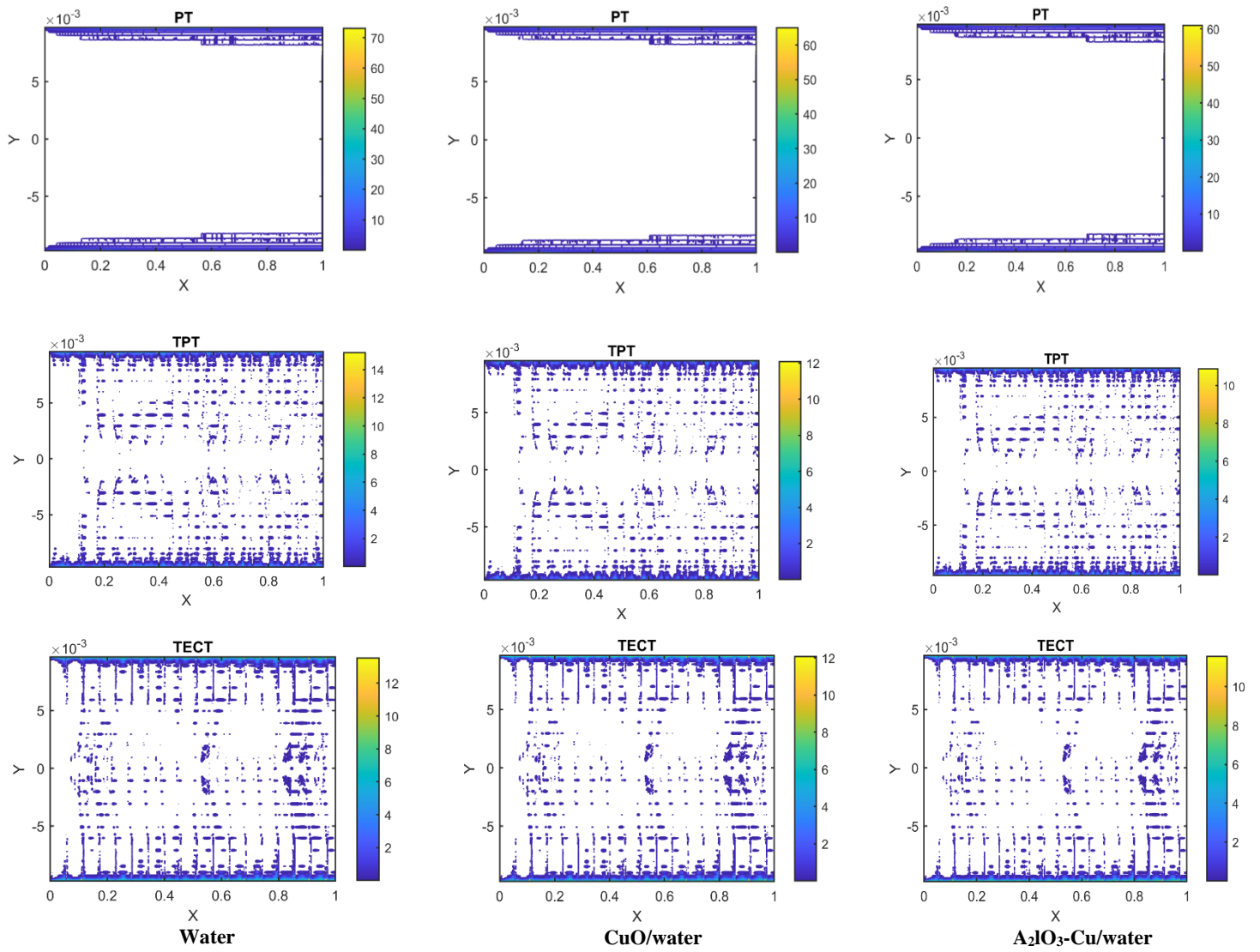
Figure 4-13 Thermal entropy production spatial distribution.
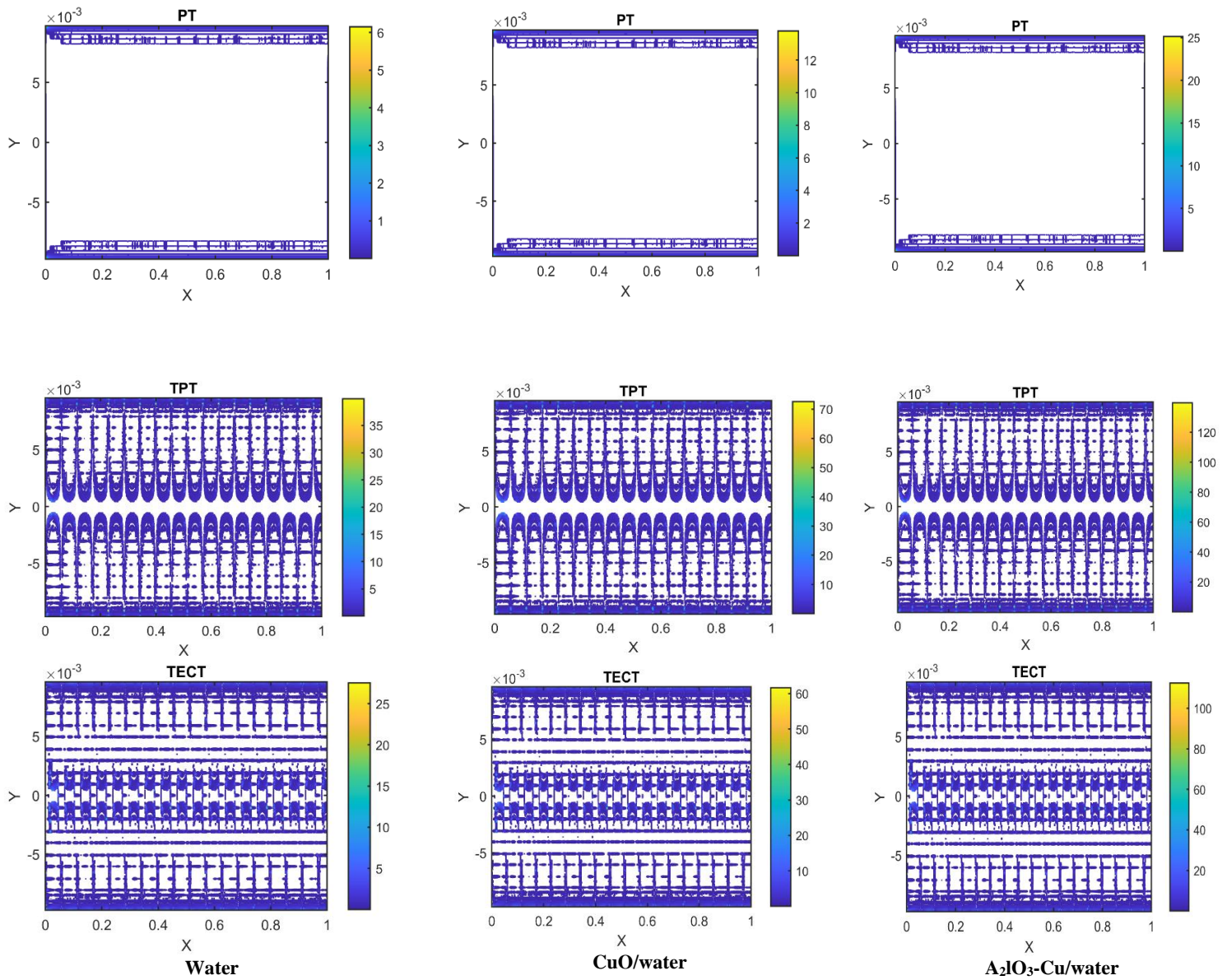
Figure 4-14 Frictional entropy production spatial distribution.

4.6.7.2 Total entropy production and Bejan number

Fluid friction and heat transfer contribute to the total amount of entropy generated. Figure 4-15 and Figure 4-16 illustrate the production of total entropy for three types of fluid flows: Al_2O_3-Cu/water, CuO/water, and water, as well as three types of configurations (PT, TPT, and TECT). The concentration of nanoparticles is at $\emptyset = 4\%$ and the Reynolds number is 7000. In addition, the total entropy generation for different values of heat flux on the wall of the absorber pipe of 600 and 4000 Wm^{-2} is shown in Figure 4-15 and Figure 4-16, respectively.

In Figure 4-16, it is evident that nanofluid and hybrid-nanofluid minimize the production of total entropy. Increasing the volume fraction of nanoparticles will decrease total entropy creation, as stated in [193, 195, 197]. Furthermore, Figure 4-15 indicates that the total entropy production in TECT is a little less than that in TPT. As a result of the analysis, the dimensions of the cut within the twisted tape play a significant role in the generation of total entropy. Consequently, tape with elliptical cuts could reduce entropy considerably by contributing to a high swirl flow. As reported by [198, 199], the production of entropy decreases as the vortex intensity is decreased. Therefore, when hybrid nanofluid is present, the vortical flow leads to further decreases in the creation of total entropy. Because of its high thermal conductivity, hybrid nanofluid contributes significantly to improving heat transmission when used with twisted tape or cut twisted tape, as previously discussed. This is derived from the fact that both elliptical-cut and classical twisted tape enhance swirling flow. Thus, swirling flows have a significant impact on temperature gradients and, therefore, on thermal entropy production and, in the end, on total entropy production. As illustrated in Figure 4-16 (c), when nanoparticles are added to the basis liquid, the creation of total entropy is reduced. Another point of Figure 4-15 and Figure 4-16 are that at low heat flux of 600 Wm^{-2}, the fluid friction is dominant, and at high heat flux of 4000 Wm^{-2} the heat transfer is dominant.

Figure 4-17 shows the effect of the Bejan number on PT, TPT, and TECT for water, CuO/water nanofluid, and Al_2O_3-Cu/water hybrid-nanofluid, (a) at a heat flux of 600 Wm^{-2}, and (b) at a heat flux of 4000 Wm^{-2}. The Bejan number is an irreversibility distribution parameter that indicates the ratio between irreversibility thermal and total irreversibility entropy production rates. Cimpean et. al. [200] define the Bejan number as a value between 0 and 1. $Be = 1$ denotes the point at which irreversible heat transmission prevails, $Be = 0$ denotes the point at which irreversibility is dominated by fluid friction effects, and $Be = 0.5$ denotes the point at which the rates of heat transfer and fluid friction entropy generation are equal [201]. The data gathered

revealed that the Bejan number decreases rapidly with increasing vortical flow, as well as when nanoparticles are added, as shown in Figure 4-17 (a). This is caused by low heat flux, as indicated by Magherbi et. al. [202], due to the commencement of convective heat transfer. The findings indicated that the Bejan number ranges from 0 to 1, $0 < Be < 1$. Figure 4-17 (b) for a heat flux of 4000 Wm^{-2}, the Bejan number is close to 1 because the thermal entropy generation is prominent.
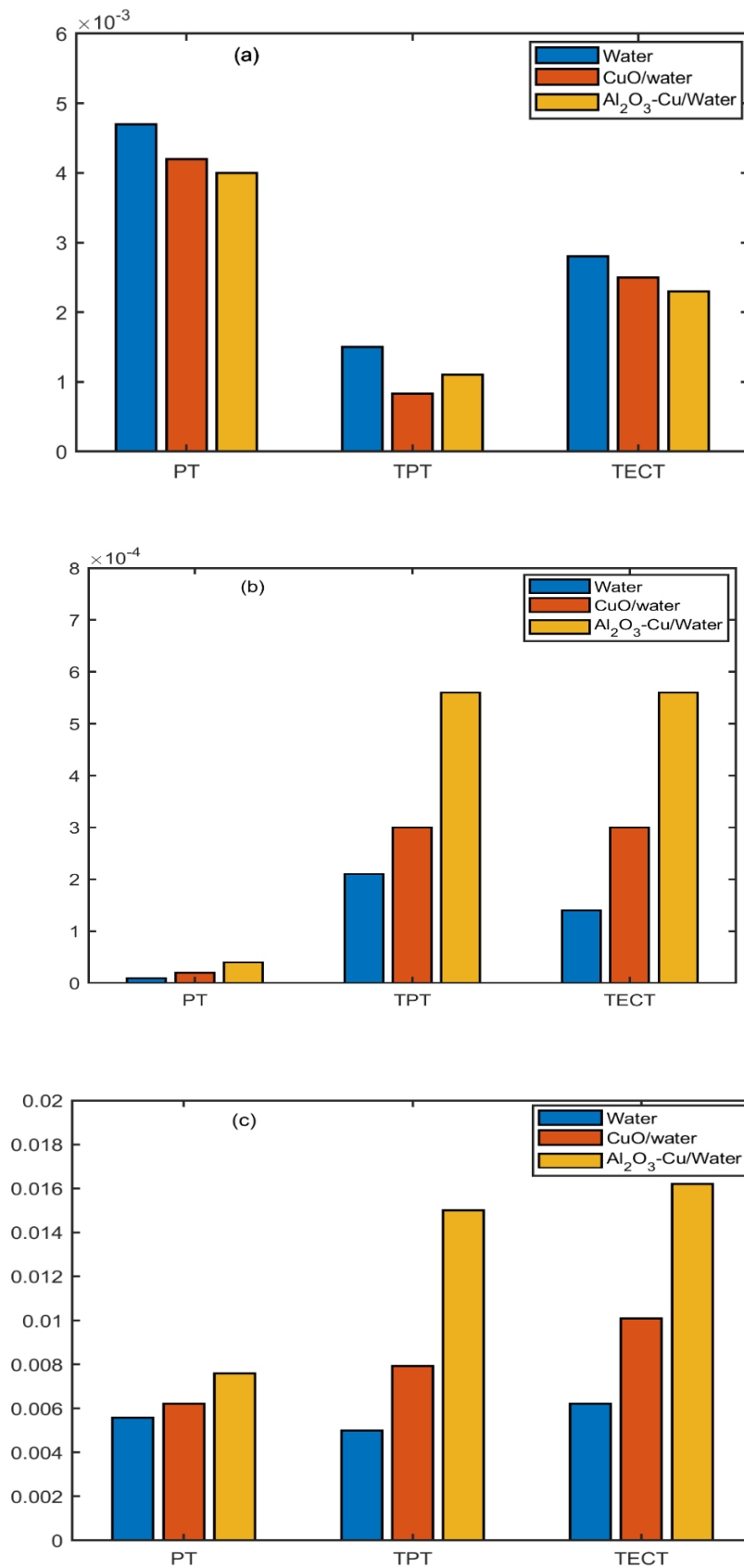
Figure 4-15 The influence of (a) entropy creation due to heat transfer (b) entropy creation due to fluid friction (c) creation of total entropy, at heat flow of 600 Wm^{-2}.
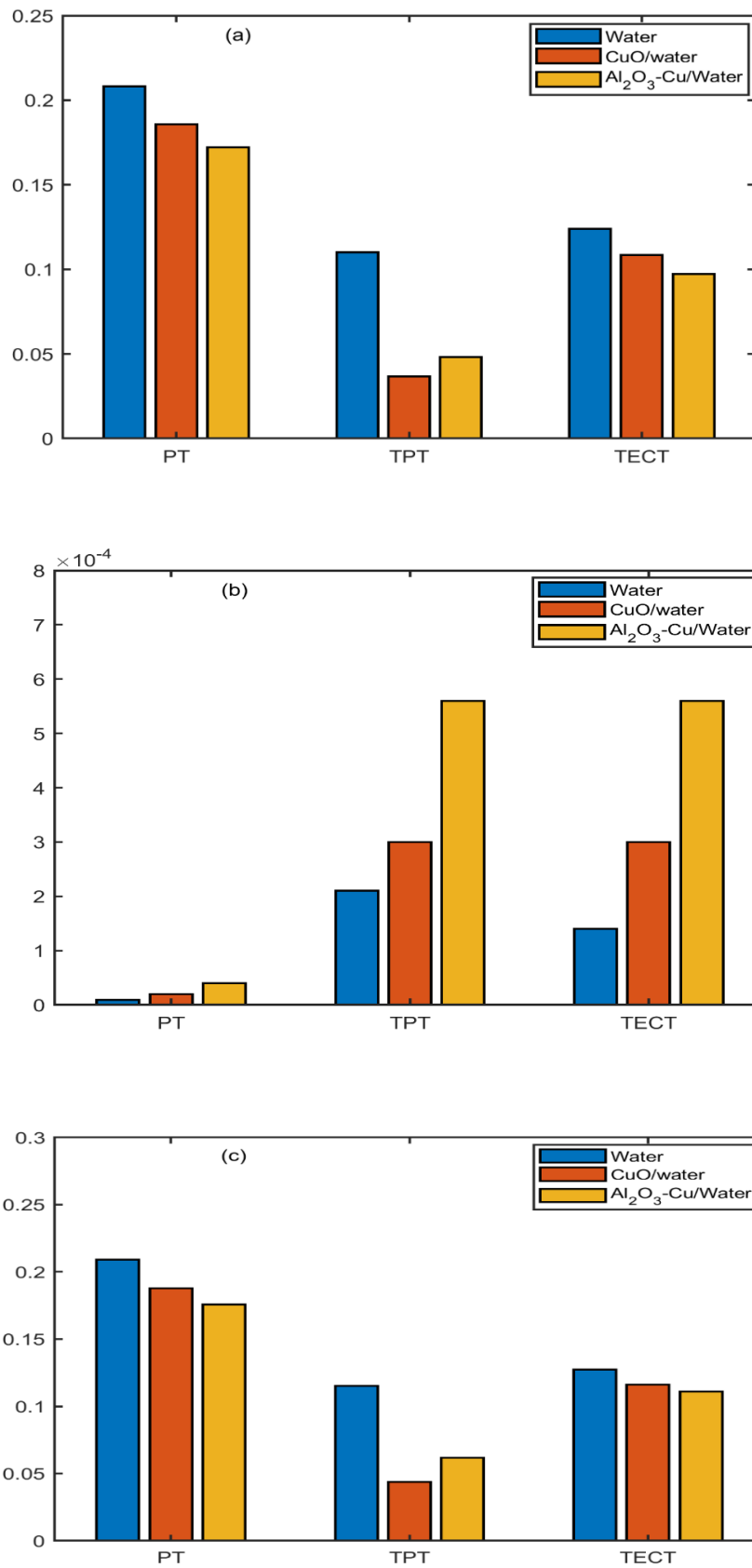
Figure 4-16 The influence of (a) thermal entropy creation (b) fractional entropy creation (c) creation of total entropy, at heat flow of 4000 Wm^{-2}.
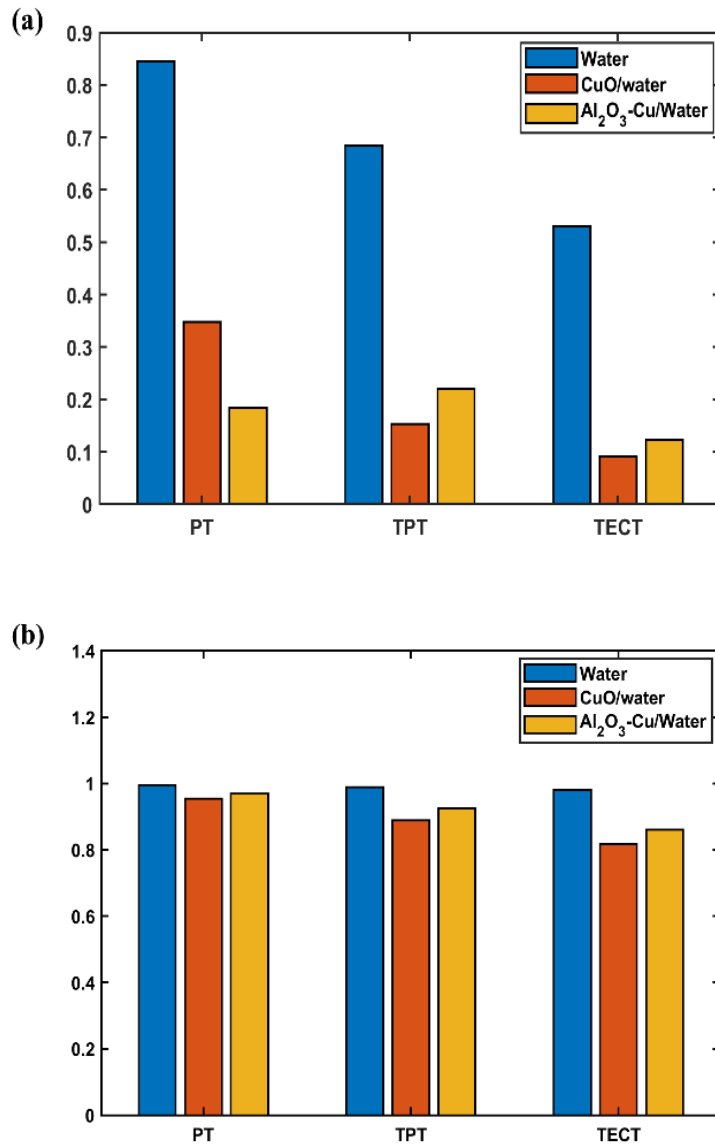
Figure 4-17 Influence of water, CuO/water, and Al₂O₃-Cu/water of PT, TPT, and TECT on Bejan number at heat flow of (a) 600 Wm^{-2} and (b) 4000 Wm^{-2}.

4.7 Conclusions

In this study, classical twisted tape inserts and elliptical-cut tape inserts were employed to calculate the rate of heat transmission Augmentation and entropy production as well as the Bejan number for turbulent hybrid nanofluid (Al_2O_3-Cu/water) flow inside a tube. In order to determine the rate of heat transmission, parameters such as thermal efficiency factor, friction behaviour, as well as nanoparticle volume fraction were studied. To do this study, Reynolds numbers ranging from 7000 and 15,000 were calculated. For the purpose of assessing the effects of parameters including nanoparticle volume fraction, elliptical-cut and solid twisted tape inserts, and a variety of entropy production types (viscous, thermal, and total) on entropy production, calculations were conducted at Reynolds numbers of 7000. Following is a summary of the results obtained:

- Heat transfer is promoted passively by inserting elliptical cut and solid twisted tape into a pipe, leading to a higher rate of heat transmission than that of a plain pipe.

- The Nusselt number of hybrid-nanofluid for TECT reaches 195, or approximately 3.9% higher than the nano-fluid Nusselt number at Re = 7000 and ($\emptyset = 4\%$).

- The Nusselt number of TECT is 1.7 times greater than PT, whereas the Nusselt number of TPT is 1.57 times higher than that of PT. With the Reynolds number of 15000 and at $\emptyset = 4\%$, the hybrid-nanofluid (Al_2O_3-Cu/water) has the highest Nusselt number of 222.

- TECT has a thermal performance factor 1.1 times higher than TPT. This is a consequence of the Nusselt number being much higher in TECT than in TPT.

- As the nanoparticle concentration increases from 1 to 4%, the thermal performance factor of TECT increases. However, as the Reynolds number increases, the thermal performance factor decreases.

- For the Al_2O_3-Cu/water at a Reynolds number of 7000, and $\emptyset = 4\%$, the thermal efficiency factor in TECT is about 1.9 which is 7.73% higher than for the CuO/water

- By utilizing hybrid nanofluids, both thermal performance and heat transfer rate improve 7.73% and 3.9%, respectively. This demonstrates the substantial improvement achieved through hybrid nanofluid incorporation in the system.

- For all geometries, the production of thermal entropy rate near the tube wall is much greater than that at the centre. Using elliptical-cut or solid twisted tape influences the

swirl flow strength near the tape surface and the wall, which results in an increase in temperature gradient.

- The incorporation of nano particles in the heat transfer process has proven to be effective in improving heat transfer rates, enhancing the thermal efficiency factor, and reducing entropy generation, with significant improvements observed as the nano particle concentration increased from 1% to 4%.

- Frictional entropy production increase by introducing a twisted tape into the pipe, as well as increasing thermal conductivity, however, the production decreases when the tape is elliptical-cut.

- When the nanoparticle concentration is increased, it can lead to enhanced heat transfer and improved fluid dynamics within the system. This improved efficiency in heat transfer reduces the energy dissipation and therefore decreases the total entropy generation. Essentially, the increased nanoparticle concentration allows for more effective energy transfer, resulting in a reduction in the overall entropy generation.

- Compared to classical twisted tape, elliptical cut twisted tape generates a stronger eddy flow. Therefore, total entropy generation decreases a bit.

- The production of entropy due to heat transfer dominates at low heat flux, while the production of entropy due to fluid friction dominates at high heat flux.

Chapter 5 Time-dependent analysis of heat transfer enhancement and entropy generation of hybrid nanofluids in a tube with a solid and elliptical-cut twisted tape insert.

5.1 Introduction

Solar receiver tubes are an important part of the system of parabolic trough solar thermal production that converts solar radiation to thermal energy, accounting for about 30% of the material costs associated with the building of a solar field [12]. Solar thermal energy can be employed effectively in a variety of applications, including solar water heating systems, solar chemistry [15], solar desalination plants, and concentrating solar power plants [16]. Recently, solar-thermal engineering has focused on optimising parabolic trough concentrators for industrial applications. In parabolic trough tubes, excessive absorber tube circumferential temperature variations produce thermal strains and may damage the receiver's glass cover [203]. Several investigations on receiver thermal performance have demonstrated that greater absorber tube temperatures lead to increased receiver thermal losses [204, 205]. It is also expected that high optical efficiency and concentration ratios would result in large heat fluxes and circumferential temperature differences in absorber tubes [162]. As a result, better heat transmission efficiency is required to minimize absorber piping temperature gradients and increase receiver performance and reliability.

Numerous experimental and numerical investigations, as described in Chapter 2, have been conducted to improve heat transfer and achieve greater performance in tubes by utilising twisted-tape inserts, uniform heat flux, and steady flow [44, 66-68, 88, 96]. The transient heat transmission for pipes with twisted tape inserts has not been addressed, despite several analytical solutions and experiments having been documented for the steady state heat transfer. Therefore, transient thermal analysis for parabolic trough solar collector tubes is crucial for using solar thermal energy with varying solar radiation. However, most researchers have only examined this heat transfer improvement utilising twisted tape under steady-state conditions: uniform wall temperature or uniform heat flow.

Most of the research on the performance analysis of tubes with or without twisted tape are based primarily on the first law of thermodynamics, which does not provide a conception of the energy quality produced by parabolic trough systems. The use of the second law is often

advised for determining the quality of energy from a system and optimising the thermal system and its components [39]. Numerous studies on entropy generation have been conducted using heat transfer augmentation techniques.

Although this numerous research has been conducted, no aspect of them has been examined: First, using twisted tape in parabolic trough collector tubes has not been analysed by transient heat transfer enhancement. Except for Kobe university researchers [139, 140, 206-212], who investigated transient heat transfer enhancement for helium gas flowing over a twisted plate in a very high temperature reactor (VHTR). Second, the transient heat transfer enhancement with non-uniform heat flux has not been investigated. Also, there has been no research on how to improve transient heat transfer in parabolic trough receivers with twisted tape inserts and non-uniform heat flux. Third, apart from Mwesigye [170], who examined the formation of minimum entropy in a parabolic trough receiver with non-uniform heat flux, no research on entropy production owing to transient heat transfer enhancement in the parabolic trough receiver with or without twisted tape, as well as non-uniform heat flow, has been conducted. Not only that, but there is also a severe lack of study on the specifics of a parabolic trough receiver's internal transient heat transport enhancement. Finally, so far, thermodynamic irreversibility has only been studied in a pipe supplied with elliptical-cut as well as classical twisted tape inserts in a steady state and uniform heat flow in our previous work [155].

In this chapter, numerical analyses were performed to investigate the transient heat transmission enhancement and the analysis of entropy production for the turbulent flow of water, nanofluid (CuO/water), and hybrid-nanofluid (Al_2O_3-Cu/water) with a volume concentration of 2% in PT, TPT, and TECT with non-uniform heat flow, to determine which tube and fluid flow provides the best performance and minimises entropy generation. Further, the hybrid nanofluid (Al_2O_3-Cu/water) was applied at concentrations ranging from 1% to 4% for TECT. The realizable k-ε model is employed to simulate turbulent flow with a Reynolds number of 20000.

5.2 Simulation method verification

5.2.1 Physical model and boundary conditions

The following physical models were defined and implemented in the STAR-CCM+ software: Three Dimensional, Implicit Unsteady (suitable for water, nanofluid and hybrid-nanofluid), Segregated Flow temperature, The Reynolds Averaged Navier-Strokes. The turbulent flow

simulation is carried out employing the realizable k-ε turbulence model. The two-layer model with all y+ wall function implemented in STAR-CCM+ is employed for near wall parameters. This technique has the potential to provide an accurate assessment of near wall viscous flow. A transient simulation with a time step of $\Delta t = 0.001$ sec is performed to get a higher degree of temporal accuracy.

The boundary conditions employed in this investigation were as follows:

(1) In Figure 4-1, the geometry of the model is described as ordinary pipes (PT) and ordinary pipes with elliptical-cut (TECT) or solid (TPT) twisted tape inserts.

(2) Non-uniform heat flow on the outside wall of the absorber pipe, the receiver angle (θ) was 40°. The distribution of local concentration ratios and the distribution of heat flux utilised in this investigation are displayed in Figure 5-3 and Figure 5-4, as determined by Eq. 5.1.

$$q = h(T_{ri} - T_b) \tag{5.1}$$

For turbulent flows, the heat transfer coefficient in STAR-CCM+ as in Eq. 5.2.

$$h = \frac{\rho_f\, C_{p.f}\, u}{T} \tag{5.2}$$

$$q = \frac{\rho_f\, C_{p.f}\, u}{T}(T_{ri} - T_b) \tag{5.3}$$

Here, T is the reference temperature.

(3) Both the wall of the pipe and the surface of solid and elliptical twisted tape are non-slip surfaces.

(4) The fluid enters the pipe at a temperature of 298.15K [134] and Reynolds number is 20,000.

(5) Water, nanofluid (CuO/water), and hybrid nanofluid (Al$_2$O$_3$-Cu/water) are used as the working fluids. Nanoparticle volume concentration is $\emptyset = 2\%$.

(6) Al$_2$O$_3$-Cu/water hybrid nanofluid was applied as the working fluids at different volume concentration from 1% to 4% for TECT.

(7) The thermophysical characteristics of hybrid-nanofluid are determined in Chapter 4.

5.2.2 Grid independence test

An investigation of the grid independence of numerical computations was performed for temperature as a monitored quantity by using four sizes of various mesh for PT, TPT, and TECT before settling on a mesh size of 842500, 2779954, and 4661961 cells, respectively. Figure 5-1 demonstrates the temperature test results for the grid resolution. The values of temperature obtained in grids with total cell counts of 665000, 742500, and 842500 differ by 0.6%, 0.9%, and 1% from those found in a grid with 527744 cells, respectively, in the PT (frame (a)). The TPT (frame (b)) indicates a difference of 0.7%, 0.9%, and 1.19% when comparing the temperature readings of grids containing 1581729, 2211149, and 2779954 cells to those of grid containing 1171427 cells. In TECT (frame (c)) there is alteration of 0.58 %, 0.88 %, and 1.1% when comparing the temperature readings in grids with 3834556, 4046985, and 4661961 cells to those in grid with 3426964 cells.

Courant number analysis in Eq. 5.4 is necessary because the solutions' stability is critical to accuracy. According to Anderson and Wendt [213], the Courant number should be less than or equal to 1. This is a significant stability criterion for maintaining equilibrium. It limits how long a time step may be or mesh cell size, finer meshes require smaller time steps.

$$Co = u.\frac{\Delta t}{\Delta x} \leq 1 \qquad\qquad (5.4)$$

Here Co is courant number, u is velocity, Δx is the grid cell dimension at each point, and Δt is time-step. Also, an independence of time step investigation regarding unsteady calculation was conducted. Different values of the time steps, (Δt) from 0.01s to 0.09s were selected, resulting in slight variations. The size of time step has been investigated from 0.0005 to 0.0015. When $\Delta t < 0.001$, the influence of the time step size is insignificant.

Time-dependent analysis of heat transfer enhancement and entropy generation of hybrid nanofluids in a tube with a solid and elliptical-cut twisted tape insert.
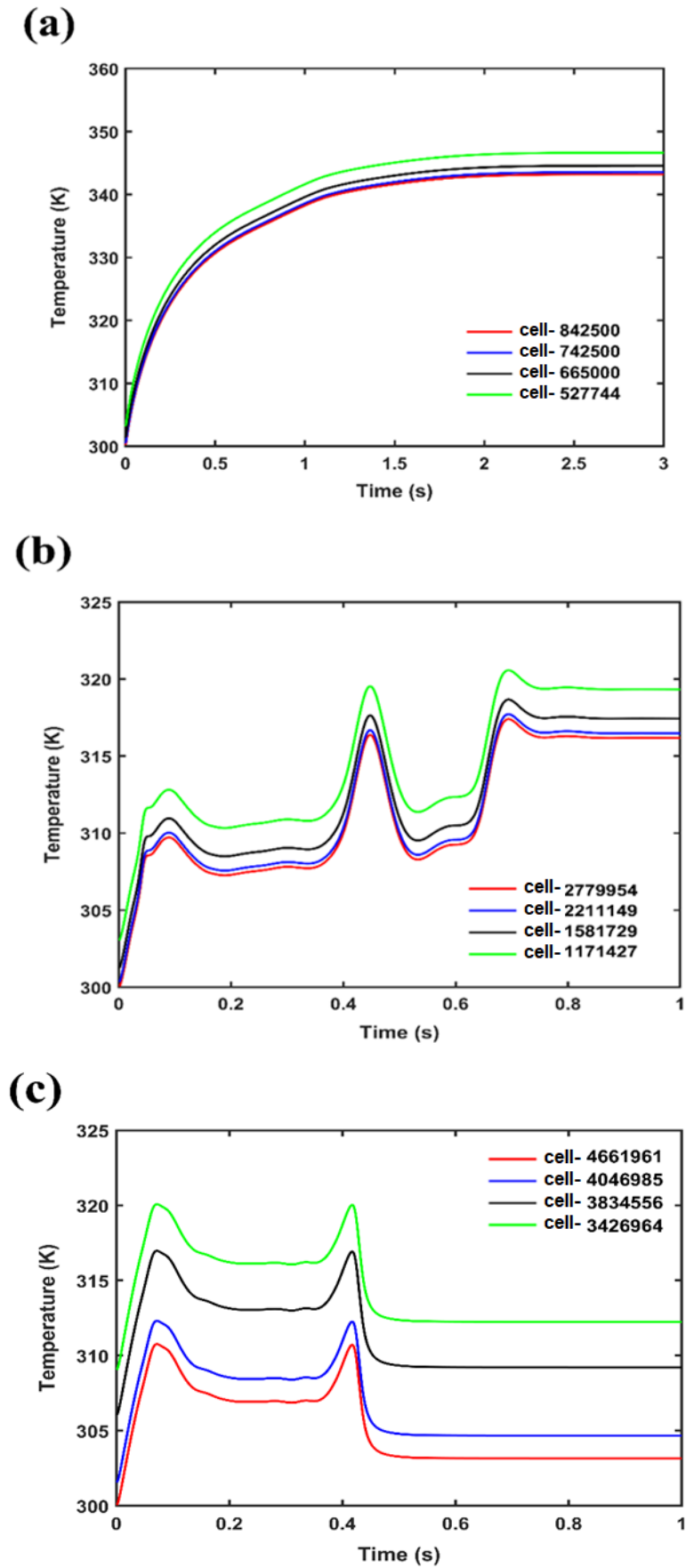
Figure 5-1 Temperature at a selected point in the middle (a) PT, (b) TPT, and (c) TECT.

5.2.3 Model validation

Numerical computations of this study were validated against Ahmet Tandiroglu's work [214], which investigated a turbulent flow with a Reynolds number of 10366. Figure 5 shows that a circular pipe with baffle plate inserts Ahmet Tandiroglu [214] was employed to validate a circular tube (PT) for transient forced convective heat transfer. The investigation was conducted by air as a working fluid with a Prandtl number of 0.71. In Figure 5-2, outlet temperature change curves from this study and the work by Ahmet Tandiroglu [214] are compared. Based on the observed data, it is evident that their similarities are considerable. The temperature variation curve of present work deviated from those of Ahmet Tandiroglu [214] by $\pm 1.3\%$, which are acceptable.
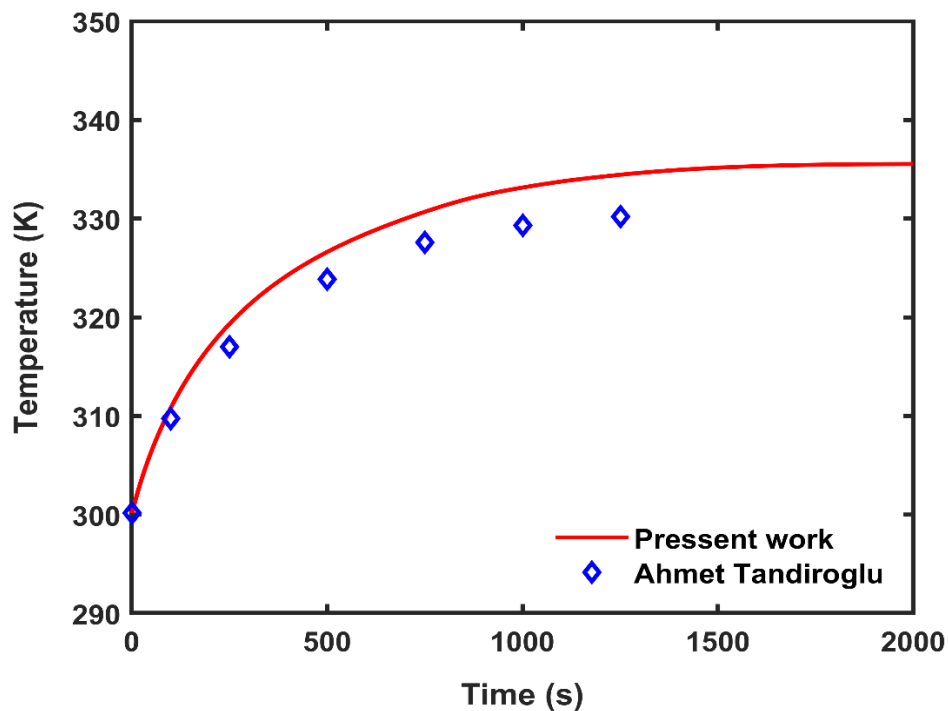
Figure 5-2 The variation of Temperature against time Ahmet Tandiroglu [214].

5.2.4 Local concentration ratio (LCR) distribution

Optimizing the parabolic trough solar collector shape involves analysing the LCR rate on the receiver pipe using Monte Carlo Ray-Trace (MCRT). To validate this approach, numerical results were compared to studies by [170, 215-217]. Jeter [217] focused on the LCR parameter, similar in nature to the distribution of heat flow. The relationship of the two parameters is illustrated in [215, 217] :

$$q = LCR. q_{sun} \qquad\qquad (5.5)$$

The curve in Figure 5-3 can be split into four parts, denoted by 1, 2, 3 and 4 as discussed by He et. al. [215]. Note that the MCRT is resolved under different conditions. Although the calculated results in this chapter are not fully consistent with the results of [215, 217], the changing trends of the curves are extremely similar. As can be seen from Figure 5-3 (b), the calculated results of LCR are consistent with the results of [215, 217] when solar rays are regarded as parallel rays. As well, the LCRs by Marugan et. al. [216] show the same trend. According to the results, MCRT's probability model in this chapter is reasonable.

Time-dependent analysis of heat transfer enhancement and entropy generation of hybrid nanofluids in a tube with a solid and elliptical-cut twisted tape insert.

(a)
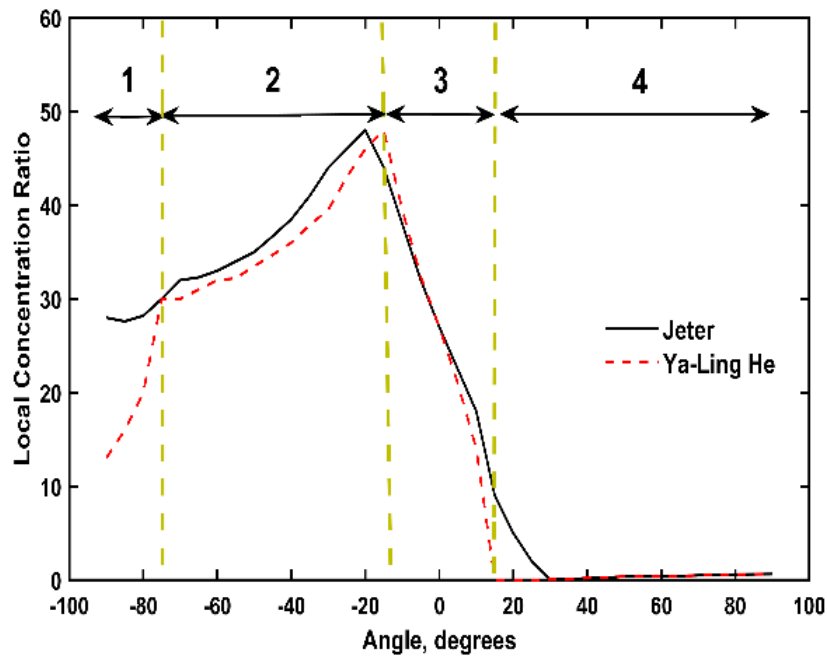
(b)
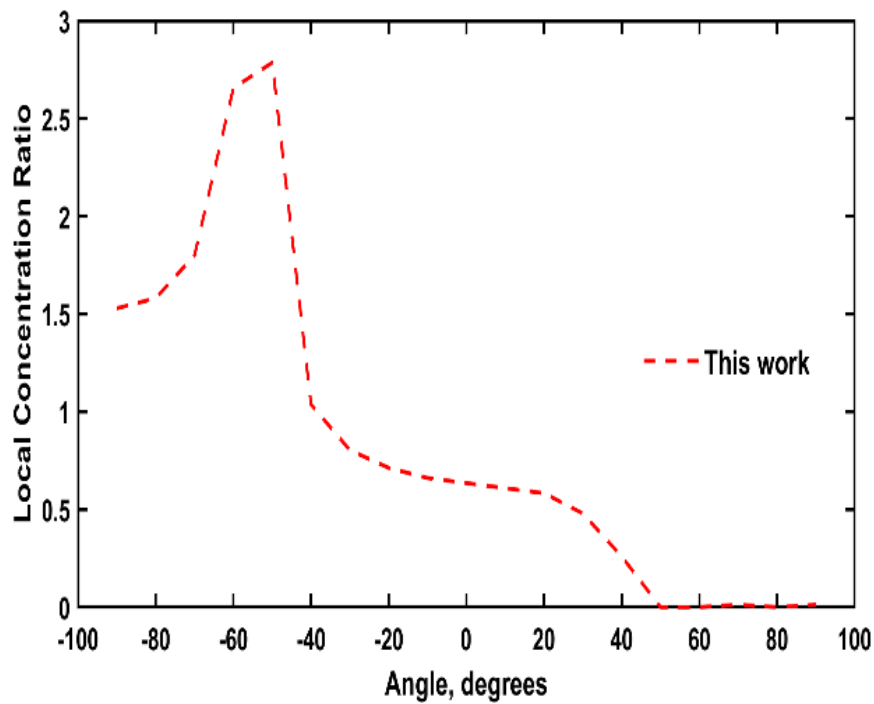
Figure 5-3 Distribution of local concentration ratios.

5.2.5 Distribution of heat flux

The heat flow distribution on the outer surface of the pipe is displayed in Figure 5-4 (a) for PT, (b) for TPT, and (c) for TECT. Due to the symmetry, only one half of the receiver, i.e, $-90^o \leq \theta \leq 90^o$, may be considered. As observed in Figure 5-4, the profile of heat flux around the absorber tube's circumference varies greatly because of the used elliptical-cut and classical twisted tape inserts. In addition, when twisted tape is inserted, the heat flux increases as the collector rim angle increases. The finite temperature difference will be increased because of the increase in peak heat flux. Furthermore, at $\theta > 30^o$, the heat flux profile consists of a direct radiation area (as seen in part 4 in Figure 5-3 (a)). In the case of different fluid flows, hybrid-nonfluids are shown to give high heat flux peaks and will give high absorber tube circumferential temperature gradients. The calculated results in this chapter closely match the receiver results for half the circumference by Mwesigye et. al. [170].

Time-dependent analysis of heat transfer enhancement and entropy generation of hybrid nanofluids in a tube with a solid and elliptical-cut twisted tape insert.

(a)
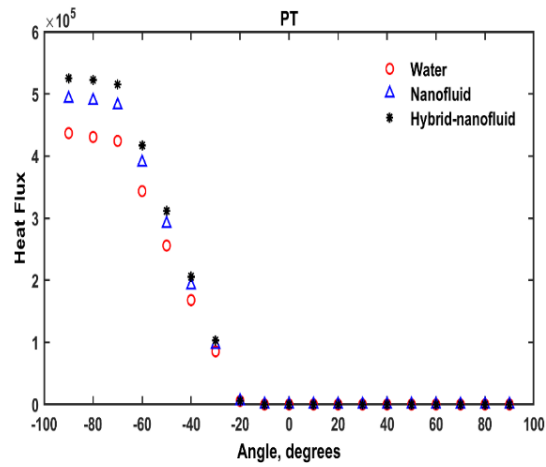
(b)
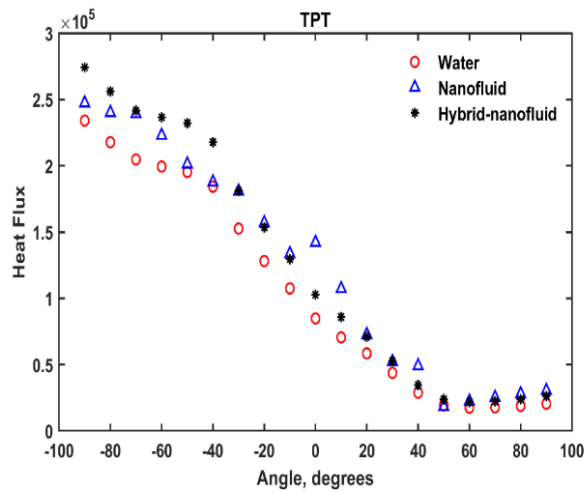
(c)
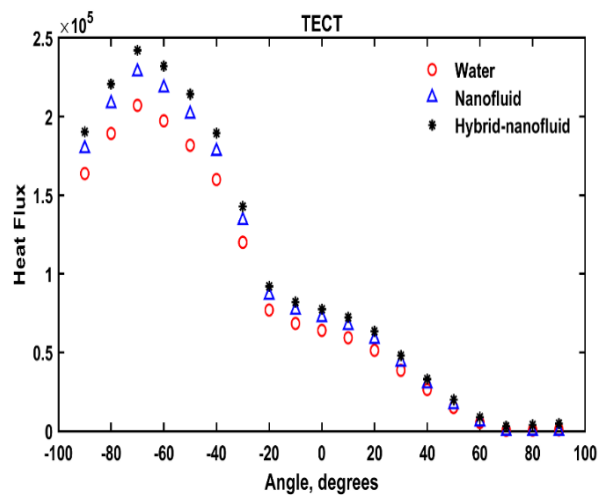
Figure 5-4 Heat flux distribution on circle direction for three different tubes.

Time-dependent analysis of heat transfer enhancement and entropy generation of hybrid nanofluids in a tube with a solid and elliptical-cut twisted tape insert.

5.3 Computational Results and Discussions

This section describes contour plots, transient heat transmission, and entropy production in turbulent flows of water, Cu/water, and Al_2O_3-Cu/water in empty pipes, and pipes with elliptical-cut and classical twisted tape inserts. To give an overview of the temperature contour, velocity contour, kinetic energy distribution in turbulent flows, and the spatial distribution of thermal and frictional entropy generation, four distinct temporal situations were studied for PT (t = 0.01s, t = 0.5s, t = 1s, and t = 3s), TPT (t = 0.01s, t = 0.5s, t =1s, and t = 1.5s), as well as TECT (t = 0.01s, t = 0.5s, t = 1 s, and t = 1.3 s). Furthermore, the results for TECT with hybrid nanofluids (Al_2O_3-Cu/water) at different concentrations are examined.

5.3.1 Temperature contours

Figure 5-5 depicts the contour plots of temperature fields in PT, TPT, and TECT for hybrid-nanofluid (Al_2O_3-Cu/water). To explore the influence of temperature, four distinct temporal situations were studied, as seen in Figure 5-5. PT is (0.01 s, 0.05 s, 1 s, and 3 s), TPT is (0.01 s, 0.05 s, 1 s, and 1.5 s), and TECT is (0.01 s, 0.05 s, 1 s, and 1.3 s). The times in Figure 5-5 (frames A-C) were chosen to demonstrate the temporal evolution of the simulation from 0.01s to 1s. However, Figure 5-5 (frame D) shows the time when the simulation solved the problem. In PT Figure 5-5, the simulation findings reveal that the temperature distribution in the pipe is significantly nonuniform because of a non-uniform flow of heat on the external pipe wall. Compared with PT, the temperature distribution on the TPT and TECT are more uniform at the exit section. One potential reason is that while the liquid is progressively heated along the direction of flow, the plate and elliptical-cut twisted tape help increase the distributions of temperature along the tube length in the flow direction. This allows for better temperature distributions in the tube. In addition, the findings show that the thermal layer near the wall of pipe grows faster in the TPT and TECT than in PT and grows even more over time. From Figure 5-5 (frame D), the temperature for Al_2O_3-Cu/Water in the PT, TPT, and TECT are 330K, 315K, and 320K, respectively. One of the most notable benefits of TPT and TECT, as shown in Figure 5-5, is that the distribution of temperature is considerably more uniform on all surfaces of the tube. From 0.01s to the end of the simulation, the temperature differences of up to 29K, 13K, and 16K occur between PT, TPT, and TECT. This temperature data is very useful for designing, optimising, controlling, and maintaining parabolic trough collectors.
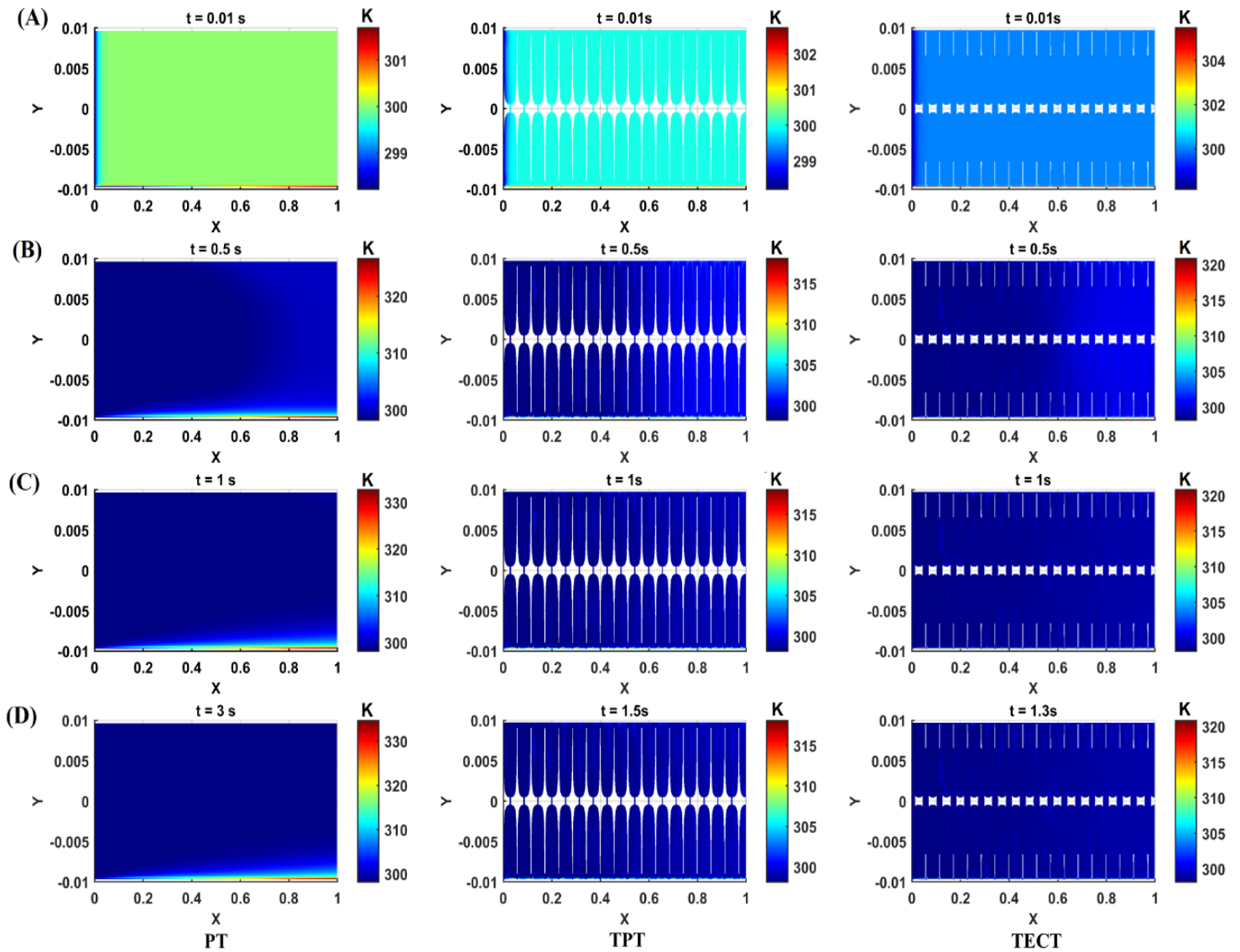
Figure 5-5 Temperature distribution of Al_2O_3-Cu/water hybrid nanofluid flow within PT, TPT, and TECT at various times.

5.3.2 Velocity contours

Figure 5-6 illustrates the time histories of velocity for three unsteady flow conditions (PT, TPT, and TECT) using hybrid-nanofluid of Al_2O_3-Cu/water. The velocity contours over the tube in the fully formed area are displayed to aid in the study of flow behaviour in the presence of elliptical-cut and solid twisted tape. The time were selected randomly in Figure 5-6 (frames A-C), but in Figure 5-6 (frame D), it was the end of the run of the simulation. The result in PT Figure 5-6 illustrates the difference in velocity between various time. As a result, it is seen that at time t = 0.01s, there is a lower vorticity, but the pattern stays the same. However, the velocities in the PT Figure 5-6 (frames B-D), are quite stable, and the highest velocities have settled towards the centre, resulting in the flow being fully developed. Swirl flows are created at the walls of pipe and in the core zone by the TPT and TECT in Figure 5-6. As a result, it promotes more fluid mixing in the interior and in the region immediately next to the walls. The TPT and TECT affect velocity homogeneity because of the whirling flow in this zone. When using TECT, the refraction rises in that zone. Consequently, the velocity gradient rises, allowing for enhanced heat transmission. This is in line with [44, 96]. Overall, as time passes in the unstable flow, the current progressively travels away from the walls and the velocity in the tube's centre rises.
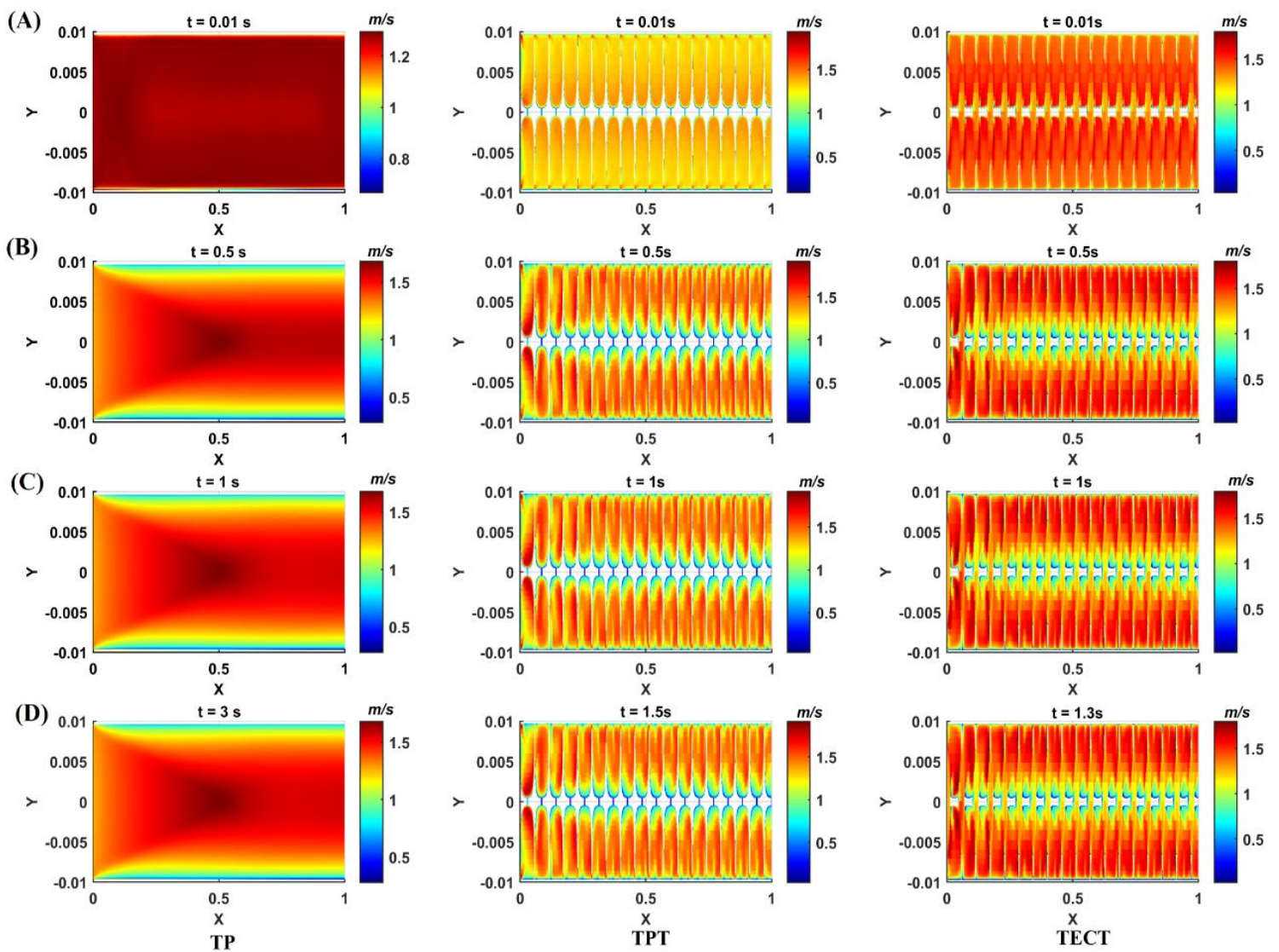
Figure 5-6 Velocity distribution of Al_2O_3-Cu/water hybrid nanofluid flow within PT, TPT,
and TECT at various times.

5.3.3 Turbulent kinetic energy contours

Figure 5-7 illustrates the time histories of turbulent kinetic energy for three unsteady flow conditions (PT, TPT, and TECT) using hybrid-nanofluid of Al_2O_3-Cu/water. Obviously, for Figure 5-7 (frame A), the prediction for the turbulent kinetic energy in the wall zone is almost indistinguishable during the early time of the three flows. However, as the time progresses in unsteady flow simulations, the changes in turbulent kinetic energy become more pronounced. This is because larger time allow for larger fluctuations in fluid motion, which can lead to the production of more turbulent kinetic energy. As seen in PT Figure 5-7 (frame B-D), the highest amount of the turbulent kinetic energy was located close to the wall, because of the low flow velocity caused by the no-slip condition on the wall [88]. As compared to the PT, the TECT and TPT have more turbulent kinetic energy. This is because the tape makes the boundary layer more turbulent [88]. The findings indicate that TECT significantly increases the intensity of the flow between the core area and the wall of the pipe. The major advantage of this type of modified twisted tape over conventional twisted tape is that the cut zone may significantly enhance flow interruptions and mixing of hot and cold flows between the core of the pipe and the pipe wall. Our prior study [155] and that of Ahmadi et. al. [44] are consistent with this finding. As discussed in Figure 5-7, TECT, combined with the high velocity magnitude by using hybrid nanofluid, improves fluid residence time, resulting in improved heat transfer.
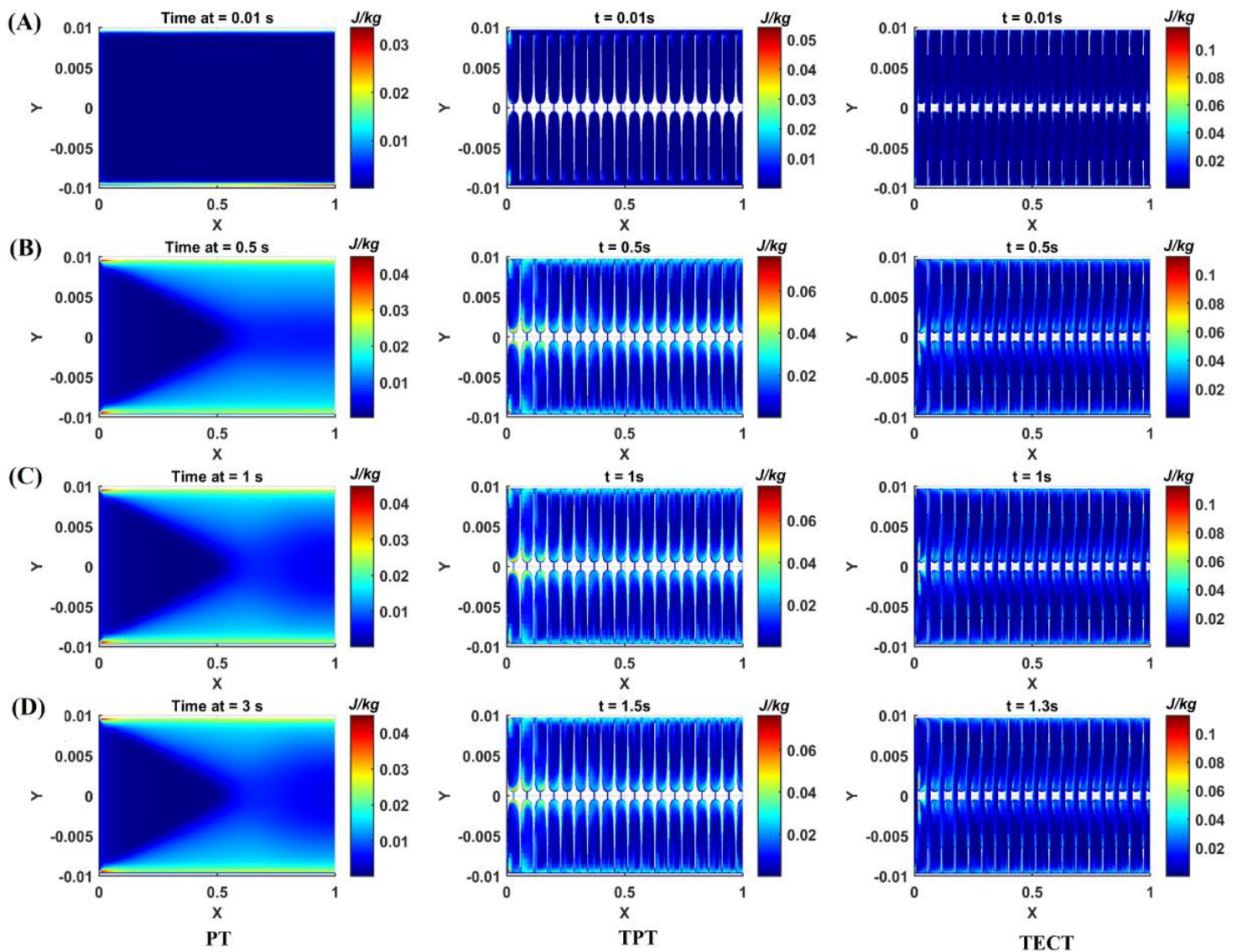
Figure 5-7 Turbulent kinetic energy distribution of Al_2O_3-Cu/water hybrid nanofluid flow within PT, TPT, and TECT at various times.

5.3.4 Transient heat transfer

Figures (5-8 to 5-10) depict three temperature variation curves obtained from STAR-CCM+ simulations for Al_2O_3-Cu/water, CuO/water, and water of PT, TPT, and TECT during the periods of time 3, 1.5, and 1.3s, respectively. For fluid heat transfer analysis, two points were selected in the tubes, one at the tube centre and the other at the tube outlet, to compare the heat transfer ability. Figures (5-8 to 5-10) frame (a) shows the fluid temperature at the selected points in the centre. Figures (5-8 to 5-10) frame (b) presents the exit fluid temperature. Temperatures at the centre and outlet of PT, TPT, and TECT were monitored every millisecond until the end of the simulation. In this work, water, CuO/water, and Al_2O_3-Cu/water were employed as working fluids to compare.

In Figure 5-8, the results of the predictions demonstrate that the variation of the fluid's temperature follows a similar pattern. As illustrated in Figure 5-8 (a), the temperature of the PT improves proportionally with time. There is minor oscillation at the beginning of the process as a consequence of excessive mesh refinement [218]. This is in agreement with [218, 219]. As seen in Figure 5-8 (a), the highest temperature reached 304.8K, 303.4K, and 302.9K of water, CuO/water, and Al_2O_3-Cu/water, respectively. The temperature differences are mostly determined by the velocity of the fluid [12]. When hybrid nanofluid is applied as the working fluid in the plain pipe PT in Figure 5-8 (b), the maximum temperature variation is reduced to around 0.7% and 0.21% when compared to water and nanofluid, respectively. Thus, employing hybrid-nanofluid of Al_2O_3-Cu/water can increase heat transmission [155]. This is owing to an increasing of thermal conductivity, and dynamic viscosity, as stated in [220].

Figure 5-9 and Figure 5-10 show the temporal evolution of the temperature of different fluids for TPT and TECT, respectively. Based on Figure 5-9 and Figure 5-10 frames (a and b) that the temperature difference rose more rapidly initially. That's because twisting tape makes the boundary layer less stable, which causes it to be disrupted and thus increases the distribution of temperature in the pipe. These short-time fluctuations have been found in the literature, for instance in [133, 134]. As a result of this breakup of the boundary layer, the heat transfer rate is increased, leading to a more rapid stabilization of the solution to steady state. In tubes with solid and elliptical-cut twisted tapes, the temperature reaches steady-state after 0.8s and 1s, respectively.

As shown in Figure 5-9 and Figure 5-10 for plate and elliptical cut twisted tape , the maximum temperature in the middle of the tube for water, nanofluid, and hybrid-nanofluid changes by

10.8K, 9.4K, 8.7K for TPT, and 9.6K, 7.9K, 7K for TECT, respectively. The figure further shows that TPT and TECT have more uniformly high temperatures compared to PT. The reason for this is that the accelerated whirling of fluid within the tubes brought about by the twisted tape causes the layer of thermal barriers to break down, allowing for better flow mixing between the surface of the heating wall and the fluids at the centre [44, 88]. Nonetheless, as displayed in Figure 5-9 (b), the exit temperature of the water, nanofluid of CuO/water, and hybrid-nanofluid Al_2O_3-Cu/water decreased from about 304.2K, 303.3K, and 302.9K at t = 0.1s to 300.1K, 300K, and 299.9K, to steady-stage (at t = 1.5s), respectively. The lower exit temperatures of different fluids indicate the improvement of heat transfer [221].

Depending on time and tape geometries, the exit temperature of the flows in the pipe supplied with elliptical-cut twisted tape was enhanced as compared to those in the TPT by about 0.2%, 0.5%, and 0.6% for water, CuO/water, and Al_2O_3-Cu/water, respectively, as demonstrated in Figure 5-9 and Figure 5-10 frame (b). This could be partially attributed to the fact that there is heat transfer between the tube's wall and the surface of elliptical-cut and classical twisted tape, though the heat flux is non-uniform. Because of the rise in turbulence intensity, the thermal/velocity boundary layer is destroyed more efficiently [44, 88, 155]. Solid and elliptical-cut twisted tape are applied to further enhance the heat transfer during the transition time when hybrid-nanofluid is employed as the working fluid [155]. For Al_2O_3-Cu/water at centre point, it is observed that the heat transfer enhancement neared the quasi-steady state for a duration of approximately 1.4s, 0.7s and 0.6s, and achieved higher values for a period of about 1.3s, 0.4s and 0.3s of PT, TPT, and TECT, respectively. Transient heat transfer increases exhibit a strong reliance on twisted tape geometries and applying Al_2O_3-Cu/water hybrid-nanofluid. This behaviour is comparable to that of a plate heater [222].

Figure 5-11 (a and b) displays the temperature curves for TECT at various concentrations of Al_2O_3-Cu/water at the selected points in the centre and the exit fluid temperature, respectively. The predicted flow temperature of the fluid at different concentrations did not show any noticeable difference in the shape of the curve. Obviously, the temperature decreased as the concentration of nanoparticles increased. That means the heat transmission is improved as the concentration of nanoparticles increases from 1% to 4%. Overall, when nanoparticles are added, the velocity and heat transmission rate were increased. Unsteady flows reach steady states as heat transfer and temperature gradient increase with increased time and flow rate.

Time-dependent analysis of heat transfer enhancement and entropy generation of hybrid nanofluids in a tube with a solid and elliptical-cut twisted tape insert.
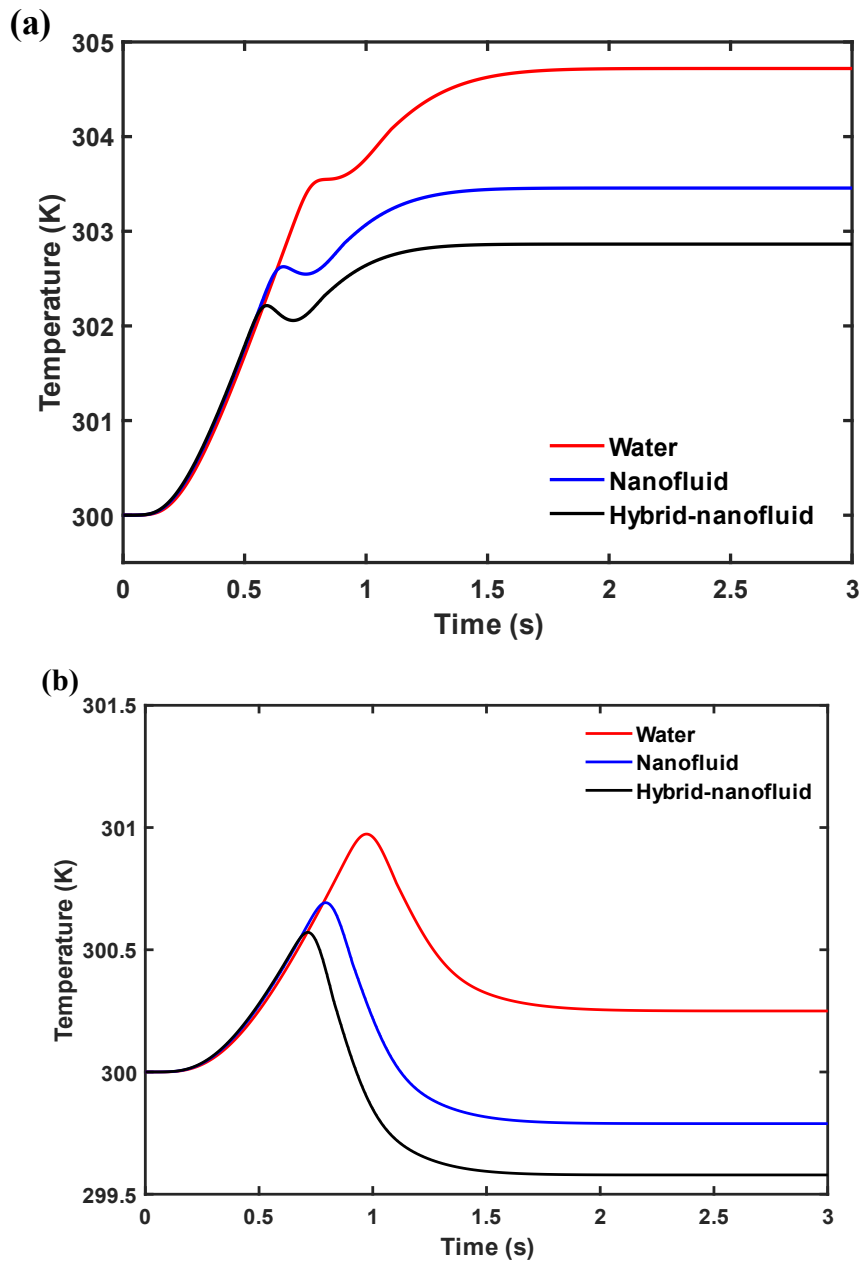
Figure 5-8 Curves of temperatures for plain tube PT.

Time-dependent analysis of heat transfer enhancement and entropy generation of hybrid nanofluids in a tube with a solid and elliptical-cut twisted tape insert.

(a)

(b)
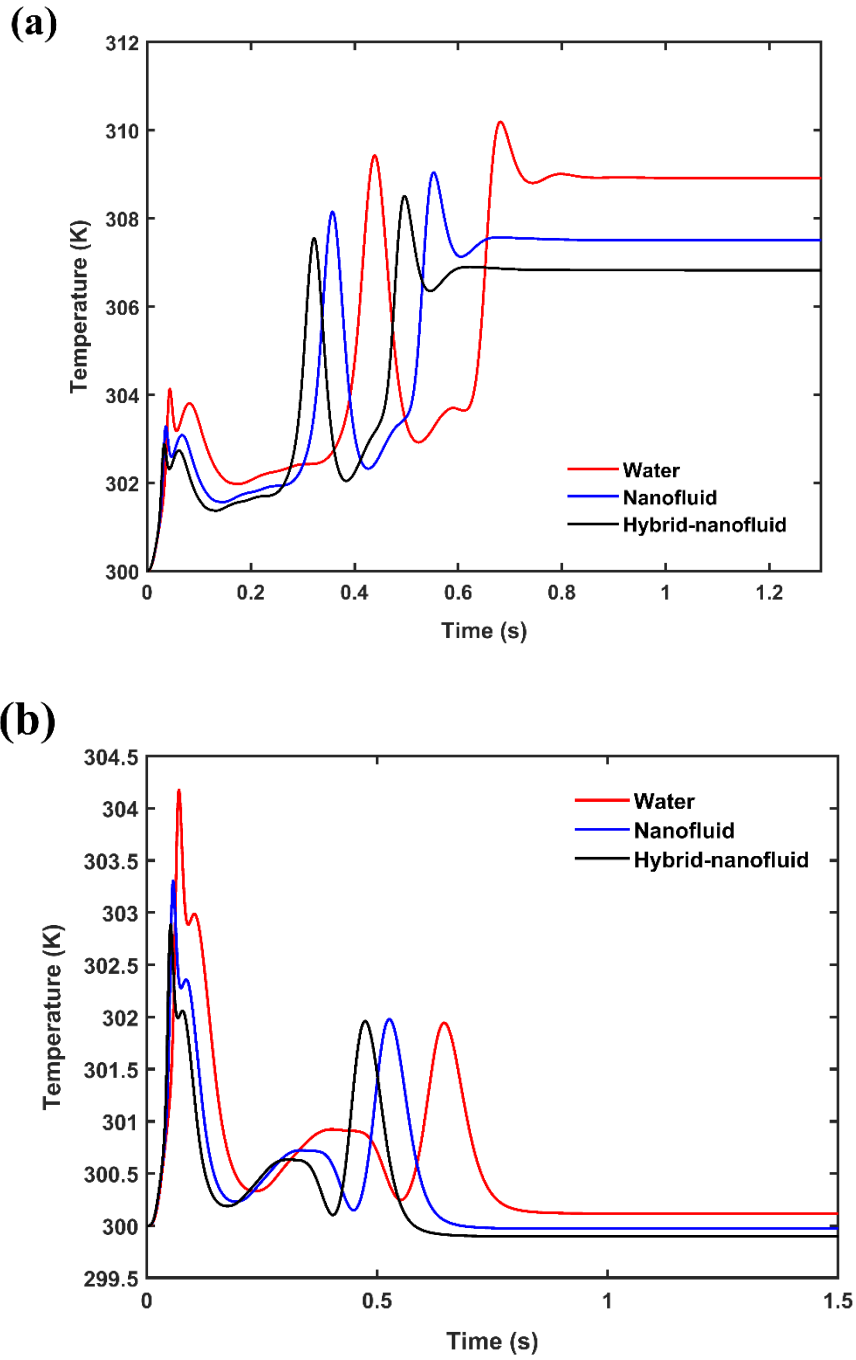
Figure 5-9 Curves of temperatures for tube fitted solid twisted tape TPT.

Time-dependent analysis of heat transfer enhancement and entropy generation of hybrid nanofluids in a tube with a solid and elliptical-cut twisted tape insert.

(a)

(b)
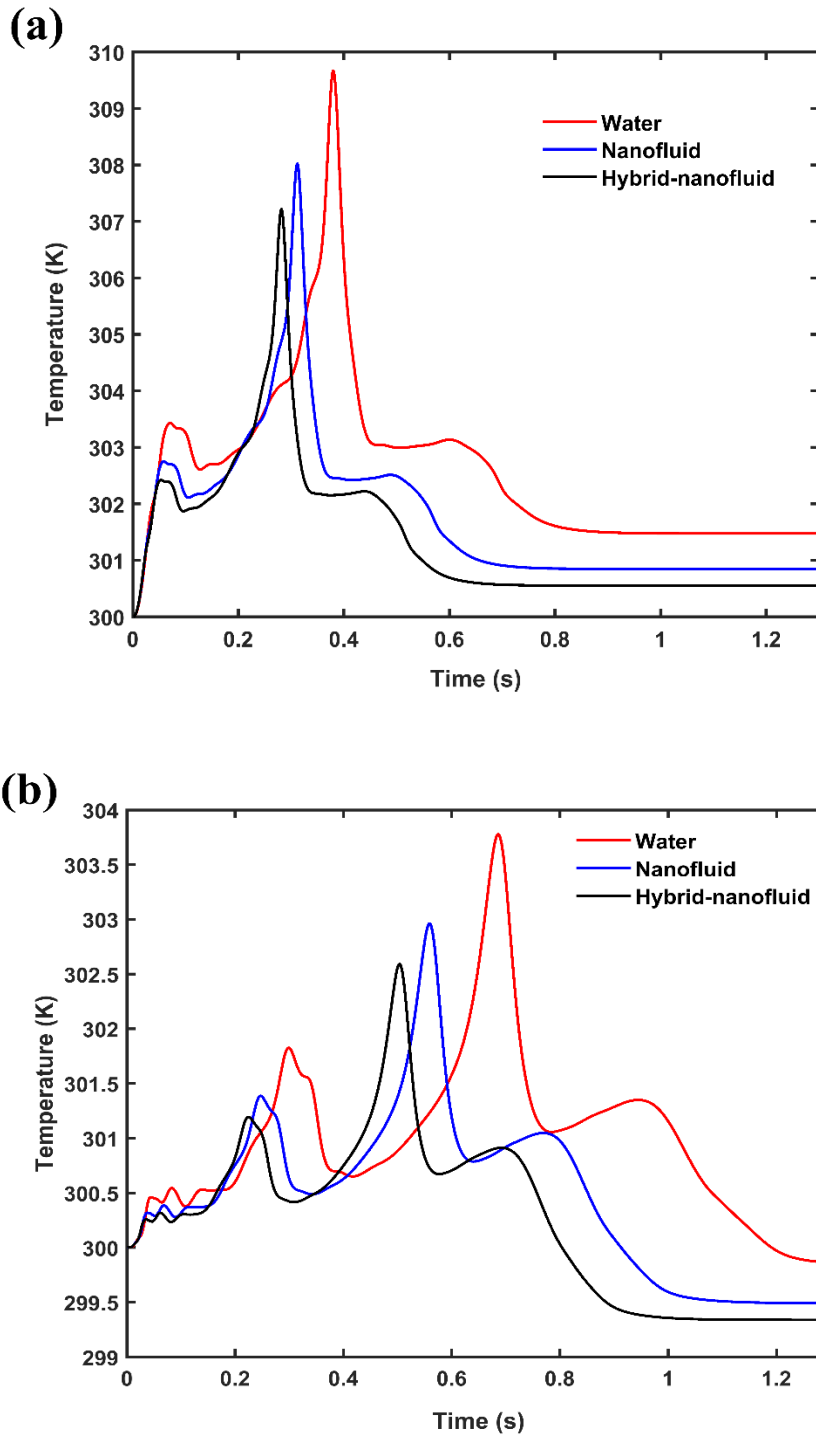
Figure 5-10 Curves of temperatures for tube fitted elliptical-cut twisted tape TECT.

Time-dependent analysis of heat transfer enhancement and entropy generation of hybrid nanofluids in a tube with a solid and elliptical-cut twisted tape insert.

(a)

(b)
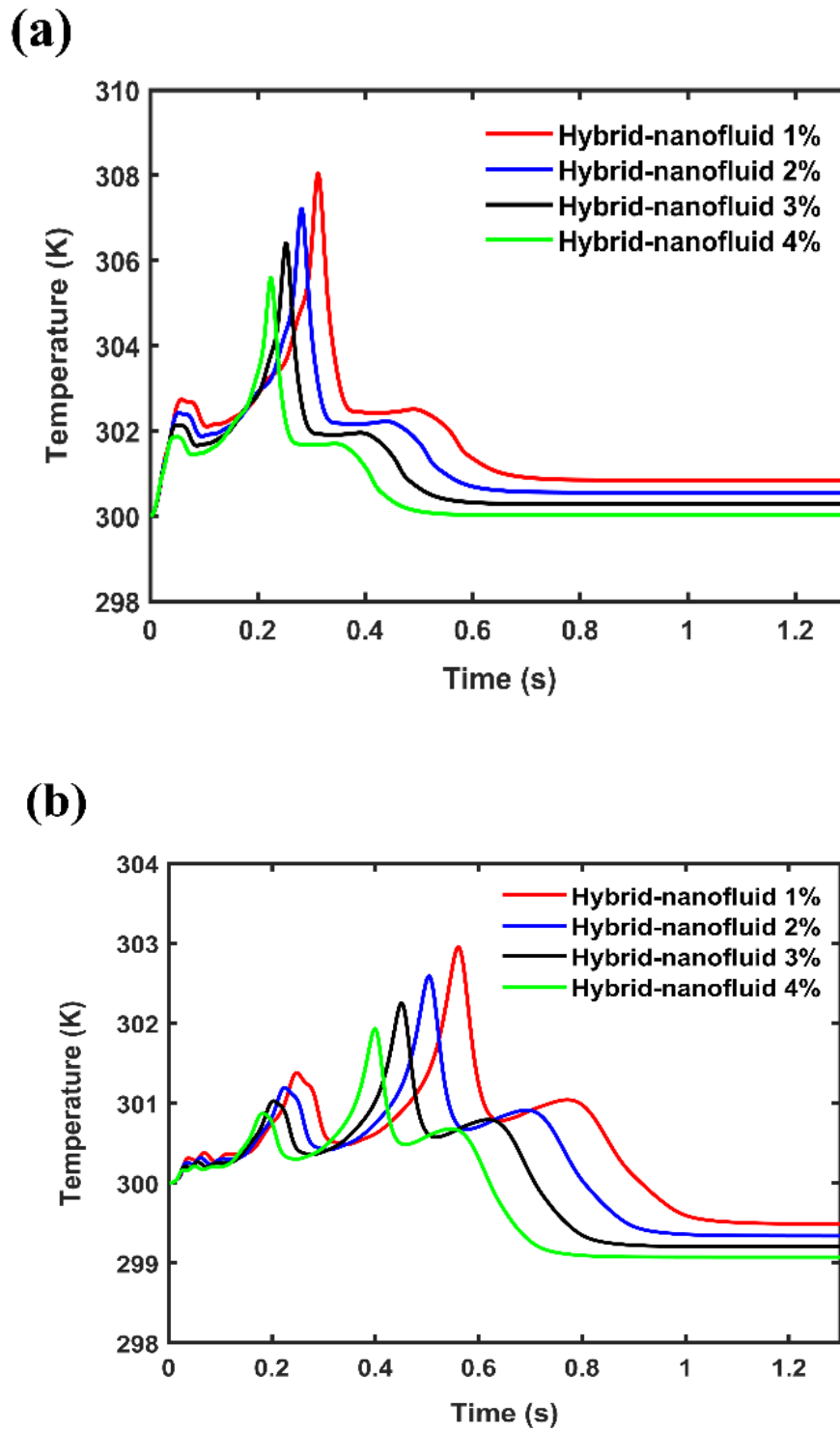
Figure 5-11 Temperature curves for TECT at different concentrations of Al2O3-Cu/water at (a) centre point (b) outlet fluid.

5.3.5 Entropy generation analysis

This section describes a study of the analysis of entropy generation during transient heat transport for, a hybrid-nanofluid of Al_2O_3-Cu/water, a nanofluid of CuO/water, and an ordinary fluid at $\emptyset = 2\%$ in PT, TPT, and TECT. Furthermore, the production total entropy and Bejan number of an Al_2O_3-Cu/water for TECT have been examined at $\emptyset$ from 1% to 4%. The irreversibilities (entropy) are generated owing to irreversible heat transmission and fluid friction [183]. Entropy production is a thermodynamic characteristic of a system. This provides insight into how the parameters are distributed throughout the vortex tube and where the irreversibility sources are concentrated. The present study's major purpose is to evaluate the impact of a pipe equipped with elliptical-cut and solid inserts of twisted tape on entropy production during transient heat transfer, with heat transmission and fluid friction effects as the sole contributors.

5.3.5.1 Local entropy generation

Figures 5-12 and 5-13 illustrate the local entropy generation during transient heat transfer. The thermodynamic irreversibilities of the process owing to heat transfer and fluid friction were analysed individually in equations 3.39 and 3.40 in section 3.5.1 by using the MATLAB code. These figures show the spatial distributions of entropy production by water, nanofluid, and hybrid-nanofluid for various time intervals. Figure 5-12 (a-c) shows the local entropy production owing to heat transport for PT, TPT, and TECT, respectively. Figure 5-12 demonstrates that there is some thermal entropy creation due to the endothermic process at t = 0.01s. At t = 0.5 and 1s, it is clear that heat transfer has increased. It is obvious that the area across which thermal entropy is created has grown dramatically. This trend matches previous research' numerical result [223]. The last row in Figure 5-12 (a-c), the time operating has terminated at 3s, 1.5s, and 1.3s for PT, TPT, and TECT. Figure 5-12 (a) shows that in plain tubes, the most thermal entropy is created in the area near the wall, where there is a bigger difference in temperatures. It is also shown in Figure 5-12 that in both (b) and (c), the spatial distribution of thermal irreversibility is created by classical and elliptical-cut twisting tape, which causes a strong eddy flow between the pipe wall and the tape surface. This leads to a rise in thermal entropy. This is to be anticipated due to the improved viscous effects in the vicinity of the near wall, as well as the greater fluid velocity because of the twisted tape. Hunt et al. observed a very similar behaviour of heat transfer irreversibility [224].

However, it is clear in Figure 5-12 (a, b, and c) that the inclusion of nanoparticles resulted in a decreased thermal entropy production compared to a normal fluid, which is consistent with the findings of Refs [155, 225]. Observably, the creation of thermal entropy reduces when using hybrid nanofluids. As an instance, applying hybrid-nanofluid in the TECT (Figure 5-12 frame c) reduces the entropy production rate by about 14.3% and 20% when compared to water and nanofluid, respectively.

Figure 5-13 depicts the creation of local entropy owing to fluid friction for PT, TPT, and TECT, respectively. As can be seen, the flow is symmetrical and temporary, as all plots vary with time. When compared to the findings of the k-ε turbulence model as seen in Figure 5-7, several similarities become visible. More precisely, as seen in Figure 5-13 (a), the formation of entropy is concentrated on the wall tube owing to an orthogonal velocity gradient. In addition to the nearby region of elliptical-cut and solid twisted tape, frictional entropy production around the rotational axis of solid and elliptical-cut twisted tape increases significantly in Figure 5-13 (b and c). Moreover, With the insert of TPT and TECT, there is an increase in both heat transmission and entropy creation due to friction factor. This increase is owing to the improved flow velocity gradients created by the usage of twisted tape at this area. As seen in Figure 5-13, the inclusion of nanoparticles contributes significantly to the increase in entropy production due to friction factor. The inclusion of nanoparticles enhances the fluid's viscosity, resulting in an increase in fluid friction [226]. A significant property of TECT geometry is that it has been discovered to decrease viscous entropy formation when compared to TPT. Figure 5-14 exhibits the plots of the local distribution of the Bejan number (Be) for TECT of Al_2O_3-Cu/water at various concentrations from 1% to 4%. It is essential to observe that the scale is not the same for each frame: when the number of nanoparticles increases, the Bejan number drops. As a consequence, entropy formation by fluid friction entirely dominates the overall local irreversibility.

Time-dependent analysis of heat transfer enhancement and entropy generation of hybrid nanofluids in a tube with a solid and elliptical-cut twisted tape insert.

(a)

Water   CuO/Water-Nanofluid   Al$_2$O$_3$-Cu/Water-Hybrid-nanofluid

(b)

Water   CuO/Water-Nanofluid   Al₂O₃-Cu/Water-Hybrid-nanofluid
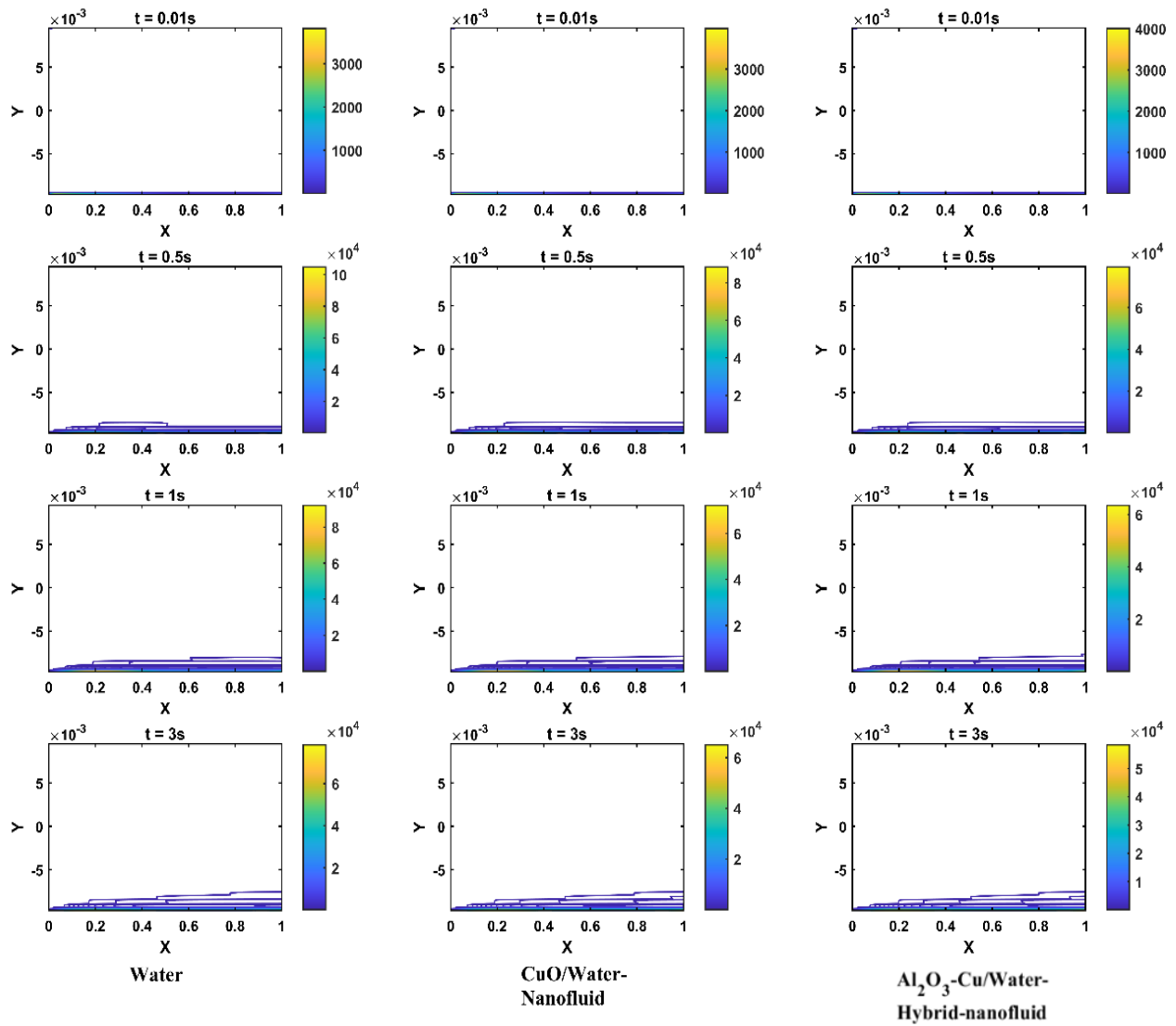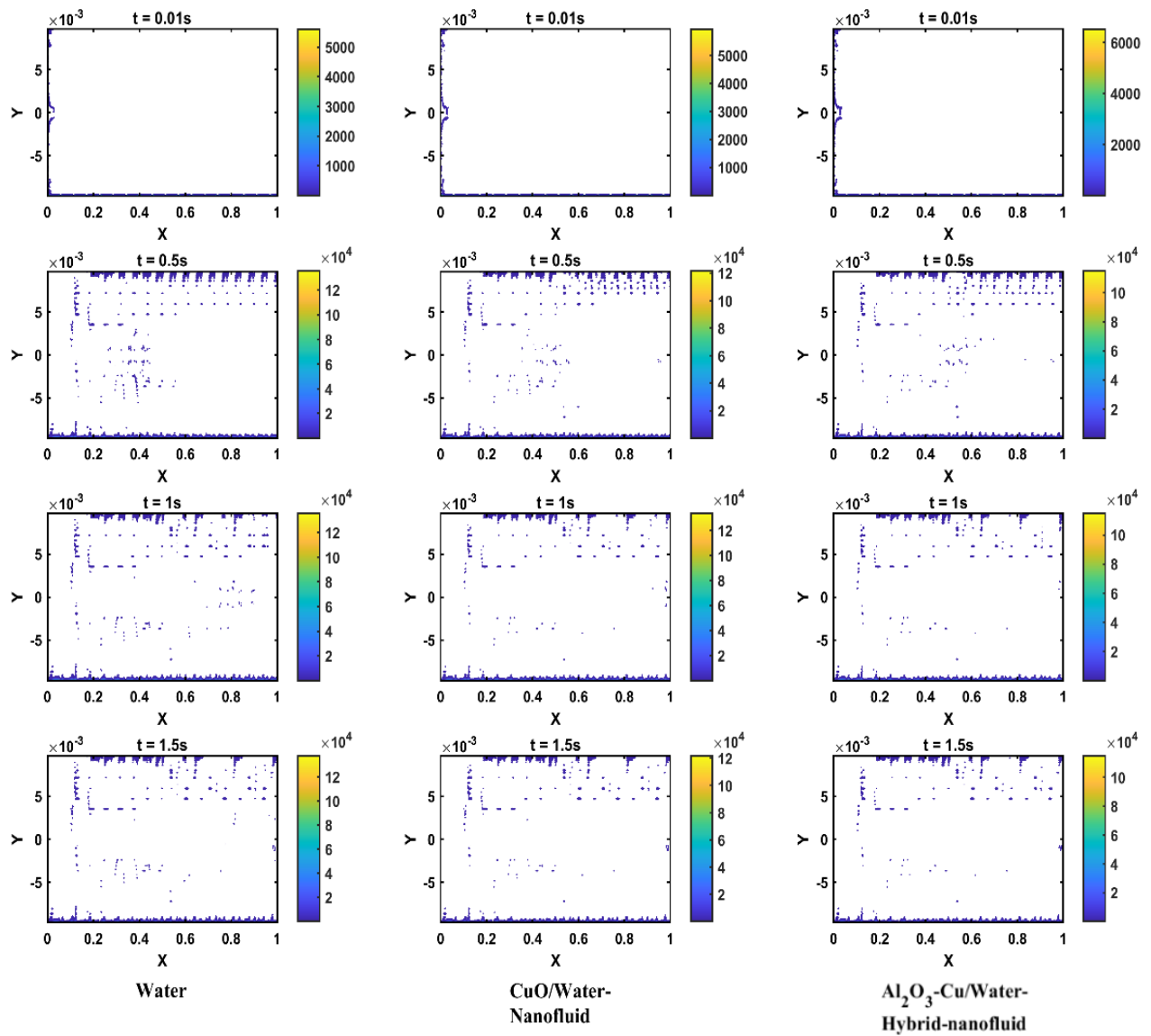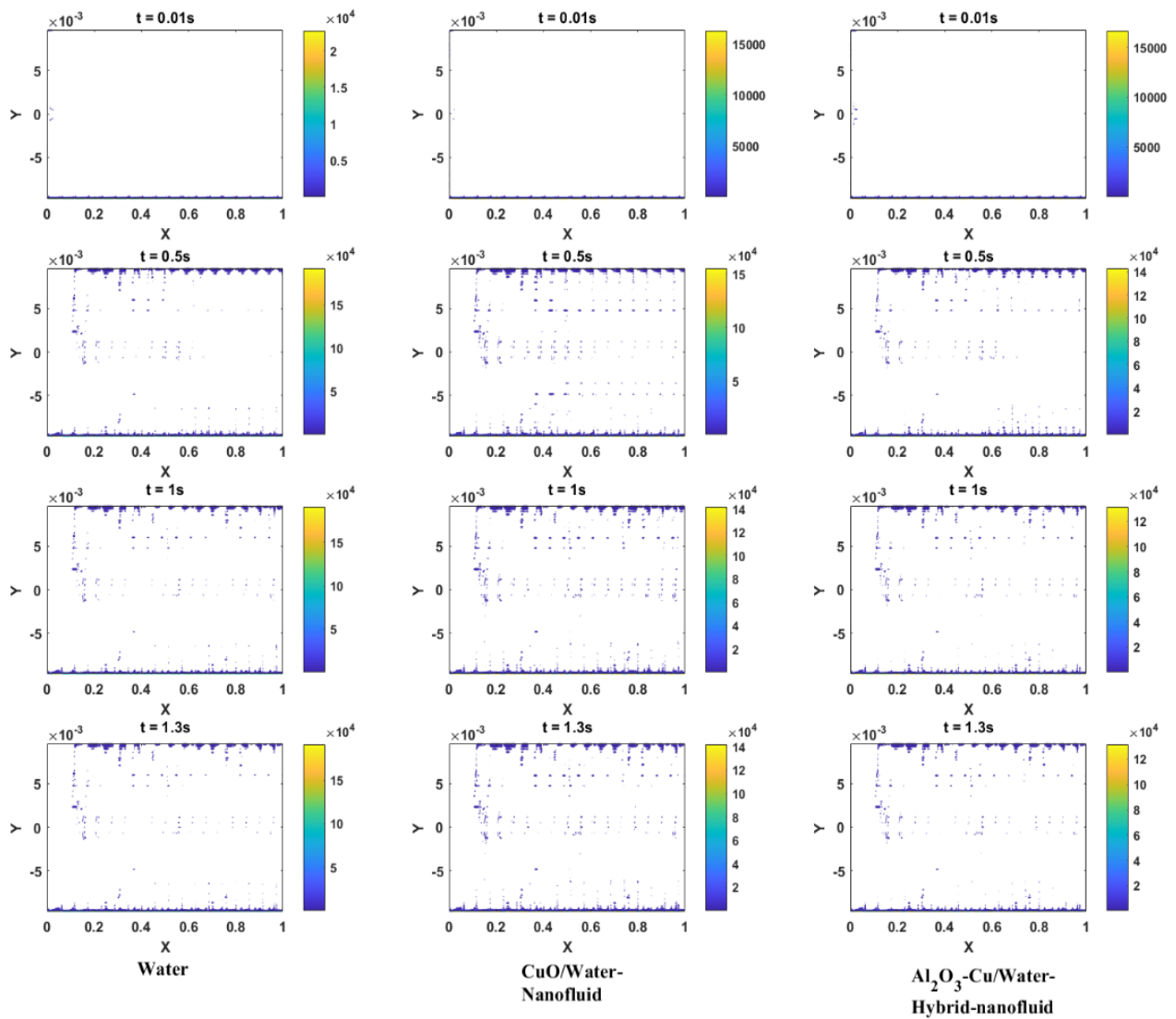
Figure 5-12 Spatio-temporal development of the rate of entropy formation owing to heat transmission in (a) PT, (b) TPT, and (c) TECT with different fluids at different times.

(a)

Water

CuO/Water-Nanofluid

Al₂O₃-Cu/Water-Hybrid-nanofluid

(b)

Water

CuO/Water-
Nanofluid

Al$_2$O$_3$-Cu/Water-
Hybrid-nanofluid

(c)

Figure 5-13 Spatio-temporal development of the rate of entropy formation due to fluid friction in (a) PT, (b) TPT, and (c) TECT for different fluids at different times.

Time-dependent analysis of heat transfer enhancement and entropy generation of hybrid nanofluids in a tube with a solid and elliptical-cut twisted tape insert.
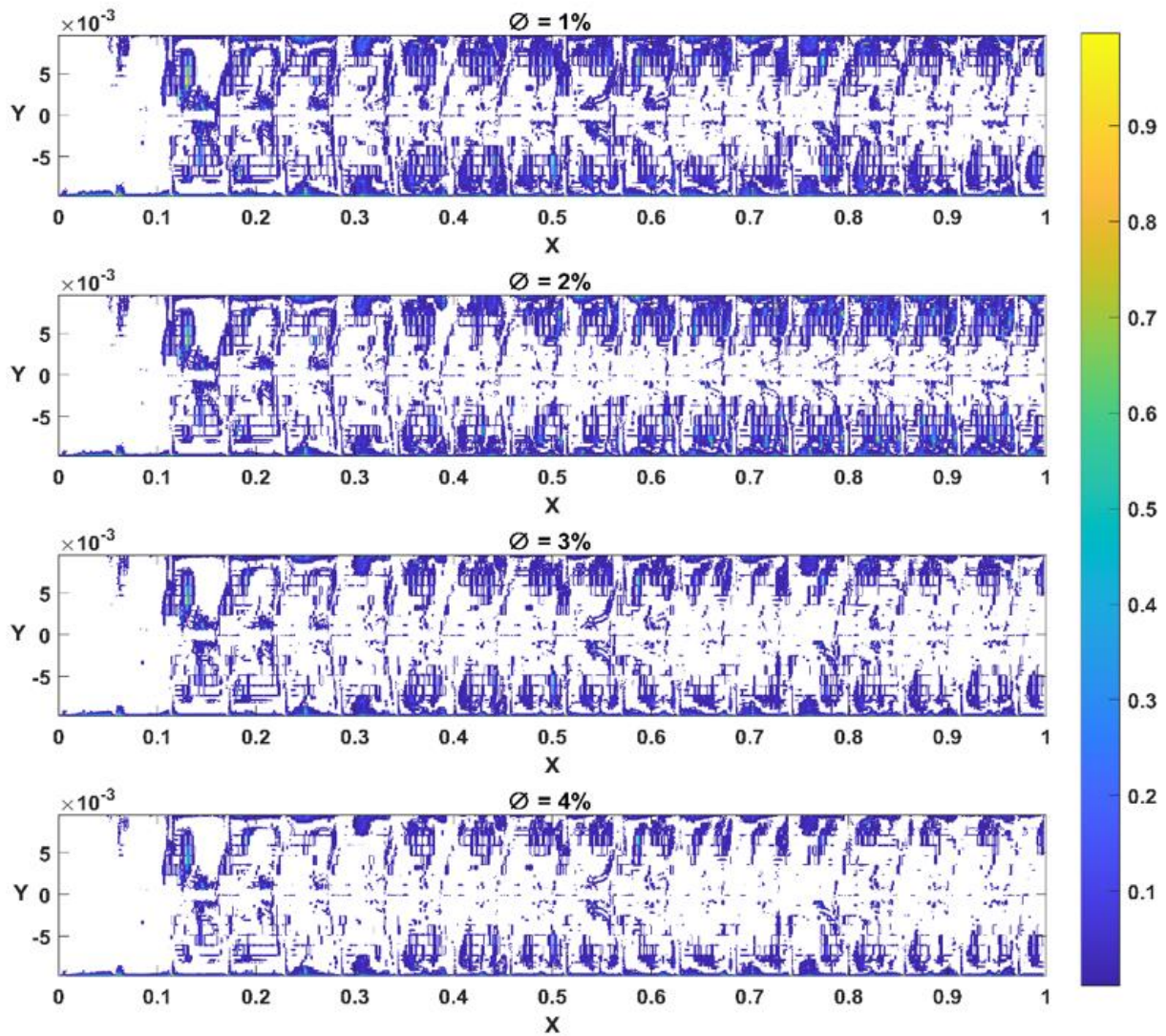
Figure 5-14 Bejan number of Al$_2$O$_3$-Cu/water for different concentration.

5.3.5.2 Entropy generation at current operating conditions

The current entropy created owing to heat transfer and fluid friction by each of the tubes (a) PT, (b) TPT, and (c) TECT can be seen in Figure 5-15 and Figure 5-16 using various values of the flows of three fluids (water, nanofluid of CuO/water, and hybrid nanofluid of Al_2O_3– Cu/water) at $\emptyset = 2\%$. Figure 5-17 and Figure 5-18 describe the heat entropy production and friction entropy production for TECT of Al_2O_3-Cu/water with the range of concentrations ranging from 1% to 4%, respectively. These figures illustrate a few key features concerning transient entropy generation. The results of Figure 5-15 shows that the thermal entropy production increases with time in all tested tubes. Figure 5-15 (a-c) further demonstrates that the thermal entropy production of hybrid nanoparticle-based fluids is lower than that of water and nanofluid. Another observation from Figure 5-15 reveals that the production of thermal entropy for TECT is lower than that of TPT and PT. That's because TECT enhances heat transfer compared to PT and TPT. The improvement of heat transfer in the TECT results in a 27.5% and 64.4% decrease in thermal entropy production compared to the TPT and PT models, respectively. This is consistent with our previous findings [155].

Figure 5-16 shows the frictional entropy production increasing with the addition of a twisted tape into the pipe due to an increasing velocity and temperature gradient. Likewise, increasing nanoparticles increases frictional entropy production. As seen in Figure 5-17 the thermal entropy production decreases gradually with increasing nanoparticle concentrations. Gabriela and Angel [227] found the same thing: that incorporating nanoparticles into the water decreased the rate of thermal entropy production. However, Figure 5-18 illustrates that, any further increase in thermal conductivity alters the irreversibilities slightly. As a working fluid, Al_2O_3-Cu/water at $\emptyset = 4\%$ may be a good choice over other hybrid nanofluids because of its reduced entropy formation rate.

Time-dependent analysis of heat transfer enhancement and entropy generation of hybrid nanofluids in a tube with a solid and elliptical-cut twisted tape insert.
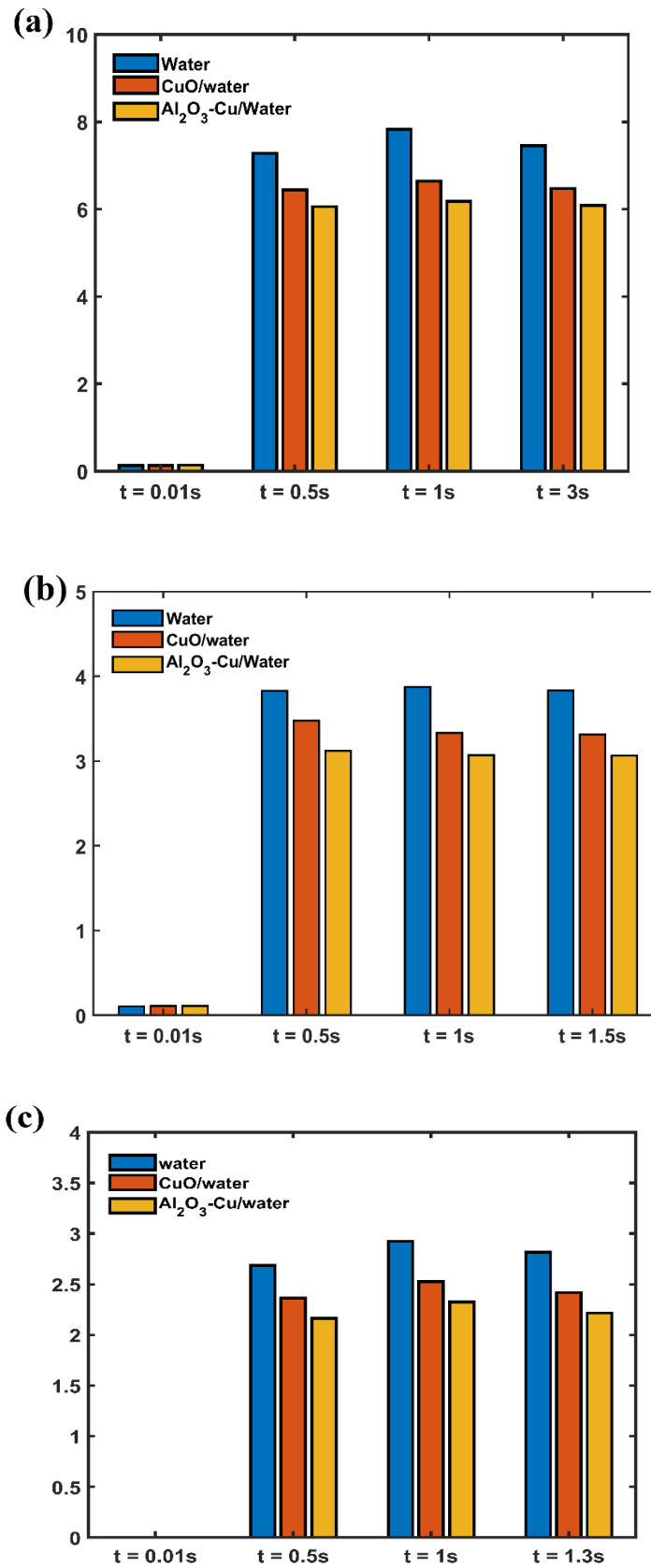
Figure 5-15 Entropy production due to heat transmission in (a) PT, (b) TPT, and (c) TECT at different times.
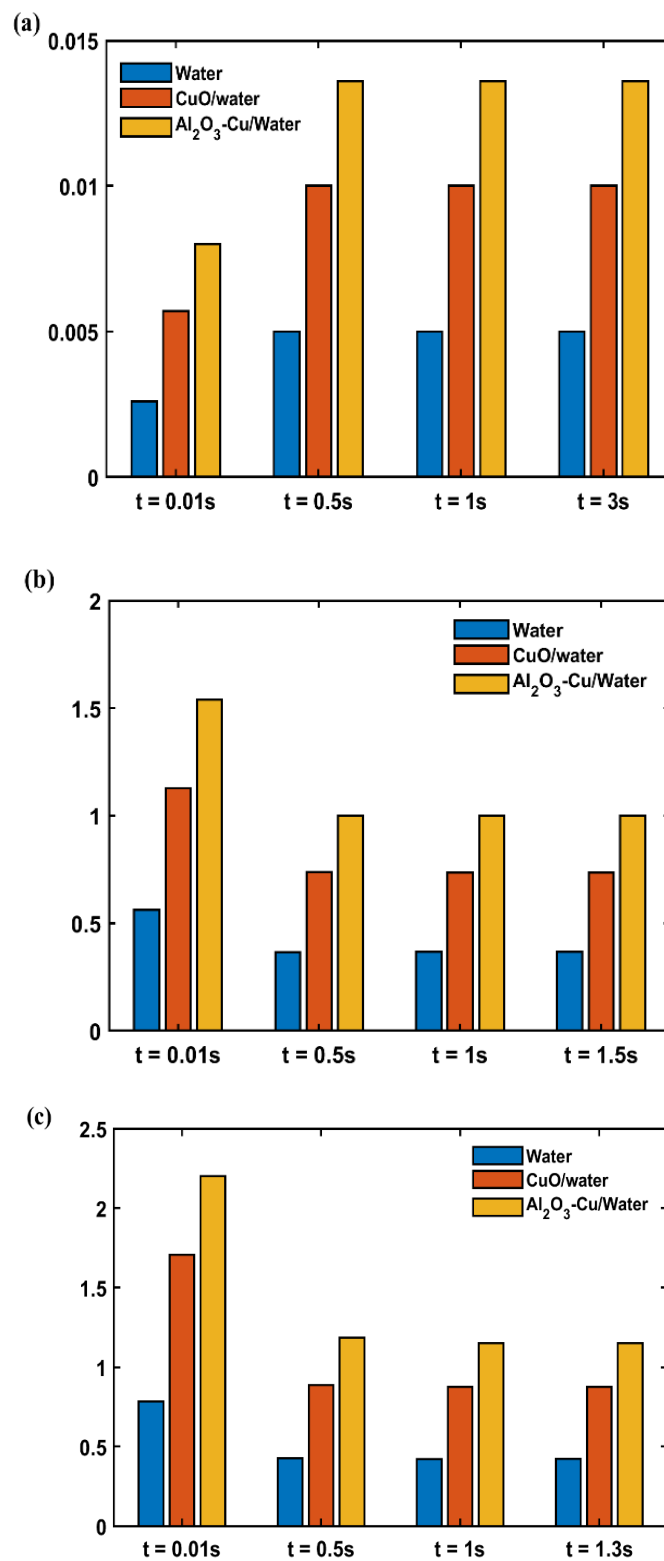
Figure 5-16 Entropy production due to Fluid friction in (a) PT, (b) TPT, and (c) TECT at different times.
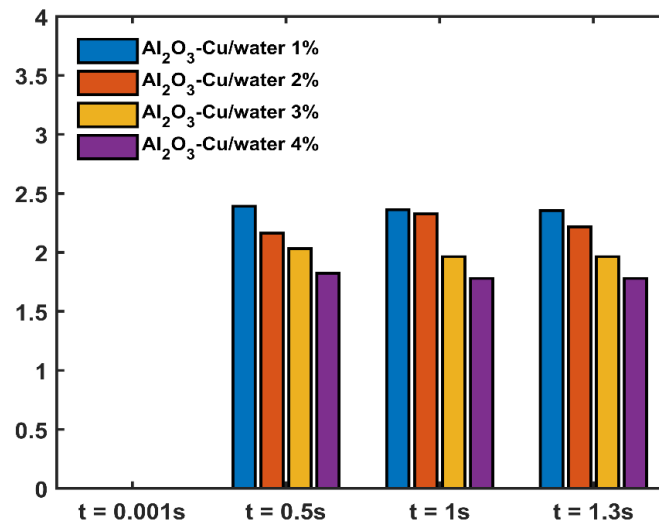
Figure 5-17 Entropy production owing to heat transmission of Al_2O_3-Cu/water at different concentrations for TECT.
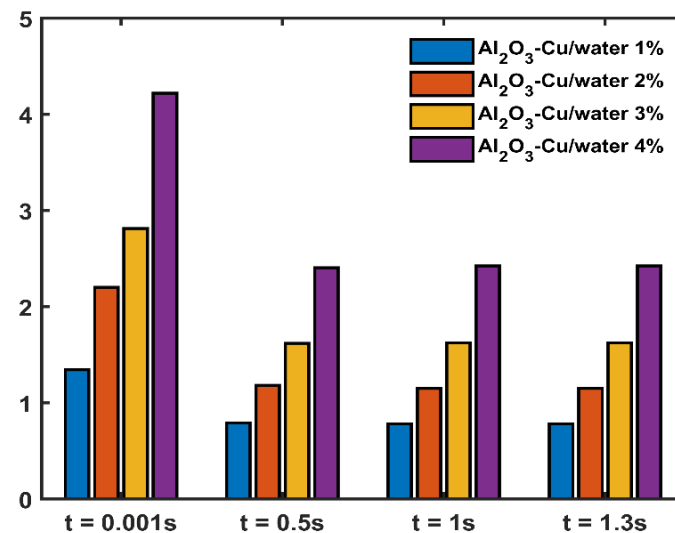
Figure 5-18 Entropy production owing to fluid friction of Al_2O_3-Cu/water at different concentrations for TECT.

5.3.5.3 Total entropy generation

Heat transfer and fluid friction contribute to the overall amount of entropy produced. The creation of total entropy for varying quantities of the flow of three fluids (water, nanofluid of CuO/water, and hybrid-nanofluid of Al_2O_3-Cu/water) and three distinct configurations are shown in Figure 5-19 (a) PT, (b) TPT, and (c) TECT. The nanoparticle concentration is equal to 2%, with four various temporal situations. When the issue is in an unstable condition, the entropy increases with increasing time due to temperature penetration into the channel's centre, an increase in the temperature gradient, and the temperature gradient's predominance in the entropy equation. As seen in Figure 5-19, the use of nanofluid and hybrid nanofluid results in a decrease in total entropy creation. According to [195, 197, 225], raising the nanoparticle volume fraction decreases the creation of total entropy. This figure clearly illustrates the impact of TPT and TECT on the system's total irreversibility. At very small-time scales, total entropy generation exhibits the same behaviour in both classical and elliptical-cut twisted tapes, as displayed in Figure 5-19 (a and b). Following that, the creation rate of total entropy grows at a slight but variable pace. That's because swirling currents have a more dramatic impact on temperature and the gradients of velocity, hence on the production of frictional and thermal entropy, which in turn leads to a reduction in total entropy.

Figure 5-19 shows that adding the plate and elliptical cut twisted tape as well as hybrid nanofluid significantly affects the rate at which total entropy generation decreases. At t = 1s, for instance, the total entropy production rates of TPT and TECT are decreased by 50% and 54%, respectively, when compared with PT. Also, in TECT, the generation of total entropy of Al_2O_3-Cu/water compared with water and CuO/water is decreased by 5.4% and 3%, respectively. Figures (5-20 and 5-21) describe the total entropy production and Bejan number as a function of the increase in the hybrid nanofluid concentration from 1% to 4% for TECT, respectively. By referring to Figure 5-20, one can notice that the total entropy production rate rises with increasing nanoparticle concentrations , this is as a result of an increase in frictional entropy production rates [228]. The Bejan number depicts the contribution of each irreversibility to the production of total entropy. Bejan number is the ratio between the irreversible thermal entropy formation rate and the total entropy formation rate. For Bejan numbers near one, irreversible heat transfer dominates, while for Bejan numbers near zero, irreversible fluid friction dominates. Based on the data in Figure 5-21, it may be deduced that increasing the number of nanoparticles decreases the Bejan number. As a result, the proportion

of frictional entropy to total entropy increases while the thermal entropy proportion decreases [229].
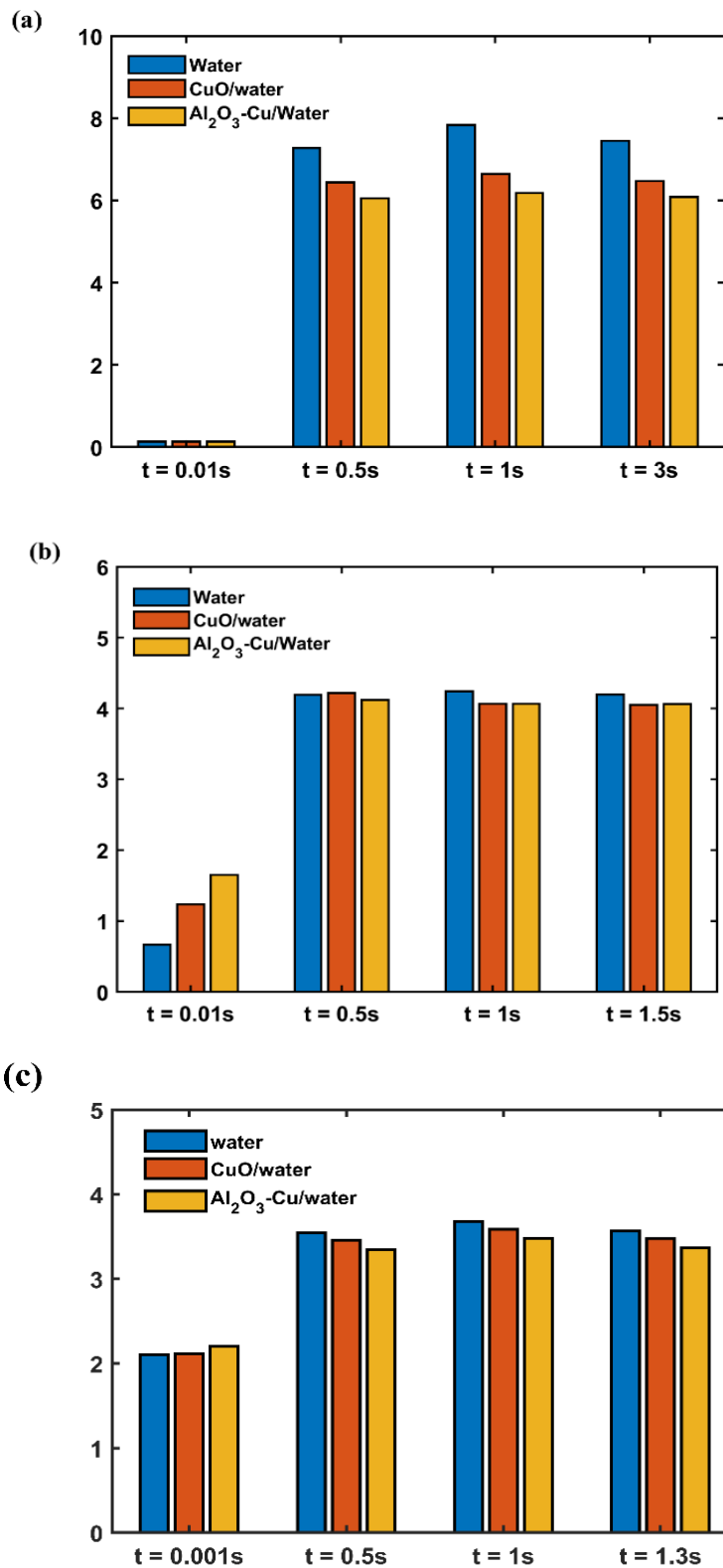
Figure 5-19 Total entropy generation in (a) PT, (b) TPT, and (c) TECT at different times.
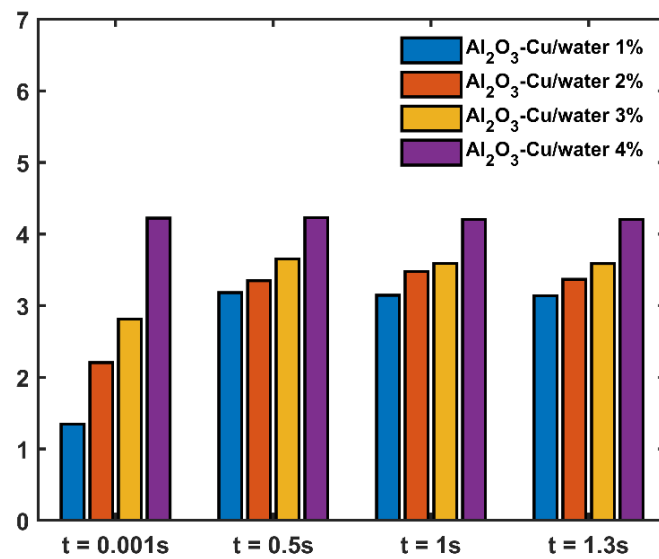
Figure 5-20 Total entropy generation of Al_2O_3-Cu/water at various concentrations for TECT.
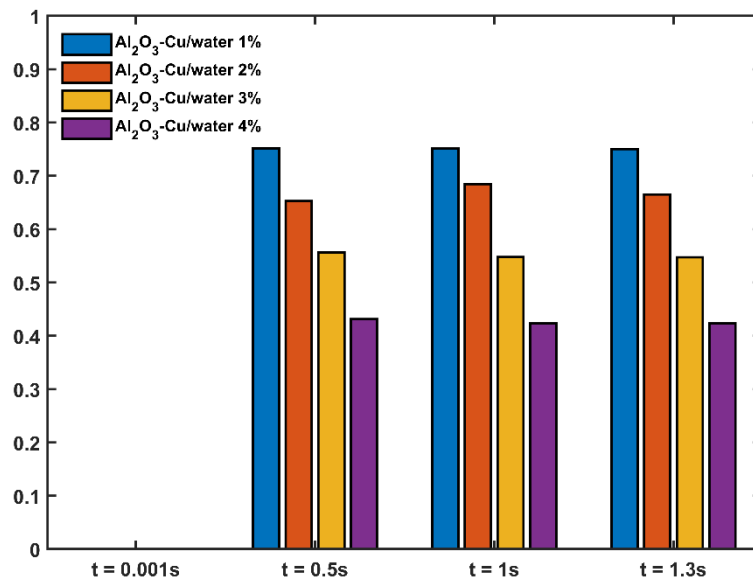
Figure 5-21 Bejan number of Al_2O_3-Cu/water at various concentrations for TECT.

5.4 Conclusions

A numerical analysis was performed to investigate the influence of transient heat transfer augmentation as well as the analysis entropy production in PT, TPT, and TECT under the non-uniform heat flux for hybrid turbulent nanofluid flow (Al_2O_3-Cu/water). The outcomes obtained are summarised as follows:

- Heat flux obtained by numerical simulation was compared to numerical and experimental data to validate the results using Monte Carlo Ray-Trace (MCRT) approach.

- In unsteady flow, the transient heat transfer enhancement is determined by temperature changes in the tube. The results found that with increasing time, the system becomes a steady state.

- Increasing the time causes a decrease in the thickness of the boundary layer and an increase in temperature gradient, which causes in a rise in heat transmission.

- Through applying the hybrid nanofluid, the heat transfer rate is improved significantly. The impact of Al_2O_3-Cu/water hybrid nanofluid in this study shows a significant influence on heat transfer. The maximum temperature difference is reduced to around 0.7% and 0.21% when compared to water and nanofluid, respectively.

- The elliptical-cut twisted tape (TECT) in this study shows a good enhancement in the heat transport as compared to those in the TPT by about 0.2%, 0.5%, and 0.6% of water, CuO/water, and Al_2O_3-Cu/water, respectively.

- The transient heat transfer is enhanced as the concentration of nanoparticles improves from 1% to 4%. By incorporating nanoparticles into the heat transfer medium, the effective thermal conductivity of the fluid increases. This is because nanoparticles possess significantly higher thermal conductivity compared to the base fluid. As a result, the nanoparticles facilitate more efficient heat conduction within the system.

- The introduction of nanoparticles into the system has notable effects on entropy generation. Specifically, it leads to a reduction in thermal entropy creation and an increase in frictional entropy production. These changes can be attributed to the enhanced heat transfer associated with the presence of nanoparticles.

- Frictional entropy generation is the dominant mode of irreversibility in this problem.

- Minimisation of the total entropy production may be sought by applying hybrid-nanofluid and using TECT.

Chapter 6 Computational study of entropy production and thermohydraulic of mixed convection of hybrid-nanofluid in a vertical tube supplied with elliptical-cut twisted tape inserts.

6.1 Introduction

In this chapter, heat transmission in turbulent flows of hybrid nanofluid (Al_2O_3-Cu/water) in a vertical tube supplied by elliptical-cut twisted tape inserts is calculated numerically. Further, the Bejan number as well as the local and total entropy production of the system are calculated. The friction factor, heat transmission, thermal performance factor, as well as entropy production analysis are conducted at different volume concentrations and Reynolds numbers between 7000 and 15000. The realizable k-ε model was applied in computational simulations of turbulent flow.

Generally, mixed convection is used when forced convection cannot disperse all of the heat needed. These devices have been used in computer system cooling, nuclear reactor technology, as well as other electronic equipment [230, 231]. The convection of mixed has also played a vital part towards satisfying industries' desire for quicker and more compact circuit technologies and packaging [232].

According to the findings of the study conducted in the preceding chapters, in all the investigated fields, a pipe with an elliptical-cut twisted tape (TECT) and applying a hybrid-nanofluid of (Al_2O_3-Cu/water) as the working fluid produced the most efficient thermal performance in terms of the enhancement of heat transport as well as entropy creation minimization. Also, a review of the literature shows that the mixed convection on pipes supplied with elliptical-cut twisted tape for turbulent flow has virtually been neglected, even though it is important in real-world applications. Therefore, this chapter looks at how buoyancy affects the thermohydraulic characteristics of steady flows of hybrid-nanofluid flow caused by a twisted tape with elliptical cuts (TECT) and an entropy generation analysis of the buoyancy. Not only that, the distribution of temperature, velocity, and kinetic energy of turbulent flow is also taken into account. In addition, the spatial distribution of thermal and frictional entropy production is indicated.

6.2 Physical model and boundary conditions

In this work, the mixed convection of hybrid nanofluid (Al_2O_3-Cu/water) in a vertical tube supplied by elliptical-cut twisted tape and uniform wall heat flux has been considered. The following physical models were defined and implemented in STAR-CCM+ software. The steady state, three-dimensional, segregated flow temperature; the Reynolds averaged Navier-Strokes, and the force of gravity acting in the direction of flow. The turbulence model of realizable k-ε was applied to simulate turbulent flow. The buoyancy force influences the thermophysical properties equation of hybrid nanofluids, which were considered Newtonian. Boussinesq's hypothesis states that the fluid's physical parameters are assumed to be fixed, except for the density of the body force, which changes linearly with temperature. Viscous dissipation was further included in this work.

The boundary conditions employed in this investigation were as follows:

(1) Model geometry consists of an ordinary tube supplied by elliptical-cut twisted tape inserts (TECT) are displayed in Figure 6-1 and Table 6.1:

(2) Tube walls receive a constant heat flux of 4000 Wm^{-2}, while elliptical-cut twisted tape is adiabatic. Further, both the elliptical twisted tape and the pipe wall have no-slip properties.

(3) There are five Reynolds numbers used in the simulations: 7000, 9000, 11000, 13000, and 15000.

(4) Al_2O_3-Cu/water hybrid nanofluid is used as the working fluids at different volume concentration from 1% to 4%.

Computational study of entropy production and thermohydraulic of mixed convection of hybrid-nanofluid in a vertical tube supplied with elliptical-cut twisted tape inserts.
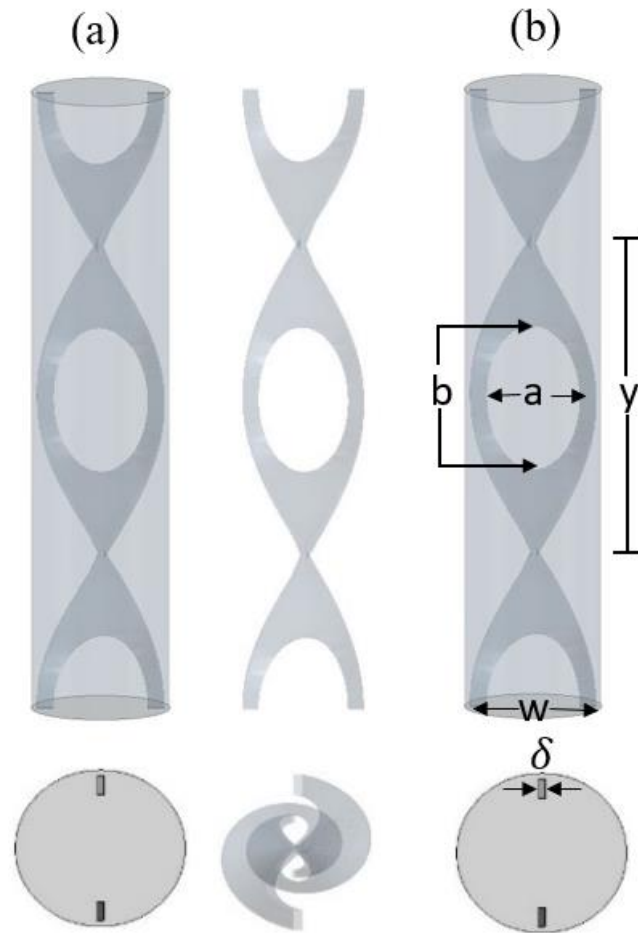
Figure 6-1 Physical model of (a) (TECT), and (b) dimensions of significant in the situation studied.

Table 6.1 Geometrical parameters of the studied parabolic trough receiver.

Feature	Value	Feature	Value
a	0.0133 m	y	0.057 m
b	0.00665 m	δ	0.0008 m
D	0.0195 m	a/w	0.7
L	1 m	b/a	2
w	0.019 m		

6.3 Thermophysical properties of the hybrid-nanofluid

For the convenience of the reader, the thermal and physical properties of hybrid nanofluids described in Chapter 4 are presented again here. As indicated in Table 6.2, the thermophysical characteristics of pure water, Al₂O₃, and Cu are identified from [233]. Equations for thermo-physical properties of the hybrid nanofluid are represented by [26-28, 234]:

Density $(\rho)_{hnf}$:

$$\rho_{hnf} = (1 - \emptyset_{hnf})\rho_f + \emptyset_A \rho_A + \emptyset_C \rho_C \tag{6.1}$$

Where *A and C* denote aluminium oxide (Al₂O₃) and copper (Cu), respectively.

$\emptyset_{hnf}$ indicates to the volume concentration of two distinct nanoparticle forms scattered in hybrid nanofluid and is computed as:

$$\emptyset_{hnf} + \emptyset_A + \emptyset_C \tag{6.2}$$

Specific heat $(C_p)_{hnf}$:

$$(\rho C_p)_{hnf} = (1 - \emptyset_{hnf})(\rho C_p)_f + \emptyset_A(\rho C_p)_A + \emptyset_C(\rho C_p)_C \tag{6.3}$$

Buoyancy $(\beta)_{hnf}$:

The thermal expansion coefficient of hybrid nanofluids may be calculated using the following formula, which has been cited in several publications [234-236]:

$$(\rho\beta)_{hnf} = (1 - \varphi_{hnf})(\rho\beta)_f + \varphi_A(\rho\beta)_A + \varphi_C(\rho\beta)_C \tag{6.4}$$

Dynamic viscosity $(\mu)_{hnf}$:

$$\mu_{hnf} = \frac{\mu_f}{(1-\emptyset_A)^{2.5}(1-\emptyset_C)^{2.5}} \tag{6.5}$$

Thermal Conductivity $(k)_{hnf}$:

$$\frac{k_{hnf}}{k_f} = \left(\frac{(\emptyset_A k_A + \emptyset_C k_C)}{\emptyset_{hnf}} + 2k_f + 2(\emptyset_A k_A + \emptyset_C k_C) - 2\emptyset k_f\right) / \left(\frac{(\emptyset_A k_A + \emptyset_C k_C)}{\emptyset_{hnf}} + 2k_f - \right.$$
$$\left. (\emptyset_A k_A + \emptyset_C k_C) + \emptyset k_f\right) \tag{6.6}$$

Here, $\emptyset_A$ and $\emptyset_C$ denote the volume fraction of sold aluminium oxide particles and solid copper nanoparticles, respectively. The water and the hybrid nanofluid are represented by *f* and *hnf*,

respectively. k_{hnf} is the thermal conductivity of hybrid nanofluid, k_f is water thermal conductivity, k_A is the thermal conductivity of aluminium oxide, and k_c is the thermal conductivity of copper.

Table 6.2 The thermophysical properties of the fluid and nanoparticles.

Substances	ρ/Kg m^{-3}	C_p/J Kg^{-1} K^{-1}	k_c /Wm^{-1} K^{-1}	$\beta \times 10^{-5}/ K^{-1}$
Water	997.1	4179	0.613	21
Al₂O₃	3970	765	40	0.85
Cu	8933	385	400	1.67

6.4 Grid independence test

Grid independence study on temperature for different mesh sizes was carried out to discover a suitable grid with high accuracy in order to assure the correctness of the computations. As part of this analysis, the independence test of grid was completed on the realizable k-ε turbulence model for a Reynolds number of 11000 in a vertical TECT to choose an appropriate grid for resolving the flow inside the domain. Five distinct grids containing the numbers 2615663, 2892319, 2990608, 3359202 and 3413798 were used. To do this, the temperature at the domain's exit was calculated from the cross-section as displayed in Figure 6-2. According to this figure, there are some discrepancies in the temperature readings of the grids. The grids with 2615663, 2892319, 2990608, and 3413798 cells differ by 0.2%, 0.1%, 0.5%, and 0.09%, respectively, compared with the grids with 3359202 cells, which were selected in this work.
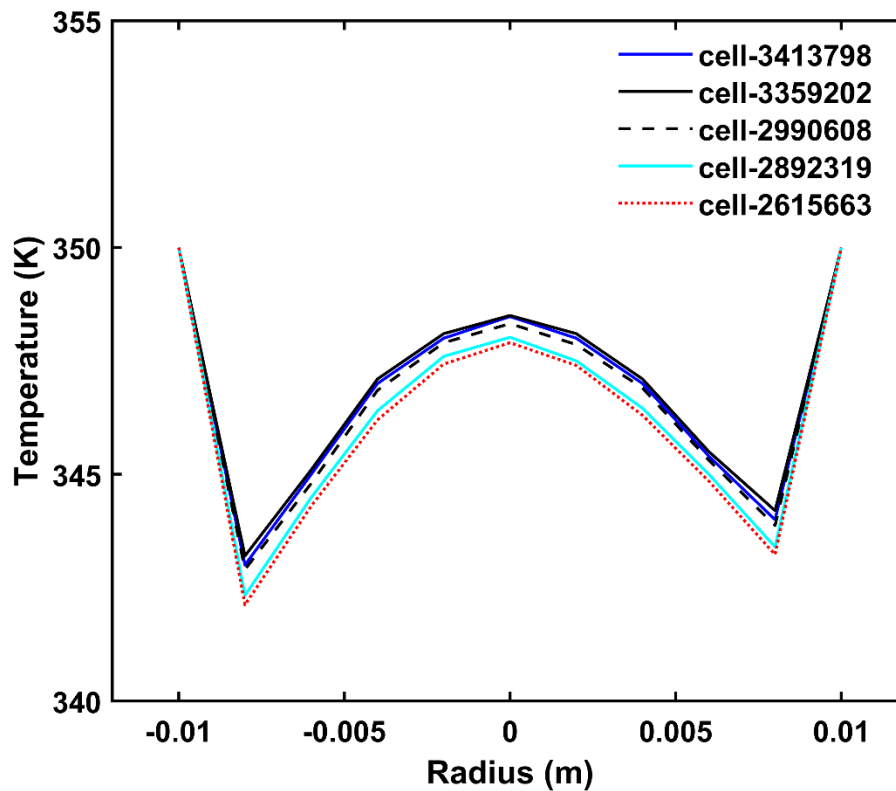
Figure 6-2 Grid independence test.

6.5 Model validation

In forced convection at a Reynolds number of 7000 and various mass concentrations of nanoparticles, the Nusselt number, friction factor, and thermal efficiency factor are validated against Ahmadi's [44] work in our previous study [155]. In Figure 6-3 a pipe made with a twisted tape cut in the shape of an alternate-axis triangle (TATCT) from Oni and Paul [151] was used to validate our tube model (TECT) for the mixed convection at 15° and turbulent flow at 5000 $\leq Re \leq$ 20000. The results were found with Prandtl number and Grashorf number of 5.83 and 3.37×10^5 respectively. In mixed convection, the Nusselt number of (TECT) has been compared with that of (TATCT), and the results are presented in Figure 6-3. Apparently, the Nusselt numbers of the present TECT deviated from those of TATCT by ± 8.3%. Comparing the results demonstrates excellent agreement under turbulent flow conditions, confirming the reliability of the present numerical method.

Computational study of entropy production and thermohydraulic of mixed convection of
hybrid-nanofluid in a vertical tube supplied with elliptical-cut twisted tape inserts.
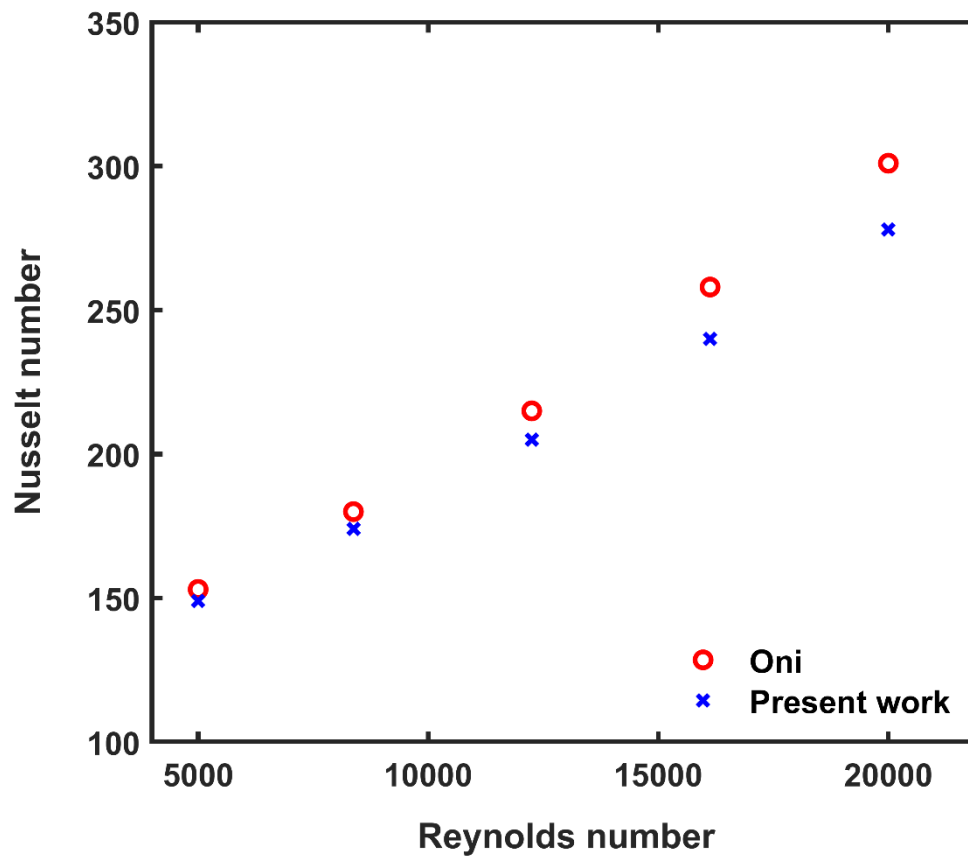
Figure 6-3 The variation of Nusselt number against Reynolds number Oni and Paul [151].

6.6 Computational Results and Discussions

The purpose of this section is to discuss the effects of the buoyant force on the steady of the system. The contour plots, thermal performance, friction factor, and Nusselt number, as well as entropy production for the turbulent flow of a hybrid nanofluid (Al_2O_3-Cu/water) in a pipe fitted with elliptical twisted tape inserts are discussed. Furthermore, the results for TECT with hybrid nanofluids (Al_2O_3-Cu/water) at different concentrations are examined. To achieve these objectives, five different Reynolds numbers (7000, 9000, 11000, 13000, and 15000) are considered to compare the results between forced and mixed convection.

6.6.1 Temperature contours

The temperature fields of an Al_2O_3/Cu-water hybrid-nanofluid ($\emptyset$ =2 %) flows are shown in Figure 6-4. The results for the temperature distribution in the tubes obtained for the turbulent flows are shown in Figure 6-4, frames (a - f), (a) forced convection at the Reynolds number of 7000, and (b-f) mixed convection with Reynolds numbers of (b) 7000, (c) 9000, (d) 11000, (e) 13000, and (f) 15000. A mixed convection tube had a higher temperature than one under forced convection at Reynolds numbers of 7000 (frames a and b) because of the buoyancy impact, as a result the fluid density changed. Under mixed convection, the tube's temperature increased slightly with increasing Reynolds numbers. There is a gradual increase in temperature along the pipe noticeably frames (b - f). This is in accordance with Oni and Pual [151].
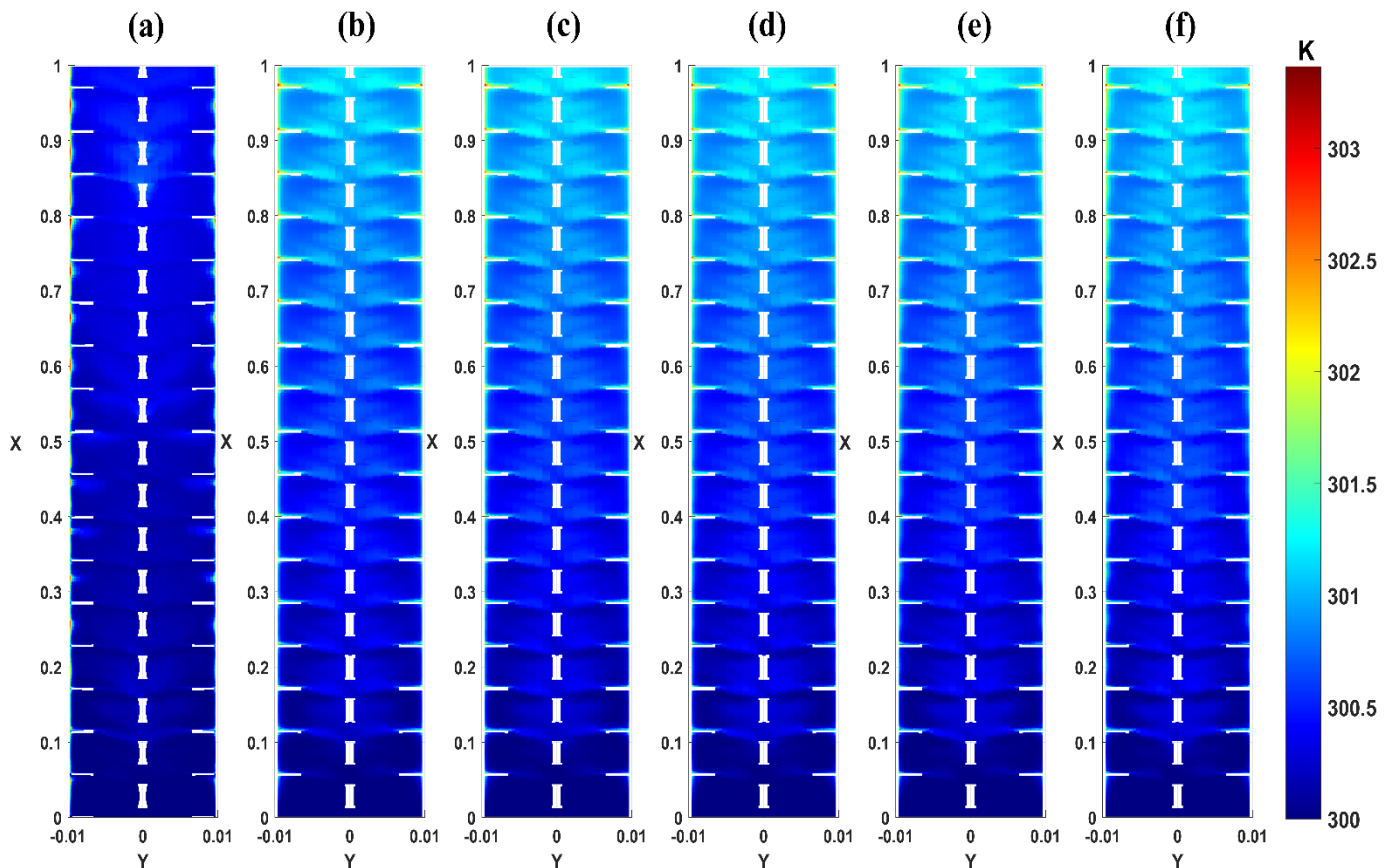
Figure 6-4 Temperature contour (a) forced convection Re =7000 (b) mixed convection Re=7000 (c) mixed convection Re=9000 (d) mixed convection Re=11000 (e) mixed convection Re=13000 and (f) mixed convection Re=15000.

6.6.2 Velocity contours

In a cross-sectional plane, the flow velocity for Al_2O_3/Cu-water hybrid-nanofluid ($\emptyset = 2$ %) in the TECT is (a) forced convection at (Re = 7000), and (b-f) mixed convection at Reynolds numbers 7000, 9000, 11000, 13000, and 15000, as exhibited in Figure 6-5. It is obvious that the velocity is larger in all instances between the surface of the twisted tape and the pipe wall. This phenomenon occurs because the rotating flow created by elliptical cut twisted tape enhances heat and mass transport from the core to the area close to the wall and vice versa [119, 155]. Furthermore, Figure 6-5 (b-f) also demonstrates that the flow rises around the twisted tape because of the buoyancy force as compared with forced convection in Figure 6-5 (a).

Computational study of entropy production and thermohydraulic of mixed convection of hybrid-nanofluid in a vertical tube supplied with elliptical-cut twisted tape inserts.
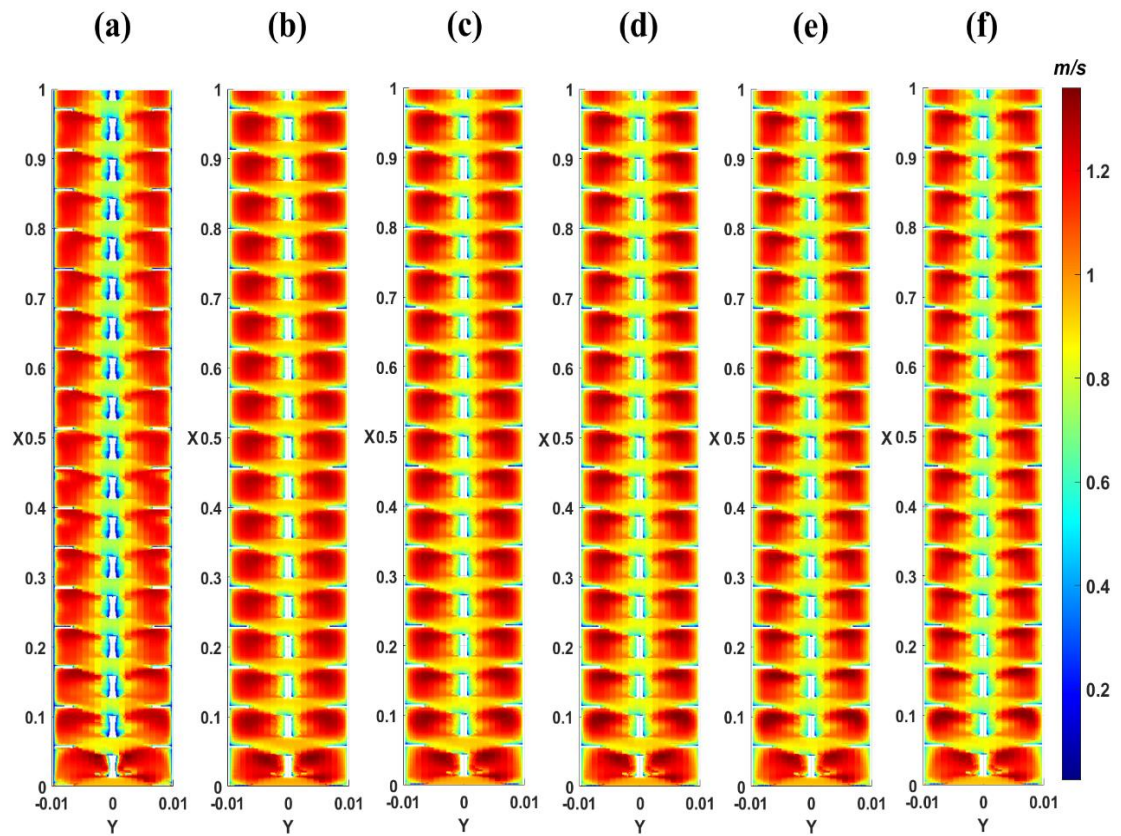
Figure 6-5 Velocity contour for (a) forced convection Re =7000 (b) mixed convection Re=7000 (c) mixed convection Re=9000 (d) mixed convection Re=11000 (e) mixed convection Re=13000 and (f) mixed convection Re=15000.

6.6.3 Turbulent kinetic energy contours

At Re = 7000 and $\emptyset$ = 2 %, Figure 6-6 (frames a and b) presents a comparison of the turbulence kinetic energy in the forced convection and the mixed convection, respectively. The turbulence kinetic energy gradually increases until it reaches the end of the tube. The maximum turbulence kinetic energy of TECT in forced convection (frame a) was around 65% lower than in TECT with mixed convection (frame b). In Figure 6-6 (frames a - f), the kinetic energy of turbulence in the region of the cuts in the tape was greater than the turbulence kinetic energy in the surrounding area. In Oni and Pual's [151] viewpoint, this is due to the disruptions the cuts cause to the flow. It is clear that when Reynolds numbers approach (b) (7000), (c) (9000), (d) (11,000), (e) (13,000), and (f) (15000), the turbulence kinetic energy improves significantly. Turbulence kinetic energy rises when the Reynolds number rises because of the increasing velocity [151].
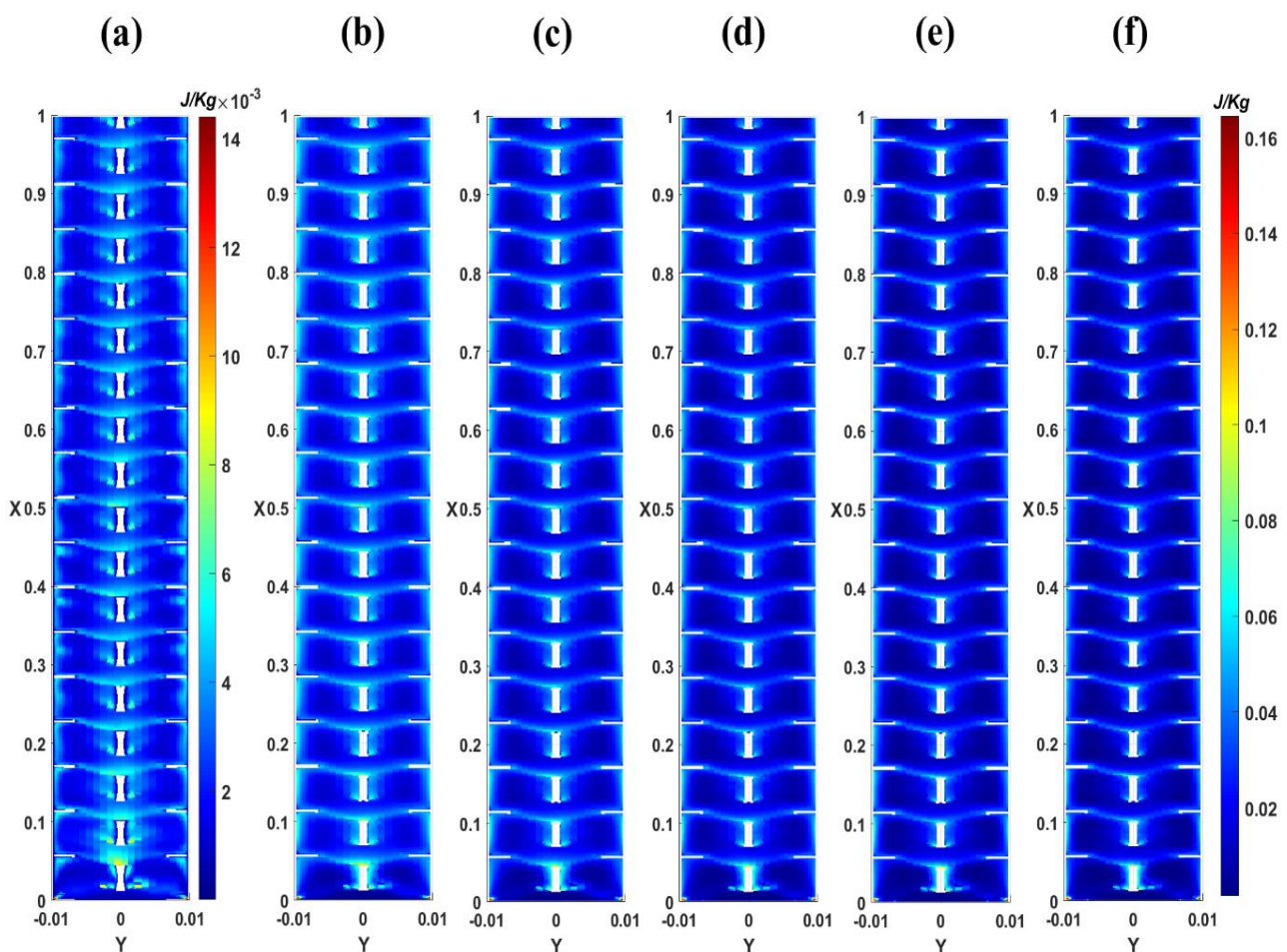
Figure 6-6 Turbulent Kinetic energy contour for (a) Forced convection at Re=7000 (b) mixed convection Re=7000 (c) mixed convection Re=9000 (d) mixed convection Re=11000 (e) mixed convection Re=13000 and (f) mixed convection Re=15000.

6.6.4 Mixed convection heat transfer

Table 6.3 displays the correlation between the Reynolds Number and Richardson Number. As seen in Table 6.3, the Richardson Number drops as the Reynolds Number rises because of higher forced convection. The effects of buoyancy are generally disregarded at the high Reynolds numbers (Re) of the impose forced flow [147]. Table 6.3 also reveals that heat transfer rates are greater for Ri ≥ 1 than for pure forced convection, showing that free convection effects are more dominant than forced convection effects. This is similar with [147].

Table 6.3 Richardson number versus Reynolds number in TECT for Al_2O_3-Cu/water.

Re	7000	9000	11000	13000	15000
Ri	8.22	4.97	3.33	2.38	1.79

6.6.5 Outlet temperature and velocity

Figure 6-7 depicts the impact of nanoparticle concentrations at varying Reynolds numbers on the outlet temperature for turbulent Al_2O_3-Cu/water hybrid nanofluids. In this case, it was observed that raising the Reynolds number resulted in a drop in the output temperature. As the concentration of nanoparticles increased, however, the normalised temperature decreased slightly. As a result, while raising $\emptyset_{hnf}$ from 1 to 4%, the outlet temperature is reduced by around 9.4%. Therefore, it seems that, for the same mass flow rate, an increase in the concentration of particles results in a degradation of secondary motion caused by buoyancy force. This is because the addition of nanoparticles leads to a significant increase in dynamic viscosity compared to pure water, particularly at high nanoparticle concentrations. These findings demonstrate that effective thermal conductivity alone is insufficient to fully define the heat transfer behaviour of nanoparticles. Various physical variables (density, thermal expansion coefficient, heat capacity) can influence nanoparticle heat transfer characteristics in forced convection [237] and free convection [238]. The impacts of nanoparticle concentrations on the outflow velocity are shown in Figure 6-8 for turbulent Al_2O_3-Cu/water hybrid nanofluids. The figure shows that the average outlet velocity rises as the Reynolds number and nanoparticles rise due to the thermophysical properties. So, when $\emptyset_{hnf}$ goes from 1 to 4%, the average outlet velocity goes up by about 10.9%.

Computational study of entropy production and thermohydraulic of mixed convection of hybrid-nanofluid in a vertical tube supplied with elliptical-cut twisted tape inserts.
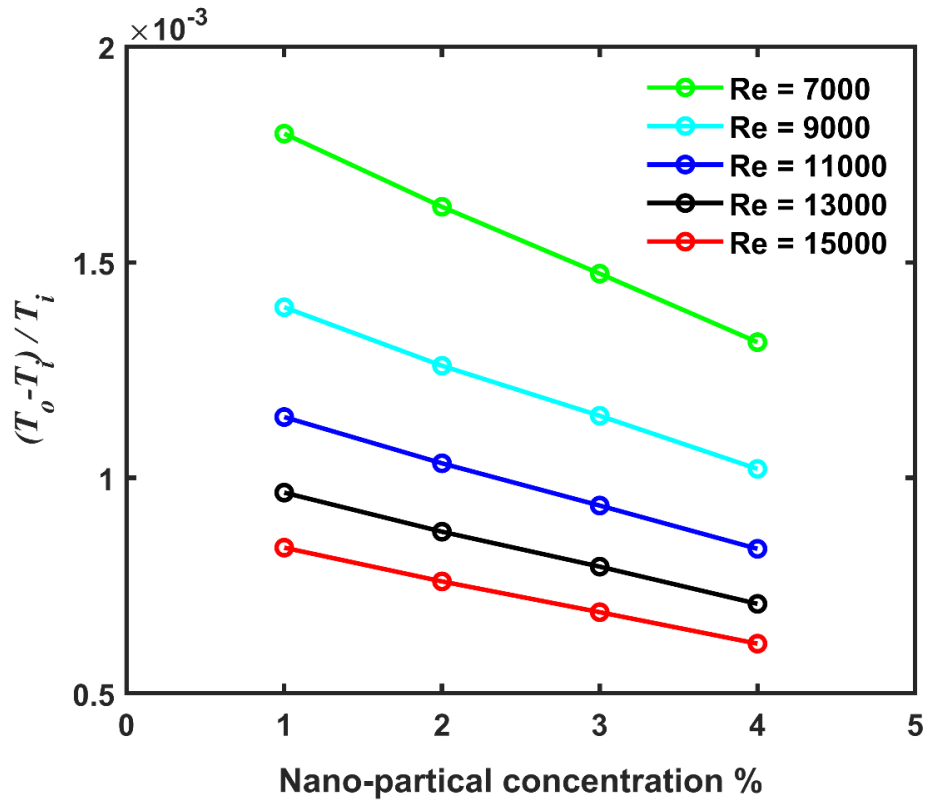
Figure 6-7 Average outlet temperature at different nanoparticle concentrations and Reynolds numbers.
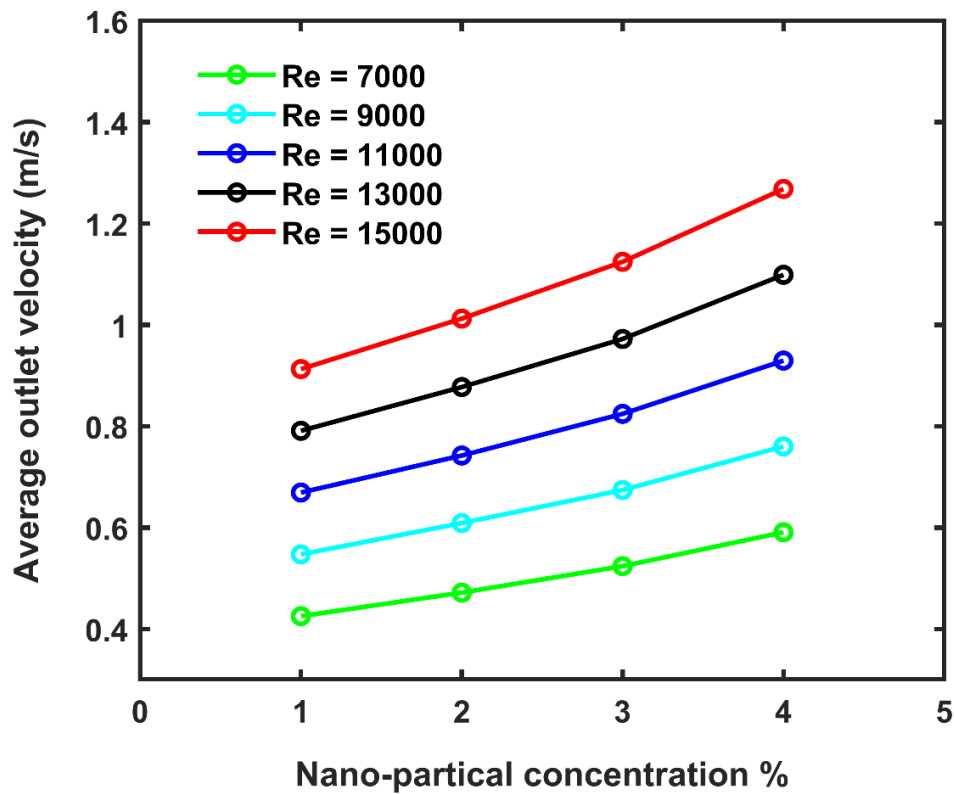
Figure 6-8 Average outlet velocity at different nanoparticle concentrations and Reynolds numbers.

6.6.6 Nusselt number

The Nusselt number was used to evaluate heat transmission in this section. Figure 6-9 (a-d) shows the comparison of the Nusselt numbers for the mixed convection and the forced convection at different nanoparticle concentrations. Mixed convection had a higher Nusselt number than forced convection, at 4.6% higher. Mixed convection improves heat transfer by using both forced and natural convection simultaneously, resulting in three distinct processes. A forced convection process produces external forces, and buoyant forces resulting from natural convection. Forced convection lowered thermal resistance and boosted heat transfer because of the external force. A reduction in thermal resistance and a rise in heat transmission were seen when buoyant force was applied in the same direction as the primary flow of the pipe. As a result, the buoyant component disrupted the boundary layer, increasing the rate of heat transmission [151, 239]. Figure 6-10 illustrates the effect of the concentration of nanoparticles in TECT on the heat transmission of hybrid nanofluid (Al_2O_3–Cu/water) flow at different Reynolds numbers. Heat transfer is improved, as expected, with both increased Reynolds number and nanoparticle concentration. According to [155, 220], this is because as the number of nanoparticles rises, the thermal conductivity increases, so the rate of heat transmission increases.

Computational study of entropy production and thermohydraulic of mixed convection of hybrid-nanofluid in a vertical tube supplied with elliptical-cut twisted tape inserts.
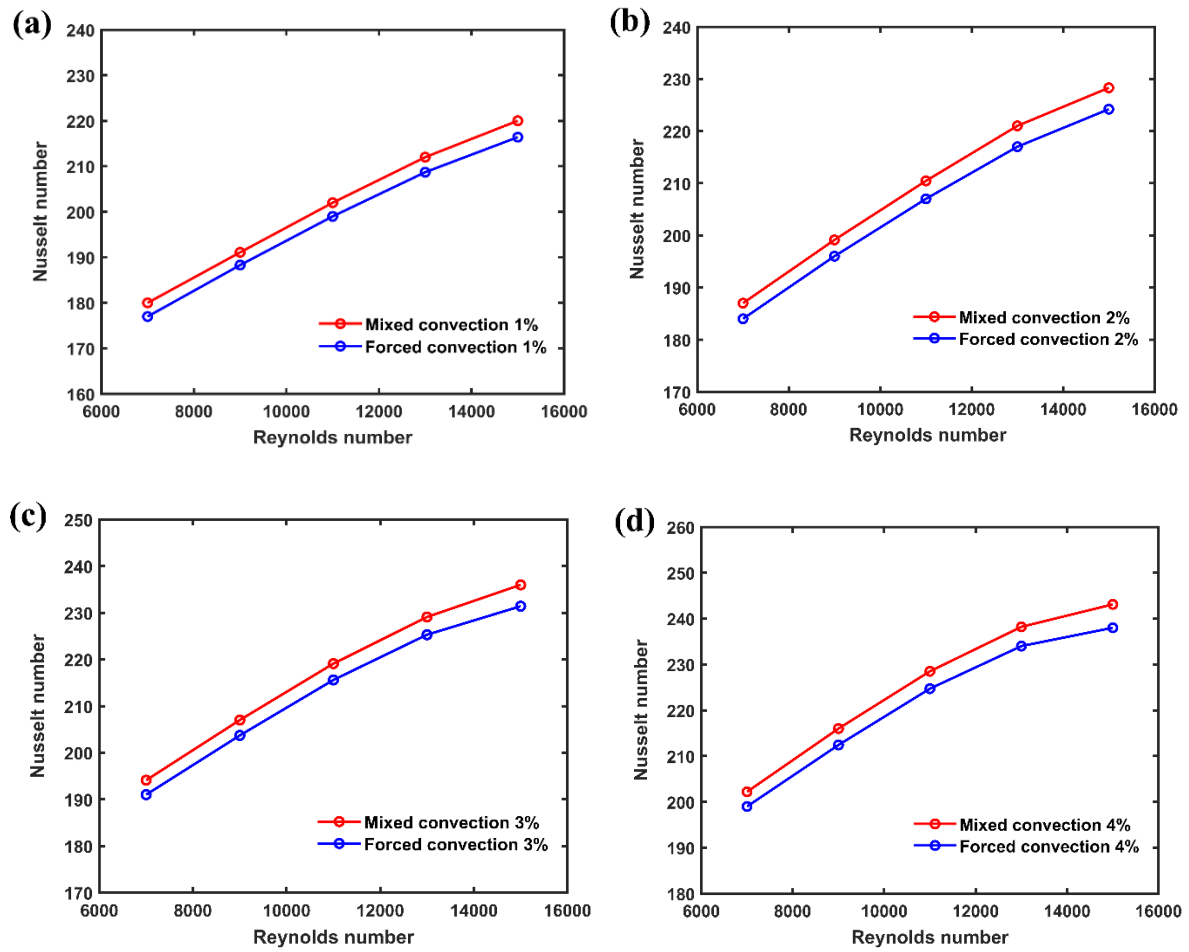
Figure 6-9 Effect of Nusselt number for various Reynolds numbers with different concentration of Al_2O_3-Cu/water (a) 1%, (b) 2%, (c) 3%, and (d) 4%
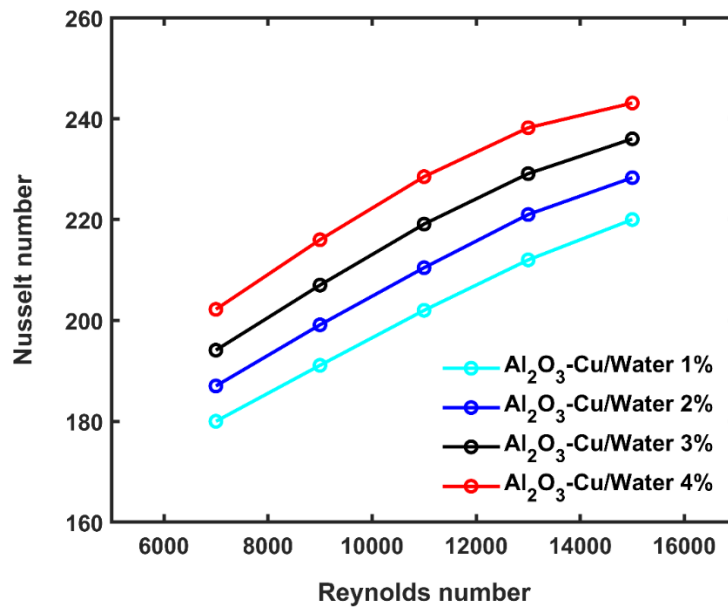
Figure 6-10 Variation of Nusselt number of Al_2O_3-Cu versus Reynolds number for different nanoparticle concentrations of mixed convection.

6.6.7 Friction factor

Figure 6-11 illustrates the friction factor vs Reynolds number of the mixed convection and the forced convection at ($\emptyset$ =2 %). As expected, mixed convection had a significantly higher friction factor than forced convection. The force of buoyancy caused by free convection operating on the flow, as well as the forces caused by forced convection operating on the flow, are responsible for this [151]. The friction factor was up to 13.6% higher in tubes with elliptical tape for mixed convection than in tubes with forced convection. Figure 6-12 depicts the impact of different nanoparticle concentrations on the friction factor for (a) mixed and forced convection at Re = 11,000, and (b) with different Reynolds numbers. As illustrated, friction factor values are found to be consistent across all tested nanoparticle concentrations. This is owing to the Reynolds number and surface roughness having the greatest influence on the friction factor [155, 240].
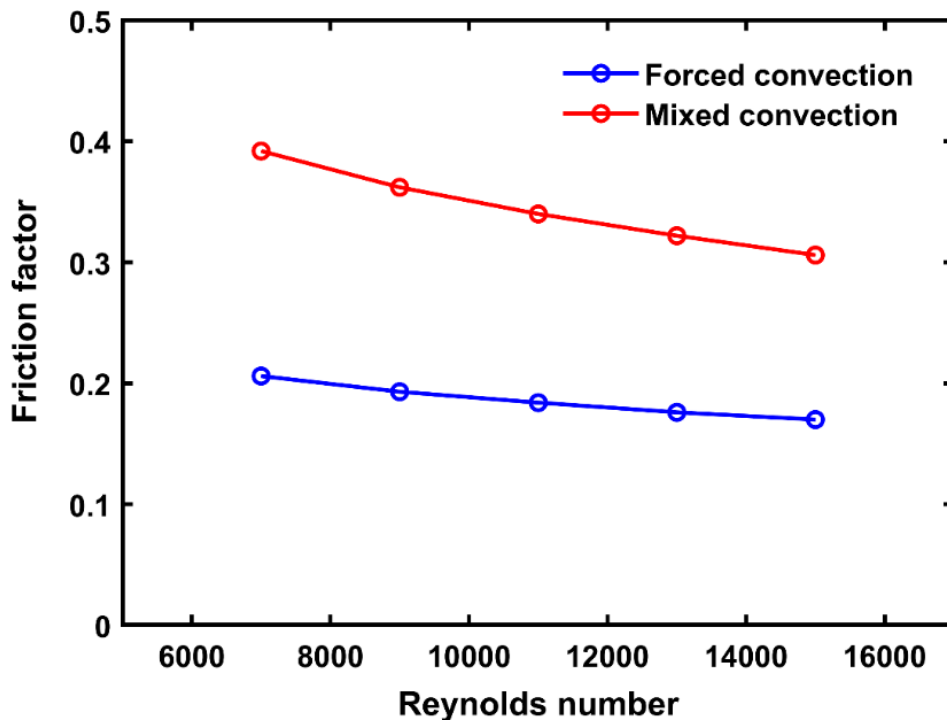
Figure 6-11 Variation of the friction factor in relation to the Reynolds number at ($\emptyset$ =2 %).
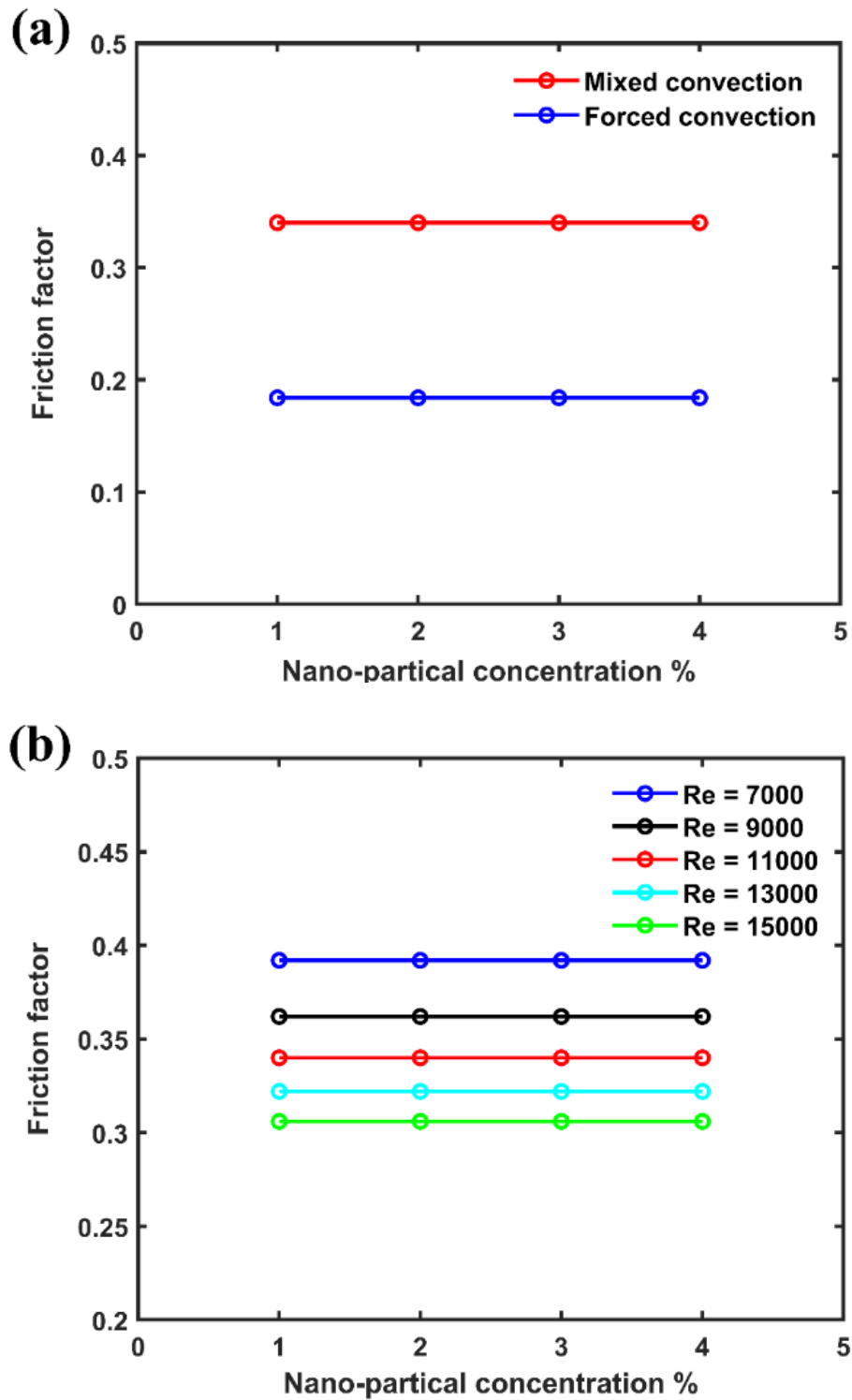
Figure 6-12 Friction factor variation with different nanoparticle concentrations of (a) mixed and forced convection with Re= 11,000 and (b) at different Reynolds numbers.

6.6.8 Thermal performance factor (TPF)

Figure 6-13 (a-d) shows the variation of the factor of thermal performance with Reynolds number in mixed convection and forced convection. The results reveal an increase in heat transmission rate for mixed convection. The thermal performance factor for mixed convection exceeded that for forced convection. Even though the use of mixed convection results in an increase in friction factor, as stated in the preceding section, thermal performance is improved due to a moderate rise in heat transfer rate [241]. Quantitatively, the mixed convection had a thermal performance factor that was up to 5.5% higher than the forced convection.
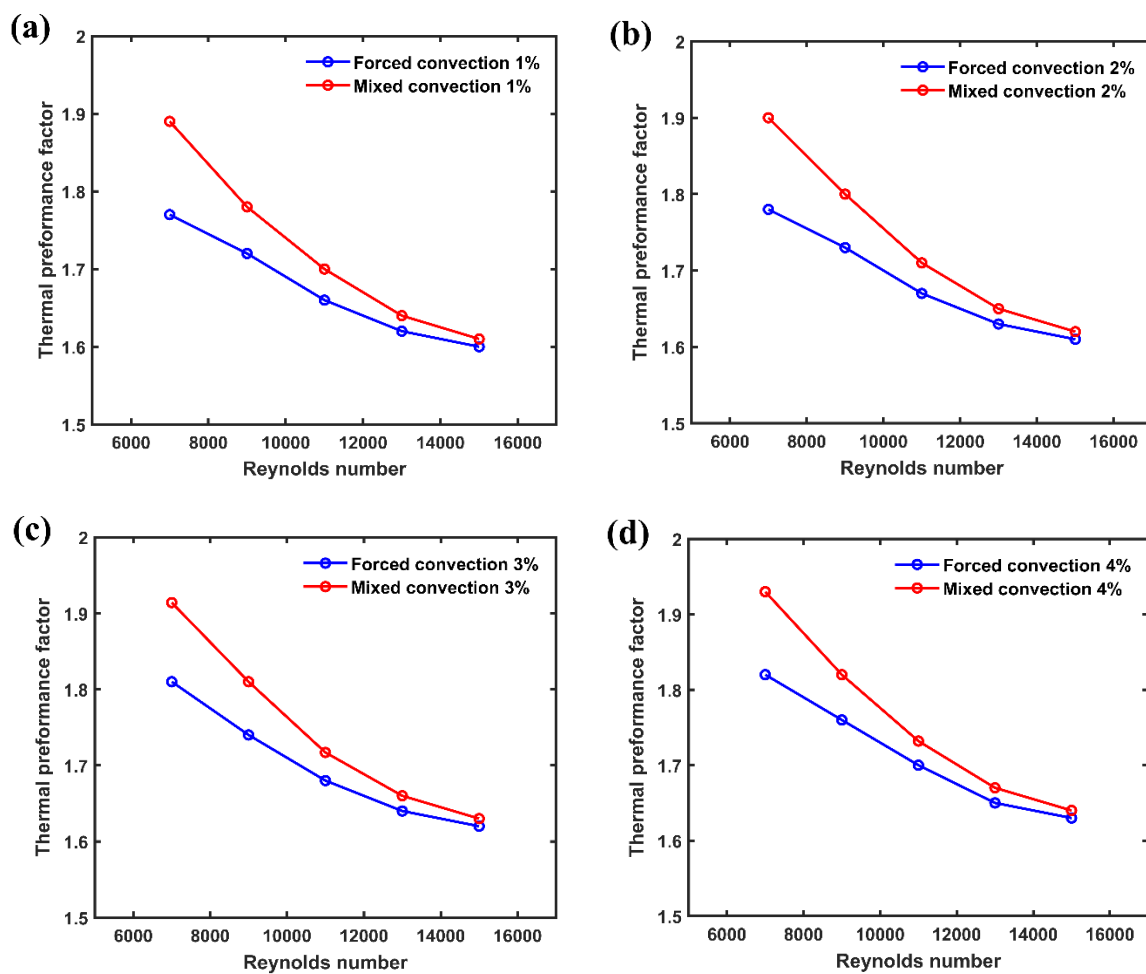
Figure 6-13 The influence of the thermal performance factor vs the Reynolds Number with various concentration of Al_2O_3-Cu/water (a) 1 %, (b) 2 %, (c) 3 %, and (d) 4%

.

6.6.9 Entropy Generation analysis

This section includes an examination of the generation of entropy during mixed convection for a hybrid nanofluid (Al$_2$O$_3$-Cu/water) at $\emptyset = 2\%$ in a tube supplied with elliptical cut twisted tape inserts for Reynolds numbers from 7000 to 15000. In addition, total entropy generation and Bejan number for a hybrid nanofluid (Al$_2$O$_3$-Cu/water) are examinate at $\emptyset$ from 1% to 4%. The irreversibilities (entropy) are generated due to irreversible fluid friction and heat transmission [183]. Thermal systems produce entropy through both irreversible dissipation of kinetic energy through fluid friction and heat transmission due to temperature differences [183]. The primary objective of this study is to assess the influence of mixed convection in a TECT within the production principles of entropy, considering solely the effects of fluid friction and transfer of heat.

6.6.9.1 The local entropy production

The improvement of local entropy creation and local Bejan numbers are shown in Figures (6-14 to 6-16). Figure 6-14 depicts the local distribution of thermal entropy generation at different Reynolds numbers (a) 7000, (b) 9000, (c) 11000, (d) 13000, and (e) 15000. The findings reveal that the highest thermal entropy production in TECT arises in the region close to the pipe wall and the twisted tape surface, where the temperature differential is greatest. This is because the elliptical-cut twisted tape creates a strong swirl flow in the pipe, thus enhances entropy production due to heat transmission [155]. Furthermore, thermal entropy generation has negligible values across wider cross sections at higher Reynolds numbers because the thermal boundary layer expands more slowly at higher Reynolds numbers, this is consistent with the findings of Refs [225, 242]. For turbulent flow, the thermal part of the rate of entropy production is no longer dependent only on conductivity, it depends on viscosity also [243]. In addition, as the buoyancy effect increases, the density of the fluid varies as well as when the Reynolds number grows. Moreover, the thermal conductivity in the system increases, while it decreases towards the wall and the twisted tape surface [242]. At different Reynolds numbers, the different thermal conductivities and temperature distributions affect both the quality of the temperature gradient changes and the way the thermal boundary layer develops. Because the thermal conductivity close to the wall as well as twisted tape is reduced at higher Reynolds numbers , the temperature gradient in these places increases more than normal, which has an influence on the rate of thermal entropy production [242].

Computational study of entropy production and thermohydraulic of mixed convection of hybrid-nanofluid in a vertical tube supplied with elliptical-cut twisted tape inserts.

Figure 6-15 depicts the local distribution of frictional entropy production at various Reynolds numbers (a) 7000, (b) 9000, (c) 11000, (d) 13000, and (e) 15000. As can be observed, the rate of frictional entropy generation improves as Reynolds number rises. The rise in Reynolds number raises the velocity gradient, which in turn increases the generation of frictional entropy. As demonstrated in Figure 6-15, the entropy production due to fluid friction around the elliptical-cut twisted tape rotational axis increases significantly. This rise is caused the use of twisted tape in this area, which makes flow velocity gradients bigger [155]. Figure 6-16 illustrates the local distribution of Bejan number for Reynolds numbers (a) 7000, (b) 9000, (c) 11000, (d) 13000, and (e) 15000. As a consequence, the contour of the local Bejan number is nearly symmetric. In Figure 6-16 (frames a-c), the range of Bejan number is between 0.8 and 1.0, showing that irreversible heat transfer occurs throughout the pipe. However, the range of Bejan numbers in (frames d-e) is less than 0.8, indicating that fluid friction irreversibilities are dominant throughout the pipe [244].
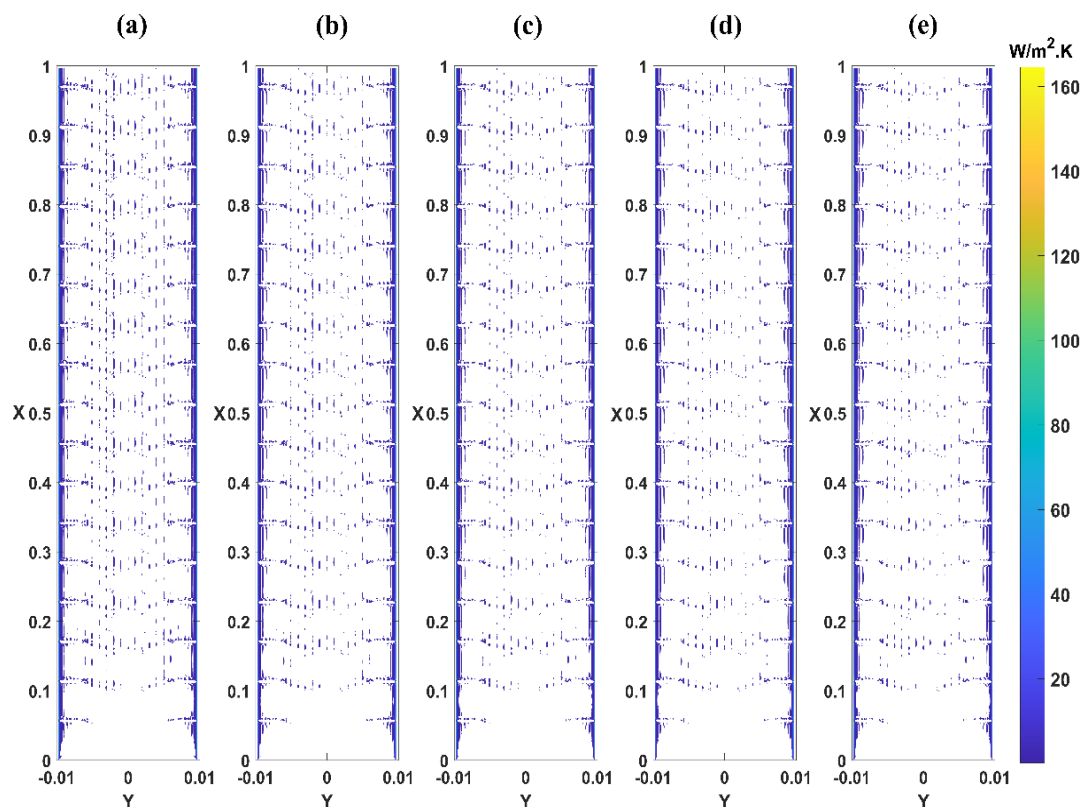
Figure 6-14 Spatial distribution of thermal entropy generation for (a) Re= 7000 (b) Re= 9000 (c) Re= 11000 (d) Re= 13000 and (e) Re= 15000.

Computational study of entropy production and thermohydraulic of mixed convection of hybrid-nanofluid in a vertical tube supplied with elliptical-cut twisted tape inserts.
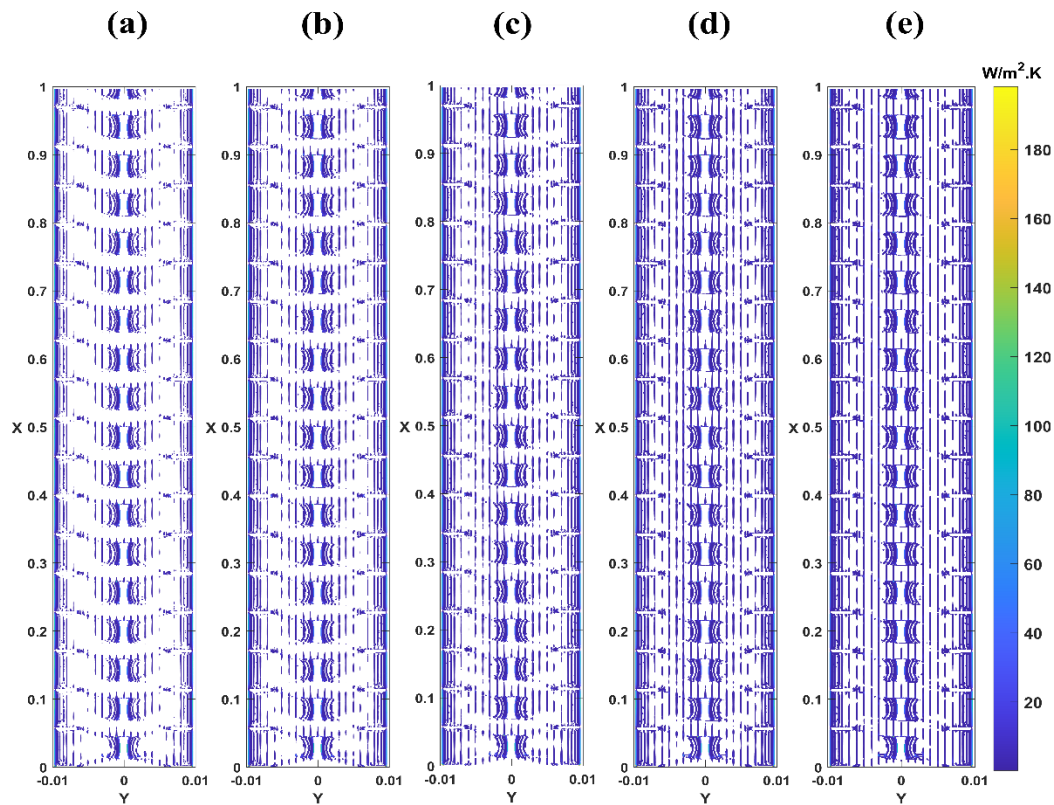
Figure 6-15 Spatial distribution of frictional entropy generation for (a) Re= 7000 (b) Re= 9000 (c) Re= 11000 (d) Re= 13000 and (e) Re= 15000.
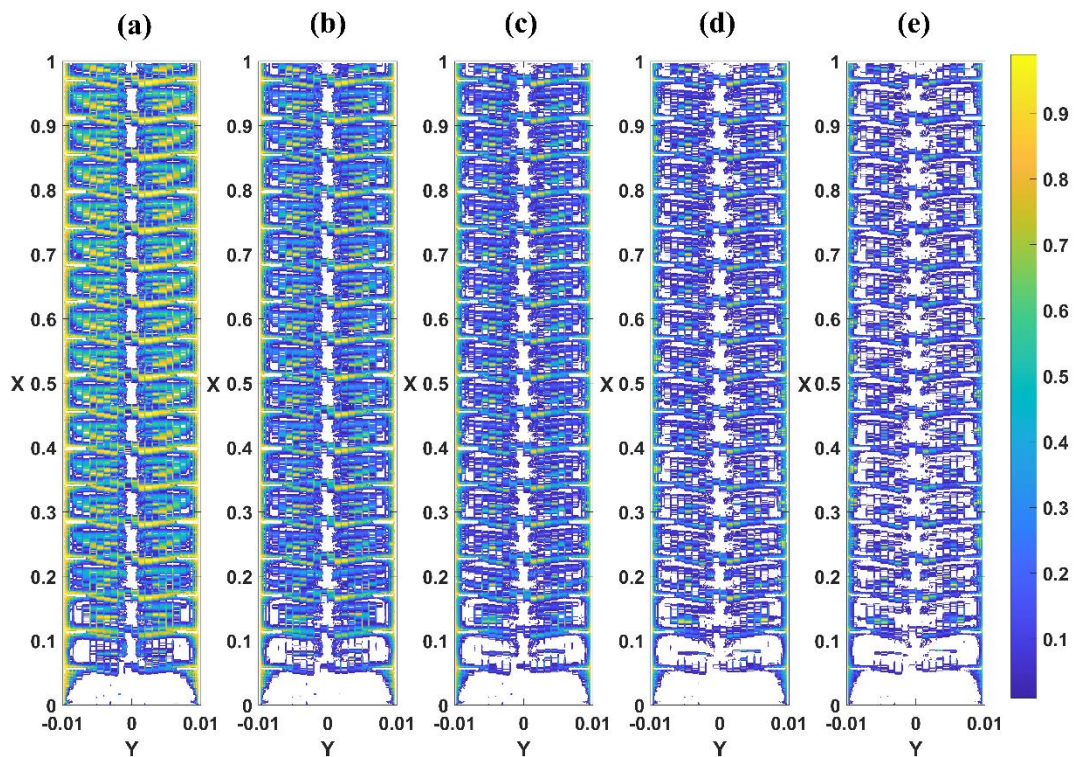
Figure 6-16 Bejan number for (a) Re= 7000 (b) Re= 9000 (c) Re= 11000 (d) Re= 13000 and (e) Re= 15000.

6.6.9.2   nTotal entropy generation and Bejan number

As previously stated, the entropy generation consists of two components: irreversibility of heat transfer across a finite temperature difference and fluid friction. Figure 6-17 (a and b) demonstrate the fluctuation of these parts and their relative contribution to the generation of total entropy as the Reynolds number rises. Figure 6-17 (a) illustrates the comparison of the thermal entropy generation for mixed convection and forced convection. It is clearly seen that as the Reynolds number improves, thermal entropy production reduces. It should be noted that the rate of heat transmission rises as the Reynolds number rises. In addition, the mixed convection heat transfer rate was higher than forced convection. Consequently, thermal entropy generation is reduced as the temperature gradients in the flow field decrease [170]. Observe that the thermal entropy generation is concentrated in the region close to the pipe wall and twisted tape where the temperature gradient is the greatest. Note also that a small amount of thermal entropy is generated between the tube's wall and the twisted tape (Figure 6-14). As a result, the temperature gradient in this area is reduced due to the formation of a secondary flow region. Quantitatively, mixed convection had a lower thermal entropy generation rate than forced convection, at 40% lower. Figure 6-17 (b) provides a study of the frictional entropy generation for forced and mixed convection versus different Reynolds numbers. As can be understood, in forced and mixed convection, when the Reynolds number rises the frictional entropy production rate intensifies. The main cause of such an increment, evident in Figure 6-5, is related to the velocity gradient increment [155].

Figure 6-18 depicts the variation of total entropy generation for various Reynolds numbers for (a) forced and mixed convection and (b) different Al_2O_3-Cu/water hybrid nanofluid concentrations. Regarding Figure 6-18 (a), as predicted, mixed convection has a significant effect on the total entropy production, such that the greatest decrease in the rate of total entropy production is 38.45%. It is evident that at lower Reynolds numbers (7000, 9000, and 11000), heat transfer irreversibility is dominating, but fluid friction is dominant at higher Reynolds numbers (13000 and 15000). This is in agreement with [170]. Furthermore, the total entropy shows a minimum value at about Re = 11000. To show the impacts of nanoparticle concentration on the total entropy production reduction, Figure 6-18 (b) depicts the total entropy production decrement as a function of the increase in the hybrid nanofluid concentration from 1% to 4%.

As can be seen in Figure 6-18 (b), the Reynolds number has a significant impact on the rate of decrease of total entropy production, with the greatest reduction of 23% and 16.89 occurring under the conditions of Re = 11000 and concentrations of 1% and 2%, respectively. However, the findings also indicate that the total entropy production rate improves with the rise of Reynolds numbers above 11000 and nanoparticle concentration with Reynolds numbers above 7000, as a result of the increased production of thermal and frictional entropy [228]. With a Reynolds number of 13000, for instance, the rate of total entropy production of Al_2O_3-Cu/water hybrid nanofluid concentrations (2%, 3%, and 4%) is increased by 8.8%, 21.1%, and 40.3%, respectively, when the nanoparticle concentration is increased from 1%. Also, raising the Reynolds number from 13000 to 15000 increases the rate of total entropy creation of hybrid nanofluids by 18.9 at a nanoparticle concentration of 4%.

The Bejan number illustrates the influence of each irreversibility to the total entropy production. The Bejan number is the ratio of the irreversible thermal entropy production rate to the total entropy production rate. For Bejan numbers close to one, irreversible heat transfer predominates, while for Bejan numbers close to zero, irreversible fluid friction predominates. For both forced and mixed convection, the Bejan number varies with Reynolds number (see Figure 6-19 (a)).

At Re (7000, 9000, and 11000), the Bejan number is found to be near to 1 and then decreases with increasing Reynolds numbers. In the mixed convection, the Bejan number is about 0.54 at a Reynolds number of 11,000. According to Varol el at [201], when Be = 0.5, the rates of fluid friction and heat transmission entropy production are equal. At high Reynolds numbers (13000 and 15000), the entropy production is due to fluid friction irreversibility, leading to a value Bejan number close to zero since the buoyancy-induced flow velocity is high.

Finally, for Reynolds numbers between 7000 and 15000, Figure 6-19 (b) shows the impact of nanoparticle shape on the Bejan number at varying nanoparticle concentrations. Based on the data, it can be concluded that increasing the concentration of nanoparticles and the Reynolds number decreases the Bejan number, which implies that the ratio of thermal entropy in the overall entropy decreases and the ratio of frictional entropy increases [229].

(a)

(b)
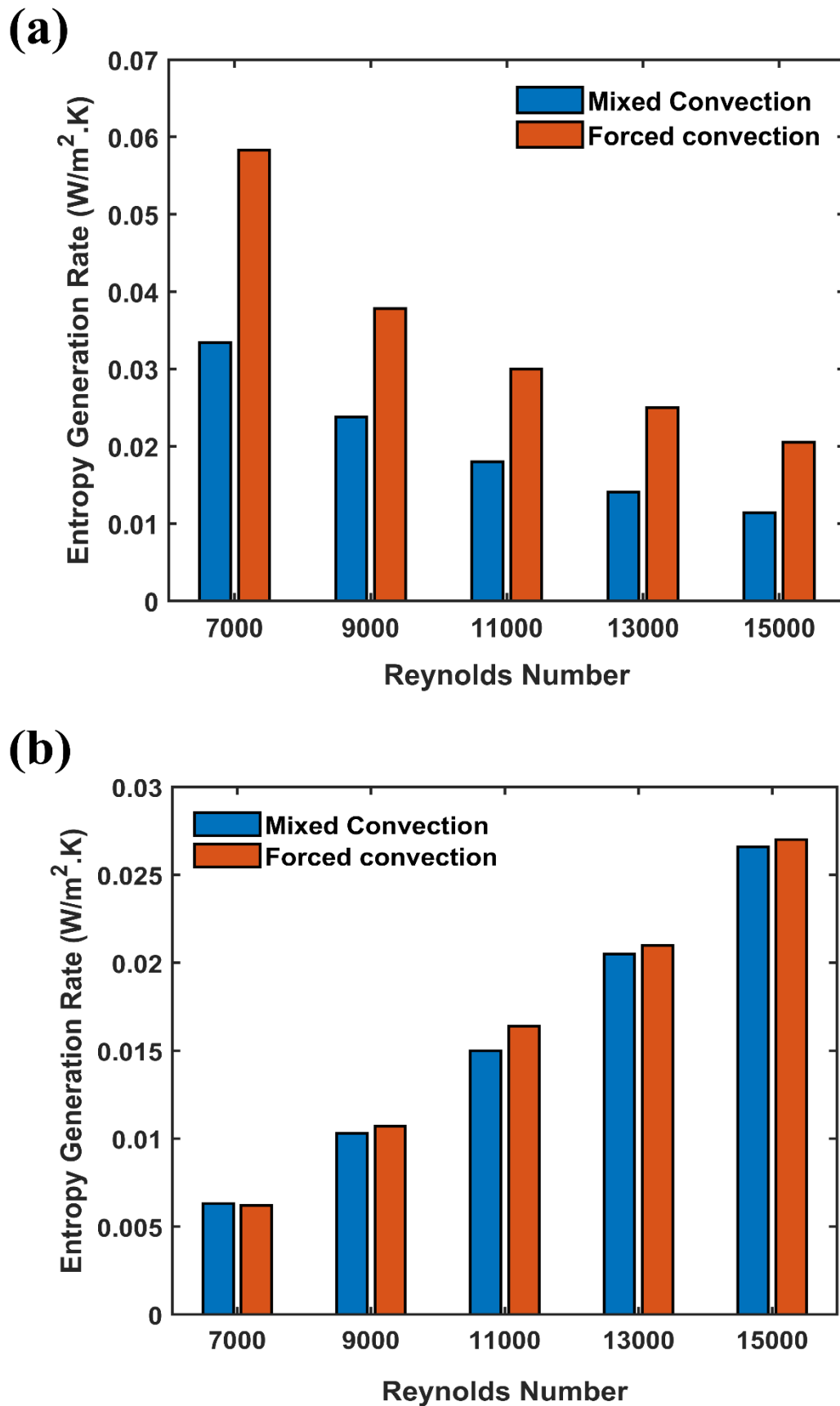
Figure 6-17 Entropy production due to (a) thermal (b) frictional

Computational study of entropy production and thermohydraulic of mixed convection of hybrid-nanofluid in a vertical tube supplied with elliptical-cut twisted tape inserts.
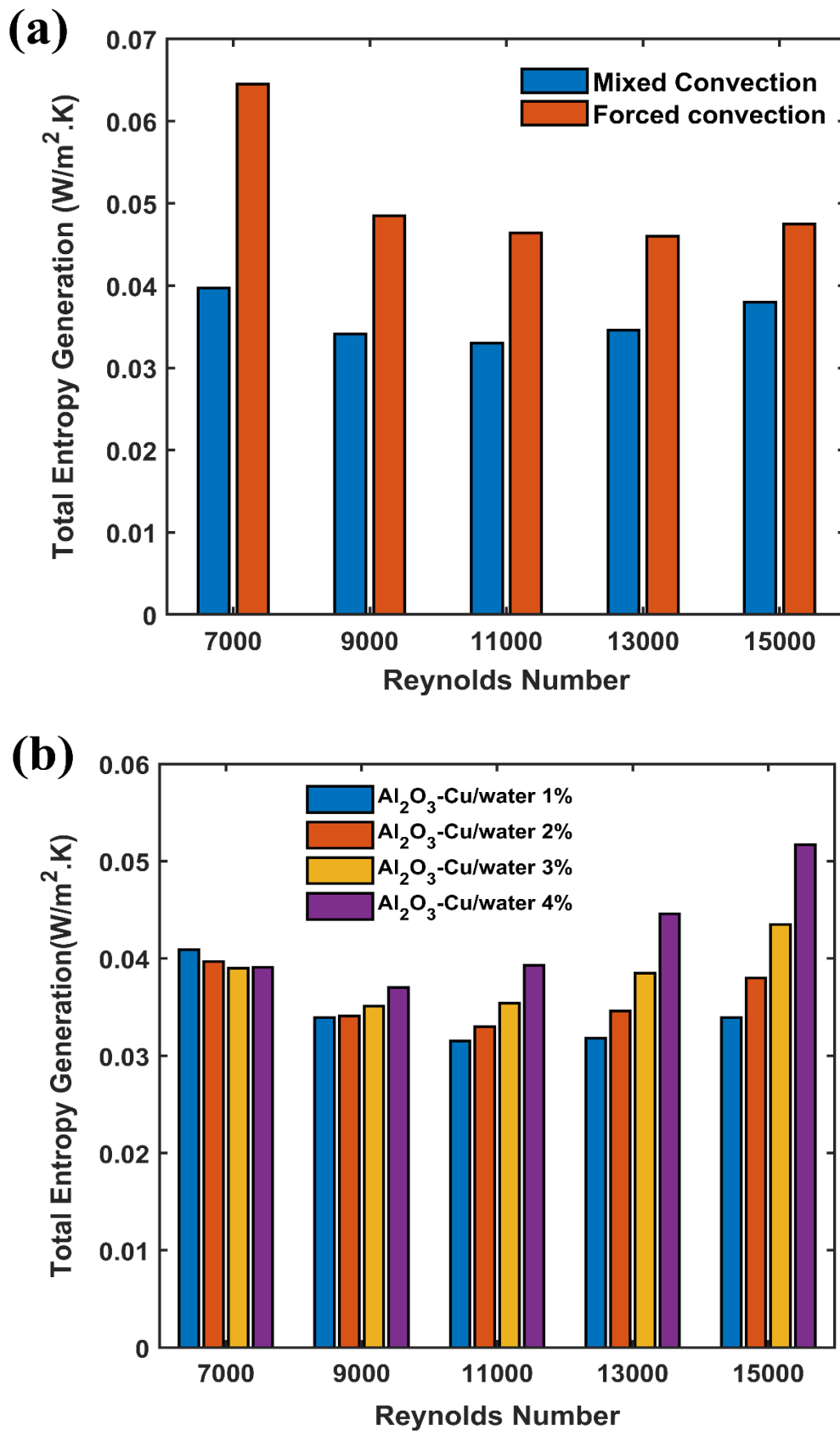
Figure 6-18 Total entropy creation (a) compare between mixed and forced convection at concentration 2% (b) varying concentrations of hybrid nanofluid.

Computational study of entropy production and thermohydraulic of mixed convection of hybrid-nanofluid in a vertical tube supplied with elliptical-cut twisted tape inserts.

(a)

(b)
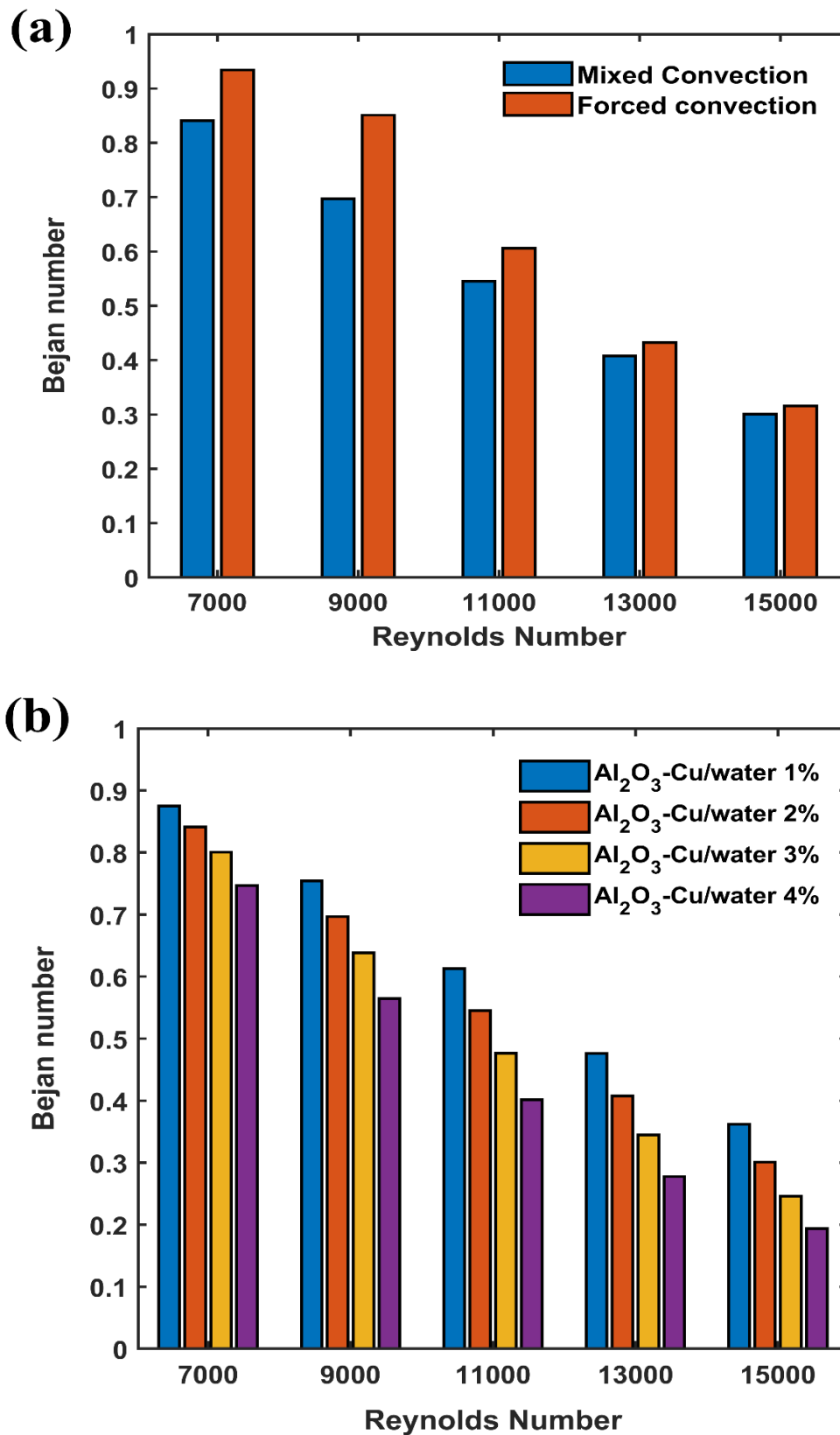
Figure 6-19 Bejan number against Reynolds number (a) compare between mixed and forced convection at concentration 2% (b) varying concentrations of hybrid nanofluid.

6.7 Comparing work with research findings

In addition to hybrid nanofluid and geometry of tube, the novel mixed convection also plays in enhancement heat transmission and reduces entropy production. The simulation findings of the proposed mixed convection of Al_2O_3-Cu/water hybrid-nanofluid in (TECT) are illustrated in Table 6.4. All data used in the comparisons are the best-observed findings in corresponding research. Novel mixed convection achieves better performance in the proposed work.

Table 6.4 Summary of research findings

References	Technique used	Fluids at Re = 7000	Heat transfer enhancement	Improve of thermal performance factor	Minimize total entropy generation
This work	Mixed convection	Al_2O_3-Cu/water	202	1.93	0.039 W/m^2.K
[155]	Forced convection	Al_2O_3-Cu/water	199	1.82	0.065 W/m^2.K
[240]	Forced convection	Nanofluid	190	1.7637	Null
[151]	Mixed convection	Water	180	Null	Null
[96]	Forced convection	Water	112	1.3	Null
[105]	Forced convection	Nanofluid	Null	Null	0.07 W/m^2. K

6.8 Conclusions

As a way to gain insight into how nanotechnology might improve heat transfer, this numerical study provided a three-dimensional simulation of turbulent mixed convection flow and entropy production analysis in a hybrid-nanofluid (Al_2O_3-Cu/water) pipe equipped with an elliptical-cut twisted tape for steady-state. The calculations were performed for Reynolds numbers ranging from 7000 to 15,000. The governing equations were solved by the finite volume method using a SIMPLE algorithm. The results obtained are summarised as follows:

- Mixed convection has greater values for the Nusselt number, friction factor, and thermal performance factor than forced convection. The Nusselt number and the thermal performance factor for mixed convection were 4.6% and 5.5% higher than for forced convection, respectively.

- As the Reynolds number increases, both the friction factor and the factor of thermal performance exhibit a reduction. This phenomenon can be attributed to the changing flow characteristics and heat transfer behaviour within the system.

- The improvement in heat transfer is observed when both the Reynolds number and nanoparticle concentrations are increased within the range of 1% to 4%. These combined factors contribute to enhanced heat transfer performance in the system.

- When the Reynolds number increases, there are two notable effects on entropy generation: a reduction in thermal entropy generation and an increase in frictional entropy production. These effects arise due to changes in the flow regime and the associated heat transfer characteristics.

- Mixed convection has a significant impact on the minimisation of the total entropy production. The rate of total entropy production is reduced by up to 38.45 % for mixed convection as compared with forced convection.

- Overall, thermal entropy production appears to be the predominant source of irreversibility in the problem at Reynolds numbers (7000, 9000, and 11000). Likewise, frictional entropy generation is the predominant mode of irreversibility in the problem at high Reynolds numbers (13000 and 15000). In turn, the minimal value of the total entropy occurs at about Re = 11000.

Chapter 7 Conclusions and Further Work

This thesis presents the results of a three-dimensional analytical study of heat transmission and fluid flow in a model parabolic trough receiver tube (an ordinary pipe and a tube supplied with elliptical-cut and classical twisted tape inserts). The investigation was carried out for turbulent flow under steady and unsteady conditions. The concept of mixed convection is also investigated. The main findings of the current study effort are given here in Section 7.1. Following this, an overview of recommendations for future studies is provided in Section 7.2.

7.1 Conclusions

In Chapter 4, numerical studies of turbulent steady flows of water, CuO/water nanofluid, and Al_2O_3-Cu/water hybrid nanofluid are investigated in a plain tube (PT) and a tube with classical (TPT) and elliptical-cut (TECT) twisted tape inserts. In this model, all tube walls are subjected to constant heat fluxes of 600 Wm^{-2} and 4000 Wm^{-2}, while the twisted tape wall condition is adiabatic. Numerical analysis of heat transmission and pressure drop was conducted at Reynolds numbers of (7000 - 15000) and volume concentrations of (1% – 4%). This research was carried out to determine which of the tubes and working fluids provides superior performance in terms of heat transmission, thermal performance factor, and entropy generation. It was observed that the TECT provides the highest performance when compared to PT and TPT. TECT has Nusselt number indices up to 170% higher than those of simple tube (PT). While the Nusselt number indices of TPT are up to 157% higher than those of simple tubes (PT). TECT has the factor of thermal performance up to 1.1 times that of TPT. In addition, by applying the hybrid nanofluid (Al_2O_3-Cu/water), the rate of heat transfer and the factor of thermal performance are enhanced substantially. The factor of thermal efficiency of hybrid nanofluid (Al2O3-Cu/water) at a Reynolds number of 7000 at $\emptyset = 4\%$ for TECT is about 1.9, which is 7.73% higher than for nanofluid (CuO/water). Furthermore, a second-law analysis revealed that at low heat flux the thermal processes dominated frictional processes, in contrast, fluid friction dominates at high heat flow regarding irreversibility.

In Chapter 5, a numerical analysis was conducted to investigate the impact of transient heat transmission enhancement as well as thermodynamic irreversibility in tubes equipped with elliptical-cut and classical twisted tape inserts under the non-uniform heat flux. In this work, water, nanofluid of CuO/water, and hybrid-nanofluid of Al_2O_3-Cu/water with a volume concentration of 2% were used as the working fluids. Part one of the results revealed that the

elliptical-cut twisted tape (TECT) in this study improves heat transfer by about 0.2%, 0.5%, and 0.6% of water, nanofluid (CuO/water), and hybrid nanofluid (Al$_2$O$_3$-Cu/water), respectively, when compared to the TPT. Second, by applying the hybrid nanofluid, the heat transfer rate experiences a significant augmentation. The effect of hybrid-nanofluid (Al$_2$O$_3$-Cu/water) in this investigate shows a good influence on the heat transmission. The maximum temperature difference is reduced to around 0.7% and 0.21% when compared to water and nanofluid, respectively. The entropy generated by thermal is the dominant source of irreversibility when the issue is in an unstable flow, the entropy increases with time due to temperature penetration into the tube's centre, increasing the gradient of temperature.

In Chapter 6, a numerical analysis was performed to study the mixed convection of hybrid-nanofluid (Al2O3-Cu/water) in a vertical tube supplied by elliptical-cut twisted tape inserts. Further, the Bejan number as well as the local and total entropy production of the system are calculated. The results show that, Due to buoyancy force, mixed convection has a higher Nusselt number, friction factor, and thermal performance than forced convection. The thermal performance factor and the Nusselt number for mixed convection were 5.5% and 4.1% higher than for forced convection, respectively. Mixed convection has a substantial impact on the minimisation of the total entropy production. Mixed convection reduces steady-state entropy generation by 38.45% compared to forced convection.

7.2 Recommendations for future work

In the present study, the thermo-hydraulic performance of various enhanced tubes and fluids was investigated with an emphasis on heat transmission augmentation, second law analysis (entropy generation), and new insights into heat transmission augmentation mechanisms have been gained, which opens the door for future research. Consequently, it is recommended that future studies consider the following:

- The influence of fluid fouling on twisted tape should be examined. Fouling may affect components such as the receiver tube of a parabolic trough, the surface of a heat exchanger, the flow channels of pipelines, turbines, solar panels, etc. Consequently, the proposed study will provide valuable outcomes.

- The flow of mixed convection in pipes fitted with twisted tape has not received adequate attention from a second-law analysis perspective. Therefore, further study is needed to fully realise the potential of the field.

- Extensive research on a variety of upgraded tubes and fluids is needed to fill out the current database on heat transfer improvement.

- Research into the Al_2O_3-Cu/water hybrid nanofluid that was studied here is required. This will undoubtedly allow for a comparison of the upcoming outcome with the existing findings on hybrid nanofluid. Additionally, an appropriate experiment has to be constructed to further evaluate the simulated outcomes of elliptical-cut twisted tape with the highest performance (TECT).

References

1.   Khalil, A. and A. Asheibe. *The chances and challenges for renewable energy in Libya*. in *the Proceedings of the Renewable Energy Conference*. 2015.

2.   Mohamed, O.A. and S.H. Masood. *A brief overview of solar and wind energy in Libya: Current trends and the future development*. in *IOP Conference Series: Materials Science and Engineering*. 2018. IOP Publishing.

3.   Aldali, Y. and K. Morad, *Numerical simulation of the integrated solar/North Benghazi combined power plant.* Applied Thermal Engineering, 2016. **108**: p. 785-792.

4.   Ummel, K. and D. Wheeler, *Desert power: the economics of solar thermal electricity for Europe, North Africa, and the Middle East.* Center for Global Development Working Paper, 2008(156).

5.   Kurokawa, K., *Energy from the Desert: Feasability of Very Large Scale Power Generation (VLS-PV)*. 2014: Routledge.

6.   Bellos, E. and C. Tzivanidis, *Alternative designs of parabolic trough solar collectors.* Progress in Energy and Combustion Science, 2019. **71**: p. 81-117.

7.   Arias, I., et al., *Modeling and Hourly Time-Scale Characterization of the Main Energy Parameters of Parabolic-Trough Solar Thermal Power Plants Using a Simplified Quasi-Dynamic Model.* Energies, 2021. **14**(1): p. 221.

8.   Collector, S.P.S. *Trough Parabolic Solar Collector*. 2011, Mar 25; Available from: https://www.energy.gov/eere/solar/articles/skytrough-parabolic-solar-collector.

9.   Jiji, L.M., *Heat convection*. 2009: Springer Science & Business Media.

10.   Ewis, K.M., *Effects of Variable Thermal Conductivity and Grashof Number on Non-Darcian Natural Convection Flow of Viscoelastic Fluids with Non Linear Radiation and Dissipations.* Journal of Advanced Research in Applied Sciences and Engineering Technology, 2021. **22**(1): p. 69-80.

11.   Holman, J.P., *Heat transfer*. 2010, McGraw Hill Higher Education.

12.   Wu, Z., et al., *Three-dimensional numerical study of heat transfer characteristics of parabolic trough receiver.* Applied Energy, 2014. **113**: p. 902-911.

13.   Wang, L. and B. Sunden, *Performance comparison of some tube inserts.* International Communications in Heat and Mass Transfer, 2002. **29**(1): p. 45-56.

14.   Kumbhar, D. and N. Sane. *Heat transfer enhancement in a circular tube twisted with swirl generator: a review*. in *Proceedings of the Third International Conference on Advances in Mechanical Engineering*. 2010.

15.   Krüger, D., et al., *Parabolic trough collector testing in the frame of the REACt project.* Desalination, 2008. **220**(1-3): p. 612-618.

16.   Hepbasli, A. and Z. Alsuhaibani, *A key review on present status and future directions of solar energy studies and applications in Saudi Arabia.* Renewable and Sustainable Energy Reviews, 2011. **15**(9): p. 5021-5050.

17.   Lane, H. and P. Heggs, *Extended surface heat transfer—the dovetail fin.* Applied thermal engineering, 2005. **25**(16): p. 2555-2565.

18.   Patil, A., *Laminar flow heat transfer and pressure drop characteristics of power-law fluids inside tubes with varying width twisted tape inserts.* J. Heat Transfer, 2000. **122**(1): p. 143-149.

19.   Saha, S., A. Dutta, and S. Dhal, *Friction and heat transfer characteristics of laminar swirl flow through a circular tube fitted with regularly spaced twisted-tape elements.* International Journal of Heat and Mass Transfer, 2001. **44**(22): p. 4211-4223.

20.   Bergles, A., *Techniques to enhance heat transfer.* Handbook of Heat Transfer, 1998. **3**: p. 11.1-11.76.

21.   Bejan, A. and A.D. Kraus, *Heat transfer handbook*. Vol. 1. 2003: John Wiley & Sons.

References

22. Manglik, R. and A. Bergles, *Heat transfer and pressure drop correlations for twisted-tape inserts in isothermal tubes: Part I—Laminar Flows.* 1993.

23. Choi, S.U. and J.A. Eastman, *Enhancing thermal conductivity of fluids with nanoparticles.* 1995, Argonne National Lab.(ANL), Argonne, IL (United States).

24. Balla, H.H., et al., *Numerical study of the enhancement of heat transfer for hybrid CuO-Cu nanofluids flowing in a circular pipe.* Journal of Oleo Science, 2013. **62**(7): p. 533-539.

25. Suresh, S., et al., *Synthesis of Al2O3–Cu/water hybrid nanofluids using two step method and its thermo physical properties.* Colloids and Surfaces A: Physicochemical and Engineering Aspects, 2011. **388**(1-3): p. 41-48.

26. Ghadikolaei, S., et al., *Investigation on thermophysical properties of Tio2–Cu/H2O hybrid nanofluid transport dependent on shape factor in MHD stagnation point flow.* Powder Technology, 2017. **322**: p. 428-438.

27. Alshare, A., W. Al-Kouz, and W. Khan, *Cu-Al2O3 water hybrid nanofluid transport in a periodic structure.* Processes, 2020. **8**(3): p. 285.

28. Anuar, N.S., N. Bachok, and I. Pop, *Cu-Al2O3/water hybrid nanofluid stagnation point flow past MHD stretching/shrinking sheet in presence of homogeneous-heterogeneous and convective boundary conditions.* Mathematics, 2020. **8**(8): p. 1237.

29. Lunsford, K.M., *Increasing heat exchanger performance.* Hydrocarbon Engineering, 1998. **77**: p. 786-793.

30. Dewan, A., et al., *Review of passive heat transfer augmentation techniques.* Proceedings of the Institution of Mechanical Engineers, Part A: Journal of Power and Energy, 2004. **218**(7): p. 509-527.

31. Manglik, R.M., *Plate heat exchangers for process industry applications: enhanced thermal-hydraulic characteristics of chevron plates.* Process, Enhanced and Multiphase Heat Transfer, 1996: p. 267-276.

32. Sidik, N.A.C., et al., *Recent progress on hybrid nanofluids in heat transfer applications: a comprehensive review.* International Communications in Heat and Mass Transfer, 2016. **78**: p. 68-79.

33. Sarkar, J., P. Ghosh, and A. Adil, *A review on hybrid nanofluids: recent research, development and applications.* Renewable and Sustainable Energy Reviews, 2015. **43**: p. 164-177.

34. Bergles, A., *The implications and challenges of enhanced heat transfer for the chemical process industries.* Chemical Engineering Research and Design, 2001. **79**(4): p. 437-444.

35. Manglik, R.M. and A.E. Bergles, *Heat transfer and pressure drop correlations for twisted-tape inserts in isothermal tubes: Part II—Transition and Turbulent Flows.* 1993.

36. Jehad, D. and G. Hashim, *Numerical prediction of forced convective heat transfer and friction factor of turbulent nanofluid flow through straight channels.* Journal of Advanced Research in Fluid Mechanics and Thermal Sciences, 2015. **8**(1): p. 1-10.

37. Lee, Y., *The use of nanofluids in domestic water heat exchanger.* J. Adv. Res. Appl. Mech, 2014. **3**(1): p. 9-24.

38. Abubakar, S. and N.C. Sidik, *Numerical prediction of laminar nanofluid flow in rectangular microchannel heat sink.* Journal of Advanced Research in Fluid Mechanics and Thermal Sciences, 2015. **7**(1): p. 29-38.

39. Bejan, A., *Entropy generation minimization: the method of thermodynamic optimization of finite-size systems and finite-time processes.* 2013: CRC Press.

40. Bejan, A., *Entropy generation minimization: The new thermodynamics of finite-size devices and finite-time processes.* Journal of Applied Physics, 1996. **79**(3): p. 1191-1218.

41. Nava, P., et al., *Status rep on solar trough power plants.* 1996, Tech. Rep. Cologne: Pilkington.

42. Maiga, S.E.B., et al., *Heat transfer enhancement by using nanofluids in forced convection flows.* International Journal of Heat and Fluid Flow, 2005. **26**(4): p. 530-546.

References

43. Minea, A.A., *A study on Brinkman number variation on water based nanofluid heat transfer in partially heated tubes.* Mechanics Research Communications, 2016. **73**: p. 7-11.
44. Ahmadi, K., et al., *Heat transfer assessment of turbulent nanofluid flow in a circular pipe fitted with elliptical-cut twisted tape inserts.* Journal of Thermal Analysis and Calorimetry, 2020.
45. Fernández-García, A., et al., *Parabolic-trough solar collectors and their applications.* Renewable and Sustainable Energy Reviews, 2010. **14**(7): p. 1695-1721.
46. Fernández-García, A., et al., *A parabolic-trough collector for cleaner industrial process heat.* Journal of Cleaner Production, 2015. **89**: p. 272-285.
47. Montes, I.E.P., et al., *Design and construction of a parabolic trough solar collector for process heat production.* Energy Procedia, 2014. **57**: p. 2149-2158.
48. Thomas, A., *Solar steam generating systems using parabolic trough concentrators.* Energy Conversion and Management, 1996. **37**(2): p. 215-245.
49. Mosleh, H.J., et al., *A new desalination system using a combination of heat pipe, evacuated tube and parabolic trough collector.* Energy Conversion and Management, 2015. **99**: p. 141-150.
50. Ullah, F. and M. Kang, *Impact of air flow rate on drying of apples and performance assessment of parabolic trough solar collector.* Applied Thermal Engineering, 2017. **127**: p. 275-280.
51. Balghouthi, M., et al., *Optical and thermal evaluations of a medium temperature parabolic trough solar collector used in a cooling installation.* Energy Conversion and Management, 2014. **86**: p. 1134-1146.
52. Elakhdar, M., et al., *A combined thermal system of ejector refrigeration and Organic Rankine cycles for power generation using a solar parabolic trough.* Energy Conversion and Management, 2019. **199**: p. 111947.
53. Wang, F., et al., *Performance assessment of solar assisted absorption heat pump system with parabolic trough collectors.* Energy Procedia, 2015. **70**: p. 529-536.
54. Eck, M., W.-D. Steinmann, and J. Rheinländer, *Maximum temperature difference in horizontal and tilted absorber pipes with direct steam generation.* Energy, 2004. **29**(5-6): p. 665-676.
55. Kalogirou, S., *Parabolic trough collector system for low temperature steam generation: design and performance characteristics.* Applied Energy, 1996. **55**(1): p. 1-19.
56. Klychev, S.I., et al., *Parameter optimization for paraboloid-cylinder-receiver system of thermal power plants.* Applied Solar Energy, 2009. **45**(4): p. 281-284.
57. Szargut, J. and W. Stanek, *Thermo-ecological optimization of a solar collector.* Energy, 2007. **32**(4): p. 584-590.
58. Bakos, G.C., *Design and construction of a two-axis Sun tracking system for parabolic trough collector (PTC) efficiency improvement.* Renewable Energy, 2006. **31**(15): p. 2411-2421.
59. Fischer, S., E. Lüpfert, and H. Müller-Steinhagen. *Efficiency testing of parabolic trough collectors using the quasi-dynamic test procedure according to the European Standard EN 12975.* in *SolarPACES 13th Symposium on Concentrating Solar Power and Chemical Energy Technologies*. 2006.
60. Liu, Q., et al., *Experimental investigation on a parabolic trough solar collector for thermal power generation.* Science in China Series E: Technological Sciences, 2010. **53**(1): p. 52-56.
61. Reddy, K., K.R. Kumar, and C. Ajay, *Experimental investigation of porous disc enhanced receiver for solar parabolic trough collector.* Renewable Energy, 2015. **77**: p. 308-319.
62. Evans, S. and R. Sarjant, *Heat transfer and turbulence in gases flowing inside tubes.* J. Inst. Fuel, 1951. **24**(9): p. 216-227.
63. Kreith, F. and D. Margolis, *Heat transfer and friction in turbulent vortex flow.* Applied Scientific Research, Section A, 1959. **8**(1): p. 457-473.

References

64. Ibragimov, M., E. Nomofelov, and V. Subbotin, *Heat transfer and hydraulic resistance with swirl-type motion of liquid in pipes.* Teploenergetika, 1961. **8**(7): p. 57-60.

65. Brevi, R., et al., *Forced convection heat transfer and burn-out measurements with twisted tapes*. 1971, Comitato Nazionale per l'Energia Nucleare.

66. Abu-Khader, M.M., *Further understanding of twisted tape effects as tube insert for heat transfer enhancement.* Heat and Mass transfer, 2006. **43**(2): p. 123-134.

67. Manglik, R.M. and A.E. Bergles, *Swirl flow heat transfer and pressure drop with twisted-tape inserts*, in *Advances in heat transfer*. 2003, Elsevier. p. 183-266.

68. Eiamsa-Ard, S., P. Seemawute, and K. Wongcharee, *Influences of peripherally-cut twisted tape insert on heat transfer and thermal performance characteristics in laminar and turbulent tube flows.* Experimental Thermal and Fluid Science, 2010. **34**(6): p. 711-719.

69. Eiamsa-ard, S., C. Thianpong, and P. Eiamsa-ard, *Turbulent heat transfer enhancement by counter/co-swirling flow in a tube fitted with twin twisted tapes.* Experimental Thermal and Fluid Science, 2010. **34**(1): p. 53-62.

70. Migay, V. and L. Golubev, *Friction and heat transfer in turbulent swirl flow with a variable swirl generator in a pipe.* Heat Transfer-Soviet Research, 1970. **2**(3): p. 68-73.

71. Burfoot, D., *Heat transfer and pressure drop characteristics of short lengths of swirl flow inducers interspaced along a circular duct.* 1983.

72. Eiamsa-Ard, S., et al., *Convective heat transfer in a circular tube with short-length twisted tape insert.* International Communications in Heat and Mass Transfer, 2009. **36**(4): p. 365-371.

73. Liao, Q. and M. Xin, *Augmentation of convective heat transfer inside tubes with three-dimensional internal extended surfaces and twisted-tape inserts.* Chemical Engineering Journal, 2000. **78**(2-3): p. 95-105.

74. Ayub, Z. and S. Al-Fahed, *The effect of gap width between horizontal tube and twisted tape on the pressure drop in turbulent water flow.* International Journal of Heat and Fluid Flow, 1993. **14**(1): p. 64-67.

75. Kumar, A. and B. Prasad, *Investigation of twisted tape inserted solar water heaters—heat transfer, friction factor and thermal performance results.* Renewable Energy, 2000. **19**(3): p. 379-398.

76. Murugesan, P., et al., *Heat transfer and pressure drop characteristics of turbulent flow in a tube fitted with trapezoidal-cut twisted tape insert.* International Journal of Academic Research, 2009. **1**(1): p. 123-128.

77. Jaisankar, S., T. Radhakrishnan, and K. Sheeba, *Experimental studies on heat transfer and friction factor characteristics of forced circulation solar water heater system fitted with helical twisted tapes.* Solar Energy, 2009. **83**(11): p. 1943-1952.

78. Murugesan, P., K. Mayilsamy, and S. Suresh, *Turbulent heat transfer and pressure drop in tube fitted with square-cut twisted tape.* Chinese Journal of Chemical Engineering, 2010. **18**(4): p. 609-617.

79. Saha, S.K., *Thermohydraulics of turbulent flow through rectangular and square ducts with axial corrugation roughness and twisted-tapes with and without oblique teeth.* Experimental Thermal and Fluid Science, 2010. **34**(6): p. 744-752.

80. Nanan, K., et al., *Investigation of heat transfer enhancement by perforated helical twisted-tapes.* International Communications in Heat and Mass Transfer, 2014. **52**: p. 106-112.

81. Skullong, S., et al., *Heat transfer and turbulent flow friction in a round tube with staggered-winglet perforated-tapes.* International Journal of Heat and Mass Transfer, 2016. **95**: p. 230-242.

82. Mengna, H., et al., *Compound heat transfer enhancement of a converging-diverging tube with evenly spaced twisted-tapes.* Chinese Journal of Chemical Engineering, 2007. **15**(6): p. 814-820.

83. Azmi, W., et al., *Comparison of convective heat transfer coefficient and friction factor of TiO2 nanofluid flow in a tube with twisted tape inserts.* International Journal of Thermal Sciences, 2014. **81**: p. 84-93.

84. Bhuiya, M., et al., *Heat transfer and friction factor characteristics in turbulent flow through a tube fitted with perforated twisted tape inserts.* International Communications in Heat and Mass Transfer, 2013. **46**: p. 49-57.

85. Ponnada, S., T. Subrahmanyam, and S.V. Naidu, *A comparative study on the thermal performance of water in a circular tube with twisted tapes, perforated twisted tapes and perforated twisted tapes with alternate axis.* International Journal of Thermal Sciences, 2019. **136**: p. 530-538.

86. Date, A.W., *Prediction of fully-developed flow in a tube containing a twisted-tape.* International Journal of Heat and Mass Transfer, 1974. **17**(8): p. 845-859.

87. Gupte, N. and A. Date, *Friction and heat transfer characteristics of helical turbulent air flow in annuli.* 1989.

88. Oni, T.O. and M.C. Paul, *Numerical investigation of heat transfer and fluid flow of water through a circular tube induced with divers' tape inserts.* Applied Thermal Engineering, 2016. **98**: p. 157-168.

89. Nakaharai, H., et al., *Numerical study of heat transfer characteristics in a tube with regularly spaced twisted tape.* Fusion Science and Technology, 2007. **52**(4): p. 855-859.

90. Eiamsa-Ard, P., et al., *A case study on thermal performance assessment of a heat exchanger tube equipped with regularly-spaced twisted tapes as swirl generators.* Case Studies in Thermal Engineering, 2014. **3**: p. 86-102.

91. Wang, Y., et al., *Configuration optimization of regularly spaced short-length twisted tape in a circular tube to enhance turbulent heat transfer using CFD modeling.* Applied Thermal Engineering, 2011. **31**(6-7): p. 1141-1149.

92. Yadav, R. and A.S. Padalkar, *CFD analysis for heat transfer enhancement inside a circular tube with half-length upstream and half-length downstream twisted tape.* Journal of Thermodynamics, 2012. **2012**.

93. Chiu, Y.-W. and J.-Y. Jang, *3D numerical and experimental analysis for thermal–hydraulic characteristics of air flow inside a circular tube with different tube inserts.* Applied Thermal Engineering, 2009. **29**(2-3): p. 250-258.

94. Eiamsa-ard, S., K. Wongcharee, and S. Sripattanapipat, *3-D Numerical simulation of swirling flow and convective heat transfer in a circular tube induced by means of loose-fit twisted tapes.* International Communications in Heat and Mass Transfer, 2009. **36**(9): p. 947-955.

95. Cui, Y.-z. and M.-c. Tian, *Three-Dimensional Numerical Simulation of Thermal-Hydraulic Performance of A Circular Tube with Edgefold-Twisted-Tape Inserts.* Journal of Hydrodynamics, 2010. **22**(5): p. 662-670.

96. Saysroy, A. and S. Eiamsa-ard, *Periodically fully-developed heat and fluid flow behaviors in a turbulent tube flow with square-cut twisted tape inserts.* Applied Thermal Engineering, 2017. **112**: p. 895-910.

97. Nakhchi, M. and J. Esfahani, *Numerical investigation of rectangular-cut twisted tape insert on performance improvement of heat exchangers.* International Journal of Thermal Sciences, 2019. **138**: p. 75-83.

98. Nakhchi, M. and J. Esfahani, *Performance intensification of turbulent flow through heat exchanger tube using double V-cut twisted tape inserts.* Chemical Engineering and Processing-Process Intensification, 2019. **141**: p. 107533.

99. Abuhatira, A.A., S.M. Salim, and J.B. Vorstius. *Numerical simulation of turbulent pipe flow with 90-degree elbow using wall y+ approach*. in *ASME International Mechanical Engineering Congress and Exposition*. 2021. American Society of Mechanical Engineers.

100. Abuhatira, A., S.M. Salim, and J. Vorstius. *Vibration-Based Leak Detection Approach in a 90-Degree Pipe Elbow: A Computational Study*. in *Proceedings of the 2022 Annual Conference of*

the UK Association for Computational Mechanics (UKACM). 2022. Nottingham University Press.

101. Azmi, W., et al., *Turbulent forced convection heat transfer of nanofluids with twisted tape insert in a plain tube.* Energy Procedia, 2014. **52**: p. 296-307.

102. Gorjaei, A.R. and A. Shahidian, *Heat transfer enhancement in a curved tube by using twisted tape insert and turbulent nanofluid flow.* J. Therm. Anal. Calorim., 2019. **137**(3): p. 1059-1068.

103. Naik, M., et al., *Comparative study on thermal performance of twisted tape and wire coil inserts in turbulent flow using CuO/water nanofluid.* Experimental Thermal and Fluid Science, 2014. **57**: p. 65-76.

104. Jafaryar, M., et al., *Nanofluid turbulent flow in a pipe under the effect of twisted tape with alternate axis.* Journal of Thermal Analysis and Calorimetry, 2019. **135**(1): p. 305-323.

105. Sheikholeslami, M., M. Jafaryar, and Z. Li, *Second law analysis for nanofluid turbulent flow inside a circular duct in presence of twisted tape turbulators.* Journal of Molecular Liquids, 2018. **263**: p. 489-500.

106. Nakhchi, M. and J. Esfahani, *Numerical investigation of turbulent CuO–water nanofluid inside heat exchanger enhanced with double V-cut twisted tapes.* Journal of Thermal Analysis and Calorimetry, 2021. **145**(5): p. 2535-2545.

107. Sundar, L.S. and K.V. Sharma, *Turbulent heat transfer and friction factor of Al2O3 Nanofluid in circular tube with twisted tape inserts.* International Journal of Heat and Mass Transfer, 2010. **53**(7-8): p. 1409-1416.

108. Sundar, L.S. and K. Sharma, *Heat transfer enhancements of low volume concentration Al2O3 nanofluid and with longitudinal strip inserts in a circular tube.* International Journal of Heat and Mass Transfer, 2010. **53**(19-20): p. 4280-4286.

109. Sundar, L.S., et al., *Effect of full length twisted tape inserts on heat transfer and friction factor enhancement with Fe3O4 magnetic nanofluid inside a plain tube: An experimental study.* International Journal of Heat and Mass Transfer, 2012. **55**(11-12): p. 2761-2768.

110. Wongcharee, K. and S. Eiamsa-ard, *Heat transfer enhancement by using CuO/water nanofluid in corrugated tube equipped with twisted tape.* International Communications in Heat and Mass Transfer, 2012. **39**(2): p. 251-257.

111. Suresh, S., et al., *A comparison of thermal characteristics of Al2O3/water and CuO/water nanofluids in transition flow through a straight circular duct fitted with helical screw tape inserts.* Experimental Thermal and Fluid Science, 2012. **39**: p. 37-44.

112. Naik, M.T. and L.S. Sundar, *Heat transfer and friction factor with water/propylene glycol-based CuO nanofluid in circular tube with helical inserts under transition flow regime.* Heat Transfer Engineering, 2014. **35**(1): p. 53-62.

113. Qi, C., et al., *Effect of rotating twisted tape on thermo-hydraulic performances of nanofluids in heat-exchanger systems.* Energy Conversion and Management, 2018. **166**: p. 744-757.

114. Sharma, K., L.S. Sundar, and P. Sarma, *Estimation of heat transfer coefficient and friction factor in the transition flow with low volume concentration of Al2O3 nanofluid flowing in a circular tube and with twisted tape insert.* International Communications in Heat and Mass Transfer, 2009. **36**(5): p. 503-507.

115. Khoshvaght-Aliabadi, M. and M. Eskandari, *Influence of twist length variations on thermal–hydraulic specifications of twisted-tape inserts in presence of Cu–water nanofluid.* Experimental Thermal and Fluid Science, 2015. **61**: p. 230-240.

116. Chougule, S.S. and S. Sahu, *Heat transfer and friction characteristics of Al2O3/water and CNT/water nanofluids in transition flow using helical screw tape inserts–a comparative study.* Chemical Engineering and Processing: Process Intensification, 2015. **88**: p. 78-88.

117. Maddah, H., et al., *Experimental study of Al2O3/water nanofluid turbulent heat transfer enhancement in the horizontal double pipes fitted with modified twisted tapes.* International Journal of Heat and Mass Transfer, 2014. **78**: p. 1042-1054.

118.   Sun, B., Z. Zhang, and D. Yang, *Improved heat transfer and flow resistance achieved with drag reducing Cu nanofluids in the horizontal tube and built-in twisted belt tubes.* International Journal of Heat and Mass Transfer, 2016. **95**: p. 69-82.

119.   Nakhchi, M.E. and J.A. Esfahani, *Cu-water nanofluid flow and heat transfer in a heat exchanger tube equipped with cross-cut twisted tape.* Powder Technology, 2018. **339**: p. 985-994.

120.   Jafaryar, M., M. Sheikholeslami, and Z. Li, *CuO-water nanofluid flow and heat transfer in a heat exchanger tube with twisted tape turbulator.* Powder Technology, 2018. **336**: p. 131-143.

121.   Farshad, S.A. and M. Sheikholeslami, *Nanofluid flow inside a solar collector utilizing twisted tape considering exergy and entropy analysis.* Renewable Energy, 2019. **141**: p. 246-258.

122.   Hosseinnezhad, R., et al., *Numerical study of turbulent nanofluid heat transfer in a tubular heat exchanger with twin twisted-tape inserts.* Journal of Thermal Analysis and Calorimetry, 2018. **132**(1): p. 741-759.

123.   Mustafa, J., et al., *The effect of using multichannel twisted tape and nanofluid on the absorber tube's heat transfer and the efficiency of a linear parabolic solar collector.* Sustainable Energy Technologies and Assessments, 2022. **52**: p. 102329.

124.   He, W., et al., *Effect of twisted-tape inserts and nanofluid on flow field and heat transfer characteristics in a tube.* International Communications in Heat and Mass Transfer, 2020. **110**: p. 104440.

125.   Bellos, E., C. Tzivanidis, and D. Tsimpoukis, *Enhancing the performance of parabolic trough collectors using nanofluids and turbulators.* Renewable and Sustainable Energy Reviews, 2018. **91**: p. 358-375.

126.   Wang, Y., et al., *Numerical simulation of flow and heat transfer characteristics of nanofluids in built-in porous twisted tape tube.* Powder Technology, 2021. **392**: p. 570-586.

127.   Salman, S., et al., *Hybrid nanofluid flow and heat transfer over backward and forward steps: A review.* Powder Technology, 2020. **363**: p. 448-472.

128.   Shah, T.R. and H.M. Ali, *Applications of hybrid nanofluids in solar energy, practical limitations and challenges: a critical review.* Solar Energy, 2019. **183**: p. 173-203.

129.   Syam Sundar, L., A.C. Sousa, and M.K. Singh, *Heat transfer enhancement of low volume concentration of carbon nanotube-Fe3O4/water hybrid nanofluids in a tube with twisted tape inserts under turbulent flow.* Journal of Thermal Science and Engineering Applications, 2015. **7**(2): p. 021015.

130.   Dalkılıç, A.S., et al., *An experimental investigation on heat transfer characteristics of graphite-SiO2/water hybrid nanofluid flow in horizontal tube with various quad-channel twisted tape inserts.* International Communications in Heat and Mass Transfer, 2019. **107**: p. 1-13.

131.   Fattahi, A., *Numerical simulation of a solar collector equipped with a twisted tape and containing a hybrid nanofluid.* Sustainable Energy Technologies and Assessments, 2021. **45**: p. 101200.

132.   Alnaqi, A.A., J. Alsarraf, and A.A. Al-Rashed, *Hydrothermal effects of using two twisted tape inserts in a parabolic trough solar collector filled with MgO-MWCNT/thermal oil hybrid nanofluid.* Sustainable Energy Technologies and Assessments, 2021. **47**: p. 101331.

133.   Li, W., et al., *A coupled optical-thermal-electrical model to predict the performance of hybrid PV/T-CCPC roof-top systems.* Renewable Energy, 2017. **112**: p. 166-186.

134.   Li, W., et al., *A three-point-based electrical model and its application in a photovoltaic thermal hybrid roof-top system with crossed compound parabolic concentrator.* Renewable Energy, 2019. **130**: p. 400-415.

135.   Xu, L., et al., *Dynamic test model for the transient thermal performance of parabolic trough solar collectors.* Solar Energy, 2013. **95**: p. 65-78.

136. Tochio, D. and S. Nakagawa, *Numerical simulation of three-dimensional thermal-hydraulic behavior for HTTR (High Temperature Engineering Test Reactor).* Nuclear Engineering and Design, 2011. **241**(5): p. 1616-1626.

137. Tandiroglu, A. and T. Ayhan, *Energy dissipation analysis of transient heat transfer for turbulent flow in a circular tube with baffle inserts.* Applied Thermal Engineering, 2006. **26**(2-3): p. 178-185.

138. Zhao, Z., Q. Liu, and K. Fukuda. *Experimental Study on Transient Heat Transfer Enhancement for Helium Gas Flowing Over a Thin Twisted Plate*. in *International Conference on Nuclear Engineering*. 2014. American Society of Mechanical Engineers.

139. Liu, Q., Z. Zhao, and K. Fukuda, *Experimental study on transient heat transfer enhancement from a twisted plate in convection flow of helium gas.* International Journal of Heat and Mass Transfer, 2015. **90**: p. 1160-1169.

140. Liu, Q., Z. Zhao, and K. Fukuda, *Width effect and local transient heat transfer characteristics for helium gas flowing over a twisted plate.* Journal of Nuclear Science and Technology, 2016. **53**(2): p. 223-231.

141. Ozsunar, A., S. Baskaya, and M. Sivrioglu, *Numerical analysis of Grashof number, Reynolds number and inclination effects on mixed convection heat transfer in rectangular channels.* International Communications in Heat and Mass Transfer, 2001. **28**(7): p. 985-994.

142. Watzinger, A. and D.G. Johnson, *Wärmeübertragung von Wasser an Rohrwand bei senkrechter Strömung im Übergangsgebiet zwischen laminarer und turbulenter Strömung.* Forschung auf dem Gebiet des Ingenieurwesens A, 1939. **10**(4): p. 182-196.

143. Martinelli, R.C. and C.J. Southwell, *Heat transfer and pressure drop for a fluid flowing in the viscous region through a vertical pipe*. 1942.

144. Kurganov, V. and A. Kaptilnyi, *Flow structure and turbulent transport of a supercritical pressure fluid in a vertical heated tube under the conditions of mixed convection. Experimental data.* International Journal of Heat and Mass Transfer, 1993. **36**(13): p. 3383-3392.

145. Piva, S., G.S. Barozzi, and M. Collins, *Combined convection and wall conduction effects in laminar pipe flow: numerical predictions and experimental validation under uniform wall heating.* Heat and Mass Transfer, 1995. **30**(6): p. 401-409.

146. Lin, W. and T. Lin, *Unstable aiding and opposing mixed convection of air in a bottom-heated rectangular duct slightly inclined from the horizontal.* 1996.

147. Patil, S. and P. Vijay Babu, *Experimental studies on mixed convection heat transfer in laminar flow through a plain square duct.* Heat and Mass Transfer, 2012. **48**(12): p. 2013-2021.

148. Chong, D., J. Liu, and J. Yan, *Effects of duct inclination angle on thermal entrance region of laminar and transition mixed convection.* International Journal of Heat and Mass Transfer, 2008. **51**(15-16): p. 3953-3962.

149. Abdelmeguid, A. and D. Spalding, *Turbulent flow and heat transfer in pipes with buoyancy effects.* Journal of Fluid Mechanics, 1979. **94**(2): p. 383-400.

150. Farouk, B. and K.S. Ball, *Convective flows around a rotating isothermal cylinder.* International Journal of Heat and Mass Transfer, 1985. **28**(10): p. 1921-1935.

151. Oni, T.O. and M.C. Paul, *Assessment of mixed convection heat transfer in a flow through an induced tube.* International Invention Journal of Engineering Science and Technology, 2015. **2**: p. 17-30.

152. Bejan, A. and J. Kestin, *Entropy generation through heat and fluid flow.* 1983.

153. Paoletti, S., F. Rispoli, and E. Sciubba. *Calculation of exergetic losses in compact heat exchanger passages*. in *Asme Aes*. 1989.

154. Bejan, A., *Convection heat transfer*. 2013: John wiley & sons.

155. Khfagi, A.M., et al., *Computational analysis of heat transfer augmentation and thermodynamic irreversibility of hybrid nanofluids in a tube fitted with classical and elliptical‑cut twisted tape inserts.* Journal of Thermal Analysis and Calorimetry, 2022: p. 1-18.

156.	Hooman, K., *Entropy-energy analysis of forced convection in a porous-saturated circular tube considering temperature-dependent viscosity effects.* International Journal of Exergy, 2006. **3**(4): p. 436-451.

157.	Ibáñez, G., S. Cuevas, and M.L. de Haro, *Minimization of entropy generation by asymmetric convective cooling.* International Journal of Heat and Mass Transfer, 2003. **46**(8): p. 1321-1328.

158.	Oliveski, R.D.C., M.H. Macagnan, and J.B. Copetti, *Entropy generation and natural convection in rectangular cavities.* Applied Thermal Engineering, 2009. **29**(8-9): p. 1417-1425.

159.	Bejan, A. and S. Lorente, *The physics of spreading ideas.* International Journal of Heat and Mass Transfer, 2012. **55**(4): p. 802-807.

160.	Ko, T.H. and C.P. Wu, *A numerical study on entropy generation induced by turbulent forced convection in curved rectangular ducts with various aspect ratios.* International Communications in Heat and Mass Transfer, 2009. **36**(1): p. 25-31.

161.	You, Y., et al., *Entropy generation analysis for laminar thermal augmentation with conical strip inserts in horizontal circular tubes.* International Journal of Thermal Sciences, 2015. **88**: p. 201-214.

162.	Mwesigye, A., T. Bello-Ochende, and J.P. Meyer, *Heat transfer and entropy generation in a parabolic trough receiver with wall-detached twisted tape inserts.* International Journal of Thermal Sciences, 2016. **99**: p. 238-257.

163.	Suri, A.R.S., A. Kumar, and R. Maithani, *Heat transfer enhancement of heat exchanger tube with multiple square perforated twisted tape inserts: experimental investigation and correlation development.* Chemical Engineering and Processing: Process Intensification, 2017. **116**: p. 76-96.

164.	Kock, F. and H. Herwig, *Entropy production calculation for turbulent shear flows and their implementation in CFD codes.* International Journal of Heat and Fluid Flow, 2005. **26**(4): p. 672-680.

165.	Liu, P., et al., *Thermal-hydraulic performance and entropy generation analysis of a parabolic trough receiver with conical strip inserts.* Energy Conversion and Management, 2019. **179**: p. 30-45.

166.	Kumar, B., et al., *Study of entropy generation in heat exchanger tube with multiple V cuts in perforated twisted tape insert.* Journal of Heat Transfer, 2019. **141**(8).

167.	Shamsabadi, H., S. Rashidi, and J.A. Esfahani, *Entropy generation analysis for nanofluid flow inside a duct equipped with porous baffles.* Journal of Thermal Analysis and Calorimetry, 2018. **135**(2): p. 1009-1019.

168.	Farshad, S.A. and M. Sheikholeslami, *Turbulent nanofluid flow through a solar collector influenced by multi-channel twisted tape considering entropy generation.* The European Physical Journal Plus, 2019. **134**(4): p. 149.

169.	Bahiraei, M., N. Mazaheri, and F. Aliee, *Second law analysis of a hybrid nanofluid in tubes equipped with double twisted tape inserts.* Powder Technology, 2019. **345**: p. 692-703.

170.	Mwesigye, A., T. Bello-Ochende, and J.P. Meyer, *Minimum entropy generation due to heat transfer and fluid friction in a parabolic trough receiver with non-uniform heat flux at different rim angles and concentration ratios.* Energy, 2014. **73**: p. 606-617.

171.	Versteeg, H.K. and W. Malalasekera, *An introduction to computational fluid dynamics: the finite volume method.* 2007: Pearson Education.

172.	ANSYS, R., *Academic Research, Release 14.5, ANSYS*. Inc.

173.	Hinze, J., *Turbulence. McGraw-Hill Publishing Co.* New York, 1975.

174.	Yan, W.-M., *Mixed convection heat and mass transfer in inclined rectangular ducts.* International Journal of Heat and Mass Transfer, 1994. **37**(13): p. 1857-1866.

175.	Fluent, I., *FLUENT user's guide 6.3.* Lebanon, USA, 2006.

176.	Shih, T.-H., et al., *A new k-ϵ eddy viscosity model for high reynolds number turbulent flows.* Computers & Fluids, 1995. **24**(3): p. 227-238.

177. Lam, C. and K. Bremhorst, *A modified form of the k-ε model for predicting wall turbulence.* 1981.

178. Fluent, I., *FLUENT 6.3 User's Guide. Fluent.* Inc, Lebanon, 2006.

179. Newell Jr, P. and A. Bergles, *Analysis of combined free and forced convection for fully developed laminar flow in horizontal tubes.* 1970.

180. Nonino, C. and S.D. Giudice, *Laminar mixed convection in the entrance region of horizontal rectangular ducts.* International journal for numerical methods in fluids, 1991. **13**(1): p. 33-48.

181. Bergman, T.L., et al., *Fundamentals of heat and mass transfer*. 2011: John Wiley & Sons.

182. Kadam, M., D. Kumbhar, and A. Pawar, *CFD and Experimentation on Heat Transfer Enrichment in Receiver Tube for Parabolic Trough Collector.* 2020.

183. Zimparov, V., *Extended performance evaluation criteria for enhanced heat transfer surfaces: heat transfer through ducts with constant heat flux.* International Journal of Heat and Mass Transfer, 2001. **44**(1): p. 169-180.

184. Warming, R. and R.M. Beam, *Upwind second-order difference schemes and applications in aerodynamic flows.* AIAA Journal, 1976. **14**(9): p. 1241-1249.

185. Patankar, S.V. and D.B. Spalding, *A calculation procedure for heat, mass and momentum transfer in three-dimensional parabolic flows*, in *Numerical prediction of flow, heat transfer, turbulence and combustion*. 1983, Elsevier. p. 54-73.

186. Mamourian, M., et al., *Optimization of mixed convection heat transfer with entropy generation in a wavy surface square lid-driven cavity by means of Taguchi approach.* International Journal of Heat and Mass Transfer, 2016. **102**: p. 544-554.

187. Lee, S., et al., *Measuring Thermal Conductivity of Fluids Containing Oxide Nanoparticles.* Journal of Heat Transfer, 1999. **121**(2): p. 280-289.

188. Suresh, S., et al., *Effect of Al2O3–Cu/water hybrid nanofluid in heat transfer.* Experimental Thermal and Fluid Science, 2012. **38**: p. 54-60.

189. Xuan, Y., Q. Li, and W. Hu, *Aggregation structure and thermal conductivity of nanofluids.* AIChE Journal, 2003. **49**(4): p. 1038-1043.

190. Kuppusamy, N.R., H.A. Mohammed, and C.W. Lim, *Numerical investigation of trapezoidal grooved microchannel heat sink using nanofluids.* Thermochimica Acta, 2013. **573**: p. 39-56.

191. Vajjha, R.S., et al., *Measurements of Specific Heat and Density of Al[sub 2]O[sub 3] Nanofluid*, in *AIP Conference Proceedings*. 2008. p. 361-370.

192. Wongcharee, K. and S. Eiamsa-ard, *Heat transfer enhancement by twisted tapes with alternate-axes and triangular, rectangular and trapezoidal wings.* Chemical Engineering and Processing: Process Intensification, 2011. **50**(2): p. 211-219.

193. Esfahani, J.A., et al., *Influences of wavy wall and nanoparticles on entropy generation over heat exchanger plat.* International Journal of Heat and Mass Transfer, 2017. **109**: p. 1162-1171.

194. Chaurasia, S.R. and R.M. Sarviya, *Numerical and experimental thermal performance with entropy generation analysis on tube with helical screw tape inserts at number of strips in turbulent flow.* Proceedings of the Institution of Mechanical Engineers, Part C: Journal of Mechanical Engineering Science, 2020. **235**(6): p. 1057-1070.

195. Mahian, O., et al., *A review of entropy generation in nanofluid flow.* International Journal of Heat and Mass Transfer, 2013. **65**: p. 514-532.

196. Feizabadi, A., M. Khoshvaght-Aliabadi, and A.B. Rahimi, *Experimental evaluation of thermal performance and entropy generation inside a twisted U-tube equipped with twisted-tape inserts.* International Journal of Thermal Sciences, 2019. **145**.

197. Belahmadi, E. and R. Bessaih, *Heat transfer and entropy generation analysis of Cu-water nanofluid in a vertical channel.* World Journal of Engineering, 2018. **15**(5): p. 604-613.

References

198. Qi, C., et al., *Influence of rotation angle of a triangular tube with a built-in twisted tape on the thermal-exergy efficiency and entropy generation of nanofluids in the heat exchange system.* Asia-Pacific Journal of Chemical Engineering, 2020. **15**(1).

199. Makhanlall, D. and L. Liu, *Entropy production analysis of swirling diffusion combustion processes.* Frontiers of Energy and Power Engineering in China, 2009. **4**(3): p. 326-332.

200. Cimpean, D., N. Lungu, and I. Pop, *A problem of entropy generation in a channel filled with a porous medium.* Creative Math and Inf, 2008. **17**: p. 357-362.

201. Varol, Y., H.F. Oztop, and A. Koca, *Entropy production due to free convection in partially heated isosceles triangular enclosures.* Applied Thermal Engineering, 2008. **28**(11-12): p. 1502-1513.

202. Magherbi, M., H. Abbassi, and A.B. Brahim, *Entropy generation at the onset of natural convection.* International Journal of Heat and Mass Transfer, 2003. **46**(18): p. 3441-3450.

203. Muñoz, J. and A. Abánades, *Analysis of internal helically finned tubes for parabolic trough design by CFD tools.* Applied Energy, 2011. **88**(11): p. 4139-4149.

204. Lüpfert, E., et al., *Experimental analysis of overall thermal properties of parabolic trough receivers.* Journal of Solar Energy Engineering, 2008. **130**(2).

205. Burkholder, F. and C. Kutscher, *Heat-loss testing of Solel's UVAC3 parabolic trough receiver*. 2008, National Renewable Energy Lab.(NREL), Golden, CO (United States).

206. Liu, Q., Z. Zhao, and K. Fukuda, *Transient heat transfer for forced flow of helium gas along a horizontal plate with different widths.* International Journal of Heat and Mass Transfer, 2014. **75**: p. 433-441.

207. Liu, Q., K. Fukuda, and Z. Zhang, *Theoretical and experimental studies on transient heat transfer for forced convection flow of helium gas over a horizontal cylinder.* JSME International Journal Series B Fluids and Thermal Engineering, 2006. **49**(2): p. 326-333.

208. Shibahara, M., Q. Liu, and K. Fukuda. *Effect of Heater Configurations on Transient Heat Transfer for Various Gases Flowing Over a Twisted Heater*. in *International Conference on Nuclear Engineering*. 2009.

209. Shibahara, M., Q. Liu, and K. Fukuda, *Effect of heater configurations on transient heat transfer for various gases flowing over a twisted heater.* Journal of Power and Energy Systems, 2010. **4**(1): p. 262-273.

210. Shibahara, M., Q. Liu, and K. Fukuda, *Enhanced Transient Heat Transfer Caused by Partially Twisted Heater in Various Gases.* Marine Engineering, 2010. **45**(Special): p. 1033-1038.

211. Wang, L., Q. Liu, and K. Fukuda, *Numerical Solution on Transient Heat Transfer for Forced Convection Flow of Helium Gas over a Twisted Plate with Different Helical Pitch.* Marine Engineering, 2015. **50**(6): p. 776-781.

212. Wang, L., Q. Liu, and K. Fukuda, *Experimental and numerical study of transient heat transfer for forced convection flow of helium gas over a twisted plate.* Journal of Thermal Science and Technology, 2016. **11**(1): p. JTST0007-JTST0007.

213. Anderson, J.D. and J. Wendt, *Computational fluid dynamics*. Vol. 206. 1995: Springer.

214. Tandiroglu, A., *Second law analysis of transient heat transfer for turbulent flow in a circular tube with baffle inserts.* International Journal of Exergy, 2005. **2**(3): p. 299-317.

215. He, Y.-L., et al., *A MCRT and FVM coupled simulation method for energy conversion process in parabolic trough solar collector.* Renewable Energy, 2011. **36**(3): p. 976-985.

216. Marugán-Cruz, C., et al., *Heat transfer and thermal stresses in a circular tube with a non-uniform heat flux.* International Journal of Heat and Mass Transfer, 2016. **96**: p. 256-266.

217. Jeter, S.M., *Analytical determination of the optical performance of practical parabolic trough collectors from design data.* Solar Energy, 1987. **39**(1): p. 11-21.

218. Boz, Z., F. Erdogdu, and M. Tutar, *Effects of mesh refinement, time step size and numerical scheme on the computational modeling of temperature evolution during natural-convection heating.* Journal of Food Engineering, 2014. **123**: p. 8-16.

References
___

219.   Erdogdu, F. and M. Tutar, *A computational study for axial rotation effects on heat transfer in rotating cans containing liquid water, semi-fluid food system and headspace.* International Journal of Heat and Mass Transfer, 2012. **55**(13-14): p. 3774-3788.

220.   Vajjha, R.S. and D.K. Das. *Measurements of specific heat and density of Al 2 O 3 nanofluid.* in *AIP Conference Proceedings.* 2008. American Institute of Physics.

221.   Zachar, A., I. Farkas, and F. Szlivka, *Numerical analyses of the impact of plates for thermal stratification inside a storage tank with upper and lower inlet flows.* Solar Energy, 2003. **74**(4): p. 287-302.

222.   Liu, Q., M. Shibahara, and K. Fukuda, *Transient heat transfer for forced convection flow of helium gas over a horizontal plate.* Experimental Heat Transfer, 2008. **21**(3): p. 206-219.

223.   Wang, L., N. Karimi, and M.C. Paul, *Gas-phase transport and entropy generation during transient combustion of single biomass particle in varying oxygen and nitrogen atmospheres.* International Journal of Hydrogen Energy, 2018. **43**(17): p. 8506-8523.

224.   Hunt, G., N. Karimi, and M. Torabi, *Two-dimensional analytical investigation of coupled heat and mass transfer and entropy generation in a porous, catalytic microreactor.* International Journal of Heat and Mass Transfer, 2018. **119**: p. 372-391.

225.   Esfahani, J., et al., *Influences of wavy wall and nanoparticles on entropy generation over heat exchanger plat.* International Journal of Heat and Mass Transfer, 2017. **109**: p. 1162-1171.

226.   Malik, S. and A. Nayak, *Effect of moving walls on heat transfer and entropy generation in a nanofluid-filled enclosure.* Journal of Engineering Mathematics, 2018. **110**(1): p. 147-165.

227.   Huminic, G. and A. Huminic, *Heat transfer and entropy generation analyses of nanofluids in helically coiled tube-in-tube heat exchangers.* International Communications in Heat and Mass Transfer, 2016. **71**: p. 118-125.

228.   Al-Rashed, A.A., et al., *Entropy generation of boehmite alumina nanofluid flow through a minichannel heat exchanger considering nanoparticle shape effect.* Physica A: Statistical Mechanics and its Applications, 2019. **521**: p. 724-736.

229.   Shahsavar, A., M. Moradi, and M. Bahiraei, *Heat transfer and entropy generation optimization for flow of a non-Newtonian hybrid nanofluid containing coated CNT/Fe3O4 nanoparticles in a concentric annulus.* Journal of the Taiwan Institute of Chemical Engineers, 2018. **84**: p. 28-40.

230.   Joye, D.D., J.P. Bushinsky, and P.E. Saylor, *Mixed convection heat transfer at high Grashof number in a vertical tube.* Industrial & Engineering Chemistry Research, 1989. **28**(12): p. 1899-1903.

231.   Peterson, G. and A. Ortega, *Thermal control of electronic equipment and devices*, in *Advances in heat transfer.* 1990, Elsevier. p. 181-314.

232.   Saha, S., et al., *Combined free and forced convection inside a two-dimensional multiple ventilated rectangular enclosure.* ARPN Journal of Engineering and Applied Sciences, 2006. **1**(3): p. 23-35.

233.   Ghasemi, B. and S. Aminossadati, *Periodic natural convection in a nanofluid-filled enclosure with oscillating heat flux.* International Journal of Thermal Sciences, 2010. **49**(1): p. 1-9.

234.   Takabi, B. and S. Salehi, *Augmentation of the heat transfer performance of a sinusoidal corrugated enclosure by employing hybrid nanofluid.* Advances in Mechanical Engineering, 2014. **6**: p. 147059.

235.   Mehryan, S.A., et al., *Free convection of hybrid Al2O3-Cu water nanofluid in a differentially heated porous cavity.* Advanced Powder Technology, 2017. **28**(9): p. 2295-2305.

236.   Nimmagadda, R. and K. Venkatasubbaiah, *Conjugate heat transfer analysis of micro-channel using novel hybrid nanofluids (Al2O3+ Ag/Water).* European Journal of Mechanics-B/Fluids, 2015. **52**: p. 19-27.

237.   Mansour, R.B., N. Galanis, and C.T. Nguyen, *Effect of uncertainties in physical properties on forced convection heat transfer with nanofluids.* Applied Thermal Engineering, 2007. **27**(1): p. 240-249.

238. Polidori, G., S. Fohanno, and C. Nguyen, *A note on heat transfer modelling of Newtonian nanofluids in laminar free convection.* International Journal of Thermal Sciences, 2007. **46**(8): p. 739-744.

239. Maughan, J. and F.P. Incropera, *Experiments on mixed convection heat transfer for airflow in a horizontal and inclined channel.* International Journal of Heat and Mass Transfer, 1987. **30**(7): p. 1307-1318.

240. Ahmadi, K., et al., *Heat transfer assessment of turbulent nanofluid flow in a circular pipe fitted with elliptical-cut twisted tape inserts.* Journal of Thermal Analysis and Calorimetry, 2020: p. 1-14.

241. Oni, T.O. and M.C. Paul, *Numerical simulation of turbulent heat transfer and fluid flow in different tube designs.* 2014.

242. Bahiraei, M., M. Jamshidmofid, and S. Heshmatian, *Entropy generation in a heat exchanger working with a biological nanofluid considering heterogeneous particle distribution.* Advanced Powder Technology, 2017. **28**(9): p. 2380-2392.

243. Singh, P.K., et al., *Entropy generation due to flow and heat transfer in nanofluids.* International Journal of Heat and Mass Transfer, 2010. **53**(21-22): p. 4757-4767.

244. Zadeh, S.M.H., et al., *Irreversibility analysis of thermally driven flow of a water-based suspension with dispersed nano-sized capsules of phase change material.* International Journal of Heat and Mass Transfer, 2020. **155**: p. 119796.